NANOPARTICLES WITH MAGNETIC CORE AS A VERSATILE CATALYST FOR ORGANIC TRANSFORMATIONS

Ph.D. Thesis

MITLESH KUMARI
(2013RCY9536)

NANOPARTICLES WITH MAGNETIC CORE AS A VERSATILE CATALYST FOR ORGANIC TRANSFORMATIONS

Submitted as a Partial Fulfillment for the Award of the
Degree of

DOCTOR OF PHILOSOPHY
IN
CHEMISTRY

Submitted by

MITLESH KUMARI
(2013RCY9536)

Under the supervision of
Dr. RAGINI GUPTA
Professor
Department of Chemistry
MNIT, Jaipur

DEPARTMENT OF CHEMISTRY
MALAVIYA NATIONAL INSTITUTE OF TECHNOLOGY JAIPUR
JAIPUR-302017 (INDIA)
December, 2019

C a n d i d a t e ' s   D e c l a r a t i o n

I, **Mitlesh Kumari,** declare that this thesis titled **"Nanoparticles with magnetic core as a versatile catalyst for organic transformations"** and the work presented in it, are my own. I confirm that:

- This work was done wholly or mainly while in candidature for a research degree at this institute.

- Where any part of this thesis has previously been submitted for a degree or any other qualification at this institute or any other institution, this has been clearly stated.

- Where I have consulted the published work of others, this is always clearly attributed.

- Where I have quoted from the work of others, the source is always given. With the exception of such quotations, this thesis is entirely my own work.

- I have acknowledged all main sources of help.

- Where the thesis is based on work done by myself, jointly with others, I have made clear exactly what was done by others and what I have contributed myself.

Date:

Mitlesh Kumari
(2013RCY9536)
Department of Chemistry
MNIT, Jaipur

Supervisor's Certificate

This is to certify that the work incorporated in the thesis entitled **"NANOPARTICLES WITH MAGNETIC CORE AS A VERSATILE CATALYST FOR ORGANIC TRANSFORMATIONS"** which is being submitted to the Malaviya National Institute of Technology Jaipur, Jaipur, Rajasthan, for the award of the degree of **Doctor of Philosophy** in Chemistry by **Mitlesh Kumari** was carried out under my supervision and guidance at Department of Chemistry, Malaviya National Institute of Technology, Jaipur, India. The matter embodied in this thesis is original and has not been submitted to any other University or Institute for the award of any other degree to the best of my knowledge and belief.

Date:

Dr. Ragini Gupta
Professor & HOD
Department of Chemistry
MNIT Jaipur

A C K N O W L E D G E M E N T

Mitlesh Kumari

Abstract

The challenging task in chemistry is to develop the practical methods, reaction media, conditions, and the use of materials based on the principles of green chemistry. The concept of ''Green Chemistry'' has emerged as one of the guiding principles of environmentally benign synthesis. The preparation and the use of nanoparticles (NPs) in organic synthesis has become a subject of intense investigation. In particular, magnetic nanoparticles (MNPs) which offer advantages in clean and sustainable chemistry as they can be non-toxic, readily accessible, and retrievable. Additionally, the activity and selectivity of magnetic nanocatalysts can be manipulated by its surface modification. The aim of this thesis is to highlight the progress in the synthesis and catalytic applications of magnetic catalyst in organic transformations. The heterogenization of the catalyst using magnetic nanoparticles allows it to be recovered and reused using an external magnet. Synthesis of functionalized magnetically recoverable nanoparticles has been carried out and successfully utilized them as an efficient catalyst for various organic transformations. Prepared nanocatalyst were well characterized by various possible techniques. Moreover, all the organic compounds were also synthesized in shorter reaction time with high yield and purity.

Contents

List of Figures

List of Tables

List of Abbreviations

S. No.	Abbreviated Form	Extended Form
1.	%	Percent
2.	Δ	Chemical Shift
3.	υ	Frequency
4.	$υ$ cm^{-1}	Wavenumber
5.	λ nm	Wavelength
6.	Å	Angstrom
7.	˚C	Degree Centigrade
8.	Ag	Silver
9.	Fe	Iron
10.	CH_2Cl_2	Dichloromethane
11.	$CHCl_3$	Chloroform
12.	CH_3CN	Acetonitrile
13.	Cu	Copper
14.	DMF	Dimethylformamide
15.	DMSO	Dimethyl sulfoxide
16.	e.g.	For example
17.	G	Gram
18.	H^+	Proton
19.	H	Hour
20.	HR-MS	High Resolution Mass Spectrum
21.	^{1}H NMR	Proton Nuclear Magnetic Resonance Spectroscopy

S. No.	Abbreviated Form	Extended Form
21.	H_2O_2	Hydrogen Peroxide
22.	Hz	Hertz
23.	FT-IR	Fourier Transform Infrared
24.	M	Multiplet
25.	m/z	Mass/Charge
26.	MHz	Megahertz
27.	M^+	Molecular Ion
28.	M	Molar
29.	Mmol	Millimole
30.	mL	Millilitre
31.	M.P	Melting Point
32.	MW	Microwave
33.	$\upsilon\ cm^{-1}$	Frequency in cm^{-1}
34.	KBr	Potassium Bromide
35.	FTIR	Fourier Transform Infrared Spectroscopy
36.	DMSO-*d6*	Deuterated Dimethyl Sulfoxide
37.	TLC	Thin Layer Chromatography

Chapter - 1

General Introduction and Literature Survey

1.1 Introduction

The phenomenon called 'catalysis' was recognized from a very former age, even though people knew nothing about the underlying mechanism and chemical process involved in it. A catalyst accelerates a chemical reaction with actually not being consumed, the process is called 'catalysis' [1]. By using catalytic reagents, one can reduce the temperature of a transformation, reduce reagent based waste, enhance the selectivity of a reaction, allowing reactions to occur faster, cheaper and greener [2]. Catalysis has a key enabling role in environmental protection, particularly in recycling waste and reduction of greenhouse gases. Anastas and Warner [3] in 1998 suggested a set of twelve principles which is the main philosophy of green chemistry to reduce or eliminate chemicals and chemical processes that have negative environmental impacts. Designing and development of a novel ideal catalyst are one of the prior application of green chemistry. According to these principles, highly selective catalytic reagents are superior to that of stoichiometric reagents. Stoichiometric reagents are used in high amounts and are not reusable while catalytic reagents are used in little amounts and can carry out a single reaction multiple times. Catalysis is the most interdisciplinary and overarching technology famously playing a key role in chemical transformations and lies at the heart of countless chemical protocols, academic research at laboratories level to the chemical industry level [4]. Catalysis research underpins several strategic industrial sectors: from energy to the manufacturing of materials and industrial processes like petrochemical, pharmaceutical and chemical industries.

Swedish chemist Jöns Jacob Berzelius first time coined the term catalysis in 1835 [5]. He summarised his concepts on 'catalysis' as a novel force, Berzelius wrote:

"It is, then, proved that several simple or compound bodies, soluble and insoluble, have the property of exercising on other bodies an action very different from chemical affinity. By means of this action, they produce, in these bodies, decompositions of their elements and different recombination of these same elements to which they remain indifferent." He called this new force as 'catalytic force' [6].

He used it to describe a wide range of observed phenomena, both in homogeneous systems, where the catalysts and the reactants happen to be in the same phase and in heterogeneous systems, where the phase differs. Berzelius recognized that common chemical principles were involved, but the two branches of catalysis have developed independently and offer the chemical industry different strengths and weaknesses [7]. The findings formulated by Berzelius were

concluded through discussions and experimental work with contemporary scientists in Europe **[8]**. The modern definition of catalyst was described by Wilhelm Ostwald in 1894. He generalized the definition and classified catalysts as species which enhance the rate of a chemical reaction through the formation of intermediate that are restored at the end of the reaction. In 1909, Ostwald was awarded with the Nobel Prize for his work on catalysis, chemical equilibrium and reaction velocities **[9]**. A significant number of Nobel laureates including Haber (1918), Bergius and Bosch (1931), Natta and Ziegler (1963), Fischer and Wilkinson (1973), Knowles, Noyori and Sharpless (2001), Chauvin, Grubbs and Schrock (2005) and recently, G.Ertl (2007), followed Ostwald contributing majorly to the field of catalysis **[1**, **6, 10]**.

In fact, we can describe the catalytic reaction as a cyclic event by conventional catalysis theory **[11]** in which the catalyst involved in the reaction and is recovered in its starting phase at the end of the cycle. Let us consider the catalytic reaction between two molecules reactant and reagent to give a product in **Figure 1.1**. The cycle starts with the bonding of molecules with the catalyst and forms the intermediates and finally gives the product. In the final step, product detaches from the catalyst, thus leaving the reaction cycle in its original state.
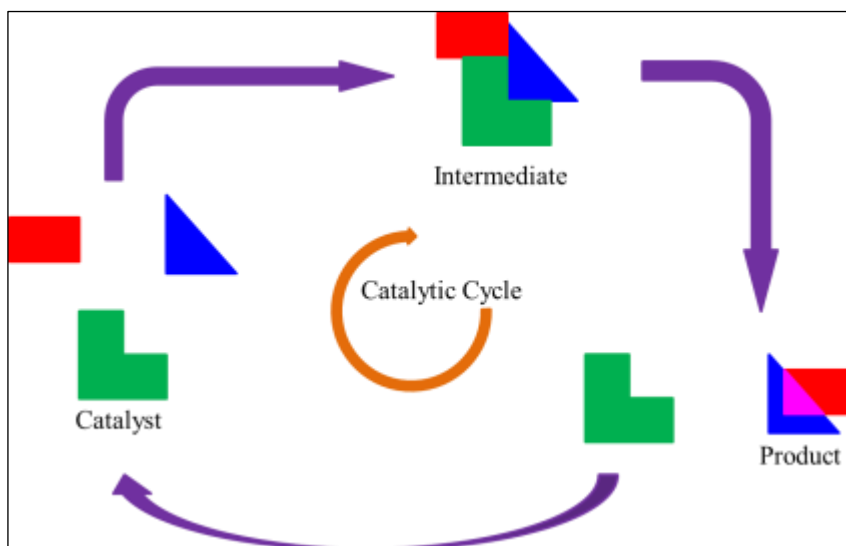
Figure 1.1. Generalized block schematic representation of energy for catalytic reaction as a sequence of elementary steps

1.2 Catalysis: Homogenous, Heterogenous and Quasi-Homogenous Phase

A homogeneous catalyst, where the catalyst is in the same phase as the reactants, is generally accepted by chemists [12]. One attractive property is that all catalytic sites are accessible because the catalyst is generally a soluble metal complex. Furthermore, it is possible to tune the chemo-, regio- and enantio-selectivity of the catalyst. Homogeneous catalysts have a number of other advantages, such as high selectivity, better yield, and easy optimization of catalytic systems by modification of ligand and metals. They are widely used in a number of commercial applications, but the difficulty of catalyst separation from the final product creates economic and environmental barriers to broadening their scope. Despite their advantages and widespread use in a number of applications, many homogeneous catalytic systems have not been commercialized because of the difficulty encountered in separating the catalyst from the final reaction product. Removal of the trace amounts of catalyst from the end product is essential since metal contamination is highly regulated, especially by the pharmaceutical industry. Even with the extensive and careful use of various techniques such as distillation, chromatography, or extraction, removal of the trace amounts of catalyst remains a challenge. To address the separation problems in homogeneous catalysis, chemists and engineers have investigated a wide range of strategies with the use of heterogeneous catalyst systems appearing to be the best logical solution [13]. The majority of the novel heterogenized catalysts are based on silica supports, primarily because silica displays some advantageous properties, such as excellent stability, good accessibility, porosity, and the fact that organic groups can be robustly anchored to its surface to provide catalytic centres [14]. The common structural feature of these materials is the entrapment or anchoring of the dopant (catalytic) molecule in the pores of silica, a phenomenon which imparts unique chemical and physical properties to the resulting hybrid silica. Anchoring can be achieved by covalent binding of the molecules or by simple adsorption; covalent anchoring is preferred as it is robust enough to withstand the harsh reaction conditions and the catalyst can be reused several times. A vast majority of the industrial heterogeneous catalysts are high-surface area solids onto which an active component is dispersed or attached. Attempts have been made to make all active sites on solid supports accessible for reaction thus allowing rates and selectivity comparable to those obtained with homogeneous catalysts. Unfortunately, often only sites on the surface are available for catalysis, which decreases the overall reactivity of the catalyst system. Another problem is the leaching of the active molecule/complex from solid supports because of

the breaking of bonds between the metal and the ligand during catalytic reactions, which again necessitates the separation of trace metals from final product. Consequently, new catalyst systems that allow for rapid, selective chemical transformations with excellent product yield coupled with the ease of catalyst separation and recovery are highly desired for "greening" the chemical manufacturing processes. Over the last decade, the use of transition metal nanoparticles (NPs) in catalysis has expanded considerably and has led to many interesting applications, with C–C bond formation reactions being one of their most important. Since the sustainable development involves the utilization of reusable catalysts, the search for new catalytic systems to replace existing homogeneous/heterogeneous ones is an important issue. In this context, the use of metal nanoparticles as catalysts or metal nanoparticle/catalyst supported over magnetic nano-surface has emerged as one of the most promising solutions as it acts as a quasi- homogeneous phase due to the nano nature of the catalyst (a bridge between homogeneous and heterogeneous phase) with efficient reactions under mild and environmentally benign conditions.
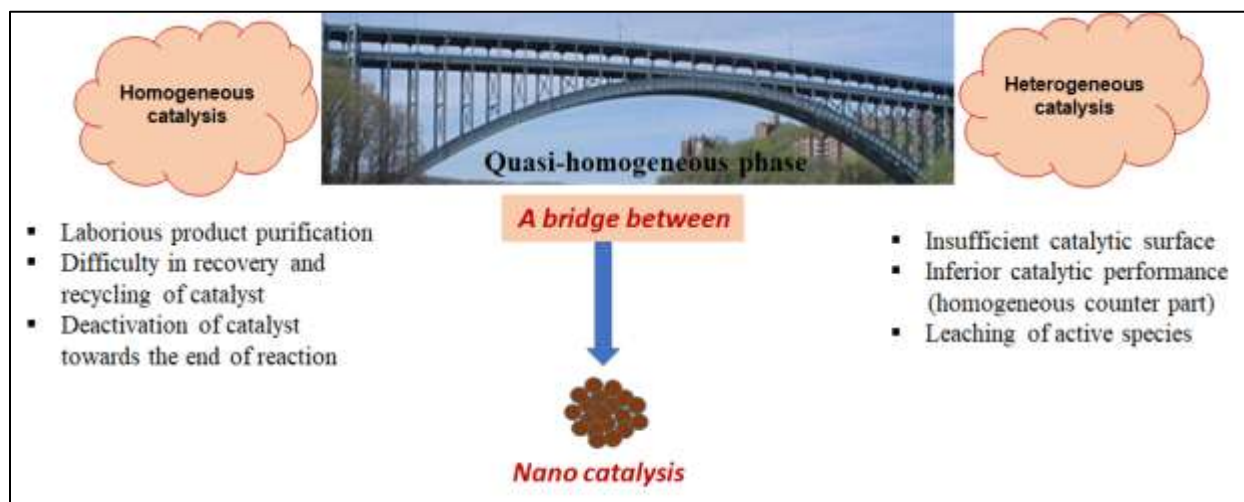
Figure 1.2. Quasi homogenous phase: A bridge between homogenous and heterogeneous phase

1.3 Magnetic nanocatalyst (Nanoparticles with magnetic core)

Green chemistry endeavours involving nanocatalysis is another fertile area of exploration, which avoids the practice of flammable organic solvents, toxic reagents, hazardous and/or harsh reaction conditions, and tedious separations **[15]**. It is essential to use benign solvents, catalysts, and alternative energy sources from the point of view of sustainable protocol development. Nanoparticles fill the gap between homogeneous and heterogeneous catalysis, but their recovery

by normal filtration technique limits their widespread utility [16]. This limitation hampers the economics and sustainability of these nanocatalytic protocols. The unique advantages of magnetically recoverable nanocatalysts stem from their capability for easy and fast separation even in large sample volumes by using external magnetic forces with respect to the mother liquor without the need for time-consuming centrifugation and filtration steps. Hence, the use of magnetically recoverable nanocatalysts is potentially a "double green dream", which not only saves time but also avoids problems such as loss of catalyst, catalyst oxidation, and need for additional solvent and subsequent generation of organic residues [17]. In the last few years, various forms of iron oxides such as FeO (wüstite), Fe_2O_3 (iron III oxides), α-Fe_2O_3 (hematite), β-Fe_2O_3 (beta phase), and γ-Fe_2O_3 (maghemite) were successfully deployed in catalysis [18-25]. Magnetite has a cubic inverse spinel structure with a space group of *Fd3m* [26]. The unit cell has interesting properties because the presence of non-equivalent cations in two valence states, Fe^{2+} and Fe^{3+}, in the crystal structure leads to formation of a unique magnetic structure. The unit cell also contains 32 O_2 ions which are regular cubic close packed along the [110] direction [27]. Generally, Fe_3O_4 crystals are distributed with octahedral and mixed octahedral/tetrahedral layers along the [111] direction [26, 28].

Magnetite is an ideal oxide support, easy to prepare, having a very active surface for adsorptions or immobilization of metals and ligands, which can be separated by magnetic decantation after the reaction, thus making it a more sustainable catalyst [29].

Bare magnetic nanoparticles (MNPs) due to their inherent instability and hydrophobic nature results in big clusters over time in the absence of any surface coating which reduces their surface energy [30]. In order to provide them stability against damage during or after being used in organic transformations, it needs to functionalize them with biocompatible organic and inorganic materials which protects them from being oxidised [31-32].
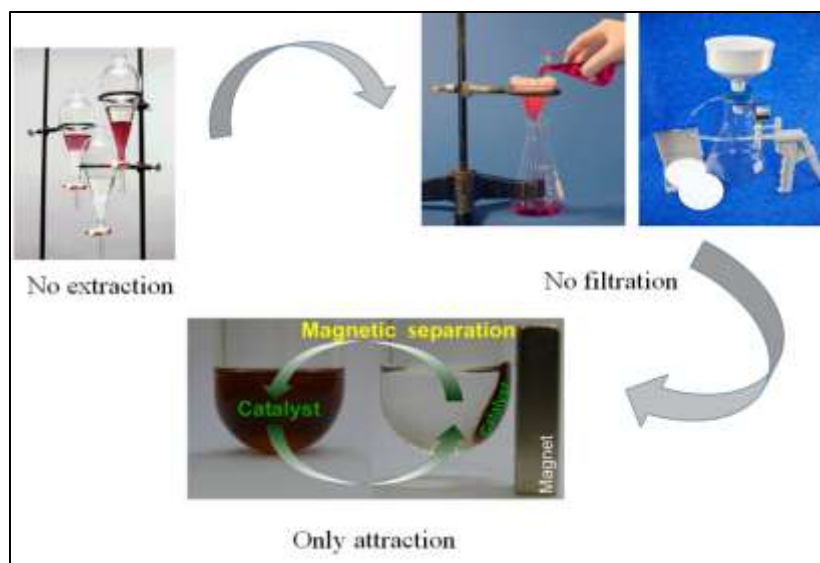
Figure 1.3 Catalytic separation by magnetic attraction

1.4 Applications of functionalized magnetic nanocatalysts in organic transformation

Magnetite-based hybrid nanomaterials have been used as catalysts for a very wide range of catalytic processes and organic transformations. This section describes the magnetite-supported typical catalytic applications and organic transformation.

Lin and co-workers **[33]** reported the preparation of magnetic Pd-NHC (NHC = N-Heterocyclic-carbene) complex using palladium diacetate and palladium chloride as Pd source with 1-(2,6-diisopropylphenyl)-1H-imidazole(1-arylimidazole) grafted on the surface of magnetic polymer support. Suzuki Miyaura reaction between phenylboronic acids with aryl bromides in ethanol–water solution successfully employed by using synthesized magnetic nanocatalyst and showed no significant loss in catalytic activity with recyclability of 21 runs (**Scheme 1.1**).

X= Cl, Br
R^1= H, p-COCH$_3$, p-CH$_3$, p-NO$_2$ etc.
R^2= H, p-CH$_3$, 2,6-Dimethyl etc.

15 examples
61-99%
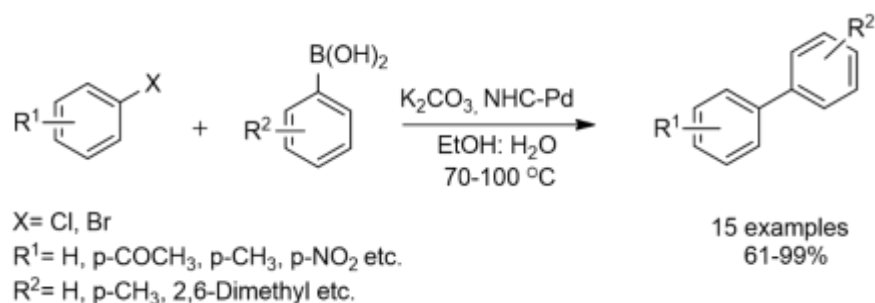
Scheme 1.1 Magnetic NHC-Pd complex catalyzed Suzuki-Miyara reaction

7

Liu and co-workers [34] have synthesized recyclable core-shell Pd/Fe$_3$O$_4$@γ-Al$_2$O$_3$ nanocomposites for Heck coupling reactions between aryl bromides and olefins. The catalysts recovered were more than 90% and after recyclability for six runs the catalyst gave 80% conversion of bromobenzene (**Scheme 1.2**).

R= H, COCH$_3$, NO$_2$, OCH$_3$ etc.
R^1= C$_6$H$_5$, COO^{i}Bu, COOCH$_3$

7 examples
58-96%
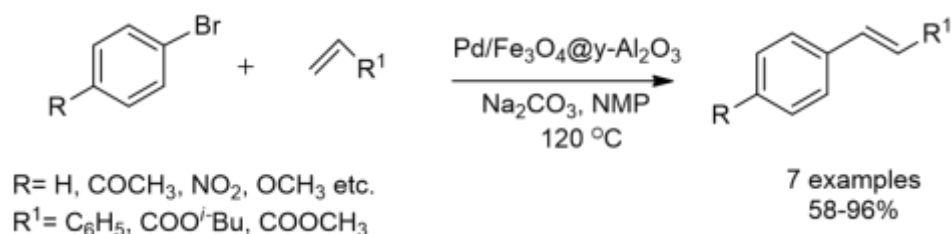
Scheme 1.2 Pd/Fe$_3$O$_4$@γ-Al$_2$O$_3$ catalyzed Heck coupling reaction

Varma and co-workers [35] synthesized heterogeneous Fe$_3$O$_4$@DOPA-Pd catalyst via immobilisation of palladium nanoparticles over dopamine decorated magnetite. The catalyst utilized for the Heck coupling reaction in aqueous media without any significant leaching of palladium (**Scheme 1.3**).

X= Br, I, Cl
R^1= CH$_3$, CH$_2$CH$_3$

10 examples
30-98%
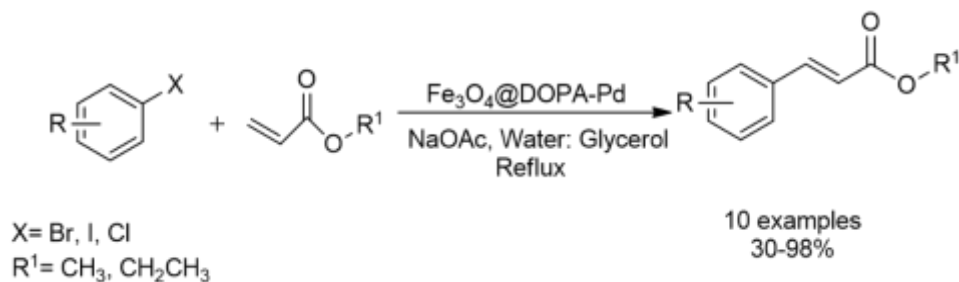
Scheme 1.3 Fe$_3$O$_4$@DOPA-Pd catalyzed Heck coupling reaction

Gawande and co-workers [36] without using any linker or ligand between metal and the magnetite support described the efficient co-precipitation method for the synthesis of magnetite-supported Pd catalyst. The catalytic application of magnetite-Pd catalyst was utilized for Buchwald-Hartwig coupling reaction between aryl halides and substituted amines with good to excellent yields (**Scheme 1.4**).
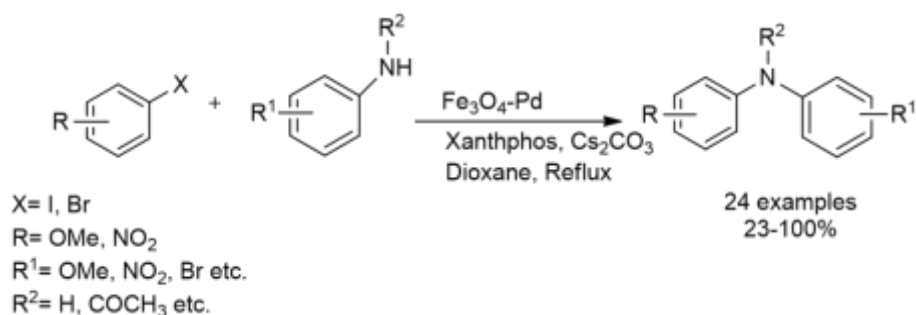
Scheme 1.4 Magnetite-Pd nanoparticle catalyzed Buchwald-Hartwig coupling reaction

Varma and co-workers **[37]** reported an environmentally benign silica-coated magnetic material, immobilized by palladium. The synthesized material was successfully used for *O*-allylation reaction between phenol and allyl acetate in open air **(Scheme 1.5)** with good yield (72-89%).
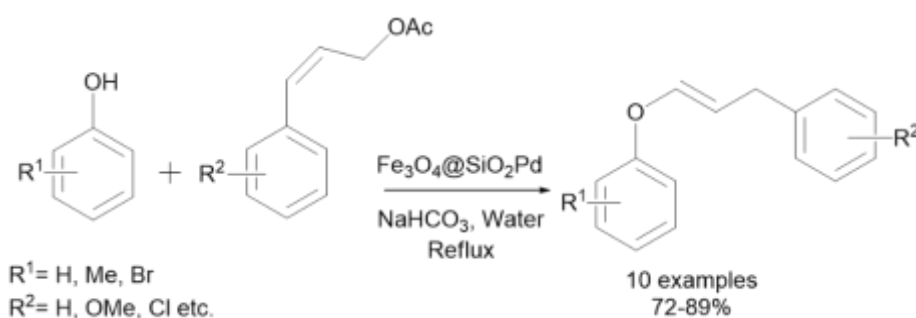
Scheme 1.5 Fe_3O_4@SiO_2Pd catalyzed O-allylation reaction

Transition metal catalyzed direct C–H bond transformation is highly valued and important strategy in organic synthesis **[38, 39]**. **R**ecently, Sharma et al. **[40]** described preparation of copper complex immobilized on amine functionalized silica-coated magnetic nanoparticles via covalent anchoring of the quinoline-2-carboimine as an efficient organic inorganic hybrid fabricated nanomaterial. The Cu-2QC@Am-SiO_2@Fe_3O_4 catalyst showed good catalytic efficiency in the carbamate synthesis in presence of TBHP (*tert*-butyl hydroperoxide) between formamide and 2-carbonyl substituted phenol/β-ketoester under solvent-free conditions **(Scheme 1.6).**
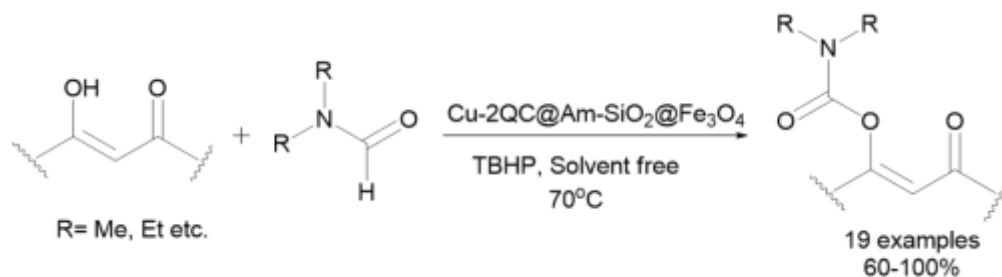
Scheme 1.6 Cu-2QC@Am-SiO$_2$@Fe$_3$O$_4$ catalyzed carbamate synthesis

Liu and co-workers **[41]** reported Fe$_3$O$_4$-CoOx catalyzed 5-hydroxymethylfurfural (HMF) conversion into 2,5-furandicarboxylic acid (FDCA) with *t*-BuOOH as oxidant (69% yield, **Scheme 1.7**); O$_2$ and H$_2$O$_2$ gave less conversion of 4.2, 1% respectively. Two consecutive step conversion of fructose to FDCA was demonstrated using Fe$_3$O$_4$@SiO$_2$-SO$_3$H (to convert fructose to HMF) followed by Fe$_3$O$_4$-CoOx for oxidation with 60% yield (from HMF to FDCA).
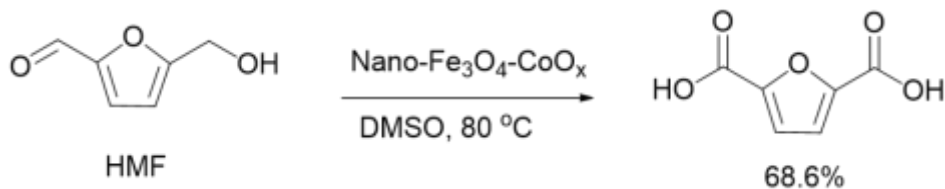
Scheme 1.7 Fe$_3$O$_4$-CoOx catalyzed 2,5-furandicarboxylic acid

Ranganath and co-workers **[42]** developed an elegant method for the synthesis of ultrafine particles of Fe$_3$O$_4$ using ferrous ammonium sulphate (NH$_4$)$_2$Fe(SO$_4$)$_2$ and ferric chloride (FeCl$_3$) mixture (Fe^{2+}: Fe^{3+} = 1:2 ratio) in alkaline medium at 80 °C via co-precipitation method. The resulting nanoparticles were used for aerobic oxidation α-hydroxyl ketone (benzoin) to benzil **(Scheme 1.8)**.
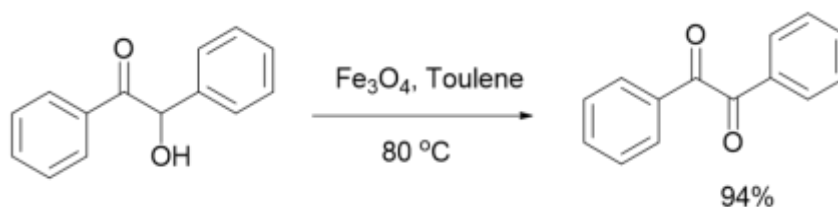
Scheme 1.8 Magnetite catalyzed oxidation of benzoin to benzil

Saikia and co-workers [43] demonstrated that their synthesized Fe_3O_4@MIL-101 (Cr) material was utilized for the solvent-free oxidation of different substituted benzyl alcohols with TBHP at 80 °C (**Scheme 1.9**).

R= H, Me etc.

6 examples
<2-79.8% conversion
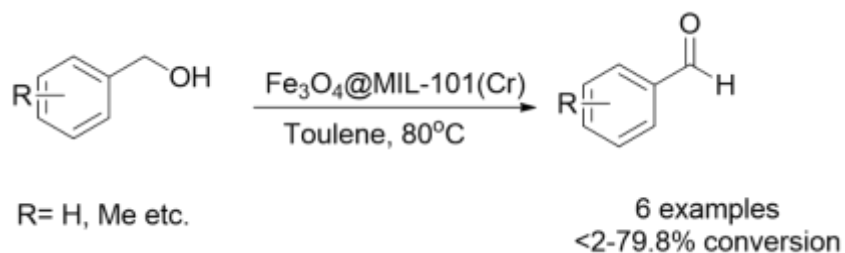
Scheme 1.9 Fe_3O_4@MIL-101 (Cr) catalyzed oxidation reaction

Lu and co-workers [44] demonstrated a method for the construction of bifunctional magnetic yolk-shell type of nanocatalysts (Fe_3O_4@*h*-C/Pt), which used for the reduction of nitrobenzene using propan-2-ol as solvent at 30 ℃ (**Scheme 1.10**).

>99% conversion
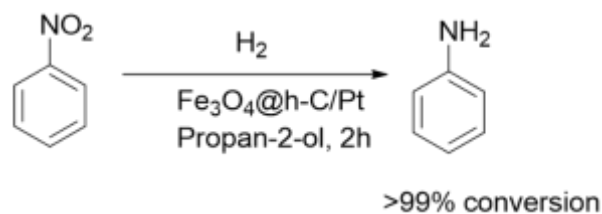
Scheme 1.10 Fe_3O_4@*h*-C/Pt catalyst for hydrogenation of nitrobenzene

Kim and co-workers [45] synthesized bimetallic Pd-Pt-Fe_3O_4 nanoparticles via hydrothermal method involving the simple one-pot co-reduction of potassium tetrachloroplatinate (II) and palladium chloride (II) in polyvinylpyrrolidone which adorned commercially available Fe_3O_4 NPs. This catalytic system catalyzed the one-pot dehydrogenation of ammonia-borane and subsequent reduction of nitroarenes to corresponding amines in methanol at room temperature within five minutes and reused up to 250 times without any loss of catalytic activity (**Scheme 1.11**). Additionally, this catalytic system showed chemoselective reduction of nitro group in presence of double bond (4-nitrostyrene) to 4-aminostyene (94 % selectivity) with 1 equivalent of ammonia-borane reagent.
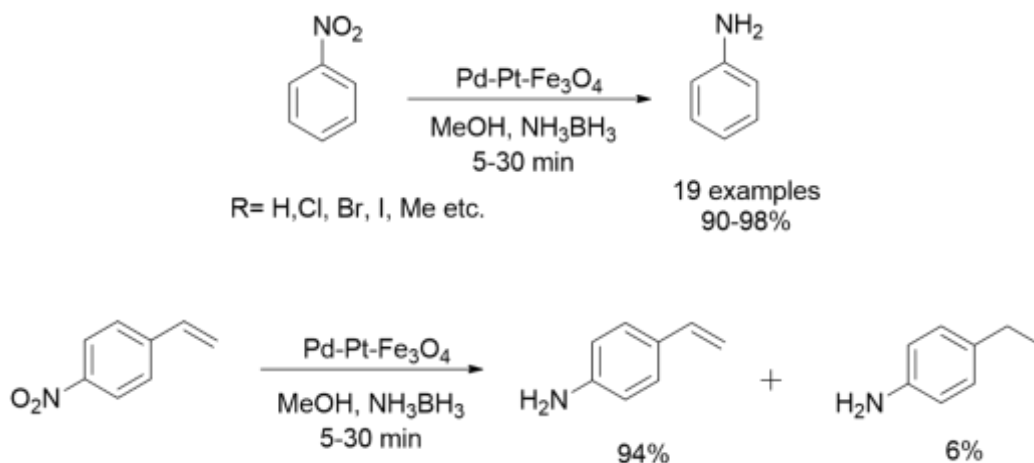
Scheme 1.11 Pd-Pt-Fe$_3$O$_4$ nanoflakes catalyzed nitroarene reduction

Akhlaghinia and co-workers **[46]** synthesized Fe$_3$O$_4$@chitin recyclable nanocatalyst via hydrothermal method. The catalyst was used for the synthesis of 5-substituted-1H-tetrazoles under solvent-free conditions using 1-butyl-3-methylimidazolium azide ([bmim][N$_3$]) ionic liquid as an azide ion source thus avoiding the highly toxic NaN$_3$ or TMSN$_3$ reagents **(Scheme 1.12)**.

R= C$_6$H$_5$, 4-BrC$_6$H$_5$, 4-CNC$_6$H$_5$ etc.

18 examples
70-98%
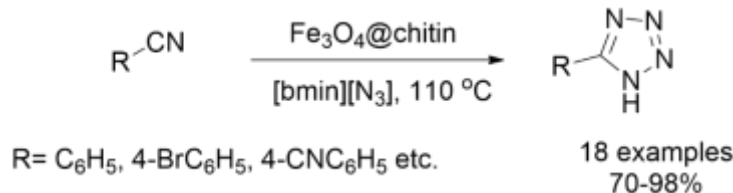
Scheme 1.12 Fe$_3$O$_4$@chitin catalyzed synthesis of 5-substituted-1H-tetrazoles under solvent free conditions

Norouzi and co-workers **[47]** described synthesis of 2,3-dihydroquinazolin-4(1H)-ones derivatives via nanoparticle-supported copper (II) (CuCl$_2$/Fe$_3$O$_4$-TEDETA) as a catalyst with a recyclability upto seven cycles without significant loss of catalytic activity **(Scheme 1.13)**.

R= Cl, CH$_3$, OCH$_3$ etc.

14 examples
95-98%
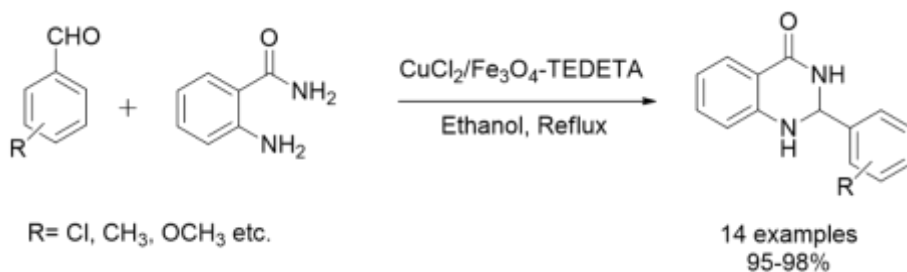
Scheme 1.13 CuCl$_2$/Fe$_3$O$_4$-TEDETA catalyzed synthesis of 2,3-dihydroquinazolin-4 (1H)-ones

Branco and co-workers **[48]** by direct addition of chlorosulfonic acid to magnetite, prepared magnetite-sulfonic acid (Nanocat-Fe-OSO₃H) nanocatalyst which was employed for a variety of important organic transformations including Strecker reaction, Ritter reaction and quinolone synthesis under solvent-free conditions with good to excellent yields **(Scheme 1.14)**.
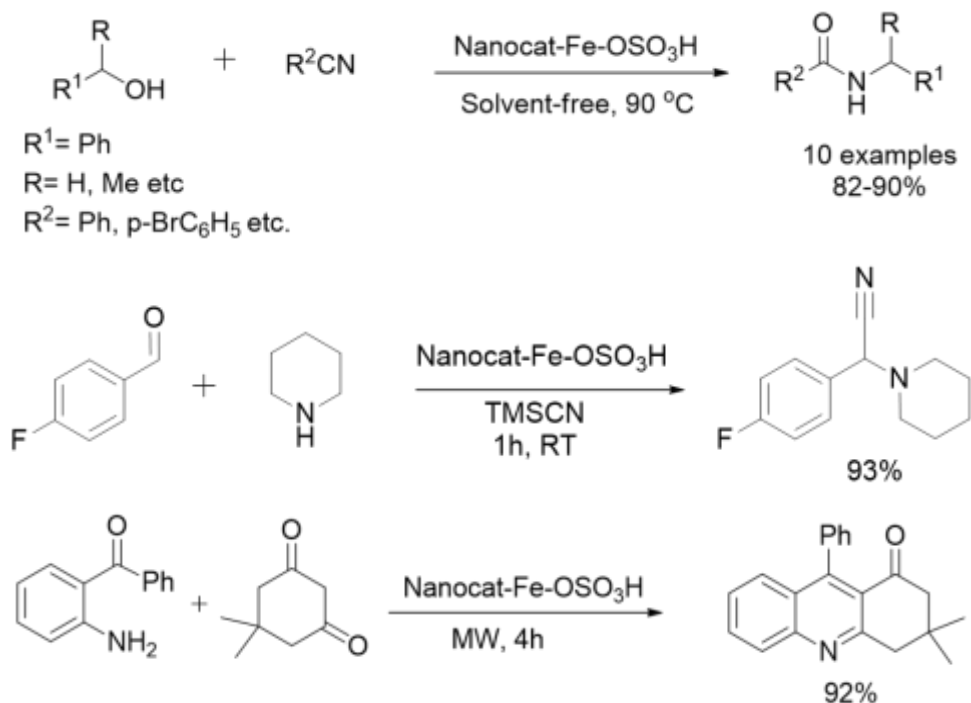
Scheme 1.14 Nanocat-Fe-OSO₃H catalyzed Ritter and multicomponent reaction under solvent - free conditions

Pramanik and co-workers **[49]**, in presence of nano magnetite Fe_3O_4–SO_3H as solid-supported acid catalyst reported one-pot condensation reaction of isatins, indane-1,3-dione and enamines under solvent-free conditions. Two different types of spiroindole fused dihydropyridine derivatives such as spiro-[indolo-3,100-indeno[1,2-b]quinolin]-2,4,110-triones and indenoquinoline-spirooxindoles products were obtained **d**epending upon the nature of *N*-substitutions of the starting isatins (N–H or N–R/Ar) **(Scheme 1.15)**.

Magnetite-supported sulfonic acid functionalized benzimidazolium based ionic liquid (IL@magnetite) was synthesized by Dadhania and co-workers **[50]**. The as-synthesized and recyclable IL@magnetite catalyst was investigated for the synthesis of 1-carbamatoalkyl-2-naphthols under solvent-free conditions in good to excellent yields **(Scheme 1.16).**
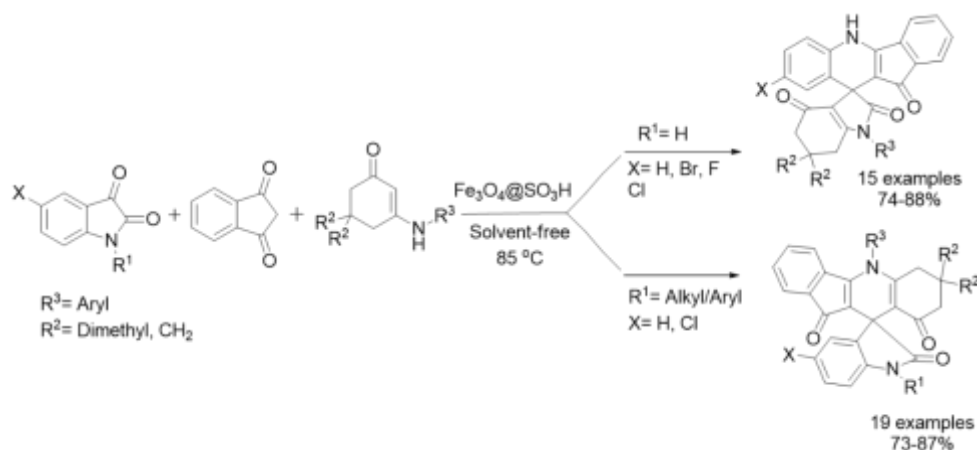
Scheme 1.15 Fe$_3$O$_4$-SO$_3$H catalyzed synthesis of spiro[indolo-3,100-indeno[1,2-b]quinolin]-2,4,110-triones (4) and indenoquinoline-spirooxindole derivatives
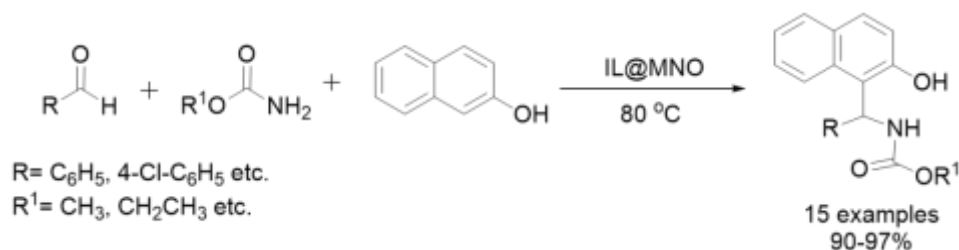
Scheme 1.16 Synthesis of 1-carbamatoalkyl-2-napthols using IL@MNP

Hosseini and co-workers **[51]** prepared a novel heterogeneous copper catalyst based on polymerization of 3-carboxymethyl-1-vinylimidazolium on the surface modified magnetic nanoparticles followed by the co-ordination of the carboxylate units in the polymer chains with copper sulfate. The polymeric nature of coating material increased the loading amount, recyclability and catalytic activity towards the one-pot synthesis of 1, 4-disubstituted 1,2,3-triazoles in water at room temperature **(Scheme 1.17)**.
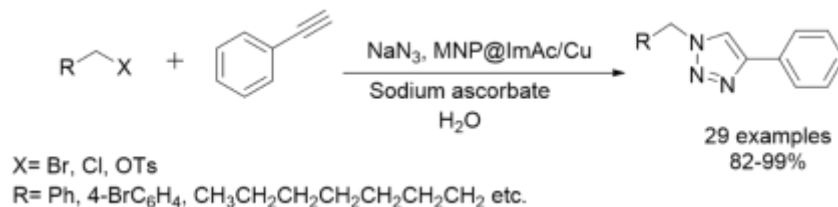
Scheme 1.17 MNP@ImAc/Cu catalyzed triazole synthesis

Maleki and co-workers **[52]** have developed an easy, convenient, inexpensive and environmental friendly synthetic approach for the preparation of polyfunctionalized pyrans and polyhydroquinolines catalyzed by Fe$_3$O$_4$@DANHA(CH$_2$)$_4$ASO$_3$H **(Scheme 1.18)**.
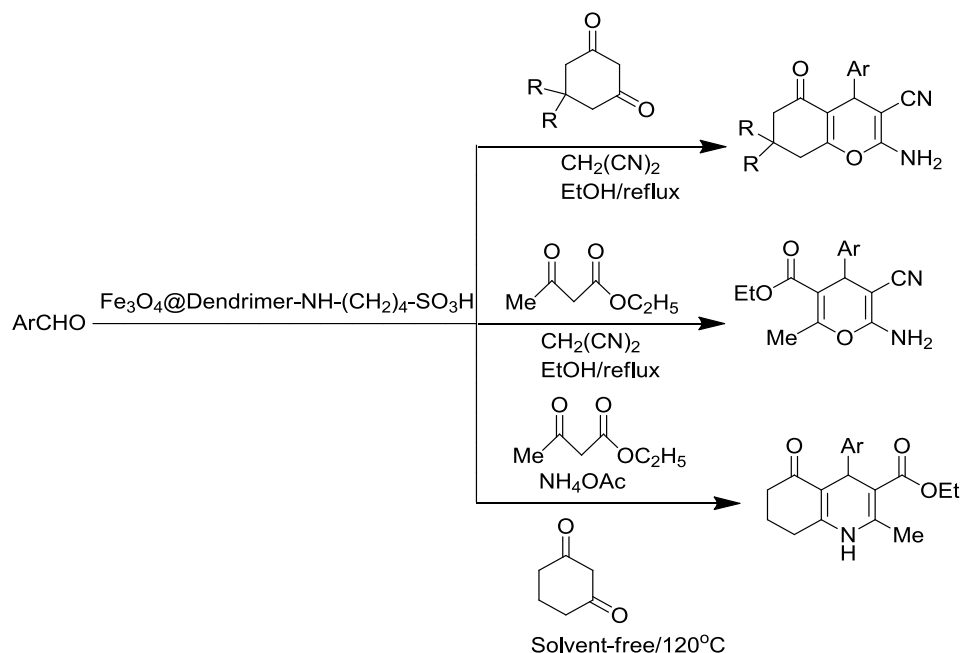
Scheme 1.18 Fe_3O_4@DANHA$(CH_2)_4$ASO$_3$H catalyzed preparation of polyfunctionalized pyrans and polyhydroquinolines

Manzoli and the group **[53]** have reported the application of a recyclable nickel silica eggshell iron-based magnetic nanoparticles (Fe_3O_4@SiO2-Ni) for the expeditious microwave-assisted reductive amination of aryl aldehydes and ketones in aqueous ammonia; several desired primary amines were produced in good-to-excellent conversions (**Scheme 1.19**)
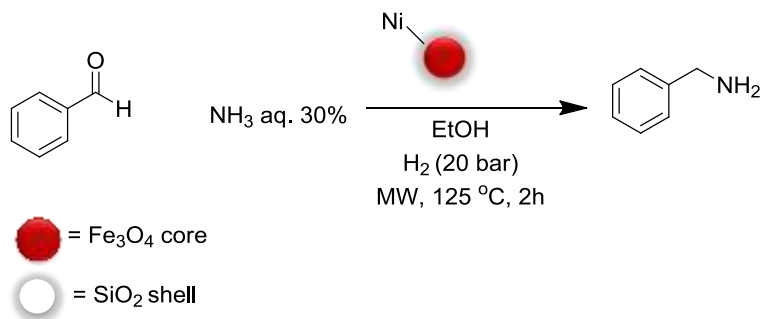
Scheme 1.19 Reductive amination of aryl aldehydes and ketones by Fe_3O_4@SiO2-Ni

Nasrollahzadeh and co-workers **[54]** reported an effective and novel magnetic catalyst composed of a Fe_3O_4 NPs core, SiO$_2$ shell and a Pd(II)- *N*- benzyl- *N*- (4- bromophenyl)- 5- amino- 1*H*- tetrazole complex. The resulting Fe_3O_4@SiO$_2$- BAT- Pd(II) nanocomplex was utilized as an effective heterogeneous catalyst for the cyanation of aryl iodides and bromides to the

corresponding aryl nitriles by using $K_4Fe(CN)_6$ as a cyanating agent under additive/ligand- free conditions (**Scheme 1.20**).

X = I & Br
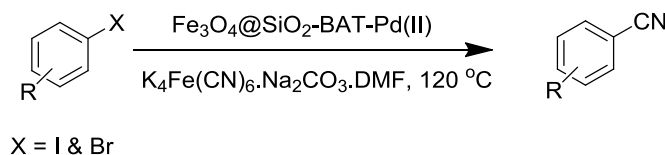
Scheme 1.20 $Fe_3O_4@SiO_2$- BAT- Pd(II) catalyzed cyanation of aryl iodides and bromides to the corresponding aryl nitriles

Ostovar and co-workers **[55]** developed a sulfathiazole- modified γ- Fe_2O_3/SiO_2 core- shell nanoarchitecture. Therefore, the catalytic performance of the prepared material was investigated in oxidation and alkylation reactions. In particular, γ- Fe_2O_3/SiO_2- STZ showed 95% of conversion and 97% of selectivity in the oxidation of benzyl alcohol to benzaldehyde, while it displayed conversion values higher than 99% in the alkylation of toluene with benzyl chloride (**Scheme 1.21**).
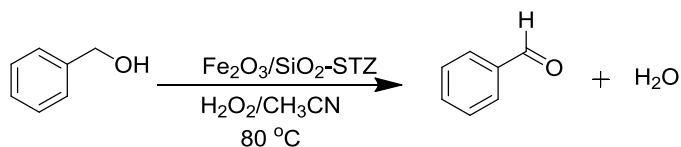
Scheme 1.21 γ- Fe_2O_3/SiO_2- STZ catalyzed oxidation of benzyl alcohol to benzaldehyde

The immobilized sulfonic acid on silica-layered magnetite was successfully synthesized and characterized by Gilanizadeh and the group **[56]**. The prepared $Fe_3O_4@SiO_2$-SO_3H MNPs were used as an efficient solid acidic nanocatalyst toward successful formylation of structurally diverse aliphatic and benzylic primary/secondary alcohols using formic acid under oil bath conditions (60 °C) (**Scheme 1.22**)
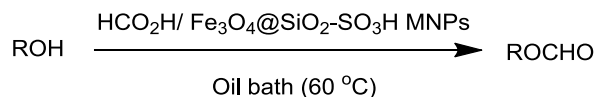
Scheme 1.22 $Fe_3O_4@SiO_2$-SO_3H MNPs catalyzed formylation of aliphatic and benzylic primary/secondary alcohols

Maleki and co-workers **[57]** report a convenient and facile method for the synthesis of $Fe_3O_4@SiO_2@$propyltriethoxysilane@o-phenylendiamine (OPSF) as a super paramagnetic heterogeneous nanocatalyst. Then, it was characterized and applied in a multicomponent one-pot synthesis of 2-amino-4H-chromes 4a–o via the condensation of dimedone, aromatic aldehydes and malononitrile **(Scheme 1.23)**.
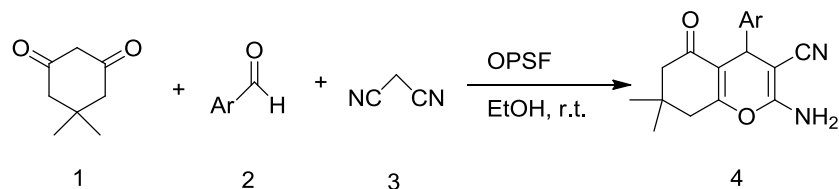
Scheme 1.23 $Fe_3O_4@SiO_2@$propyltriethoxysilane@o-phenylendiamine catalysed synthesis of 2-amino-4H-chromes.

Azizi and coworkers **[58]** prepared $Fe_3O_4@SiO_2@$GMSI-VB1 catalyst by modifying thiamine (VB1) with (3-glycidyloxypropyl)trimethoxysilane (GMSI) moiety and grafted onto magnetic nanoparticles and applied as a magnetically retrievable catalyst for an efficient and environmental friendly synthesis of 2,3-dihydroquinazolin-4(1H)-ones in aqueous media **(Scheme 1.24)**.
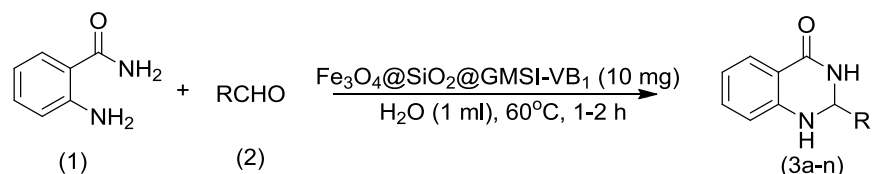
Scheme 1.24 $Fe_3O_4@SiO_2@$GMSI-VB1 catalysed synthesis of 2,3-dihydroquinazolin-4(1H)-ones in aqueous media.

Rahimzadeh and coworkers **[59]** prepared a novel imidazole ionic liquid (IL)-functionalized silica@γ-Fe_2O_3 (IL-$SiO_2@$MNP) by functionalizing $SiO_2@$MNP with 1-butyl-3-(3-trimethoxypropyl)-1H-imidazol-3-ium chloride as the IL moiety. IL-$SiO_2@$MNP showed good activity in the synthesis of 6H-chromeno[4,3-b]quinolin-6-one derivatives via multicomponent reaction of 4-hydroxycoumarin, anilines and benzaldehydes **(Scheme 1.25)**.
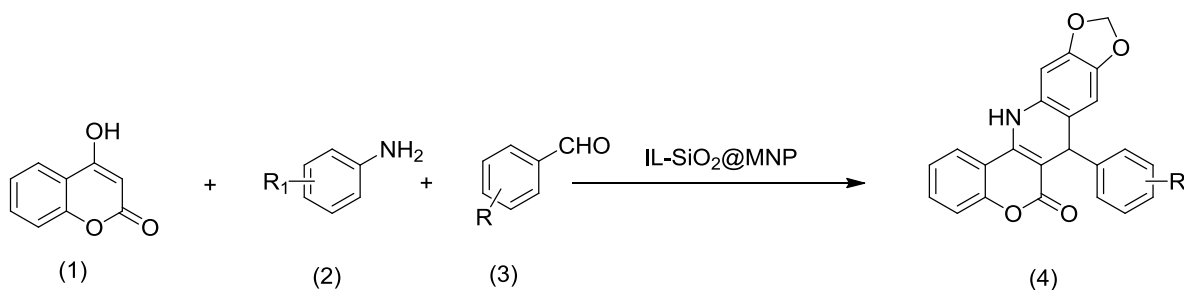
Scheme 1.25 (IL)-functionalized silica@γ-Fe$_2$O$_3$ (IL-SiO$_2$@MNP) catalysed synthesis of 6H-chromeno[4,3-b]quinolin-6-one derivatives.

Elhamifar and coworkers **[60]** reported a novel magnetic iron oxide nanoparticle supported phenyl sulfonic acid (Fe$_3$O$_4$@Ph-SO$_3$H), characterized and applied as effective nanocatalyst in synthesis of biologically active and chemically useful tetrahydrobenzo[b]pyrans **(Scheme 1.26)**.
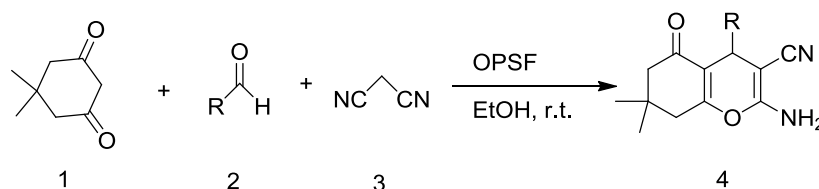
Scheme 1.26 Fe$_3$O$_4$@Ph-SO$_3$H catalysed synthesis of tetrahydrobenzo[b]pyrans.

Mousavifar and coworkers **[61]** reported a Fe$_3$O$_4$@PS@His[HSO$_4^-$] by converting the imidazole group of prepared Fe$_3$O$_4$@Propylsilane@Histidine MNPs to imidazolium hydrogen sulfate and applied as effective support for one-pot synthesis of 9-aryl-1,8-dioxooctahydroxanthenes and spiro[indoline-3,9'-xanthene]triones derivatives.

Nikoorazm and coworkers **[62]** synthesized a novel and reusable nanocatalyst by anchoring a nickel Schiff base complex onto Fe$_3$O$_4$@MCM-41 (Fe$_3$O$_4$@MCM-41@Ni-P2C). This catalytic system was efficiently used for oxidation of sulfides to sulfoxides and oxidative coupling of thiols to corresponding disulfides using H$_2$O$_2$ as green oxidant at room temperature **(Scheme 1.27)**.
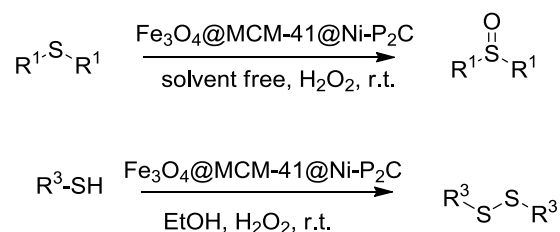
Scheme 1.27 Fe$_3$O$_4$@MCM-41@Ni-P2C catalyzed oxidation of sulfides to sulfoxides and oxidative coupling of thiols into disulfides using H$_2$O$_2$.

Nano-magnetite-supported catalysts are emerging and versatile reagents in the heterogeneous catalysis domain for the development of sustainable protocols. Recently MNPs have found remarkable niche in diverse areas ranging from magnetic resonance imaging, magnetic targeting drug delivery to chemical catalysis, they increasingly serve as catalyst supports or are incorporated in the hybrid nano composite as sustainable catalyst for convenient separation and recycling. Bare MNPs due to their inherent instability and hydrophobic nature results in big clusters over time in the absence of any surface coating which reduces their surface energy. Therefore it needs to be minimized by surface immobilization of MNPs with biocompatible and organic and inorganic materials which protects them from being oxidized and provides them stability against damage during or after being used in organic transformations. However most of the techniques require several steps to introduce functional groups to the magnetic surface and often involve the use of organosilica precursors as an organic shell to prepare a suitable support for incorporation of different transition metal ions. Therefore, the preparation of modified MNPs *via* simple method and without using organoalkoxysiloxane compounds is highly desirable from both an environmental and economic point of view. The most important aspect in magnetic catalysis is the design and synthesis of a catalyst for specific organic reaction, considering the mechanistic pathway and the feasibility to perform such reactions on a laboratory scale with potential for industrial applications. In this respect, to improve the properties of magnetic nanoparticles derived catalysts there is still demand for synthesis of highly water-dispersible magnetic nanoparticles, end-functionalized with non-toxic, biodegradable materials like citric acid, amino acids, L-DOPA etc. having amino and carboxyl groups as these are the most attractive functional groups, which are especially suitable for the immobilization of transition metal ions.

Present thesis describe the synthesis of magnetite nanoparticle functionalize with various biocompatible moieties with further immobilisation of transition metal ions over them and their applications in different organic transformations.

1.5 The Scope of the Work

Sustainable and economical synthetic methodologies are highly desired requisites of the modern chemical industries. The searches for the new, improved and economic catalysts are the prime requirements in the present scenario. Finding further applications of the magnetic nanocatalyst

and search for cost-effective alternative developing reaction methodologies to work economically and with high efficiency are the critical goals of this research. Development of new and active catalysts can be used for industrial applications is the motivation for this study. In the preparation of magnetic nanoparticle-supported catalysts; significant progress has been made in the development of functionalized magnetic nanocatalyst which provides identical or better reactivity than the corresponding homogenous catalysts.

The present thesis describes a straight forward and more efficient methodology for efficient synthesis of the Schiff's bases, reduction of nitroarenes, an array of multicomponent reaction catalyzed by recyclable magnetic nanocatalyst under ultrasonication and microwave irradiation. The detail investigations and results are presented in the subsequent chapters.

1.6 References

[1] Chorkendorff, I.; Niemantsverdriet, J. W. *WILEY-VCH Verlag GmbH & Co. KGaA: Weinheim,* **2007**.

[2] Hemalatha, K.; Madhumitha, G.; A. Kajbafvala, N. Anupama, R. Sompalle, S. Mohana Roopan, *J. Nanomater.* **2013**, *2013*, 23.

[3] Anastas, P. T.; Warner, J. C. *Oxford University Press: New York*, **1998**.

[4] Patai, S. *Wiley-Interscience: New York,* **1966**.

[5] Berzelius, J. J. *Årsberättelsen Om Framsteg I Fysik Och Kemi*. Royal Swedish Academy of Sciences: **1835**.

[6] Robertson, A. J. B. *Platin. Met. Rev.* **1975,** *19*, 64.

[7] Green, S. *Macmillan Company: New York*, **1928**.

[8] Berzelius, J. J.; *Reseanteckningar*. P. A. Norstedt & Söne: Stockholm, **1903**.

[9] Van Houten, J. *J. Chem. Educ.* **2002**, *79*, 21.

[10] Santen, R. V. *Wiley-VCH Verlag: Weinheim* **2012**.

[11] Koshland Jr., D. E. *Angew. Chem. Int. Ed.* **1995**, *33*, 2375.

[12] a) Cole-Hamilton, D. J. *Science* **2003**, *299*, 1702; b) Baker, R. T.; Tumas, W. *Science* **1999**, *284*, 1477.

[13] a) Coperet, C.; Chabanas, M.; Saint-Arroman, R. P.; Basset, J. M. *Angew. Chem., Int. Ed.* **2003**, *42*, 156; b) Basset, J. M.; Choplin, A. *J. Mol. Catal.* **1993**, *21*, 95; (c) Mizuno, N.; Misono, M. *Chem. Rev.* **1998**, *98*, 199; d) Lefebvre, F.; Basset, J. M. *J. Mol. Catal.*, *A. Chem.*, **1999**, *146*, 3.

[14] a) Polshettiwar, V.; Len, C.; Fihri, A.; *Coord. Chem. Rev.* **2009**, *253*, 2599; b) V. Polshettiwar and A. Molnar, *Tetrahedron* **2007**, *63*, 6949.

[17] Gawande, M. B.; Luque, R.; Zboril, R. *ChemCatChem* **2014**, *6*, 3312.

[18] Sonavane, S. U.; Gawande, M. B.; Deshpande, S. S.; Venkataraman, A.; Jayaram, R. V. *Catal. Commun.* **2007**, *8*, 1803.

[19] Xu, L.; Ma, Y.; Zhang, Y.; Jiang, Z.; Huang, W. *J. Am. Chem. Soc.* **2009**, *131*, 16366.

[20] Anand, N.; Reddy, K. H. P.; Satyanarayana, T.; Rao, K. S. R.; Burri, D. R. *Catal. Sci. Technol.* **2012**, *2*, 570.

[21] Khoudiakov, M.; Gupta, M. C.; Deevi, S. *Appl. Catal. A* **2005**, *291*,151.

[22] Rostamizadeh, S.; Shadjou, N.; Azad, M.; Jalali, N. *Catal. Commun.* **2012**, *26*, 218.

[23] Carraro, G.; Barreca, D.; Comini, E.; Gasparotto, A.; Maccato, C.; Sada, C.; Sberveglieri, G. *Cryst. EngComm.* **2012**, *14*, 6469.

[24] Rosario-Amorin, D.; Gaboyard, M.; Clerac, R.; Vellutini, L.; Nlate, S.; Heuze, K. *Chem.–Eur. J.* **2012**, *18*, 3305.

[25] Cornell, R. M.; Schwertmann, U. *Wiley-VCH Verlag GmbH & Co. KGaA*, **2004.**

[26] Cornell, R. M.; Schwertmann, U. *Wiley-VCH Verlag GmbH & Co. KGaA*, **2004.**

[27] Yang, C.; Wu, J. J.; Hou, Y. L. *Chem. Commun.* **2011**, *47*, 5130.

[28] Schwertmann, U.; Cornell, R. M. *Wiley-VCH Verlag GmbH*, **2007.**

[29] (a) Ranganath, K. V. S.; Glorius, F. *Catal. Sci. Technol.* **2011**, *1*, 13; (b) Polshettiwar, V.; Luque, R.; Fihri, A.; Zhu, H. B.; Bouhrara, M.; Bassett, J. M. *Chem. Rev.* **2011**, *111*, 3036.

[30] Nasr-Esfahani, M.; Rafiee, Z.; Montazerozohori, M.; Kashi, H. *RSC Adv.* **2016**, *6*, 47298.

[31] Gawande, M. B.; Branco, P. S.; Varma, R. S. *Chem, Soc. Rev.* **2013**, *42*, 3371.

[32] Shelke, S. N.; Bankar, S. R.; Mhaske, G. R.; Kadam, S. S.; Murade, D. K.; Bhorkade, S. B.; Rathi, A. K.; Bundaleski, N.; Orlando, M. N. D.; Zboril, T. R.; Varma, R. S.; Gawande, M. B. *ACS Sustainable Chem and Eng.* **2014**, *2*, 1699.

[33] Wang, Z.; Yu, Y.; Zhang, Y. X.; Li, S. Z.; Qian, H.; Lin, Z. Y. *Green Chem.* **2015**, *17*, 413.

[34] Yang, H.; Shi, D.; Ji, S.-F.; Zhang, D.-N.; Liu, X.-F. *Chin. Chem. Lett.* **2014**, *25*, 1265.

[35] Baig, R. B. N.; Leazer, J.; Varma, R. S. *Clean Technol. Environ. Policy* **2015**, *17*, 2073.

[36] Sa, S.; Gawande, M. B.; Velhinho, A.; Veiga, J. P.; Bundaleski, N.; Trigueiro, J.; Tolstogouzov, A.; Teodoro, O. M. N. D.; Zboril, R.; Varma, R. S.; Branco, P. S. *Green Chem.* **2014**, *16*, 3494.

[37] Nasir Baig, R. B.; Varma, R. S. *Ind. Eng. Chem. Res.* **2014**, *53*, 18625.

[38] Gensch, T.; Hopkinson, M. N.; Glorius, F.; Wencel-Delord, J. *Chem. Soc. Rev.* **2016**, *45* (10), 2900.

[39] McNally, A.; Haffemayer, B.; Collins, B. S. L.; Gaunt, M. J. *Nature* **2014**, *510*, 129.

[40] Sharma, R. K.; Dutta, S.; Sharma, S. *Dalton Trans.* **2015**, *44*, 1303.

[41] Wang, S.; Zhang, Z.; Liu, B. *ACS Sustainable Chem. Eng.* **2015**, *3*, 406.

[42] Shaikh, M.; Sahu, M.; Gavel, P. K.; Ranganath, K. V. S. *Catal. Commun.* **2015**, *64*, 18.

[43] Saikia, M.; Bhuyan, D.; Saikia, L. *New J. Chem.* **2015**, *39*, 64.

[44] Sun, Q.; Guo, C.-Z.; Wang, G.-H.; Li, W.-C.; Bongard, H.-J.; Lu, A.-H. *Chem. Eur. J.* **2013**, *19*, 6217.

[45] Byun, S.; Song, Y.; Kim, B. M. *ACS Appl. Mater. Interfaces* **2016**, *8*, 14637.

[46] Zarghani, M.; Akhlaghinia, B. *RSC Adv.* **2016**, *6*, 31850.

[47] Ghorbani-Choghamarani, A.; Norouzi, M. *J. Mol. Catal. A: Chem.* **2014**, *395*, 172.

[48] Gawande, M. B.; Rathi, A. K.; Nogueira, I. D.; Varma, R. S.; Branco, P. S. *Green Chem.* **2013**, *15*, 1895.

[49] **D**ebnath, K.; Singha, K.; Pramanik, A. *RSC Adv.* **2015**, *5*, 31866.

[50] Dadhania, H. N.; Raval, D. K.; Dadhania, A. N. *Catal. Sci. Technol.* **2015**, *5*, 4806.

[51]

[52] Maleki, B.; Reiser, O.; Esmaeilnezhad, E.; Choi, H. J. *Polyhedron* **2019**, *162*, 129.

[53]   Manzoli, M.; Gaudino, E. C.; Cravotto, G.; Tabasso, S.; Baig, R. B. N.; Colacino, E.; Varma, R. S. *ACS Sustainable Chem. Eng.* **2019**, *7* (6), 5963.

[54]   Nasrollahzadeh, M.; Maryami, M.; Sajjadi, M.; Mehdipour, E. *Appl. Organomet. Chem.* **2019**, *33* (5), e4730.

[55]   Ostovar; Rodríguez, P.; Saberi; Balu; Luque. *Catalysts* **2019**, *9* (4), 348.

[56]   Gilanizadeh, M.; Zeynizadeh, B.; Gholamiyan, E. *Iranian J. Sci. Technol. A: Science* **2018**, *43* (3), 819.

[57] Maleki, A.; Ghalavand, R.; Firouzi Haji, R. *Appl. Organomet. Chem.* **2018**, *32*, 3916.

[58] Azizi, N.; Abbasi, F.; Abdoli-Senejani, M. *Mater. Chem. Phys.* **2017,** *196*, 118.

[59] Rahimzadeh, G., Bahadorikhalili, S., Kianmehr, E., Mahdavi, M. *Mol. Divers*. **2017**, *21*, 597.

[60] Elhamifar, D.; Ramazani, Z.; Norouzi, M.; Mirbagheri, R. *J. Colloid Interface Sci.* **2018**, *511*, 392.

[61] Mousavifar, S. M.; Kefayati, H.; Shariati, S., *Appl. Organomet. Chem.* **2018,** *32* (4), 4242.

[62] Nikoorazm, M.; Ghorbani, F.; Ghorbani-Choghamarani, A.; Erfani, Z. *Phosphorus, Sulfur, and Silicon and the Related Elements* **2018,** *193* (9), 552.

Chapter - 2

Preparation of a simple biocompatible magnetite@citric acid: An

efficient reusable solid acid catalyst for the rapid synthesis of antipyrine

Schiff's bases and study of their radical scavenging potential
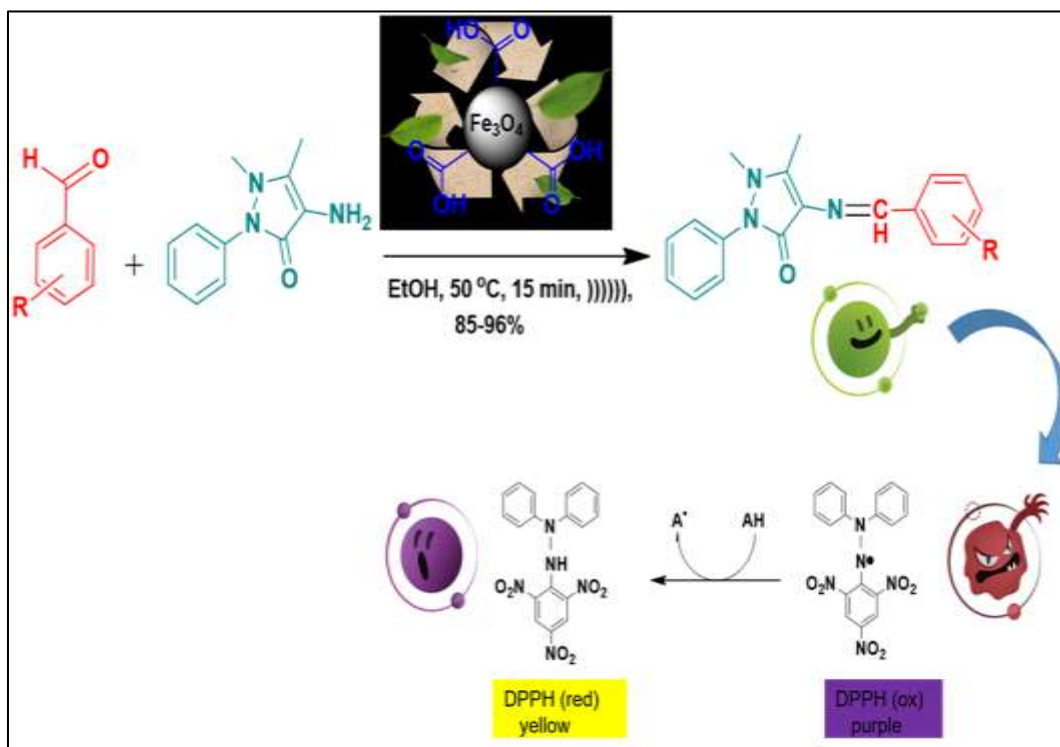
2.1 Introduction

Nanotechnology is one of the most versatile areas of current research and wide range applications. Their unique properties arise from particularly their high surface to volume ratio [1-3]. Various methods have been reported for their synthesis, among them the biological methods, plant-mediated synthesis of nanoparticles are more attractive because of its simplicity, easy availability and stability of the resulting products [4-14]. Now a days they have attracted great deal of attention due to catalytic application such as synthesis of spirooxindoles [15], carbonitriles [16], 4-H chromenes [17-18], decahydroacridine 1,8 diones [19], oxidation of sulfides to sulfoxides [20], synthesis of propargylamines [21], quinoxaline [22] etc.

Nanoparticles fill the gap between homogeneous and heterogeneous catalysis, but recovery by normal filtration technique limits their widespread utility which results in their loss disturbing the economics and sustainability of these nano-catalytic protocols [23]. In recent decades magnetic nanoparticles (MNPs) have gained popularity due to their ease of preparation and surface functionalization, facile separation *via* magnetic force as well as low toxicity and price [24]. Bare MNPs due to their inherent instability and hydrophobic nature results in big clusters over time in the absence of any surface coating which reduces their surface energy [25]. Therefore it needs to be minimized by surface immobilisation of MNPs with biocompatible organic and inorganic materials which protects them from being oxidised and provides them stability against damage during or after being used in organic transformations [26-27]. Surface functionalization of MNPs with PO_4^{3-}, sulphate and carboxylate are attractive surface modifications which can be easily accomplished. It is observed that carboxylate binding to MNPs is the strongest preventing leaching out during reaction, as well as protecting the bare NP's against damage hence it can be used undoubtedly in catalysis with good stability [28].

Schiff bases are some of the most widely used organic compounds. They are used as pigments & dyes [29], catalysts [30], intermediates in organic synthesis [31] and a polymer stabilizers [32]. Recently they have been utilised for optical recording technology [33], as electrical conductor [34], electrode materials [35] and micro-electronic equipment [36], organic batteries or electrochromic display devices [37]. The Schiff's base of 4-aminoantipyrine are considered to be pyrazolone derivatives and are reported to demonstrate biological, clinical, pharmacological and analytical applications [38]. Synthesis of Schiff's base is often carried out with or without acid catalyzed by various previously reported synthetic methods like microwave assisted [39],

irradiation by UV **[40]**, ultrasonication **[41]** etc. The main drawback of these reported methods is the utilisation of large amount of solvent and longer reaction time. Therefore there is need to vary or modify the conventional methods which are not eco-friendly and less efficient. Separation of the catalyst and final product from the reaction mixture is one of the most vital aspects of synthetic protocols. Catalytic recovery by filtration is relatively inefficient. Another technique, extractive isolation of products also requires excessive amount of organic solvents. The development of versatile and efficient procedures for the preparation of these types of compounds by using a new catalyst and active ongoing research area, and there will be a scope for further improvement towards lower reaction times, improved yields and milder reaction conditions. In view of this MNP@CA has been prepared by the adsorption of citric acid on the surface of magnetite nanoparticles by co-ordinating whereby one or two of the carboxylate functionality co-ordinate depending upon steric necessity and the curvature of surface **[42]**. The catalytic property of MNP@CA for the activation of carbonyl group of aromatic aldehyde to obtain the desired compounds (3a-k) was successfully explored. Due to trouble free ease of separation using an external magnet, this method provides a rapid and effective way to synthesise Schiff's bases along with the added advantage of reusability and recyclability up to 8 runs without any significant loss of yield. In addition all the compounds were screened for radical scavenging potential by DPPH method taking ascorbic acid as standard. Indeed, to the best of our knowledge this is the first report of hassle free synthesis of bio-important antipyrine Schiff's bases using MNP@CA. Antioxidants are molecules, which can safely interact with free radicals and terminate the chain reaction before vital molecules are damaged. Free radicals are major factors leading to more than sixty different health problems including ageing, cancer and atherosclerosis etc. Addition of hydrogen would remove the odd electron feature which is responsible for radical reactivity. The different synthesized compounds 3a-k showed good antioxidant activity taking ascorbic acid as standard in DPPH free radicals scavenging, which indicates that the compounds have potential to prevent free radical mediated oxidative damage.

2.2 Results and Discussion

2.2.1 Characterization of magnetite@citric acid

Figure 2.1 gives a pictorial depiction for the synthesis of magnetic nanoparticles decorated by citric acid. The magnetite nanoparticles were synthesized by chemical co-precipitation method

similar to previously reported method with slight modification **[43]**. Detail description has been provided in experimental section. After that in order to improve the chemical stability, surface modification was performed by immobilisation of citric acid on its surface **[44-45].** Prepared catalyst (MNP@CA) was then characterized by using various microscopic and spectroscopic techniques such as FESEM, FTIR, XRD, HRTEM and TGA.
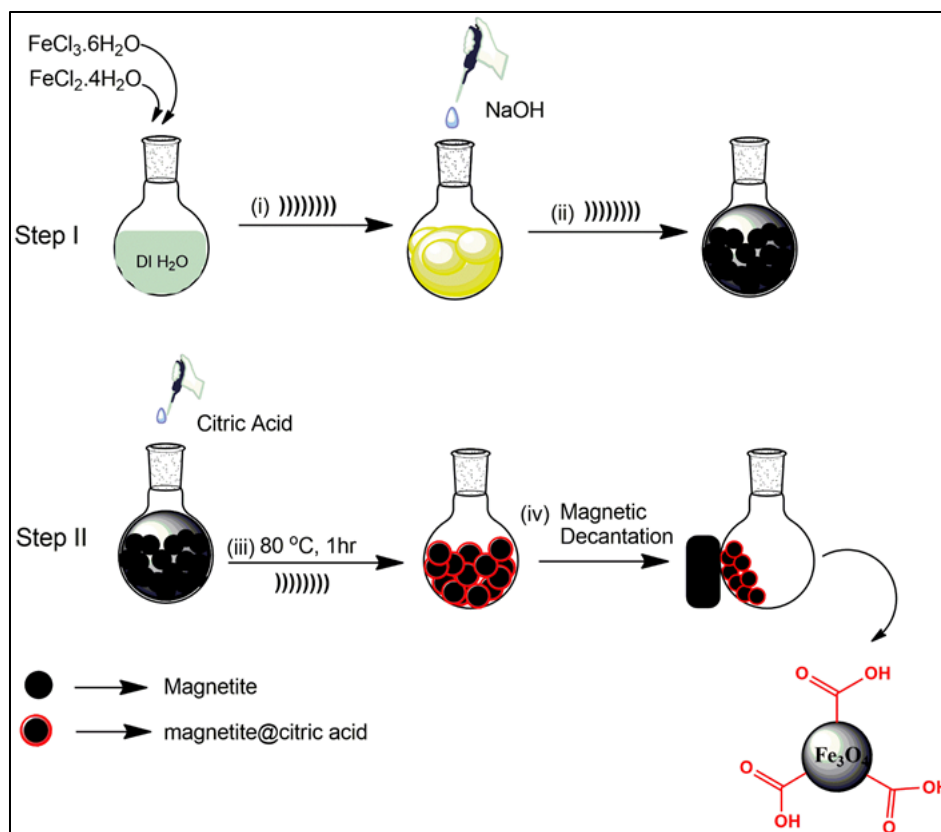
Figure 2.1 Pictorial depiction for the preparation of magnetite@citric acid nanoparticles (MNP@CA)

A comparative study of FTIR spectrum of magnetite, citric acid, magnetite@citric acid was done to validate the immobilisation of citric acid on magnetite. In the IR spectrum of magnetite the characteristic Fe–O stretching peak initially comes at 573.71 cm^{-1} **(Figure 2.2 (a))** shifted to 583 cm^{-1} after grafting of citric acid on the surface of magnetite as shown in **Figure 2.2 (c)**. The FTIR spectrum of pure citric acid **(Figure 2.2 (b))** shows that peaks are well resolved and broaden when CA gets attached to Fe_3O_4. An intense band at 1753 cm^{-1} **Figure 2.2 (b)** indicates the presence of stretching vibration of C=O group of carboxylic acid of the citric acid, which shifted to a band at about 1627 cm^{-1} for MNP-CA as showed in graph **(c)** of **Figure 2.2**,

displaying that the citric acid ions gets attached to the surface of magnetite by carboxylate groups forming ester bond with the –OH group present on the surface of magnetite. In **Figure 2.2 (b)** peak around 3300 cm^{-1} show the non-dissociated symmetric vibration of –OH group of citric acid. The bending vibration peak due to –OH group present on the surface of magnetite comes at 1648 cm^{-1} **(Figure 2.2 (a))**. Very small peaks at 2910 cm^{-1} and 2862 cm^{-1} is due to coupled vibration of $>CH_2$ of citric acid **[23]**. Hence it can be said that immobilisation of the citric acid on the surface of magnetite has been done successfully by carboxylate **[24]**.
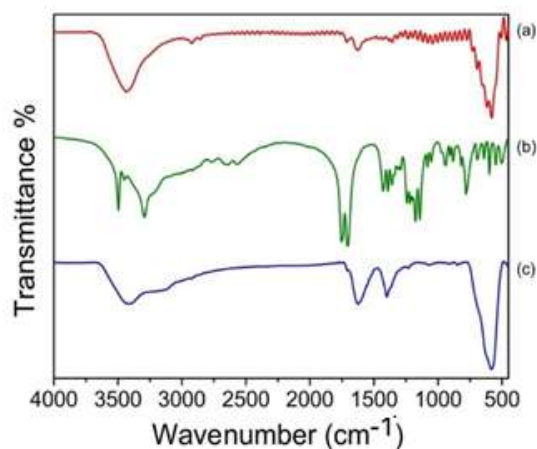
Figure 2.2 FT-IR spectrum of (a) magnetite, (b) neat citric acid and (c) magnetite@citric acid

The materials were characterized by using X-ray diffraction. Crystallite size of MNP@CA was estimated using Debye scherrer's equation $n\lambda/\beta\cos\theta$. Maximum intensity peak (311) was used to estimate the average crystallite size and it is found to be 14 nm. The investigation of the structure of prepared nanoparticles by powdered XRD diffraction pattern has also been carried out. It is clear that no impurity peaks appear but the sample has polycrystalline pattern with face centered cubic structure. Almost the same characteristic peaks of the magnetite and MNP@CA were obtained in **Figure 2.3 (a)** and **(b)** indicating that morphology and crystalline cubic spinel structure has been also preserved during immobilization. The XRD pattern of MNP@CA and magnetite have similar diffraction peaks at around 30.4, 35.8, 43.5, 53.8, 57.3 and 63.0 corresponds to the (220), (311), (400), (422), (511), (440) reflections respectively which coincides with JCPD 00-001-1111 standard. As shown in **Figure 2.4** SEM images of magnetite@citric acid revealed that the nanocatalyst was almost spherical in shape.
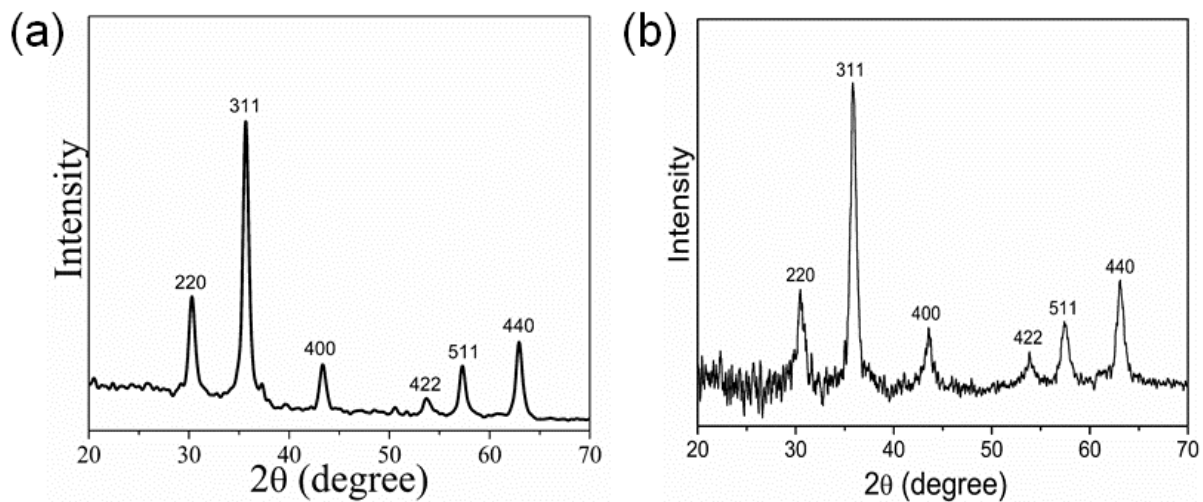
Figure 2.3 XRD of (a) magnetite (b) magnetite@citric acid
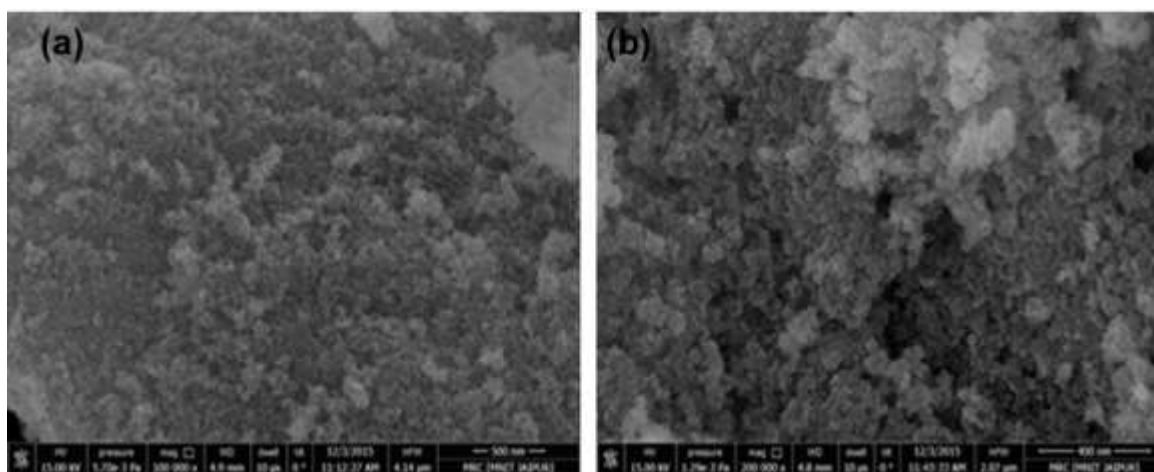
Figure 2.4 SEM images of (a) magnetite (b) magnetite@citric acid
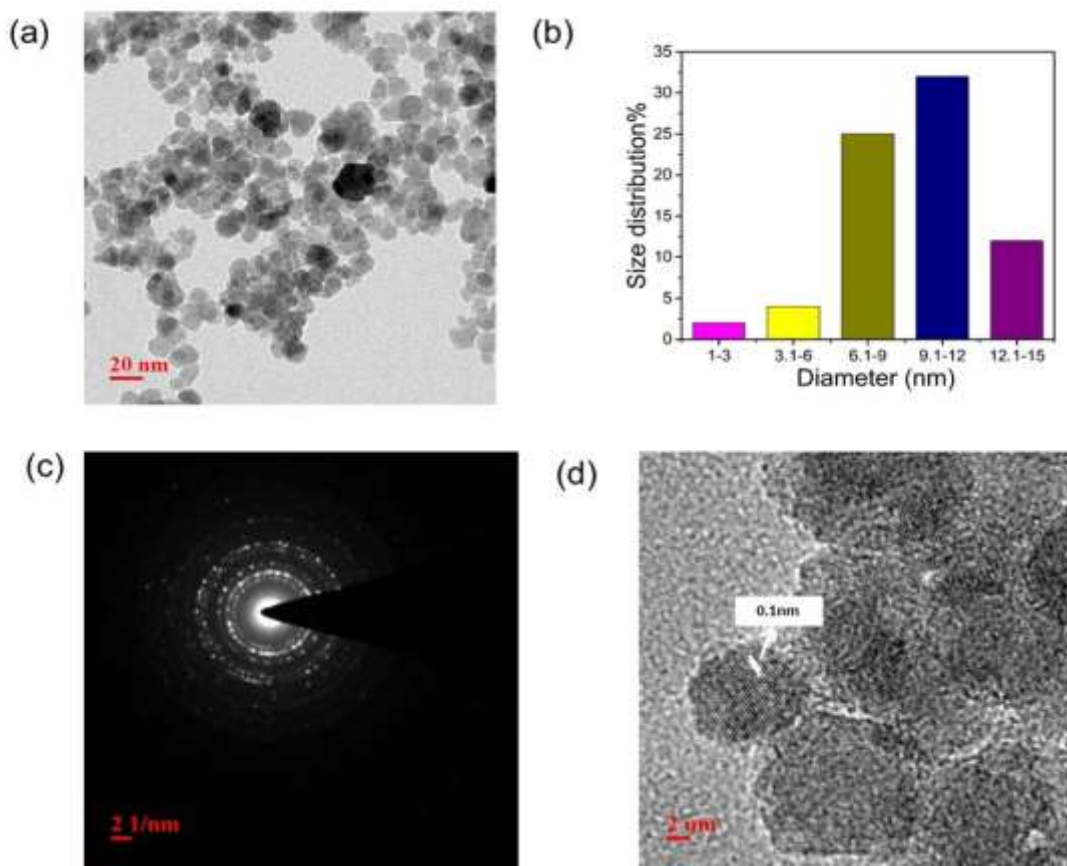
Figure 2.5 (a) Low magnification TEM image of the magnetite@citric acid, (b) Histogram showing size distribution of magnetite@citric acid nanoparticles, (c) SAED pattern of the corresponding low magnification TEM image, (d) HRTEM image showing the interlayer planes.

Figure 2.5 (a) depicts the low magnification TEM image of the magnetite@citric acid nanoparticles showing that the particles are almost spherical in shape while the histogram **Figure 2.5 (b)** shows that the size ranges from 2-15 nm with dominant particles in the range of size 9-12 nm. The high resolution TEM image of the nanoparticles **(Figure 2.5 (d))** shows the estimated interlayer gap is 0.1 nm. Thermal gravimetric analysis (TGA) of magnetite@citric acid was performed within the range of 25-900˚C under an inert atmosphere of nitrogen. As shown in **Figure 2.6 (a)**, 3.5% weight loss of bare magnetite was observed due to degradation of hydroxyl group on the surface of magnetite. In **Figure 2.6 (b)** major weight loss at high temperature was observed which confirms that citric acid is chemically bound to the magnetic nanoparticles. It implies that the immobilization loading of citric acid in the optimal catalyst was 18.5 %. It implies that thermal stability of synthesized magnetite@citric acid catalyst is maintained at

higher temperature.
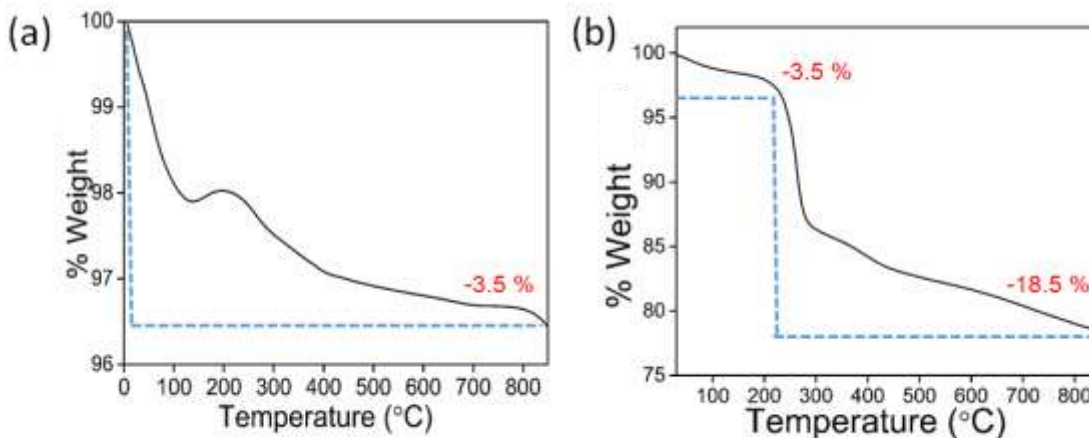
Figure 2.6 TGA curve of (a) magnetite (b) magnetite@citric acid

2.2.2 Optimization Studies

After characterization, catalytic activity of the magnetite@citric acid was assessed for synthesis of Schiff's base. As shown in **Table 2.1**, initially a trial reaction has been carried out using benzaldehyde (1 mmol), 4-aminoantipyrine (1 mmol) under ultrasonication at 50°C with and without catalyst. When the reaction was performed in the absence of catalyst, the yield obtained was in traces (**Table 2.1**, **Entries 1 and 2**). Further when the reaction was carried out by using 0.15 mol% of the catalyst under the same conditions, product was obtained with improved yield. Increased yield with MNP@CA may be attributed firstly due to the activation of carbonyl group of benzaldehyde through acidic proton of the carboxylic group of citric acid immobilised on magnetite and secondly due to the availability of enhanced surface area. The plausible mechanism for the reaction is given in the **Scheme 2.1**. Owing to the improved yield, the model reaction was performed using different mol% of the catalyst i.e. 0.25, 0.50, 0.65, 0.80 at different temperatures by varying the reaction time. Interestingly yield was increased up to 95% when 0.65 mol% of the catalyst was used (**Table 2.1, Entry 13, 14, 15**). With further increase of the catalyst to 0.80 mol%, efficiency did not change significantly. We have also studied individual effect of various reaction parameters as solvent standardization, catalyst loading and effect of temperature variation on %yield and the results proved that 0.65 mol% of catalyst, ethanol solvent and 80 ℃ of temperature are the best optimized condition for the reaction (**Figure 2.7 (a-c)**)

31

TABLE 2.1 Optimization for the synthesis of (E)-4-(benzylideneamino)-1,5-dimethyl-2-phenyl-1,2-dihydro-3H-pyrazol-3-one under various reaction conditions[a]

S. No.	Catalyst (mol%)	Time (min.)	Temperature (°C)	Yield (%)[b]
1	No catalyst	15	50	28
2	No catalyst	120	50	42
3	No catalyst	120	80	44
4	0.25	15	50	58
5	0.25	30	50	64
6	0.25	60	50	64
7	0.25	60	80	65
8	0.45	15	50	66
9	0.45	30	50	68
10	0.45	60	50	70
11	0.45	60	80	72
12	0.65	15	50	90
13	0.65	30	50	92
14	0.65	60	50	94
15	0.65	15	80	95
16	0.80	15	50	92
17	0.80	30	80	94
18	0.80	60	80	94

[a]Reaction conditions: benzaldehyde (1mmol), 4-amino antipyrine (1mmol), solvent-ethanol (2mL), 80°C, ultrasonicated in open air [b]Isolated yield   Without catalyst (**Entry 1-3**), WithMNP@CA (**Entry 4-18**)

With the optimal conditions in hand (**Table 2.1, Entry 15**), we next studied the substrate scope of this reaction by screening the different aromatic benzaldehydes. A variety of different substituted aromatic aldehydes possessing electron withdrawing and electron donating groups gave good yield (86-96%). Several aromatic aldehydes containing electron releasing substituents, electron withdrawing substituents and halogens on their aromatic ring were utilized in the

reaction and the corresponding products was obtained with high yields and in shorter reaction times. As evident from **Table 2.2**, ease of the reaction is directly related to the substituent on benzene ring. The electron withdrawing groups (such as nitro, cyano, halo) were found to activate the aldehydes towards nucleophilic attack and increases the reaction rate (**Entry 3f, 3g, 3h, 3i**).

TABLE 2.2 Synthesis of various Schiff's base using MNP@CA[a]

Entry	R_1	R_2	R_3	R_4	R_5	Time (min)	Yield (%)
3a	H	H	H	H	H	15	95
3b	OH	H	H	H	H	20	90
3c	H	H	OH	H	H	20	90
3d	OH	H	OH	H	H	15	91
3e	OH	OCH_3	H	H	H	15	88
3f	OH	H	H	NO_2	H	10	96
3g	NO_2	H	H	H	H	10	96
3h	H	H	CN	H	H	15	92
3i	H	H	Cl	H	H	10	86
3j	OH	H	H	$N(C_2H_5)_2$	H	15	88
3k	2-hydroxy naphthaldehyde					10	92

[a]Reaction conditions: benzaldehyde (1mmol), 4-amino antipyrine (1mmol), solvent-ethanol (2mL), 80℃, 0.65 mol% of MNP@CA, ultrasonicated in open air

[b]Isolated yield
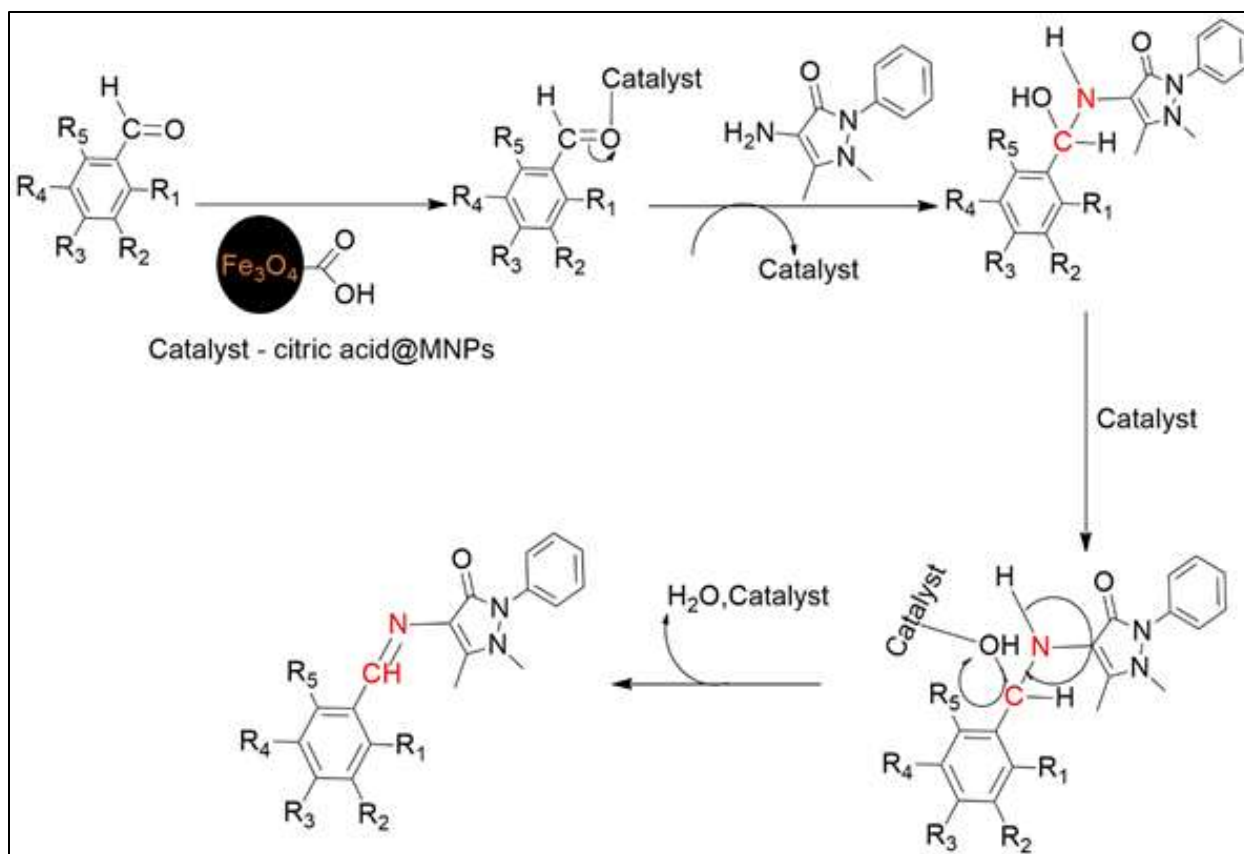
Scheme 2.2 Plausible mechanism for the synthesis of Schiff's base

The level of reusability of MNP@CA catalyst was also checked. For this the model reaction (benzaldehyde, 4-aminoantipyrine) was examined under optimized conditions. When the reaction was completed, the catalyst was separated out using an external magnet and then thoroughly washed with hot ethanol (2 x 10 ml) and dried in an oven for 3 h at 80 ˚C and was used for next run. The recycled catalyst could be reused 8 times without any significant decrease in its catalytic activity **(Figure 2.7 (d)).**
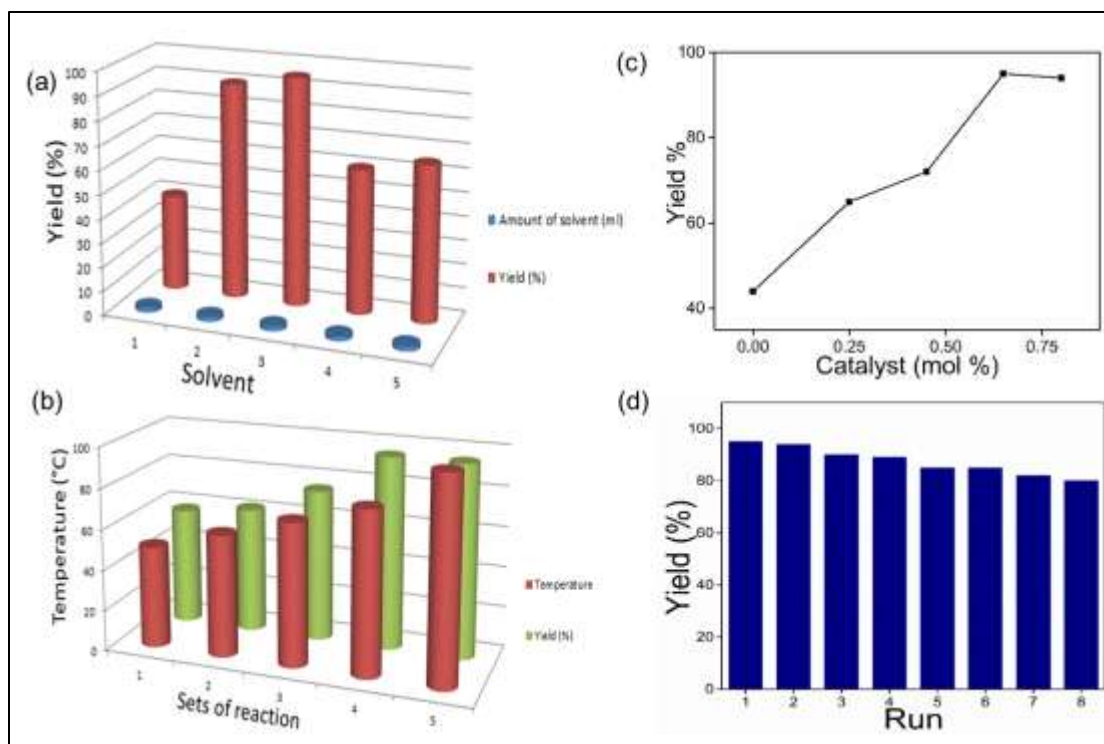
Figure 2.7 (a) Solvent standardization 1) H_2O, 2) MeOH, 3) EtOH, 4) $CHCl_3$, 5) H_2O/ EtOH (b) temperature variation (c) catalyst amount variation (d) reusability of magnetite@citric acid in the model reaction

As explained earlier FTIR analysis of magnetite@citric acid was carried out and it has been observed that the characteristics peaks of citric acid immobilization on magnetite through carboxylate groups forming ester bond with the OH group present on the surface of magnetite comes at 1627 cm^{-1} and the symmetric vibration due to non dissociated OH group of citric acid appeared at 3300 cm^{-1}. After eight runs same peaks were observed in FTIR spectrum but with lower intensity as depicted in **Figure 2.8 (A)** which might be due to gradual leaching of CA from Fe_3O_4 surface as well as catalyst loss during recovery process resulting in decrease of overall conversion in subsequent cycles. Almost the same characteristic peaks of magnetite@citric acid were obtained in **Figure 2.8 (B) (a)** and **(b)** which may explained that only Fe_3O_4 gives characteristic peaks in XRD and no peaks of CA were obtained. The morphology and crystalline cubic spinel structure has been also preserved during catalytic reaction and after the reaction similar diffraction peaks observed.
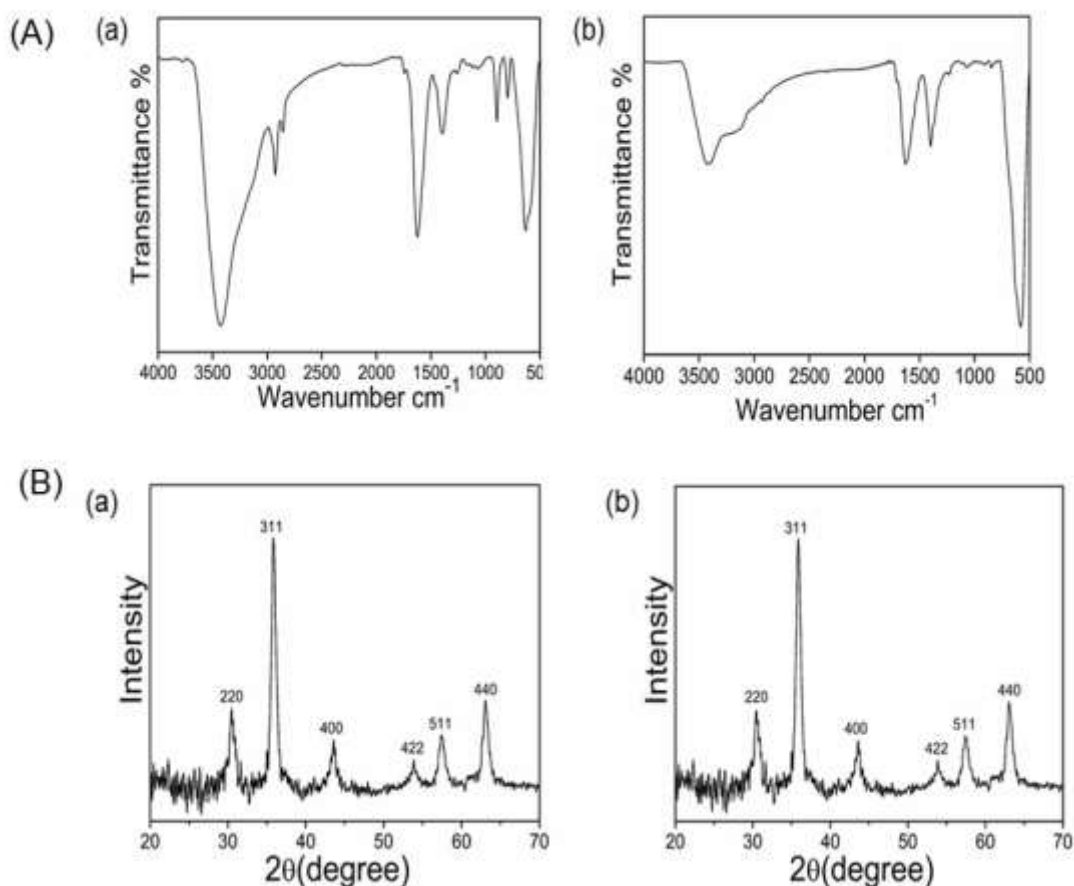
Figure 2.8. Comparative of MNP@CA nanocatalyst before and after the reaction (A) FTIR analysis (B) XRD analysis

2.2.3 Biological evaluation

All the compounds were screened for radical scavenging potential by DPPH method taking ascorbic acid as standard. The inhibitory effect of DPPH was calculated according to the following formula:

$$\text{Scavenging activity (\%)} = 100 \times (1 - (A_{sample} / A_{control}))$$

$A_{control}$ is the absorbance of the control solution (containing all reagents except the compounds being tested) and A_{sample} is the absorbance of the test compound. IC_{50} of the samples were determined by the method described by Molyneux (2004). The IC_{50} value is the concentration of inhibitor at which 50% of the DPPH radicals are scavenged. A low IC_{50} value indicates a high ability of the compound to act as a DPPH scavenger **(Figure 2.9)**. The effects of functional

36

groups on activity of the diphenolic antioxidants were observed. Bond Dissociation Energy (BDE) is the amount of energy needed to break a given bond to produce two fragments (in this case AO–H → AO$^{.}$ + H). BDE is an important factor in determining the efficacy of an antioxidant since the weaker the –OH bond, the faster will be the reaction with the free radicals. The addition of electron-donating substituents to an aromatic ring can increase radical scavenging activity as a result of increased electron density at carbon atoms in the ring **[46]**. In contrast, the presence of electron-withdrawing substituents decreases electron density around the ring, hence decreasing its ability to scavenge free radicals due to poor aromatic ring resonance of the phenoxyl radical. On the basis of above discussed factors some of them **3c, 3i, 3d, 3g, 3b** gave very good results. The rest synthesized compounds showed average antioxidant activity taking ascorbic acid as standard in DPPH free radicals scavenging, which indicates that the compounds have potential to prevent free radical mediated oxidative damage.
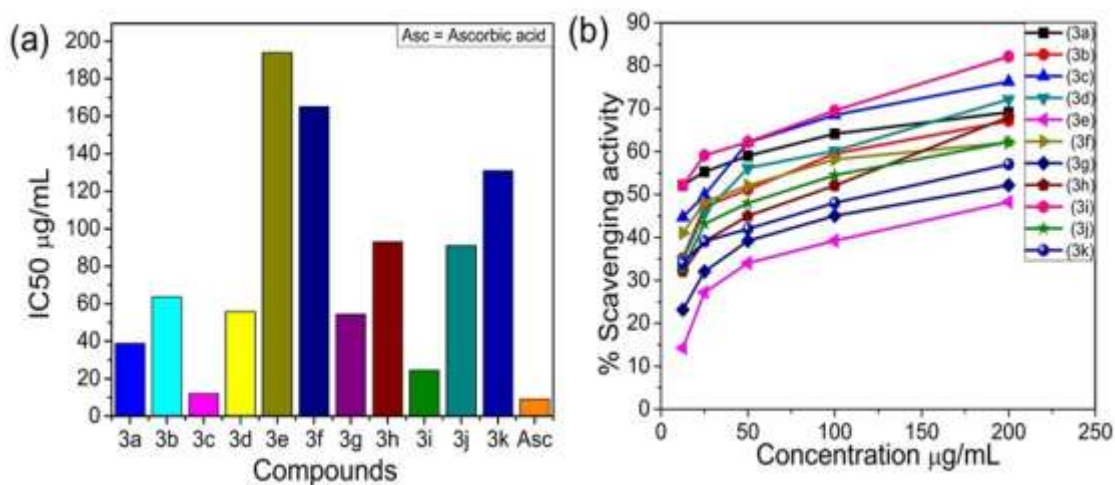
Figure 2.9 Antioxidant activity performances of synthesized Schiff's bases (**3a-3k**).

2.3 Experimental

2.3.1 Materials and methods

All chemicals and solvents purchased are of analytical grade and used without further purification. Ferric chloride hexahydrate (FeCl$_3$.6H$_2$O, CDH), ferrous chloride tetra hydrate (FeCl$_2$.4H$_2$O, Sigma Aldrich), sodium hydroxide (NaOH, 98% Alfa Aesar), citric acid (99.5%, ACS), 4-aminoantipyrine (99%, Loba Chemie), substituted aldehyde (Loba Chemie, CDH, Spectrochem, Molychem). The visualization of surface morphology of MNPs was done by using a field- emission scanning electron microscope (FESEM; NOVA nano SEM) operated at a voltage 10 kV. Samples were prepared by putting a little amount of fine powdered nanoparticles on black carbon tape. Their TEM images were recorded with a Tecnai G^2 20 (FEI) S-Twin high-resolution transmission electron microscope (HRTEM) operating at 200 kV. Samples were prepared by drying the droplet of dispersed solution of MNPs on a 400 mesh carbon coated copper grid under 100 W table lamp. Powder X-ray diffraction (XRD) pattern of the sample was obtained with X-ray Diffractometer (Panalytical X Pert Pro) using Cu Kα radiation. Thermo gravimetric analysis (TGA) was performed on a Mettler thermal analyzer in an inert atmosphere at a heating rate of 10 ℃/min. Melting points were determined in open glass capillaries and are reported uncorrected. Infrared spectrum were collected on a Bruker Fourier transform infrared spectrophotometer (FTIR) (Alpha) with pressed KBr pellets and were recorded in the range of 4000-400 wave number (cm^{-1}). ^{1}H NMR were recorded on a Jeol ECS 400 MHz spectrophotometer and ^{1}H NMR were recorded on a Jeol ECS 100 MHz spectrophotometer using DMSO d$_6$ as a solvent. TMS was taken as an internal standard and chemical shifts are reported in δ ppm. Resonance multiplicities are described as s (singlet), d (doublet), t (triplet), q (quartet) and m (multiplet). Ultrasonic bath; Elma S 70 H with 37 KHz with an output frequency was used to carry out the sonochemical reactions. The purity of all the compounds was checked by TLC using silica gel as adsorbent and solvents of increasing polarity as mobile phase.

2.3.2 Synthesis of the catalyst

In a 250 ml round bottom flask 16 mmol of FeCl$_3$.6H$_2$O (4.32 g) and 8 mmol of FeCl$_2$.4H$_2$O (1.59 g) were taken in 50 ml of deionised (DI) water and ultrasonicated for 15 minutes at room temperature (25 ℃). Then slowly the temperature was raised to 60 ℃ and maintained for further

30 minutes. After that 50 ml of 1M NaOH solution was added dropwise at the same temperature till the pH of the solution became 10-11. It was further sonicated for another 30 minutes. The resulting black dispersion was then allowed to remain undisturbed for one night and the desired nanoparticles were separated by using an external magnet then washed thoroughly with deionised water (100 x 3 ml) followed by acetone, (2 x 50 ml) and finally dried in a vacuum oven for 6 h at 60 ℃. The synthesised magnetite nanoparticles (1 g) were taken in a 250 ml round bottom flask and dispersed in 5 ml of deionised water under ultrasonication for 5 minutes. Then 4 ml of aqueous solution of citric acid (0.6 g/ml) was added dropwise to the reaction mixture and the temperature was slowly raised to 80 ℃. The reaction mixture was sonicated for another 1 h after which it was cooled down to room temperature and the black precipitate of functionalised magnetic nanoparticles settled down under the influence of an external magnet. They were retrieved by magnetic decantation and washed with deionised water (20 ml x 5) and then with acetone to remove any unbound citric acid. Thereafter they were dried in vacuum oven for 5 h at 60 ℃
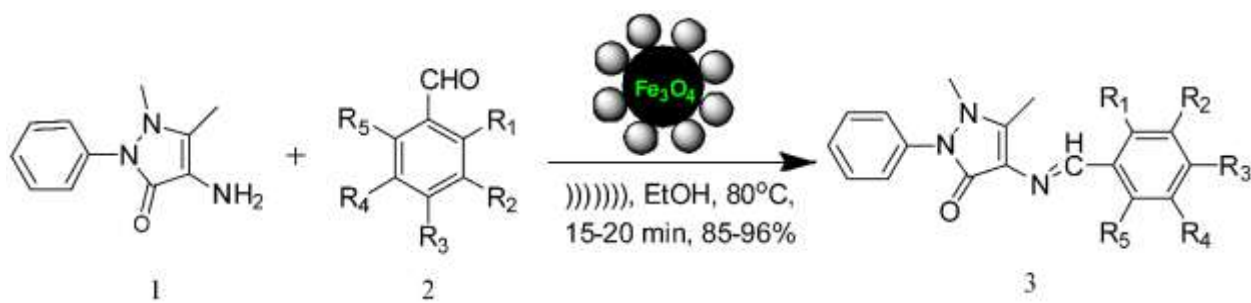
Scheme 2.1 Synthesis of Schiff's base by using MNP@CA

2.3.3 Synthesis of (E)-4-((2-methylbenzylidene) amino)-1,5-dimethyl-2-phenyl-1,2-dihydro-3H-pyrazol-3-one (3a)

As shown in **Scheme 2.1** initially benzaldehyde (1 mmol) dissolved in 3 ml of ethanol was taken in a 50 ml round bottom flask and 0.65 mol% of the catalyst was added to it which was then sonicated for 2 min to activate the carbonyl group of the benzaldehyde by the MNP@CA nano

catalyst. Then 1 mmol 4-aminoantipyrine was added to the reaction mixture and sonication continued till the completion of the reaction indicated by TLC (8:2 petroleum ether: ethyl acetate). The catalyst was then separated by using a strong external magnet. The reaction mixture was concentrated in a rota vapour under reduced pressure. The final solid of the desired product was obtained which was further purified by recrystallization using ethanol as a solvent.

2.3.4 Analytical Data

4-(benzylideneamino)-1,5-dimethyl-2-phenyl-1H-pyrazol-3(2H)-one (3a)[47]

Off white solid, yield: 95%, mp: found:177-178 °C, Reported: 178-179 °C. IRν (KBr):1643 (>C=O), 1560 (>C=N) cm^{-1}, ^{1}H NMR (400 MHz, DMSO d$_6$): δ = 9.55 (-N=CH-,s), 7.81-7.32 (m, Ar 9H), 3.14 (s , -N-CH$_3$, 3H), 2.45 (, s, 3H, =C-CH$_3$) , ^{13}C NMR (100 MHz, DMSO d$_6$) δ = 10.29, 35.86, 116.82, 125.11, 127.41, 127.91, 129.26, 129.67, 130.68, 135.08, 138.04, 152.76, 154.83, 160.12, HRMS (ESI) (C$_{18}$H$_{17}$N$_3$O) [M+H]$^+$ calcd. 292.1445; found: 292.1442

4-((2-hydroxybenzylidene)amino)-1,5-dimethyl-2-phenyl-1H-pyrazol-3(2H)-one (3b)

Lemon yellow color solid, yield: 92%, mp 282-283 °C. IRν (KBr):1643 (>C=O), 1557 (>C=N) cm^{-1}, ^{1}H NMR (400 MHz, DMSO d$_6$): δ = 9.63 (s ,-N=CH-,), 7.57 -6.87 (m, Ar 9H,), 3.17 (s, 3H, -N-CH$_3$), 2.36 (s, 3H, =C-CH$_3$,) ^{13}C NMR (100 MHz, DMSO d$_6$) δ= 10.61, 35.47, 114.70, 117.07, 119.62, 120.83, 125.48, 127.78, 129.86, 131.59, 132.28, 134.76, 150.89, 158.03, 159.60, 159.93. HRMS (ESI) (C$_{18}$H$_{17}$N$_3$O$_2$) [M+H]$^+$ calcd. 308.1394; found: 308.1398

4-((4-hydroxybenzylidene)amino)-1,5-dimethyl-2-phenyl-1H-pyrazol-3(2H)-one (3c)[47]

Pale dull yellow color solid, yield: 90%, mp found: 233-235 °C, reported 232-234 °C; IRν (KBr):1663 (>C=O), 1602 (>C=N) cm^{-1}; ^{1}H NMR (400 MHz, DMSO d$_6$) : δ = 9.42 (s, -N=CH-), 7.61 -6.78 (m, Ar 9H), 3.08 (s, 3H, -N-CH$_3$), 2.37 (s, 3H, =C-CH$_3$); ^{13}C NMR (100 MHz, DMSO d$_6$) δ 10.38, 35.84, 113.17, 121.60, 122.68, 123.17, 125.92, 128.31, 129.69, 130.93, 134.46, 150.58, 154.49, 155.07, 159.09; HRMS (ESI) (C$_{18}$H$_{17}$N$_3$O$_2$) [M+H]$^+$ calcd. 308.1394; found: 308.1398

4-((2,4-dihydroxybenzylidene)amino)-1,5-dimethyl-2-phenyl-1H-pyrazol-3(2H)-one (3d)[48]

Shiny yellow color solid, yield: 91%, mp found: 231-234 °C, reported: 232 °C; IRν (KBr):1624 (>C=O), 1510 (>C=N) cm^{-1}; ^{1}H NMR (400 MHz, DMSO d$_6$) : δ = 9.51 (-N=CH-,s), 7.53 -6.31 (m, Ar 7H), 6.22 (s, 1H, ArH), 3.14 (-N-CH$_3$, 3H, s), 2.31 (s, 3H, =C-CH$_3$); ^{13}C NMR (100

MHz, DMSO d$_6$) δ = 10.31, 35.83, 102.97, 108.52, 113.43, 115.53, 125.34, 127.50, 129.60, 133.72, 150.19, 158.97, 159.98, 161.73, 162.80; HRMS (ESI) (C$_{18}$H$_{17}$N$_3$O$_3$) [M+H]$^+$ calcd. 324.1343 found: 324.1342

4-((2-hydroxy-3-methoxybenzylidene)amino)-1,5-dimethyl-2-phenyl-1H-pyrazol-3(2H)-one (3e)

Fluorescent yellow color solid; yield: 88%; mp: 204-206 ℃. IRν (KBr):1649 (>C=O), 1558 (>C=N) cm^{-1}; ^{1}H NMR (400 MHz, DMSO d$_6$): δ = 9.55 (s, -N=CH-), 7.81-7.32 (m, Ar 9H), 3.14 (s, 3H, -N-CH$_3$), 2.45 (s, 3H, =C-CH$_3$); ^{13}C NMR (100 MHz, 25℃, Si(CH$_3$)$_4$, DMSO d$_6$) δ = 10.58, 35.81, 56.61, 114.49, 114.84, 119.20, 120.66, 123.23, 125.51, 127.90, 129.88, 134.78, 148.30, 149.73, 150.91, 158.18, 159.75; HRMS (ESI) (C$_{19}$H$_{19}$N$_3$O$_3$) [M+H]$^+$ calcd. 338.1499 found: 338.1495

4-((2-hydroxy-5-nitrobenzylidene)amino)-1,5-dimethyl-2-phenyl-1H-pyrazol-3(2H)-one (3f)

Bright yellow color solid; yield: 96%, mp: 220-224 ℃; IRν (KBr):1637 (>C=O), 1554 (>C=N) cm^{-1}, ^{1}H NMR (400 MHz, DMSO-d$_6$): δ = 9.75 (s, -N=CH-), 8.50-7.06 (m, Ar 8H), 3.21 (s, 3H, -N-CH$_3$), 2.40 (s, 3H, =C-CH$_3$); ^{13}C NMR (100 MHz, DMSO d$_6$) δ = 10.63, 35.42, 114.54, 117.71, 121.55, 125.78, 127.13, 128.45, 129.57, 135.13, 141.06, 151.56, 153.40, 159.25, 164.88; HRMS (ESI) (C$_{18}$H$_{16}$N$_4$O$_4$) [M+H]$^+$ calcd. 353.1245 found: 353.1246

1,5-dimethyl-4-((2-nitrobenzylidene)amino)-2-phenyl-1H-pyrazol-3(2H)-one (3g)

Saffron color solid; yield: 96%; mp: 248-251 ℃; IRν (KBr):1643 (>C=O), 1560 (>C=N) cm^{-1}; ^{1}H NMR (400 MHz, DMSO-d$_6$): δ = 9.77 (s, -N=CH-), 7.31-8.16 (m, Ar 9H), 3.19 (s, 3H, -N-CH$_3$), 2.42 (s, 3H,=C-CH$_3$); ^{13}C NMR (100 MHz, DMSO d$_6$) δ = 10.64, 36.08, 115.95, 124.68, 125.68, 127.85, 128.83, 129.87, 131.60, 131.65, 133.42, 135.14, 148.79, 149.49, 153.37, 159.65; HRMS (ESI) (C$_{18}$H$_{16}$N$_4$O$_3$) [M+H]$^+$ calcd. 337.1295 found: 337.1295

4-(((1,5-dimethyl-3-oxo-2-phenyl-2,3-dihydro-1H-pyrazol-4-yl)imino)methyl)benzonitrile (3h)

Lemon yellow color solid; yield (92%); mp: 282-283 ℃; IRν (KBr):1643 (>C=O), 1557 (>C=N) cm^{-1}; ^{1}H NMR (400 MHz, DMSO d$_6$): δ = 9.56 (s, -N=CH-), 7.99 -7.32 (m, Ar 9H), 3.16 (s, 3H, -N-CH$_3$,), 2.41 (s, 3H, =C-CH$_3$); ^{13}C NMR (100 MHz, DMSO d$_6$) δ = 10.62, 36.96, 116.82, 117.78, 124.82, 128.95, 127.75, 129.68, 129.82, 129.81, 135.65, 152.12, 155.87, 160.52, 160.99; HRMS (ESI) (C$_{19}$H$_{16}$N$_4$O) [M+H]$^+$ calcd. 317.1397 found: 317.1397

4-((4-chlorobenzylidene)amino)-1,5-dimethyl-2-phenyl-1H-pyrazol-3(2H)-one (3i)[48]

Creamy yellow color solid; yield: 86%; mp: 252-253 ℃; IRν (KBr):1644 (>C=O), 1583 (>C=N) cm^{-1}; ^{1}H NMR (400 MHz, 25℃, Si(CH$_3$)$_4$, DMSO d$_6$): δ = 9.52 (s, -N=CH-), 7.82-7.34 (m, Ar 9H,), 3.15 (s, 3H, -N-CH$_3$,), 2.41 (s, 3H, =C-CH$_3$,); ^{13}C NMR (100 MHz, DMSO d$_6$) δ =10.66, 36.56, 116.57, 117.68, 124.74, 127.45, 129.07, 129.18, 135.45, 151.95, 155.41, 160.01, 160.54; HRMS (ESI) (C$_{18}$H$_{16}$ClN$_3$O) [M+H]$^+$ calcd. 326.1055 found: 326.1051

4-((4-(diethylamino)-2-hydroxybenzylidene)amino)-1,5-dimethyl-2-phenyl-1H-pyrazol-3(2H)-one (3j)

Yellow color solid, yield: 88%, mp: 234-236 ℃. IRν (KBr):1663 (>C=O), 1610 (>C=N) cm^{-1}, ^{1}H NMR (400 MHz, DMSO-d$_6$): δ 9.44 (-N=CH-,s), 7.50-6.03 (m, Ar 8H), 3.07 (s, 3H, -N-CH$_3$), 2.29 (s, 3H, =C-CH$_3$) ^{13}C NMR (100 MHz, DMSO d$_6$) δ =10.63, 35.84, 44.91, 97.73, 104.08, 108.93, 115.93, 124.69, 127.43, 129.91, 133.73, 135.16, 149.52, 151.56, 158.57, 156.32, 163.44; HRMS (ESI) (C$_{22}$H$_{26}$N$_4$O$_2$) [M+H]$^+$ calcd. 379.2129 found: 379.2129

4-(((2-hydroxynaphthalen-1-yl)methylene)amino)-1,5-dimethyl-2-phenyl-1H-pyrazol-3(2H)-one (3k)[49]

Dark yellow color solid; yield: 92%; mp: 172-175 ℃; IRν (KBr):1649 (>C=O), 1557 (>C=N) cm^{-1}; ^{1}H NMR (400 MHz, DMSO d$_6$): δ = 10.62 (-N=CH-,s), 8.06 -7.11 (m, Ar 9H), 3.18 (s, 3H, -N-CH$_3$), 2.41 (s, 3H, =C-CH$_3$); ^{13}C NMR (100 MHz, DMSO d$_6$) δ = 10.62, 36.18, 110.42, 114.50, 119.79, 120.13, 124.01, 125.50, 127.85, 128.04, 128.44, 129.63, 129.75, 123.46, 133.99, 134.69, 149.87, 154.61, 159.79, 161.33; HRMS (ESI) (C$_{22}$H$_{19}$N$_3$O$_2$) [M+H]$^+$ calcd. 358.1550 found: 358.1552
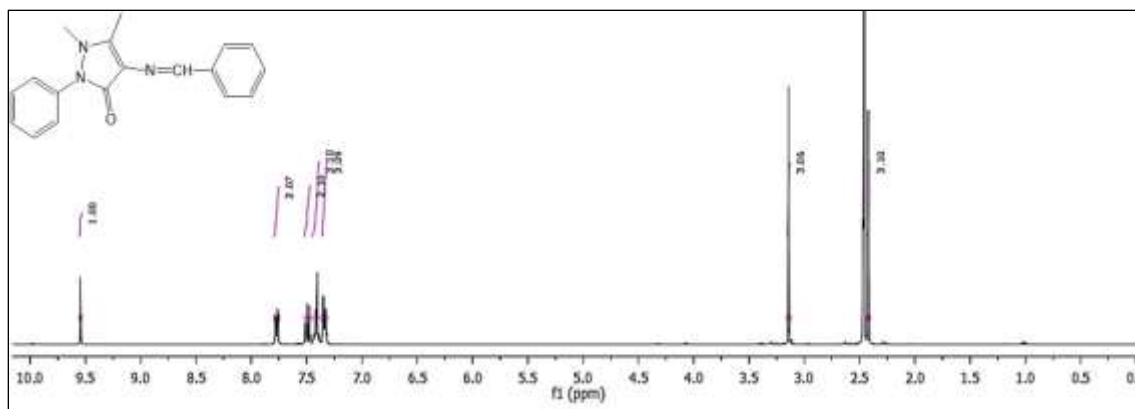
Figure 2.10 ^{1}H NMR spectrum of 4-(benzylideneamino)-1,5-dimethyl-2-phenyl-1H-pyrazol-3(2H)-one **(3a)**
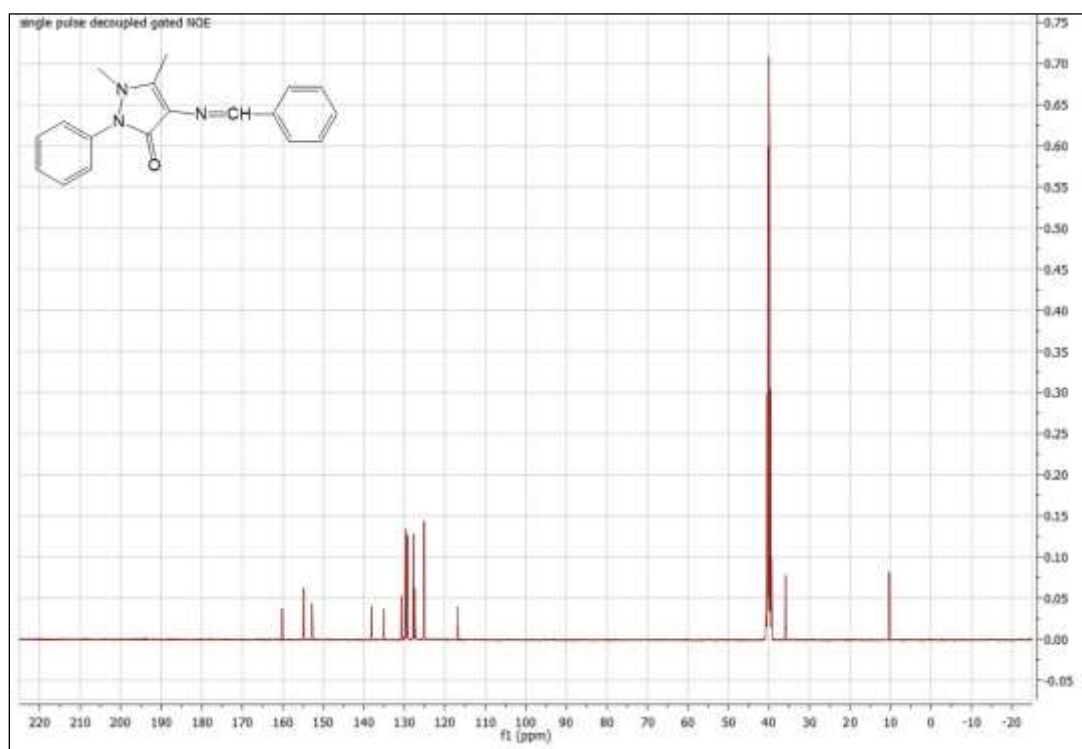
Figure 2.11 ^{13}C NMR spectrum of 4-(benzylideneamino)-1,5-dimethyl-2-phenyl-1H-pyrazol-3(2H)-one **(3a)**
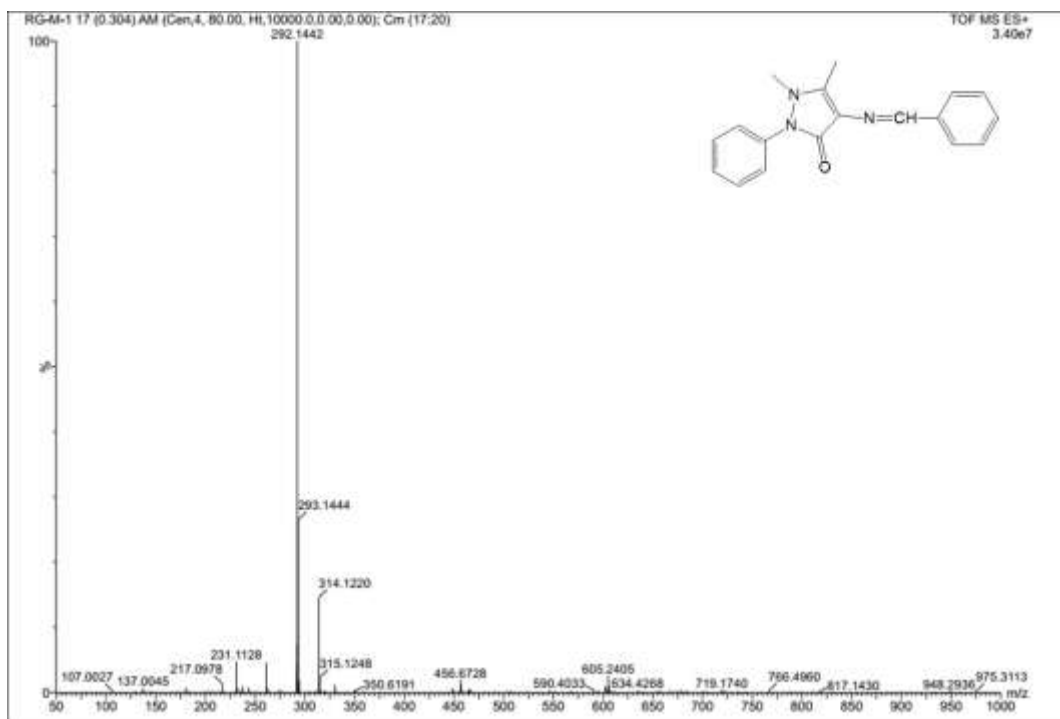
Figure 2.12 ESI mass spectrum of 4-(benzylideneamino)-1,5-dimethyl-2-phenyl-1H-pyrazol-3(2H)-one **(3a)**
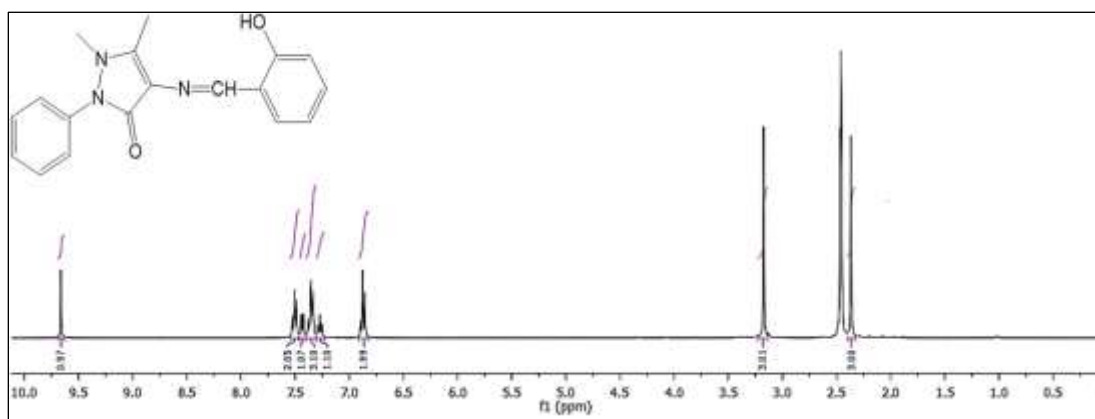
Figure 2.13 ¹H NMR spectrum of 4-((2-hydroxybenzylidene)amino)-1,5-dimethyl-2-phenyl-1H-pyrazol-3(2H)-one **(3b)**

44
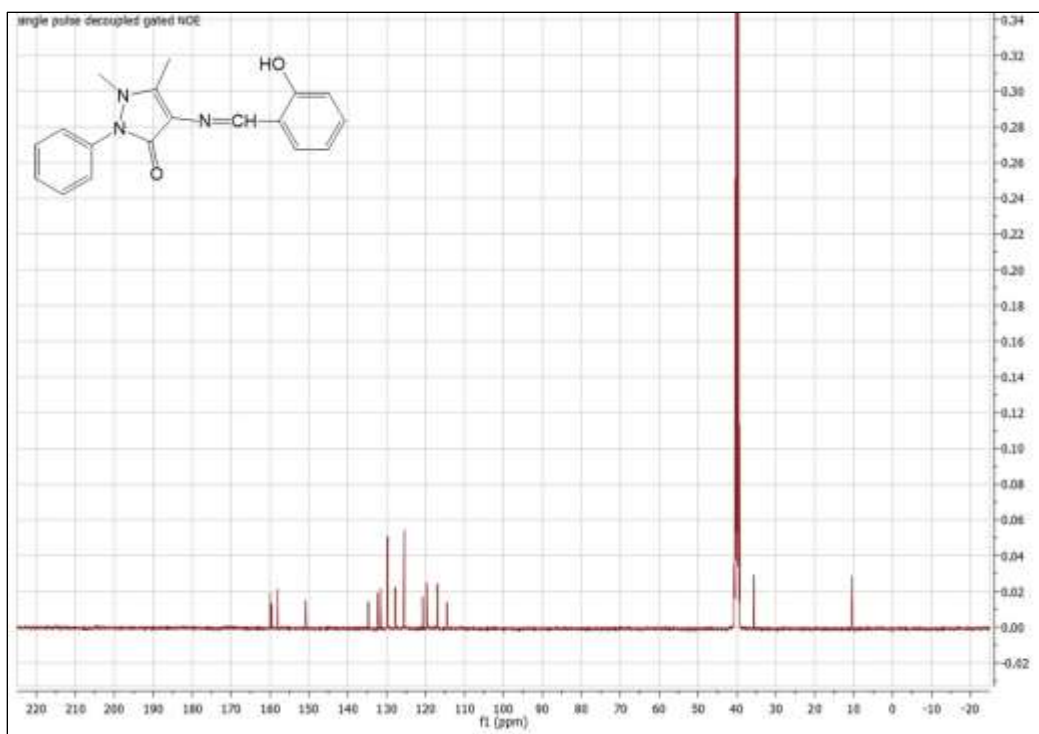
Figure 2.14 ^{13}C NMR spectrum of 4-((2-hydroxybenzylidene)amino)-1,5-dimethyl-2-phenyl-1H-pyrazol-3(2H)-one **(3b)**
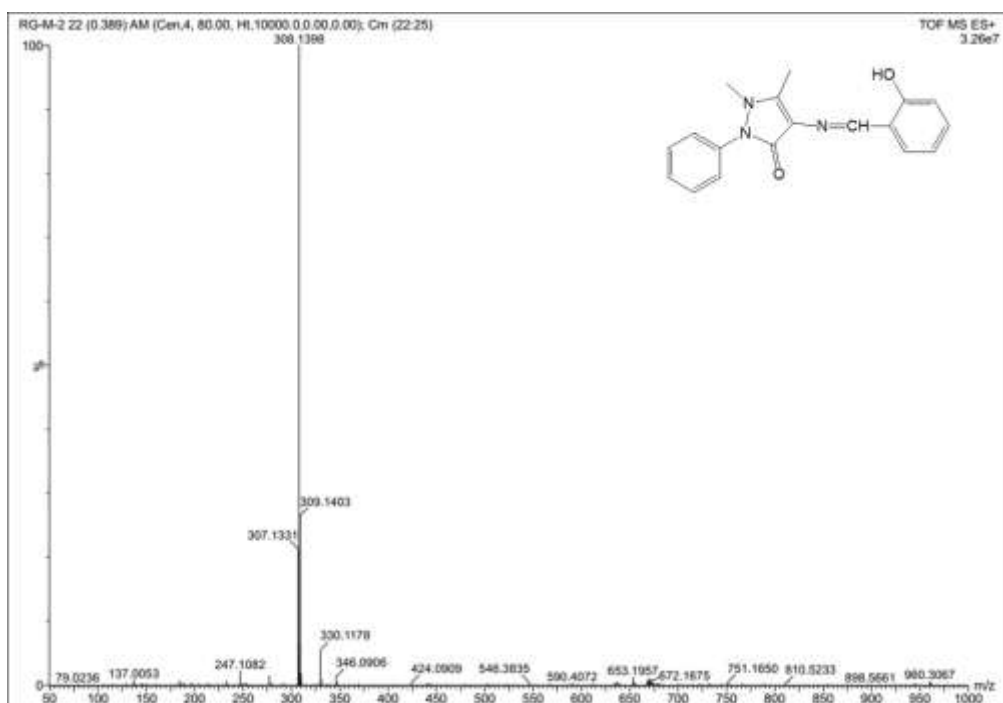
Figure 2.15 ESI mass spectrum of 4-((2-hydroxybenzylidene)amino)-1,5-dimethyl-2-phenyl-1H-pyrazol-3(2H)-one **(3b)**
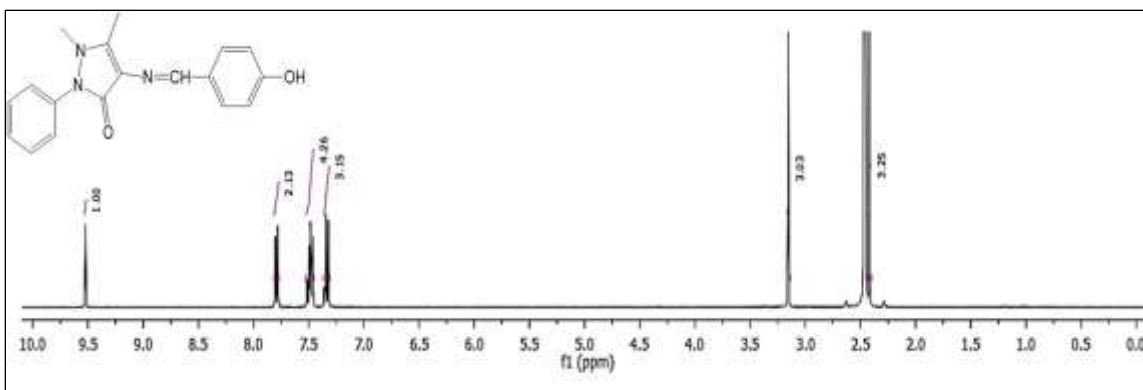
Figure 2.16 ^{1}H NMR spectrum of 4-((4-hydroxybenzylidene)amino)-1,5-dimethyl-2-phenyl-1H-pyrazol-3(2H)-one **(3c)**
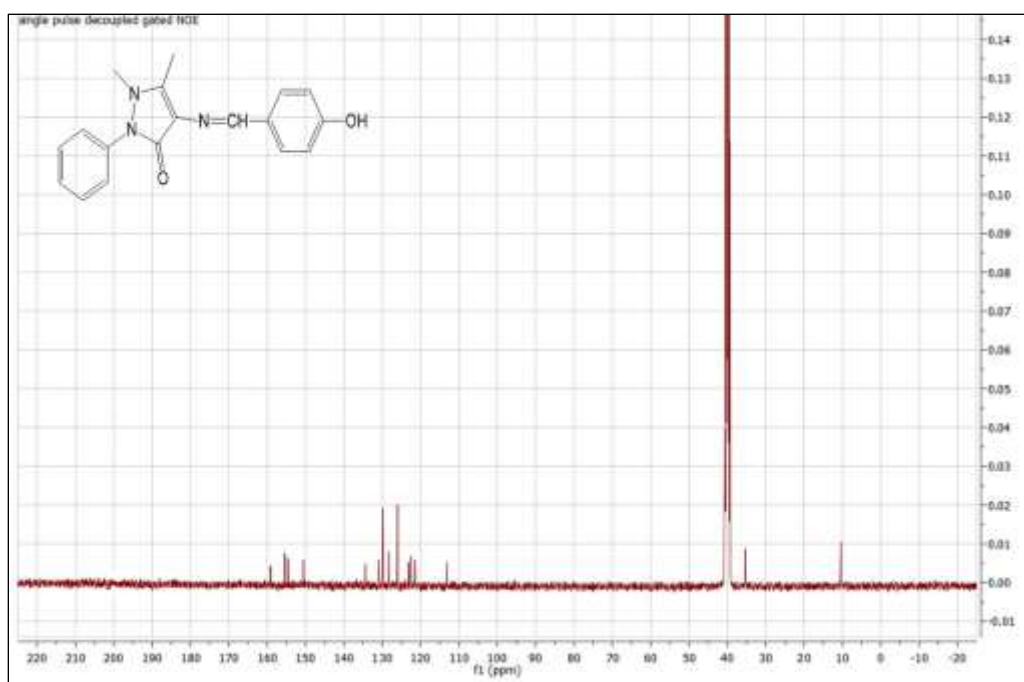
Figure 2.17 ^{13}C NMR spectrum of 4-((4-hydroxybenzylidene)amino)-1,5-dimethyl-2-phenyl-1H-pyrazol-3(2H)-one **(3c)**
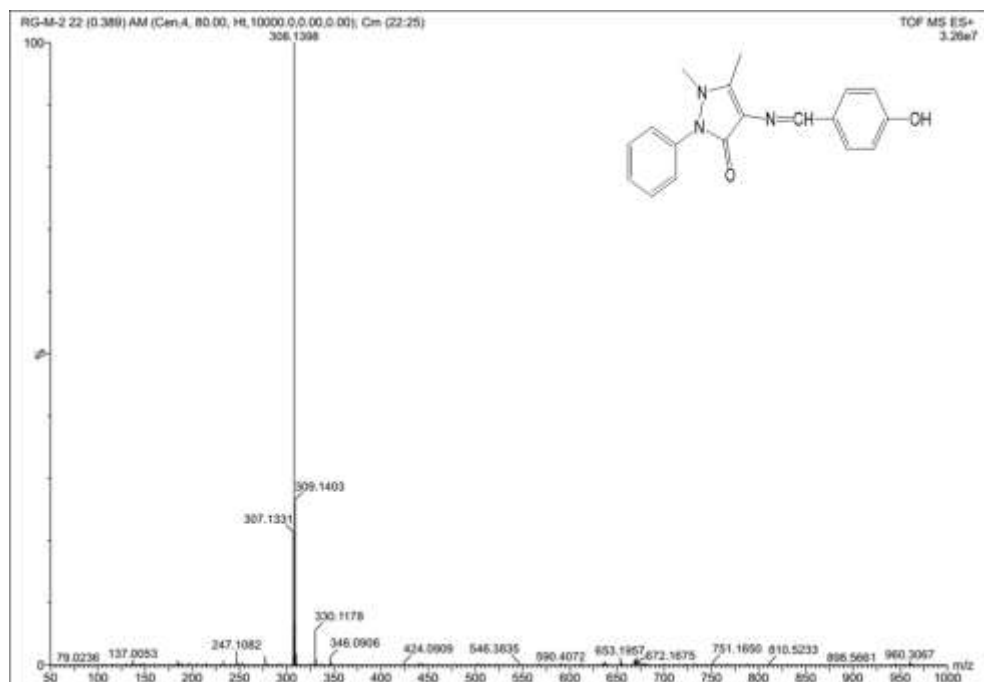
Figure 2.18 ESI mass spectrum of 4-((4-hydroxybenzylidene)amino)-1,5-dimethyl-2-phenyl-1H-pyrazol-3(2H)-one **(3c)**
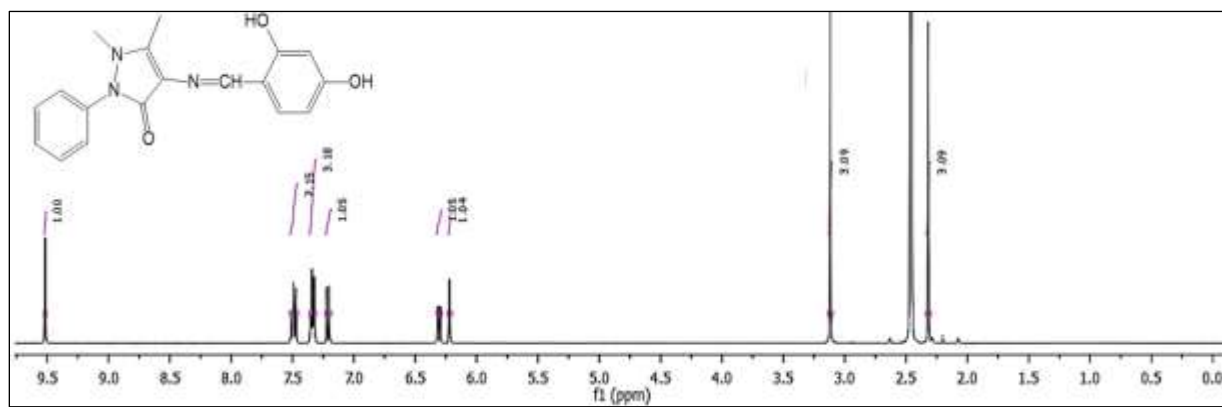
Figure 2.19 ^{1}H NMR spectrum of 4-((2,4-dihydroxybenzylidene)amino)-1,5-dimethyl-2-phenyl-1H-pyrazol-3(2H)-one **(3d)**

47
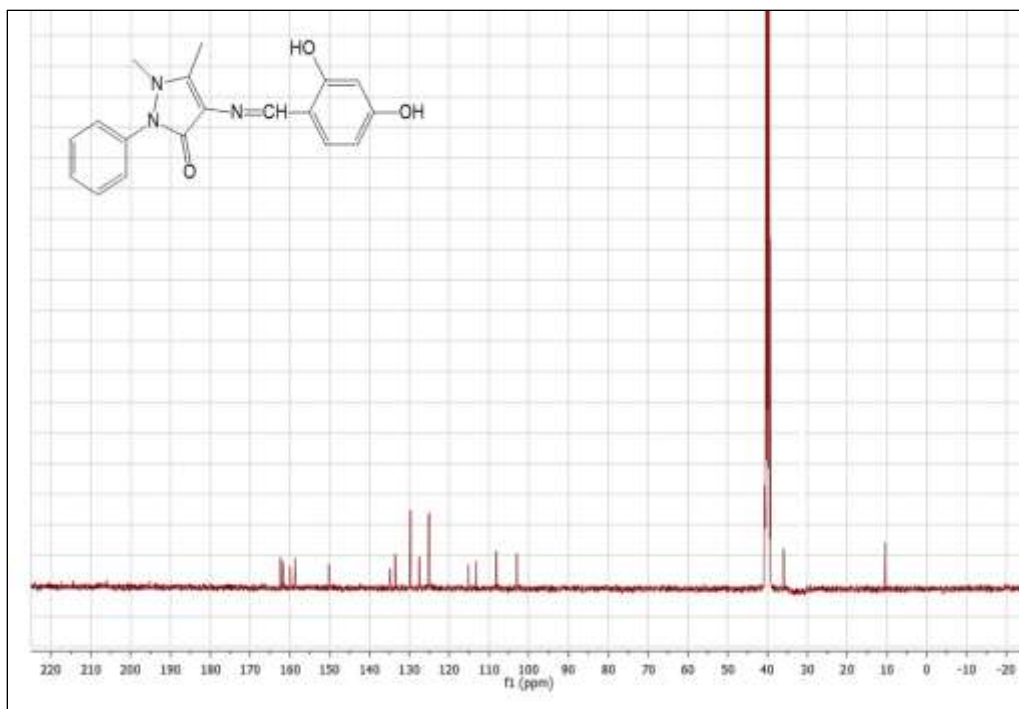
Figure 2.20 ^{13}C NMR spectrum of 4-((2,4-dihydroxybenzylidene)amino)-1,5-dimethyl-2-phenyl-1H-pyrazol-3(2H)-one **(3d)**
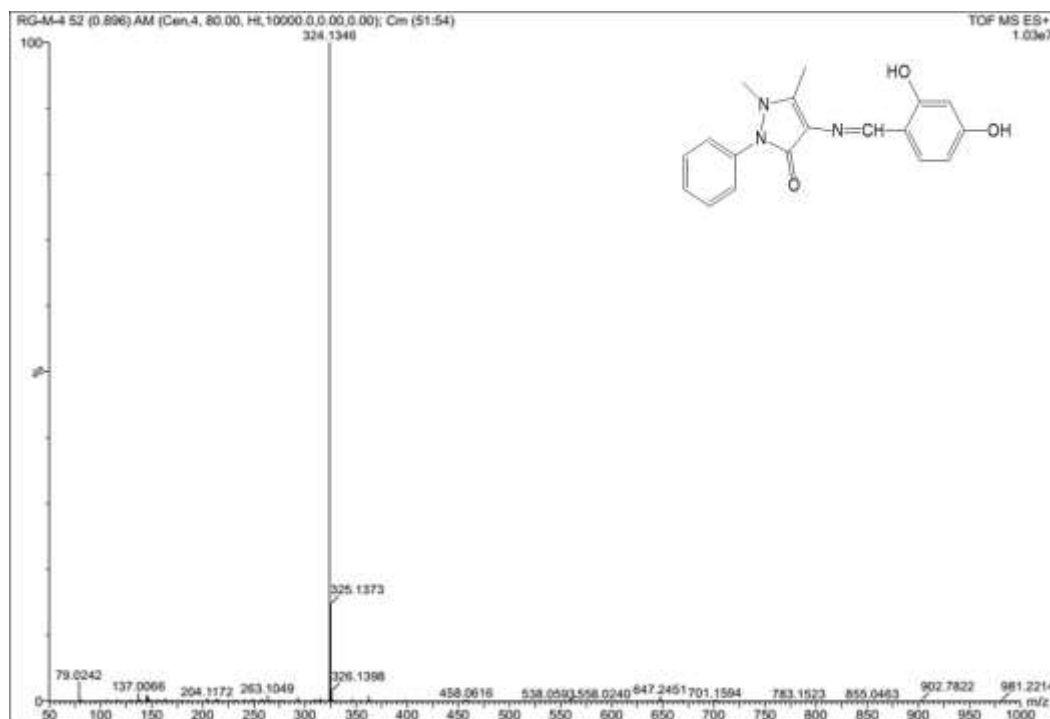
Figure 2.21 ESI mass spectrum of 4-((2,4-dihydroxybenzylidene)amino)-1,5-dimethyl-2-phenyl-1H-pyrazol-3(2H)-one **(3d)**
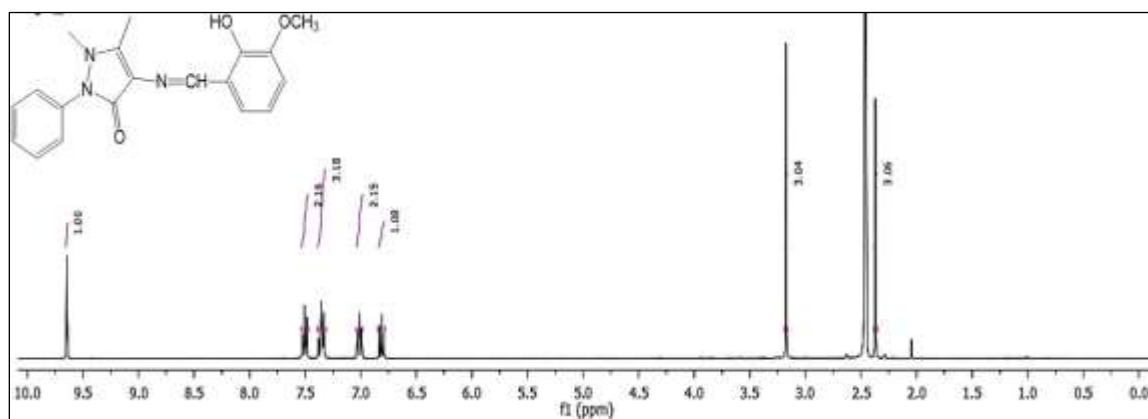
Figure 2.22 ^{1}H NMR spectrum 4-((2-hydroxy-3-methoxybenzylidene)amino)-1,5-dimethyl-2-phenyl-1H-pyrazol-3(2H)-one **(3e)**
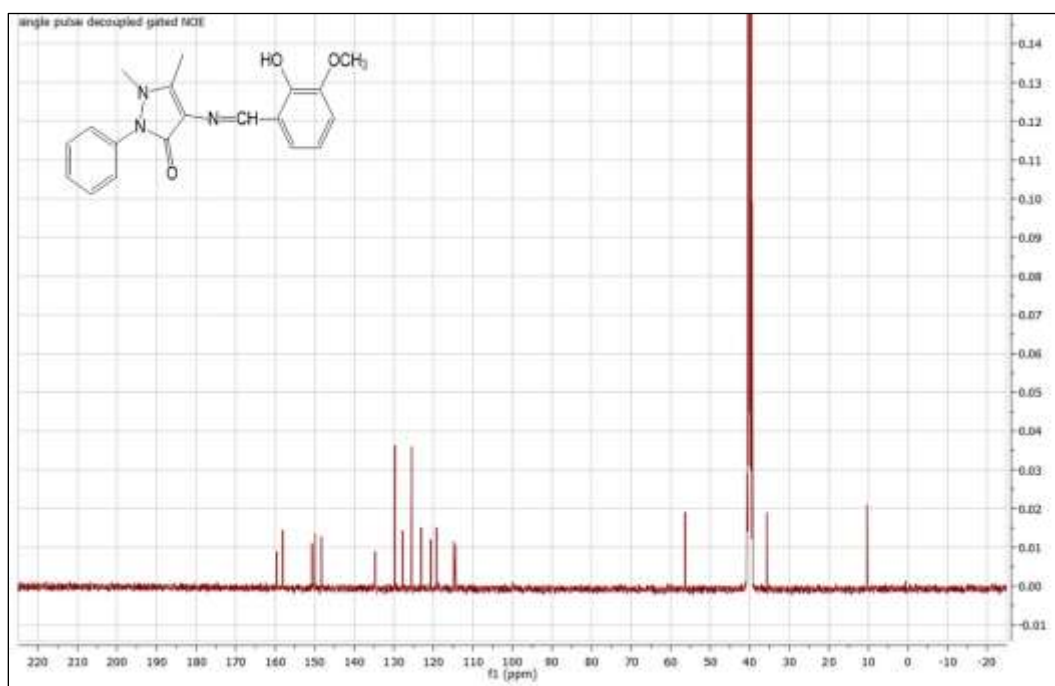
Figure 2.23 ^{13}C NMR spectrum of 4-((2-hydroxy-3-methoxybenzylidene)amino)-1,5-dimethyl-2-phenyl-1H-pyrazol-3(2H)-one **(3e)**
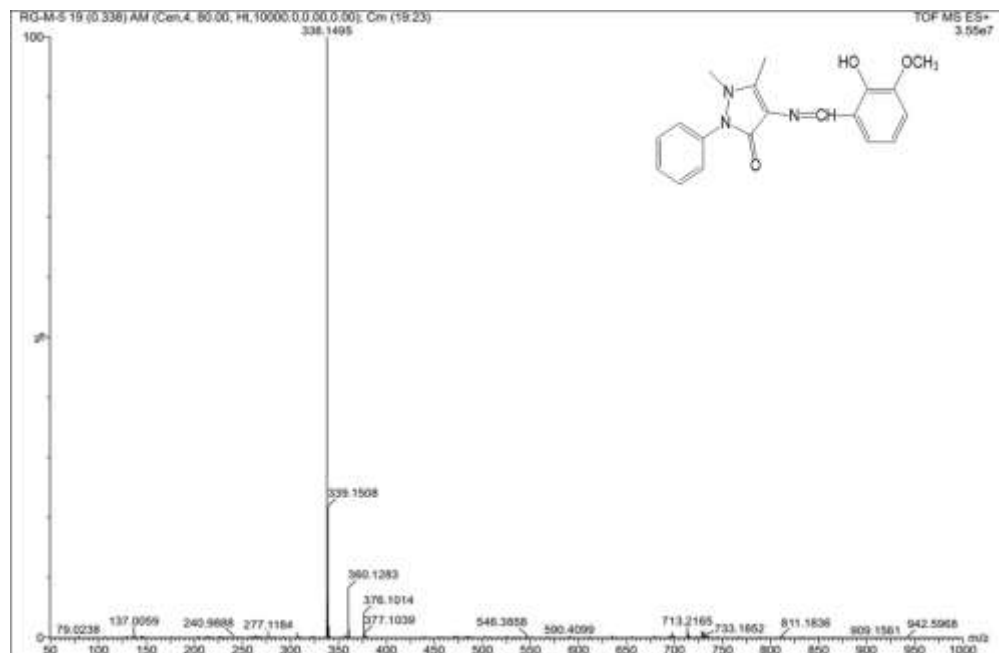
Figure 2.24 ESI mass spectrum of 4-((2-hydroxy-3-methoxybenzylidene)amino)-1,5-dimethyl-2-phenyl-1H-pyrazol-3(2H)-one **(3e)**
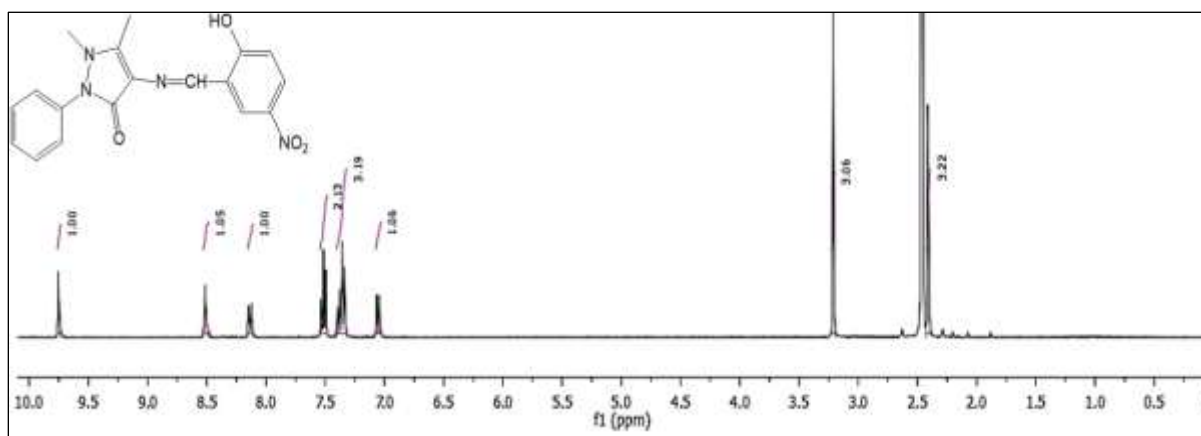
Figure 2.25 ¹H NMR spectrum of 4-((2-hydroxy-5-nitrobenzylidene)amino)-1,5-dimethyl-2-phenyl-1H-pyrazol-3(2H)-one **(3f)**
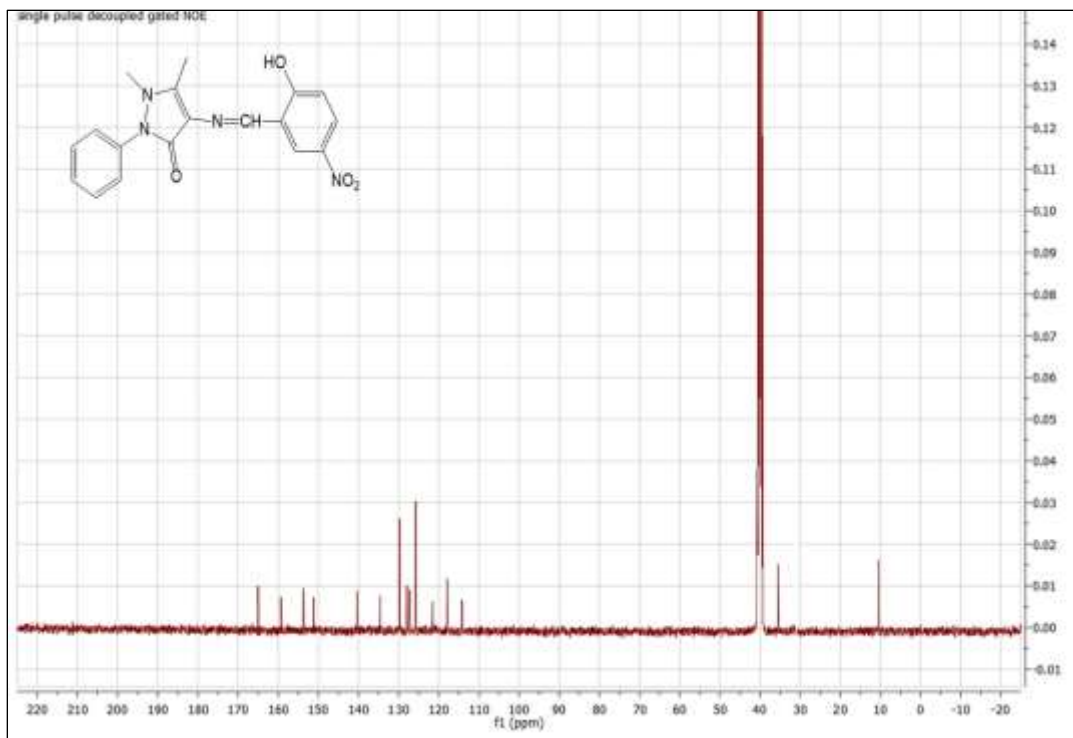
Figure 2.26 ^{13}C NMR spectrum of 4-((2-hydroxy-5-nitrobenzylidene)amino)-1,5-dimethyl-2-phenyl-1H-pyrazol-3(2H)-one **(3f)**
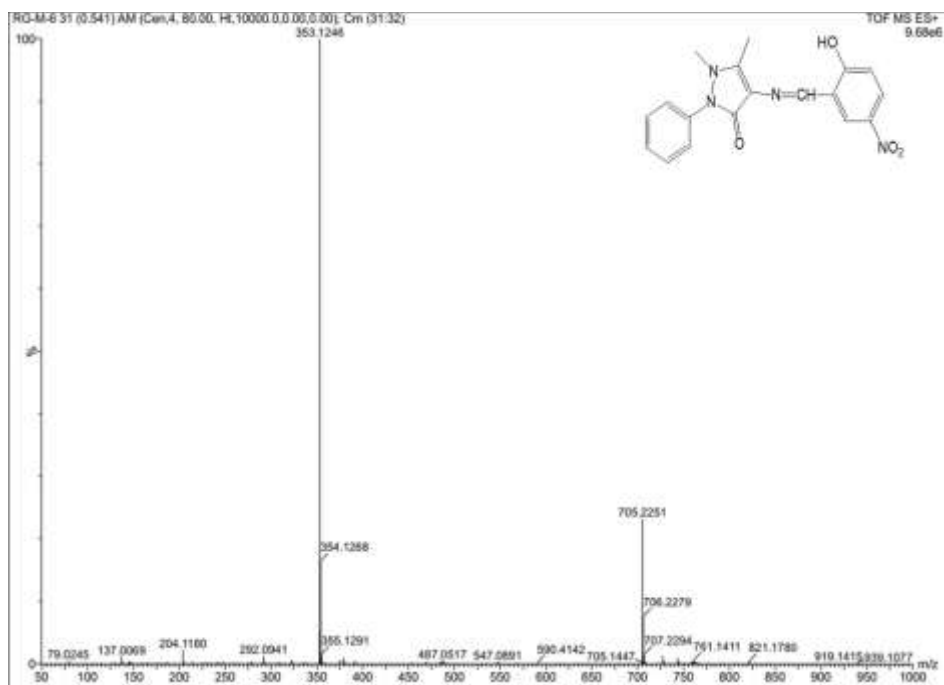
Figure 2.27 ESI mass spectrum of 4-((2-hydroxy-5-nitrobenzylidene)amino)-1,5-dimethyl-2-phenyl-1H-pyrazol-3(2H)-one **(3f)**
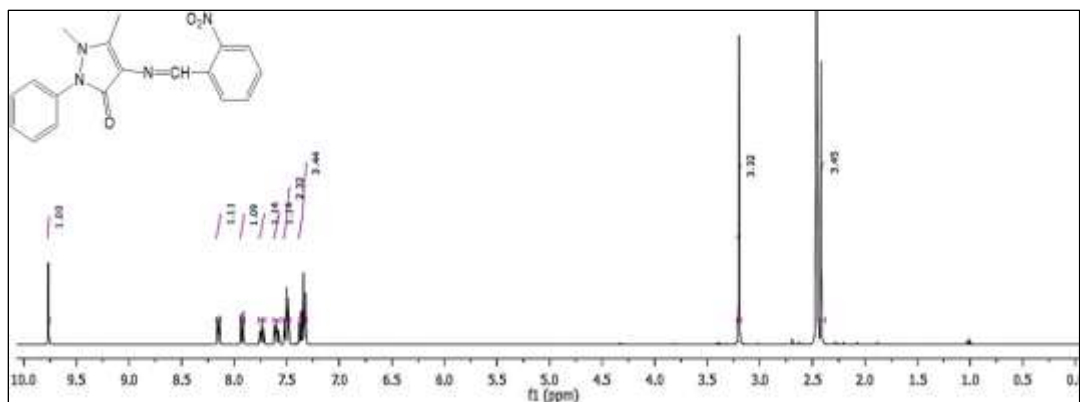
Figure 2.28 ^{1}H NMR spectrum of 1,5-dimethyl-4-((2-nitrobenzylidene)amino)-2-phenyl-1H-pyrazol-3(2H)-one **(3g)**
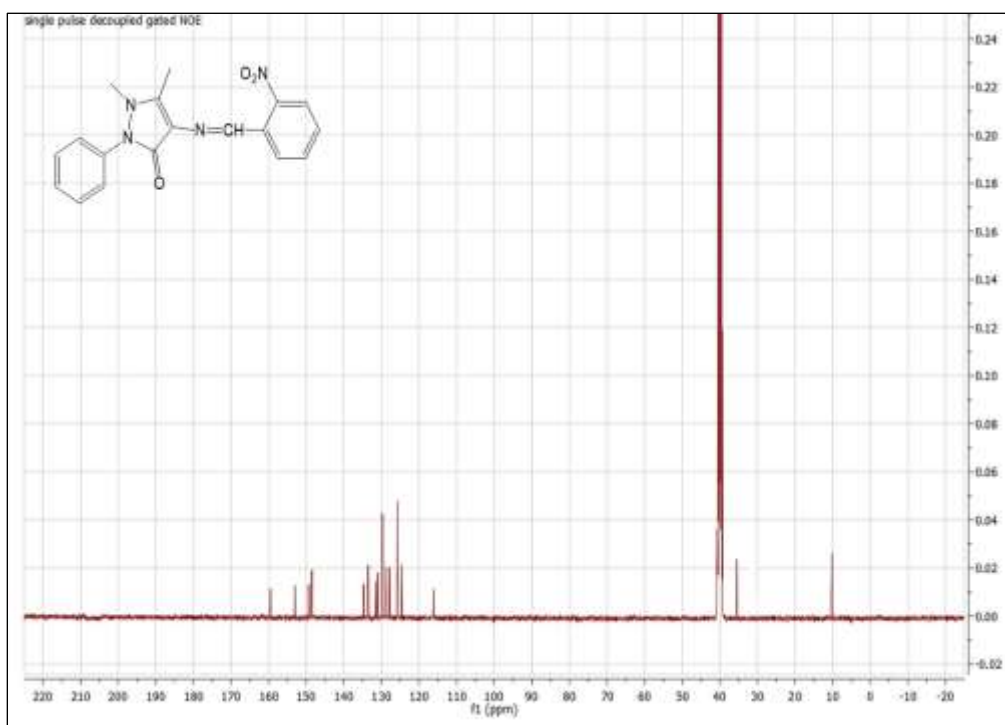
Figure 2.29 ^{13}C NMR spectrum of 1,5-dimethyl-4-((2-nitrobenzylidene)amino)-2-phenyl-1H-pyrazol-3(2H)-one **(3g)**
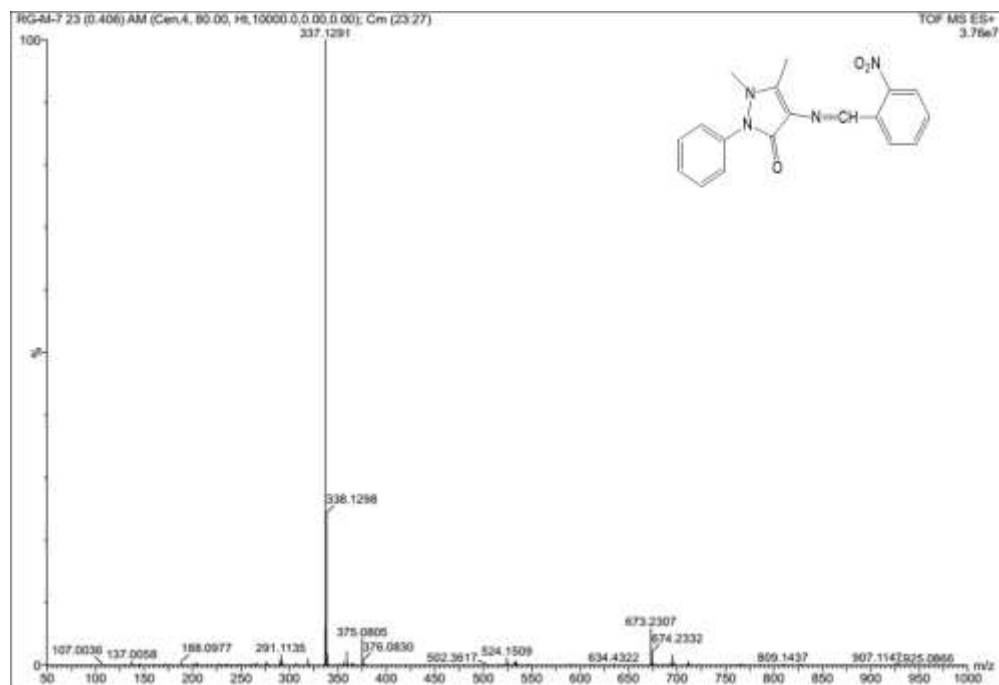
Figure 2.30 ESI mass spectrum of 1,5-dimethyl-4-((2-nitrobenzylidene)amino)-2-phenyl-1H-pyrazol-3(2H)-one **(3g)**
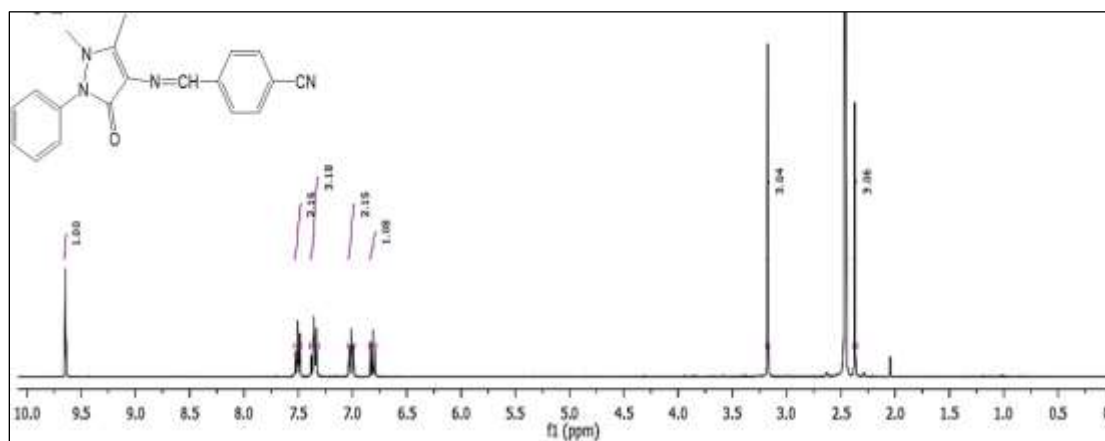
Figure 2.31 ^{1}H NMR spectrum of 4-((((1,5-dimethyl-3-oxo-2-phenyl-2,3-dihydro-1H-pyrazol-4-yl)imino)methyl)benzonitrile **(3h)**
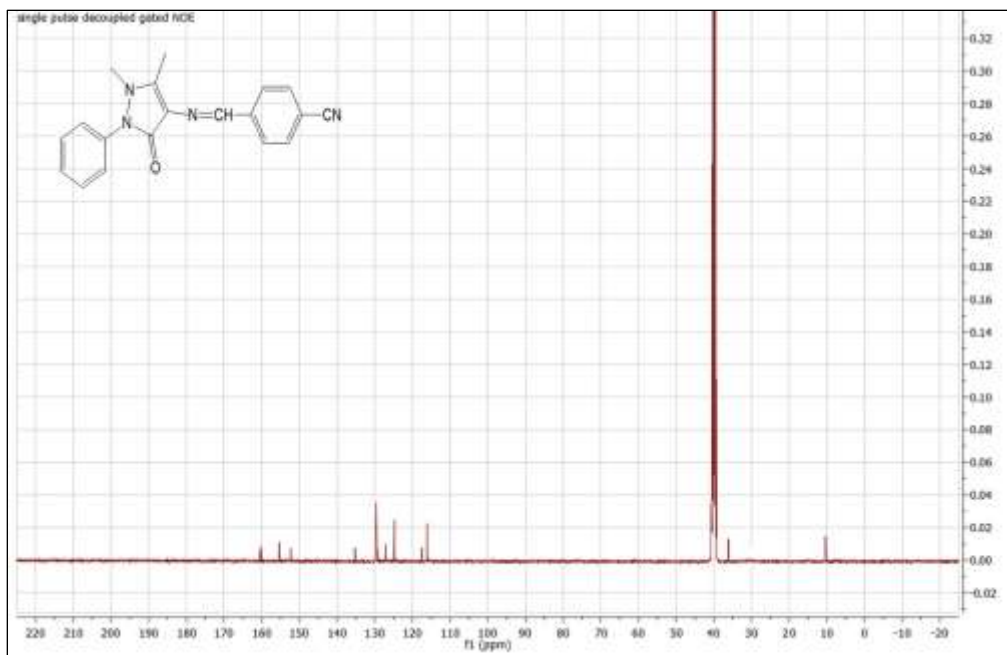
Figure 2.32 ¹³C NMR spectrum of 4-(((1,5-dimethyl-3-oxo-2-phenyl-2,3-dihydro-1H-pyrazol-4-yl)imino)methyl)benzonitrile **(3h)**
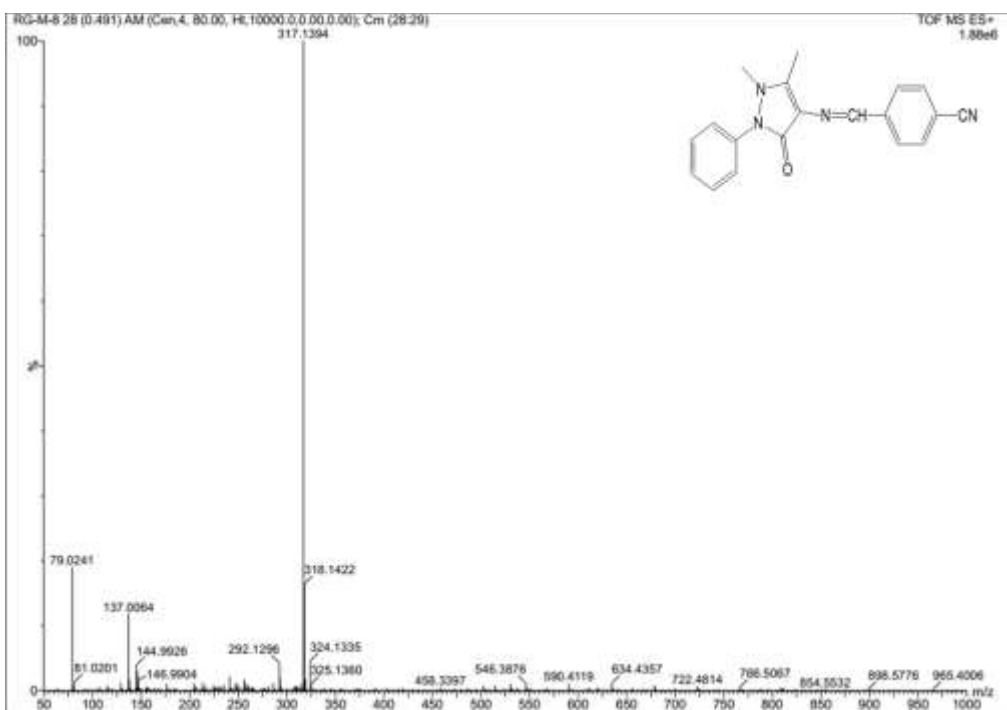
Figure 2.33 ESI mass spectrum of 4-(((1,5-dimethyl-3-oxo-2-phenyl-2,3-dihydro-1H-pyrazol-4-yl)imino)methyl)benzonitrile **(3h)**
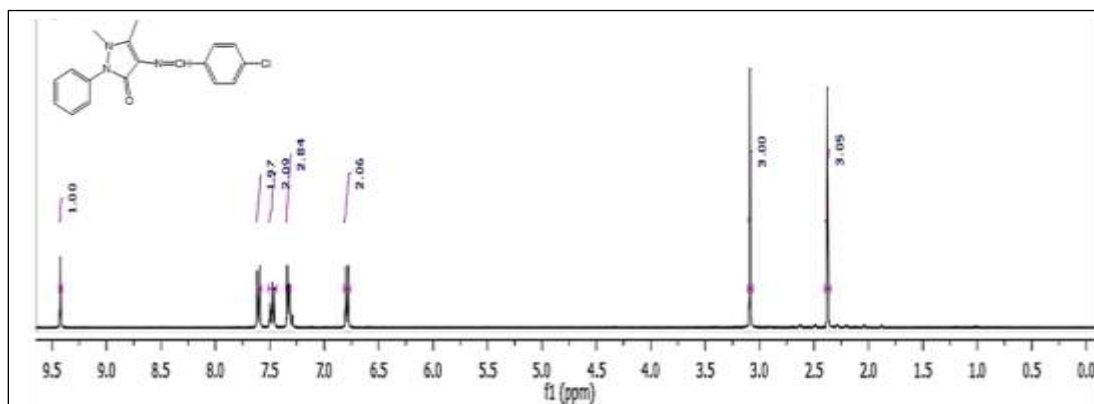
Figure 2.34 ^{1}H NMR spectrum of 4-((4-chlorobenzylidene)amino)-1,5-dimethyl-2-phenyl-1H-pyrazol-3(2H)-one **(3i)**
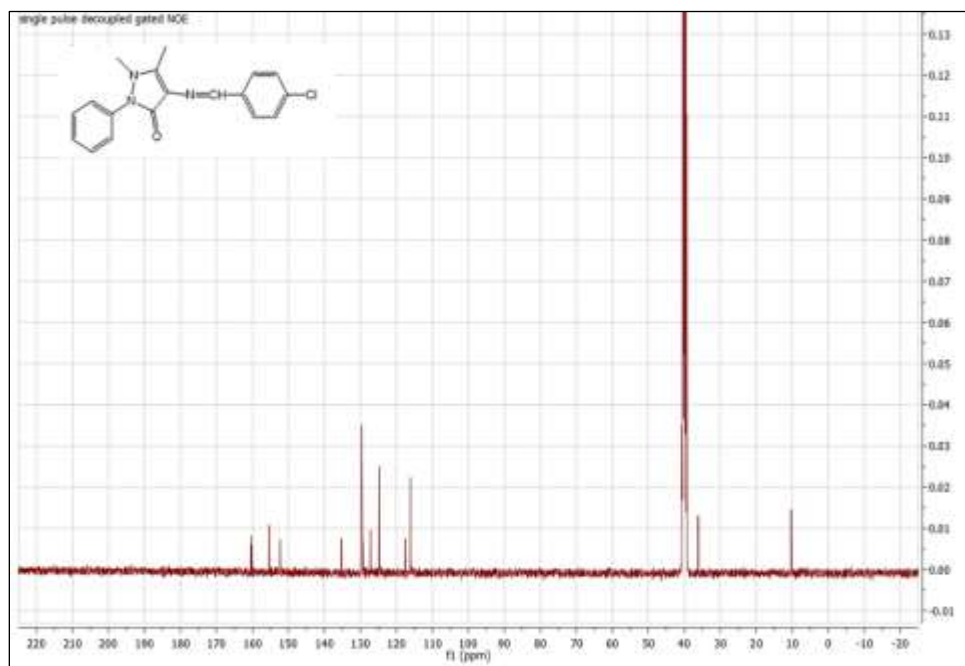
Figure 2.35 ^{13}C NMR spectrum of 4-((4-chlorobenzylidene)amino)-1,5-dimethyl-2-phenyl-1H-pyrazol-3(2H)-one **(3i)**
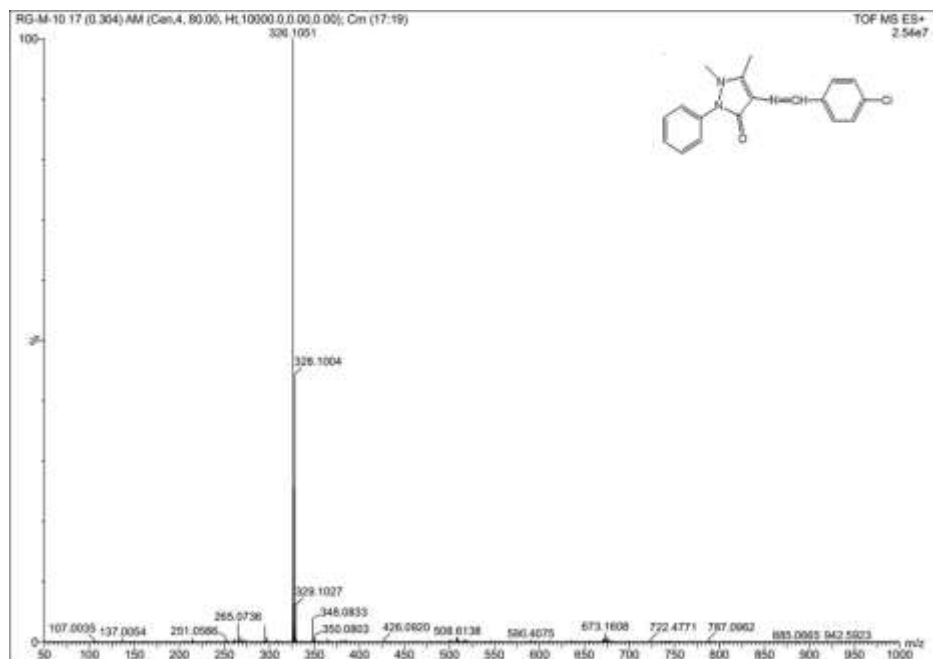
Figure 2.36 ESI mass spectrum of 4-((4-chlorobenzylidene)amino)-1,5-dimethyl-2-phenyl-1H-pyrazol-3(2H)-one **(3i)**
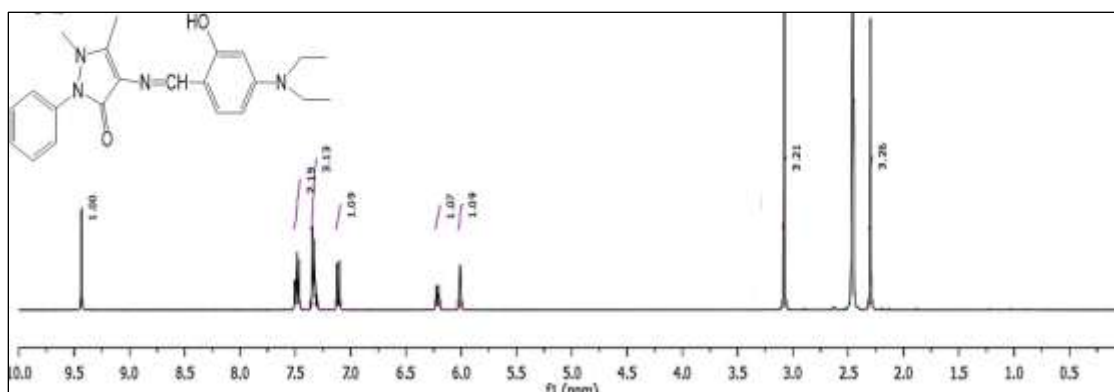
Figure 2.37 ^{1}H NMR spectrum of 4-((4-(diethylamino)-2-hydroxybenzylidene)amino)-1,5-dimethyl-2-phenyl-1H-pyrazol-3(2H)-one **(3j)**
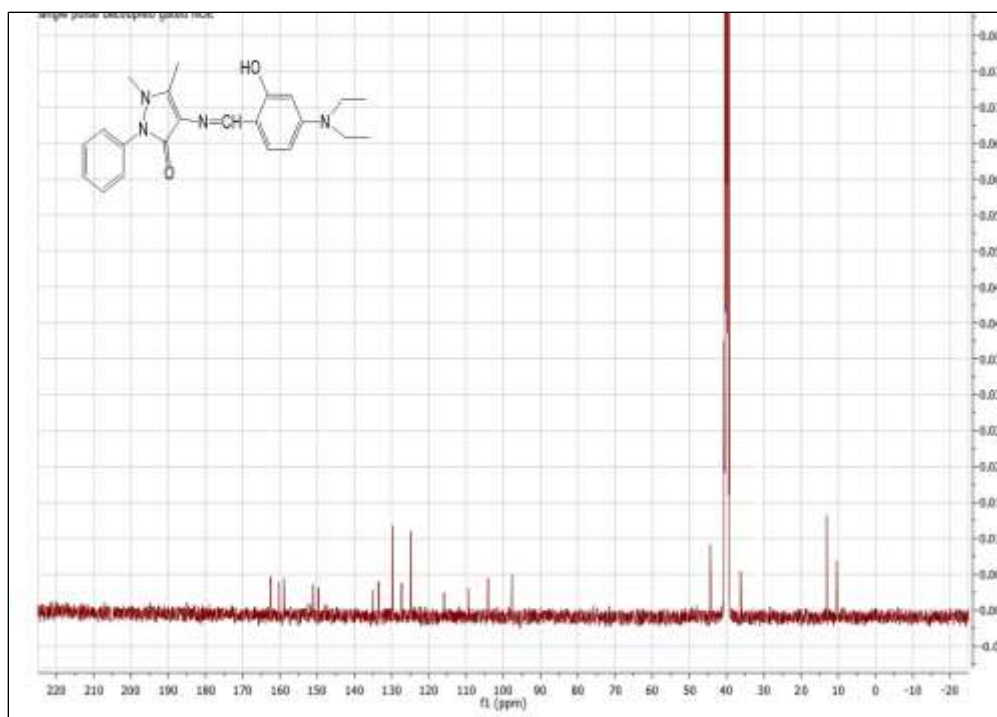
Figure 2.38 ^{13}C NMR spectrum of 4-((4-(diethylamino)-2-hydroxybenzylidene)amino)-1,5-dimethyl-2-phenyl-1H-pyrazol-3(2H)-one **(3j)**
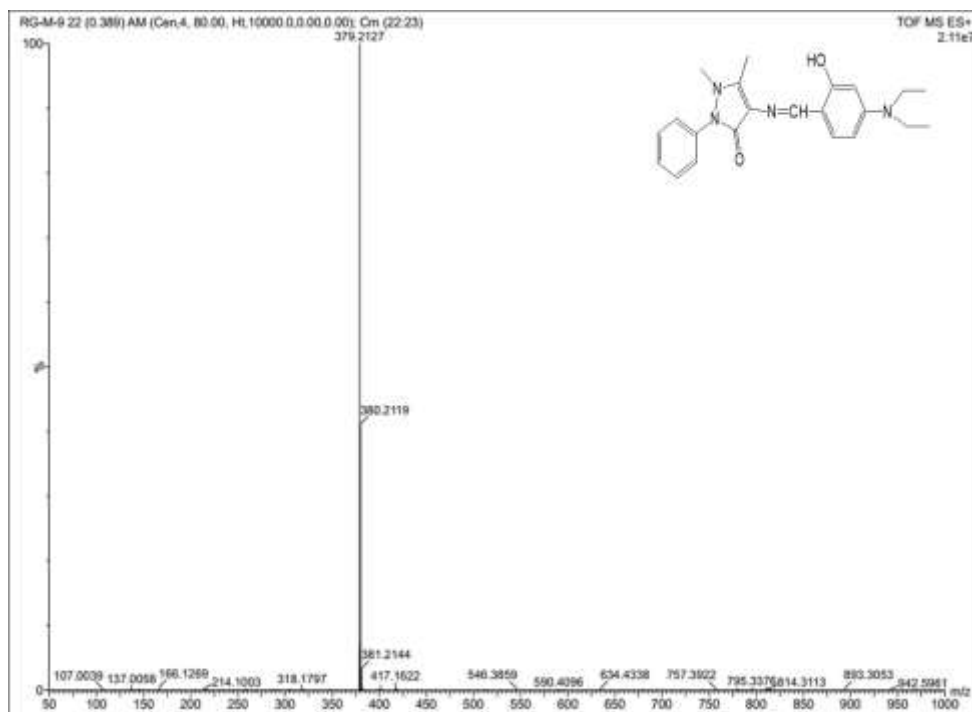
Figure 2.39 ESI mass spectrum of 4-((4-(diethylamino)-2-hydroxybenzylidene)amino)-1,5-dimethyl-2-phenyl-1H-pyrazol-3(2H)-one **(3j)**
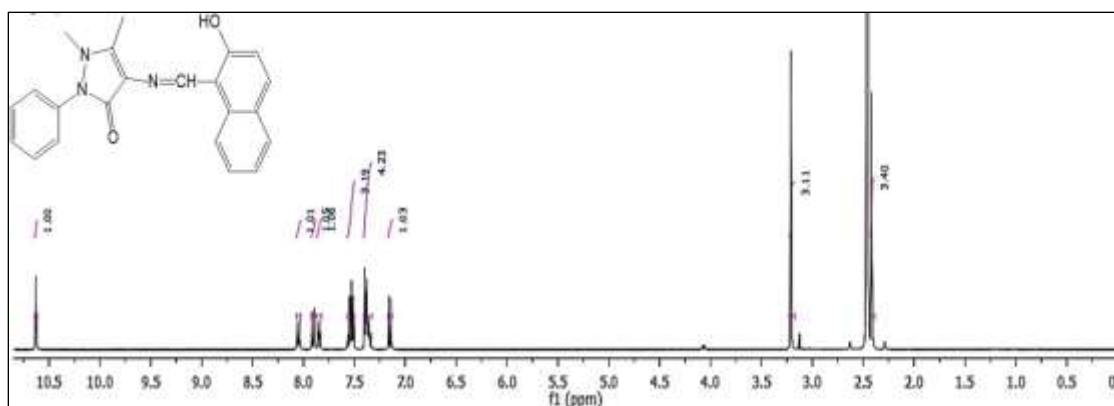
Figure 2.40 ¹H NMR spectrum of 4-(((2-hydroxynaphthalen-1-yl)methylene)amino)-1,5-dimethyl-2-phenyl-1H-pyrazol-3(2H)-one **(3k)**
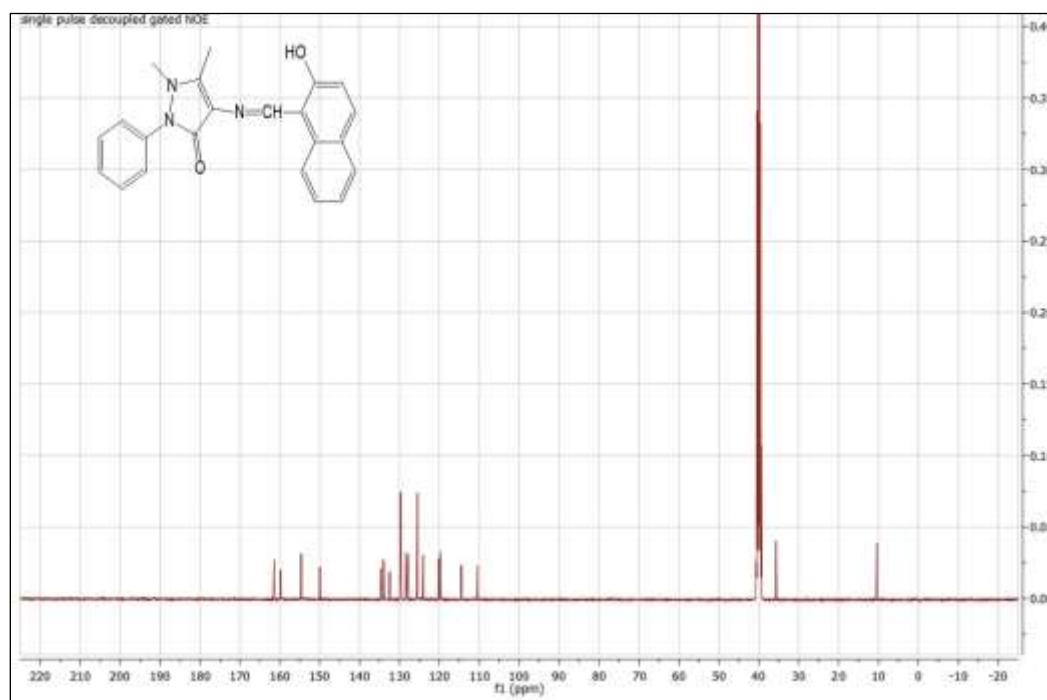
Figure 2.41 ¹³C NMR spectrum of 4-(((2-hydroxynaphthalen-1-yl)methylene)amino)-1,5-dimethyl-2-phenyl-1H-pyrazol-3(2H)-one **(3k)**
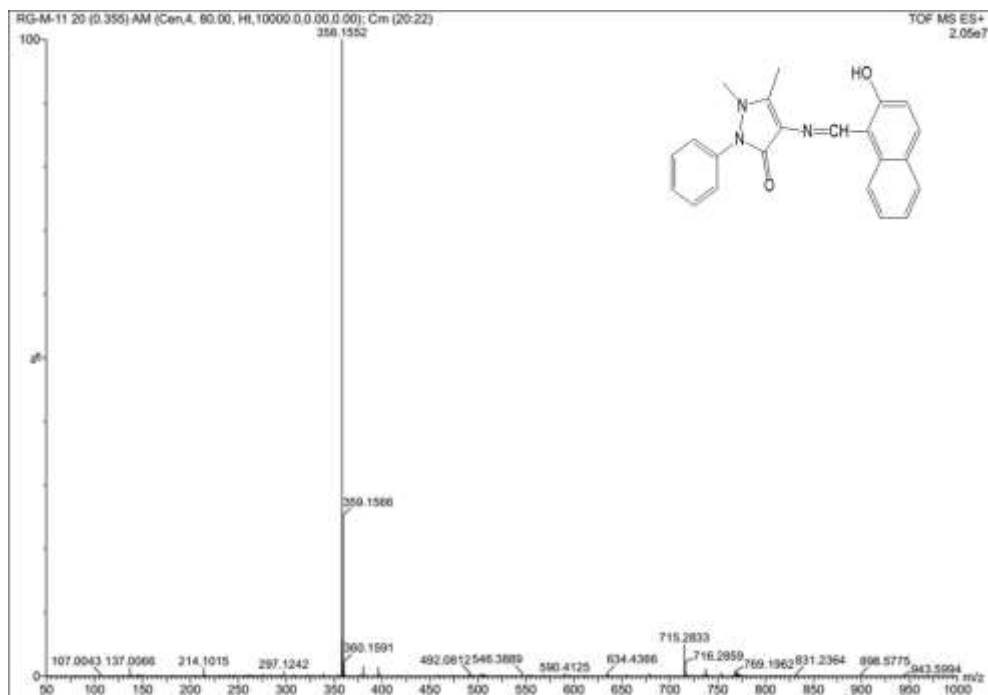
Figure 2.42 ESI mass spectrum of 4-(((2-hydroxynaphthalen-1-yl)methylene)amino)-1,5-dimethyl-2-phenyl-1H-pyrazol-3(2H)-one **(3k)**

2.4 Conclusion

We have developed a green protocol for the synthesis of biological active Schiff's base. These Schiff's bases have been synthesized using antipyrine and various aromatic aldehyde derivatives catalysed by citric acid@MNPs which has been recovered and reused upto 8 cycles without any significant loss in yield. On the basis of presented results, the investigated compounds **3a-k** can be considered as good source of antioxidants. This study could be beneficial for the development of such heterocyclic moiety containing derived compounds for pharmaceutical applications.

2.5 References

[1] Sharma, J.; Bansal, R.; Soni, P. K.; Singh, S.; Halve, A. K. *Asian J. Nano. Mat.* **2018**, *1*, 135.

[2] Sorbiun, M.; Mehr, S. E.; Ramazani, A.; Fardood, S. T. *Int. J. Environ. Res.* **2018**, *1*, 29.

[3] Saeedi, H.; Taghizadeh, M. J.; Afghahi, S. S. S. *Asian J. Nano. Mat.* **2018**, *1*, 74.

[4] Ahmadi, F.; Hekmati, M.; Yousefi, M.; Veisi, H. *Asian J. Nano. Mat.* **2018**, *1*, 104.

[5] Atrak, K.; Ramazani, A.; Fardood, S. T. *J. Mater. Sci. Mater. Electron.* **2018**, *8*, 6702.

[6] Atrak, K.; Ramazani, A.; Fardood, S. T. *J. Mater. Sci. Mater. Electron.* **2018,** *10*, 8347.

[7] Moradi, S.; Fardood, S. T.; Ramazani, A. *J. Mater. Sci. Mater. Electron.* **2018**, *16*, 14151.

[8] Sorbiun, M.; Mehr, S. E.; Ramazani, A.; Fardood, S. T. *J. Mater. Sci. Mater. Electron.* **2017**, 123456789.

[9] Mehr, S. E.; Sorbiun, M.; Ramazani, A.; Fardood, S. T. *J. Mater. Sci. Mater. Electron.* **2017**.

[10] Mehr, S. E.; Sorbiun, M.; Ramazani, A.; Fardood, S. T. *J. Mater. Sci. Mater. Electron.* **2017**.

[11] Fardood, S. T.; Golfar, Z.; Ramazani, A. *J. Mater. Sci. Mater. Electron.* **2017**, *18*, 13596.

[12] Tobin, Z. M.; Posada, L. F.; Bechu, A. M.; Carroll, M. K.; Bouck, R. M.; Anderson, A. M.; Bruno, B. A. *J. Sol-Gel Sci. Technol*. **2017**, *2*, 432.

[13] Fani, M.; Ghandehari, F.; Rezayi, M. *J. Med. Chem. Sci.* **2018**, *1*, 28.

[14] Alem, M.; Teimouri, A.; Salavati, H.; Kazemi, S. *Chem. Methodol.* **2017**, *1*, 49.

[15] Hasani, H.; Irizeh, M. *Asian J. Green Chem.* **2018**, *2*, 85.

[16] Mohammadi, B.; Salmani, L. *Asian J. Green Chem.* **2018**, *2*, 51.

[17] Ahankar, H.; Ramazani, A.; Ślepokura, K.; Lis, T. *Turk. J. Chem*. **2018**, 719.

[18] Aghahosseini, H.; Ramazani, A.; Ślepokura, K.; Lis, T. *J. Colloid Interface Sci.*, **2018,** *511*, 222.

[19] Motamedi, R.; Bardajee, G. R.; Rad, S. M. *Asian J. Green Chem.* **2017**, *1*, 89.

[20] Mirzaie, A. *J. Med. Chem. Sci.* **2018**, *1*, 5.

[21] Aghahosseini, H.; Rezaei, S. J. T.; Tadayyon, M.; Ramazani, A.; Amani, V.; Ahmadi, R.; Abdolahnjadian, D. *Eur. J. Inorg. Chem.* **2018**, *22*, 2589.

[22] Sajjadifar, S. *Chem. Methodol.* **2017**, *1*, 1.

[23] Baig, R. B. N.; Varma, R. S. ***Chem. Commun.*** **2013**, *49*, 752.

[24] Khalafi-Nezhad, A.; Nourisefat, M.; Panahi, F. *Org. Biomol. Chem.* **2015**, *13***,** 7772.

[25] Nasr-esfahani, M.; Rafiee, Z.; Montazerozohori, M.; Kashi, H. *RSC Adv.* **2016**, *6*, 47298.

[26] Abu-Dief, A. M.; Abdel-Fatah, S. M. *J. Basic Appl. Sci.* **2018**, *7*, 55.

[27] Mosayebi, J.; Kiyasatfar, M.; Laurent, S. *Adv. Healthcare Mater*. **2017**, *1700306*, 1.

[28] Cheraghipour, E.; Javadpour, S.; Mehdizadeh, A. R. *J. Biomed. Sci. Eng*. **2012**, *5*, 715.

[29] Şenol, D. *J. Biol. &amp* Chem. **2017**, *45*, 67.

[30] Zoubi, W. A.; Ko Y. G. *Appl. Organomet. Chem.* **2017**, *31*, 1.

[31] Sabaa, M. W.; Mohamed, R. R.; Oraby, E. H. *Eur. Polym. J.* **2009**, *45,* 3073.

[32] Kajal, A.; Bala, S.; Kamboj, S.; Sharma, N.; Saini, V. *J. Catal.* **2013**, 1.

[33] Fenoll, S.; Navarro-Fuster, V*.;* Ortuño, M.; Serrano, J. L.; Márquez, A.; Gallego, I. P.; Beléndez, A. *Polymers.* **2017**, *9*, 298.

[34] Li, H.; Liu, C.; Dai, B.; Tang, X.; Zhang, Z. J.; Xiong, Z.; Liu, X. *J. Appl. Polym. Sci.* **2015.**

[35] Herraiz, M. L.; Martínez, E. C.; González, J. C.; Carrasco, J.; Rojo, T.; Armand, M. *Energy & Environmental Science.*

[36] Brodowska, K.; Chruścińska, E. L. *Chemik.* **2014**, 68, *2*, 129.

[37] Wen, H.; Niu, H.; Ma, B. X.; Bai, X. Y.; Wang, W. Z. *Synth. Met.* **2015**, *202*, 89.

[38] Deshmukh, P.; Soni, P. K.; Kankoriya, A.; Halve, A. K.; Dixit, R. *Int. J. Pharm. Sci. Rev. Res.* **2015**, *26*, 162.

[39] Chakraborty, M.; Baweja, S.; Bhagat, S.; Chundawat, T. S. *Int. J. Chem. React. Eng.* **2012***, 10, A53.*

[40] Thomas, A. B.; Tupe, P. N.; Badhe, R. V.; Nanda, R. K.; Kothapalli, L. P.; Paradkar, O. D.; Sharma, P. A.; Deshpande, A. D. *Green Chem. Lett. Rev.* **2009**, *2*, 23.

[41] Venkatesan, K.; Satyanarayana, V. S. V.; Sivakumar, A. *J. Chin. Chem. Soc.* **2011**, *58*, 583.

[42] Ghonchepour, E.; Yazdani, E.; Saberi, D.; Arefi, M.; Heydari, A. *Appl. Organometal. Chem.* **2017**, *12*, 1.

[43] Yazdani, F.; Seddigh, M. *Mater. Chem. Phys.* **2016**, *184*, 318.

[44] Cheraghipour, E.; Javadpour, S.; Mehdizadeh, A. R. *J. Biomed. Sci. Eng.* **2012**, 5, 715.

[45] Nigam, S.; Barick, K. C.; Bahadur, D. *J. Magn. Magn. Mater.* **2011**, 323, 237.

[46] Kaur, R.; Kaur, K., Bansal, M. *Asian J. Chem.* **2016**, *28*, 1921.

[47] Alam, M. S.; Choi J. H.; Lee D. U. *Bioorg. Med. Chem.* **2012,** *20*, 4103.

[48] Ali, P.; Meshram, J.; Sheikh, J.; Tiwari, V.; Rajendra Dongre, R.; Ben Hadda, T. *Med. Chem. Res.* **2012**, *21*, 157.

[49] Maity, S.; Shyamal, M.; Das, D.; Mazumdar, P.; Sahoo, G. P.; Misra, A. *Sensors and Actuators B*, **2017**, *248*, 223.

Chapter - 3

Synthesis of Fe$_3$O$_4$-DOPA-Cu Magnetically Separable Nanocatalyst: A Versatile and Robust Catalyst for an Array of Sustainable Multicomponent Reactions under Microwave Irradiation
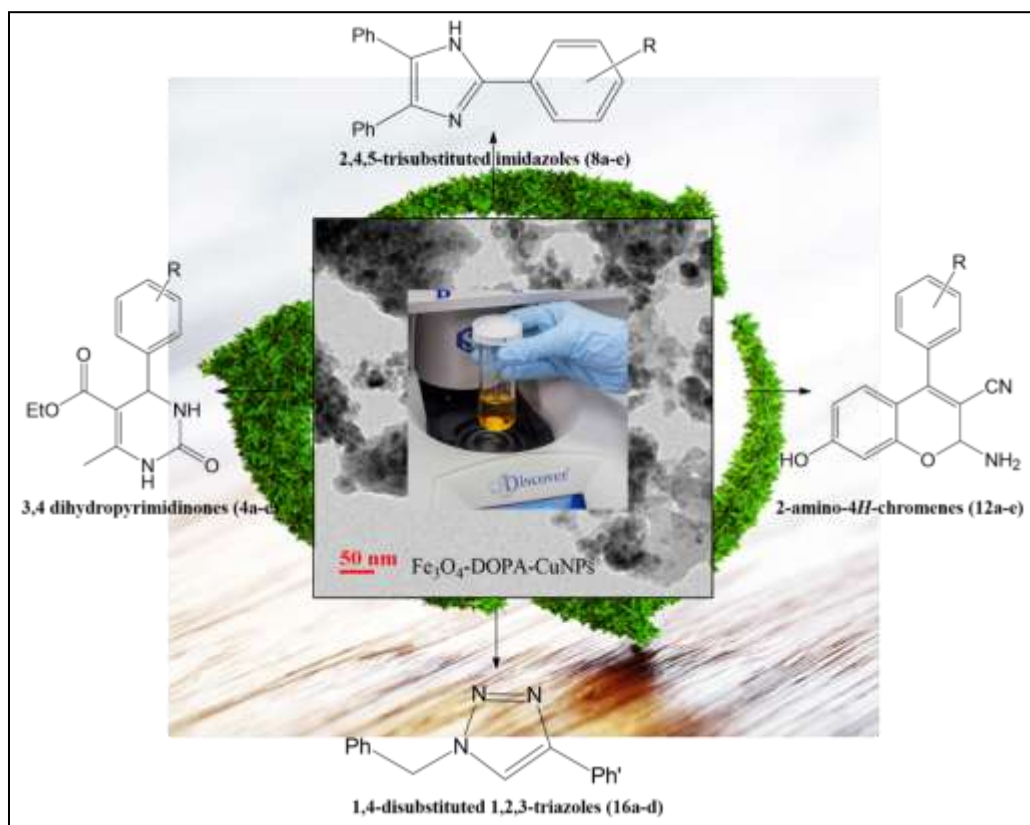
3.1 Introduction

MNPs have emerged as viable alternatives to conventional materials as robust, readily available, high surface area heterogeneous catalyst supports [1- 2]. Recently MNPs have found remarkable niche in diverse areas ranging from magnetic resonance imaging, magnetic targeting drug delivery to chemical catalysis, they increasingly serve as catalyst supports or are incorporated in the hybrid nanocomposite as sustainable catalyst for convenient separation and recycling [3-5]. Bare MNPs due to their inherent instability and hydrophobic nature results in big clusters over time in the absence of any surface coating which reduces their surface energy [6]. Therefore it needs to be minimized by surface immobilization of MNPs with biocompatible and organic and inorganic materials which protects them from being oxidized and provides them stability against damage during or after being used in organic transformations [7-9]. However most of the techniques require several steps to introduce functional groups to the magnetic surface and often involve the use of organosilica precursors as an organic shell to prepare a suitable support for incorporation of different transition metal ions [10-11]. Therefore, the preparation of modified MNPs *via* simple method and without using organoalkoxysiloxane compounds is highly desirable from both an environmental and economic point of view. The chemistry of copper is extremely rich because it can easily access Cu°, Cu^{I}, Cu^{II}, and Cu^{III} oxidation states allowing it to act through one electron or two electron process. This unique characteristic of Cu based nanocatalyst have made it suitable for many applications in nanotechnology, including catalytic organic transformations, electrocatalysis and photocatalysis. Because of the leaching effect and poor recyclability neat metal and oxide must be incorporated on some supports [12-13]. In this respect, we introduce a simple and facile ultrasonication method for synthesis of highly water-dispersible magnetic nanoparticles, end-functionalized with non-toxic, biodegradable L-DOPA (L-3,4- dihydroxyphenylalanine) having amino and carboxyl groups as these are the most attractive functional groups, which are especially suitable for the immobilization of Cu nanoparticles. Multicomponent reactions (MCRs) whereby three or more reactants come together in a single vessel to create extremely ideal route for rapidly creating a library of diverse heterocyclic scaffolds. These reactions are highly atom economic since target compound obtained in one pot with much fewer steps containing all the atoms which are present in the substrates [14]. The combination of magnetic nanocatalyst and multicomponent reactions is an

attractive research area and is an ideal blend for the development of sustainable methods in green synthetic chemistry **[15].** In view of this we have investigated the catalytic activity of the synthesized Fe_3O_4-DOPA-Cu nanocatalyst towards four important multicomponent reactions: (i) 'Biginelli reaction' for the synthesis of DHPMs derivatives (ii) synthesis of 2,4,5-trisubstituted imidazole (iii) synthesis of 2-amino-4*H*- chromene and (iv) 'Click reaction' for the synthesis of 1,2,3 triazole derivatives.

Synthesis of DPHM and derivatives are important because of their wide range pharmaceutical and therapeutic applications such as calcium channel blockers, anti-inflammatory agents, antihypertensive, anti-tumor, adrenergic and neuropeptide antagonists **[16-20]** etc. Biginelli multicomponent reaction pathway is the most direct and elegant methodology for synthesis of DHPMs. Imidazoles have various biological applications as they are well known to anti-inflammatory, antiparasitic, antifungal, antiviral **[21]**, in addition they are used in photography as photosensitive compounds **[22]**, selective antagonists of the glucagon receptors and inhibitors of the IL-1 biosynthesis **[23]**. They are also the core structural skeleton in many important biological molecules like histidine, histamine, and biotin, as well as several drug moieties such as trifenagrel, eprosartan, and losartan **[24]**. The 4H-chromenes are major classes of natural oxygen-containing heterocyclic compounds, which are extensively found in ripe fruits and vegetables. Because of their different biological and pharmacological activities such as antioxidant, antileishmanial, antibacterial, antifungal, hypotensive, anticoagulant, antiviral, diuretic, antiallergenic, and antitumor activities **[25-34]**, these compounds have occupied a key place in drug research. Synthesis of 1,4-disubstituted 1,2,3-triazoles by 'click reaction' has gained immense interest because it acts as scaffold for large number of biological active chemicals, pharmaceuticals, agrochemicals, drug molecules with significant anti-HIV activity, anti-microbial activity against Gram positive bacteria etc. **[35-37]**. Most of the synthetic methods are associated with one or more disadvantages such as using expensive reagents, prolonged reaction time, low yield of products, complex work-up procedures, formation of undesirable side products which can be resolved by microwave-assisted organic synthesis which is one of the most powerful and sustainable tools in synthetic chemistry due to its specific features including efficient atomic utilization, improved temperature regulation, reaction homogeneity, lesser reaction time and high product yield **[38-39]**. Inspite of all these factors, one more factor that is tedious recoverability of the catalyst particles hamper the sustainability and economics of the

nanocatalytic strategy. Therefore to address all these issue, the development of such catalyst which will exhibit high catalytic activity along with easy recyclability and reusability for the synthesis of above described important MCRs is highly needed. So in continuation of our research endeavours towards the development of sustainable protocols and application of nanocatalyst **[40-41]**, herein we report on a highly efficient, versatile magnetically separable and recyclable Fe_3O_4-DOPA-Cu catalyst towards four important multicomponent reactions.

3. 2 Results and Discussion

3.2.1 Characterization of the Fe_3O_4-DOPA-Cu nanocatalyst

In the present protocol, we have synthesized an efficient and magnetically recoverable catalyst, Fe_3O_4-DOPA-CuNPs and the detail process of its preparation described in experimental section under synthesis part. Firstly Fe_3O_4 nanoparticles were prepared by the co-precipitation method and were reacted with L-3,4 dihydroxyphenylalanine (L-DOPA) in water to yield the Fe_3O_4-DOPA and these obtained nanoparticles were further metallated with copper chloride in the presence of aqueous $NaBH_4$ solution to obtained the final copper decorated L-DOPA functionalized magnetic nanoparticles. The synthesized catalyst was characterized by various techniques such as FTIR, SEM-EDS, HRTEM, XPS, VSM, PXRD and TGA.
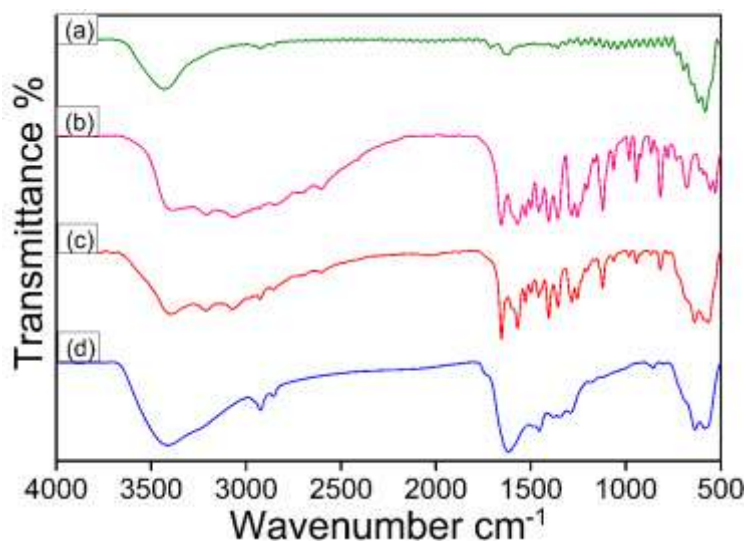
Figure 3.1 FTIR spectrum of (a) Fe_3O_4 (b) L-DOPA (c) Fe_3O_4-DOPA (d) Fe_3O_4-DOPA-CuNPs

FTIR is one of the best technique to characterize the functionalization and modification of magnetite nanoparticles. The FTIR spectrum of the magnetite, L-DOPA, Fe_3O_4-DOPA and Fe_3O_4-DOPA-Cu nanocomposites were recorded to confirm the modification of the magnetite surface with the L-DOPA and metal ion (**Figure 3.1(a) – (d)**). The IR spectrum of Fe_3O_4 shows a broad band at 578 cm^{-1} due to the Fe-O stretching vibrational mode [43], **Figure 3.1 (a)**. The IR spectrum of L-DOPA show a peak at 1656 cm^{-1} due to C=O stretching of carboxylic acid. The IR bands appearing at about 3408 cm^{-1} and 679 cm^{-1} correspond to the N-H stretching and bending vibration mode of L-DOPA as shown in **Figure 3.1 (b)**. Fe_3O_4-DOPA shows IR peak at 3402, 3206, 3071, 2919, 2840, 1651, 1465, 1405, 1274, 561 cm^{-1}. It has been observed that the stretching vibrational mode of the C-H of CH_2 group of L-DOPA appeared at 2919 cm^{-1} and 2840 cm^{-1} while the bending vibrational mode appeared at 1465 cm^{-1} [44]. Moreover, IR peaks at 1651 cm^{-1} and 1405 cm^{-1} could be ascribed to the carboxylate group of L-DOPA whereas the IR peak at 1274 cm^{-1} to the C-O stretching vibrational mode of the carboxylate group [43]. These results show that a large number of L-DOPA molecules are grafted over the Fe_3O_4 support. In terms of Fe_3O_4-DOPA-Cu (**Figure 3.1 (d)**), all the peaks become broaden and appears as band , and one of the noticeable change was a red shift of the band at 1651 cm^{-1} was observed (1651 cm^{-1} to 1617 cm^{-1}), which was probably characteristic of the asymmetrical fluctuations of the carbonyl group after interaction with the metal ion [45]. Overall, the IR results suggested that Cu was successfully immobilized onto the surface of Fe_3O_4-DOPA nanoparticles.
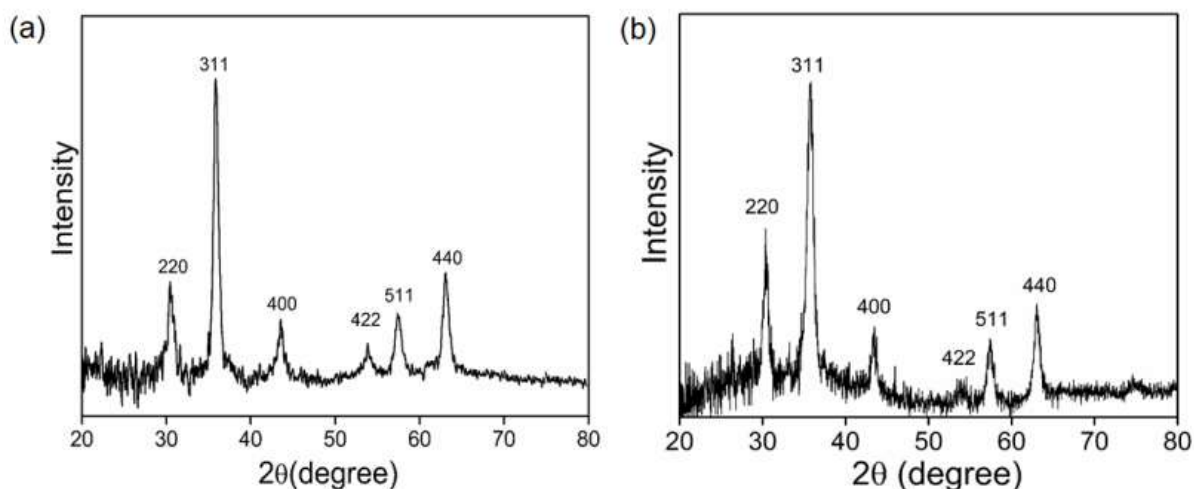
Figure 3.2 XRD of (a) Fe_3O_4 (b) Fe_3O_4-DOPA-CuNPs

The crystalline structure of Fe_3O_4 and Fe_3O_4-DOPA-CuNPs were analysed by powder X-ray diffraction (XRD). As displayed in **Figure 3.2 (a)** and **(b)**, according to the JCPDS card no. 19-0629, all the samples show diffraction peaks at around 30.4°, 35.5°, 43.3°, 53.4°, 57.2° and 62.8° which can be assigned to diffraction of Fe_3O_4 crystal with an inverse spinal structure from the (220), (311), (400), (422), (511), and (440) faces of the crystals, respectively. On assessment of the diffractograms of nanoparticles, the very distinguishable FCC peaks of the magnetite crystal were not changed, which means that these particles have phase stability, but there is a slight decrease in the intensity with broadening of the corresponding peak. The signals of Cu metal were not detected in XRD, indicating that Cu species is highly dispersed on ferrites.
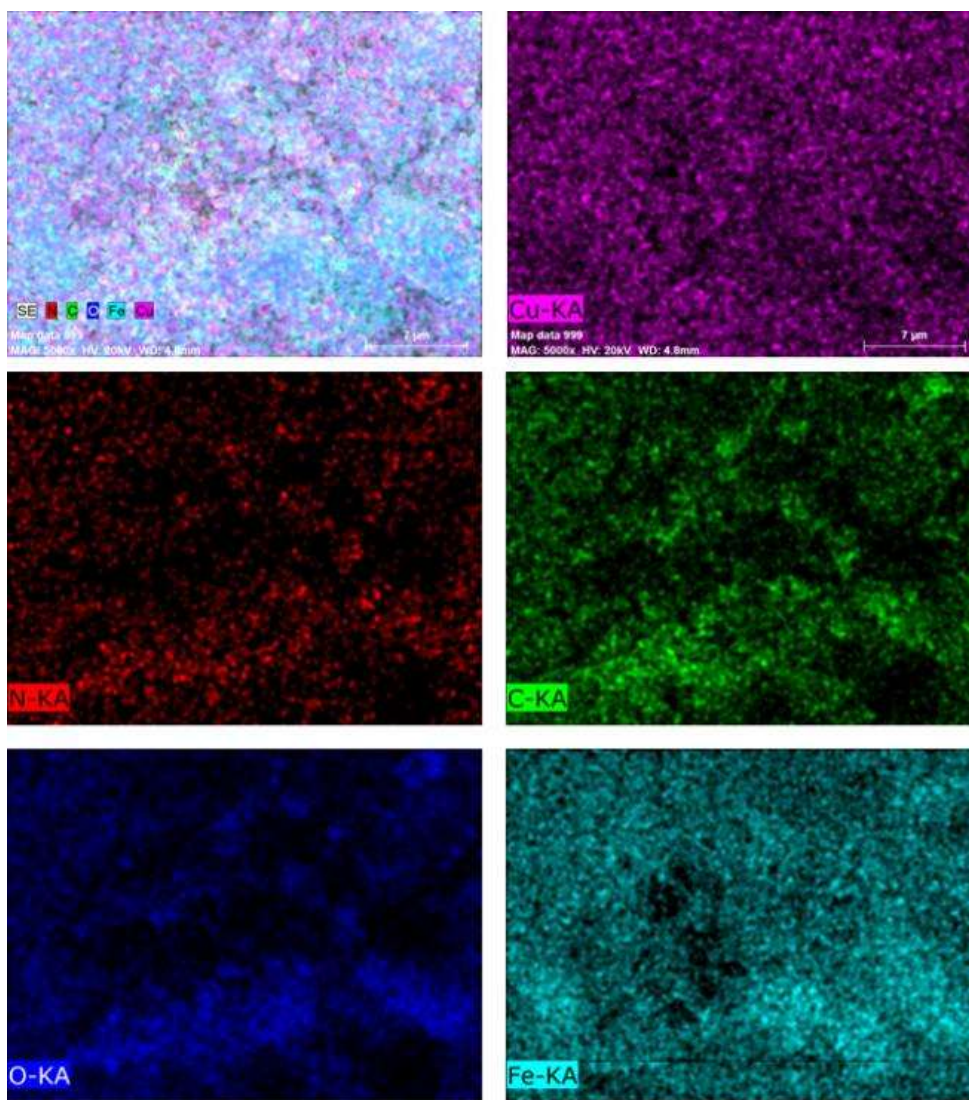
Figure 3.3 EDS elemental mapping of the Fe_3O_4-DOPA-CuNPs

Furthermore, the chemical composition of the Fe_3O_4-DOPA-Cu nanocomposite was determined by energy X-ray spectroscopy (SEM-EDX). The presence of C, N, O, Fe and copper centers in the nanocomposite was confirmed by elemental mapping images **(Figure 3.3).** The result showed uniform distribution of Cu nanoparticles over the structure of the L-DOPA supported magnetite nanoparticles. The percentage of each element present in nanocatalyst were obtained from energy dispersive X-ray spectrum and the results obtained were in good agreement with the proposed catalyst composition **(Figure 3.4)**.
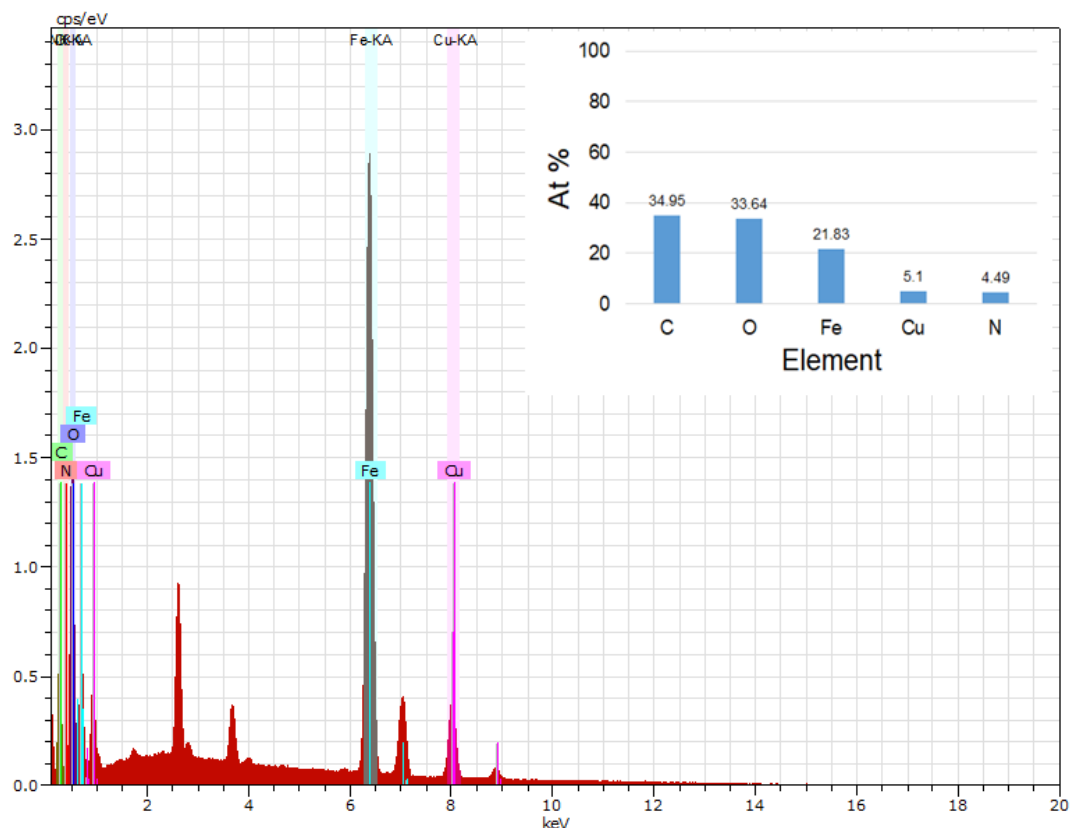
Figure 3.4 EDS spectrum of Fe_3O_4-DOPA-CuNPs
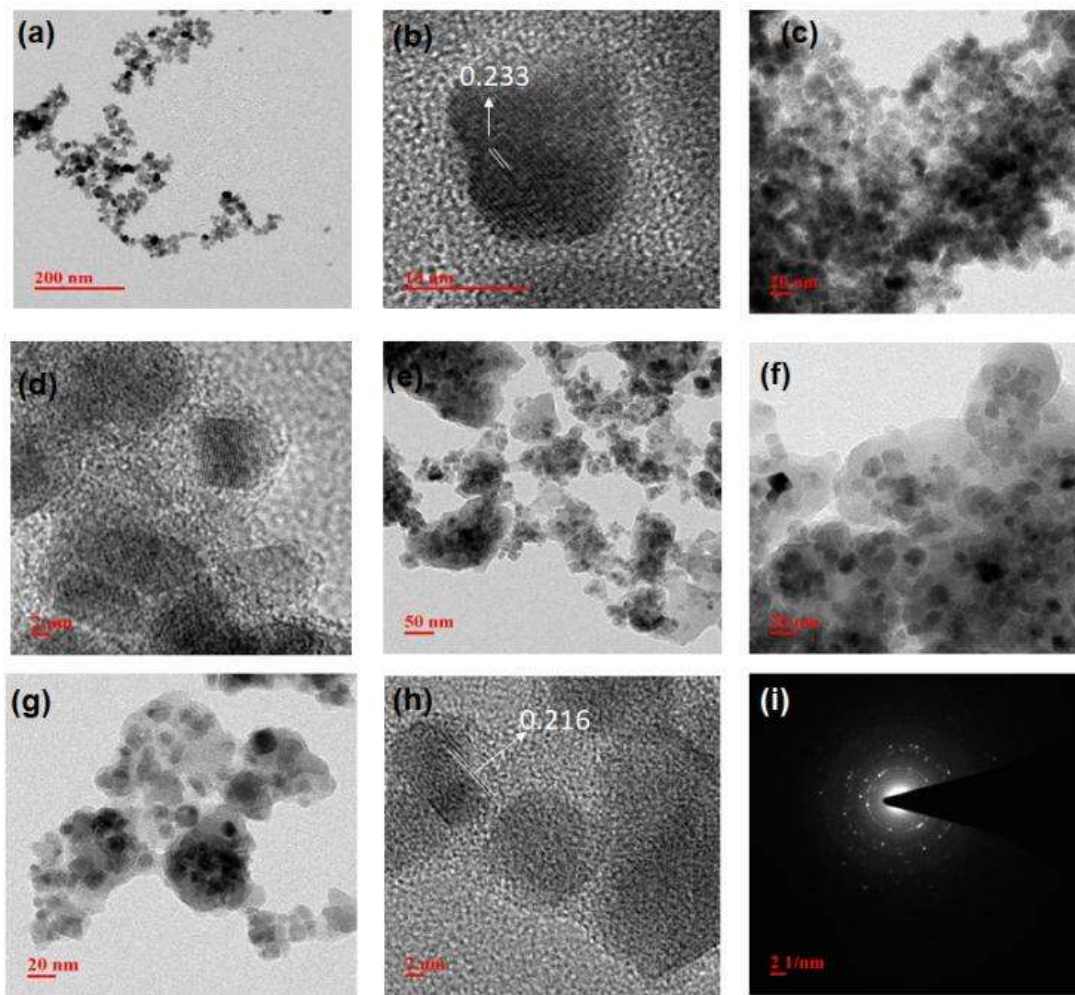
Figure 3.5 (a) TEM image of Fe_3O_4 (b) HRTEM image of Fe_3O_4 (c) TEM image of Fe_3O_4 – DOPA (d) HRTEM image of Fe_3O_4 (e), (f) and (g) TEM image of Fe_3O_4- DOPA-CuNPs (h) HRTEM image of Fe_3O_4- DOPA-CuNPs (i) SAED pattern of the of Fe_3O_4-DOPA-CuNPs

TEM image of the Fe_3O_4-DOPA-Cu nanocatalyst shows a somewhat spherical morphology, with some cubic partials, and an average size range of 8-20 nm with a mean particle size of 12 nm. The HRTEM image in **Figure 3.5 (b)** shows the characteristic lattice fringes of Fe_3O_4 nanoparticles with the d-spacing of 0.233 nm corresponds to the [311] plane of Fe_3O_4 **[46]**. Additional HRTEM image (**Figure 3.5 (h)**) of Fe_3O_4-DOPA-Cu showed the lattice fringes with an interplanar spacing of approximately 0.216 nm corresponding to the [111] lattice plane of metallic Cu **[47]**. **Figure 3.5 (i)** showed selected area electron diffraction pattern of the Fe_3O_4-DOPA-Cu nanocatalyst which revealed its polycrystalline nature.
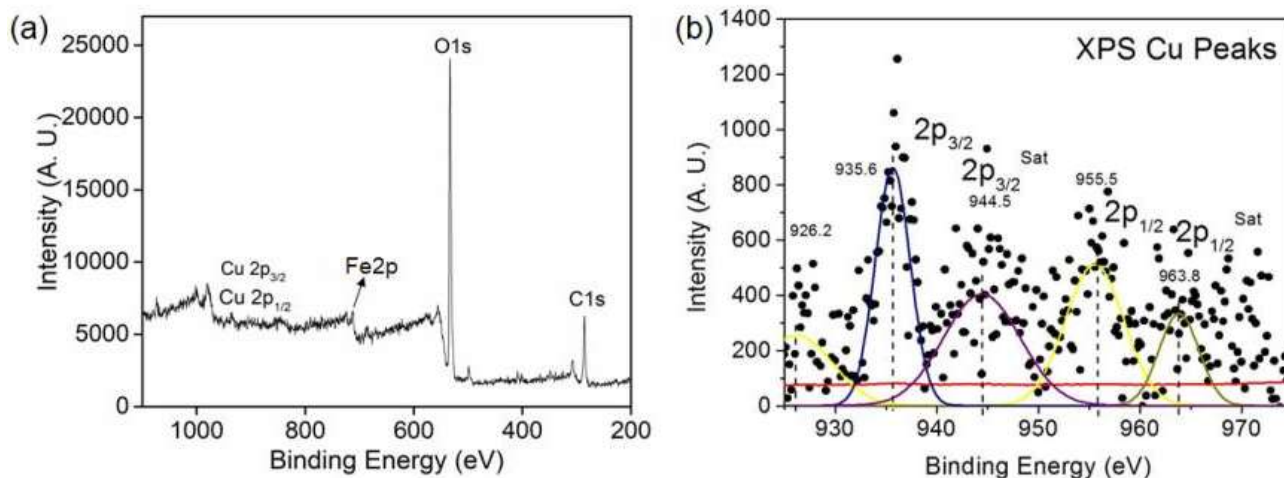
Figure 3.6 X-ray photoelectron spectrum of Fe_3O_4-DOPA-CuNPs showing Cu 2p3/2 and Cu 2p1/2 binding energies

In order to provide further evidence of the formation of Cu^{2+} complex over the iron oxide core and to determine the oxidation state of copper, the XPS resolution spectroscopy have been investigated. For a better understanding of the oxidation state of copper, the binding energy obtained from the catalyst was compared with the Cu^{2+} $2p_{3/2}$ and $2p_{1/2}$ peak positions. The binding energies of the main peaks were about 935.6 eV and 955.5 eV due to Cu $2p_{3/2}$ and $2p_{1/2}$, respectively [48]. Two other peaks were also obtained at 944.5 eV and 963.8 eV that attributed to the Cu $2p_{3/2}$ and $2p_{1/2}$ satellite peaks (**Figure 3.6(b)**). Since all these lie within the given literature, it can be concluded that the oxidation state of copper in the catalyst is +2.
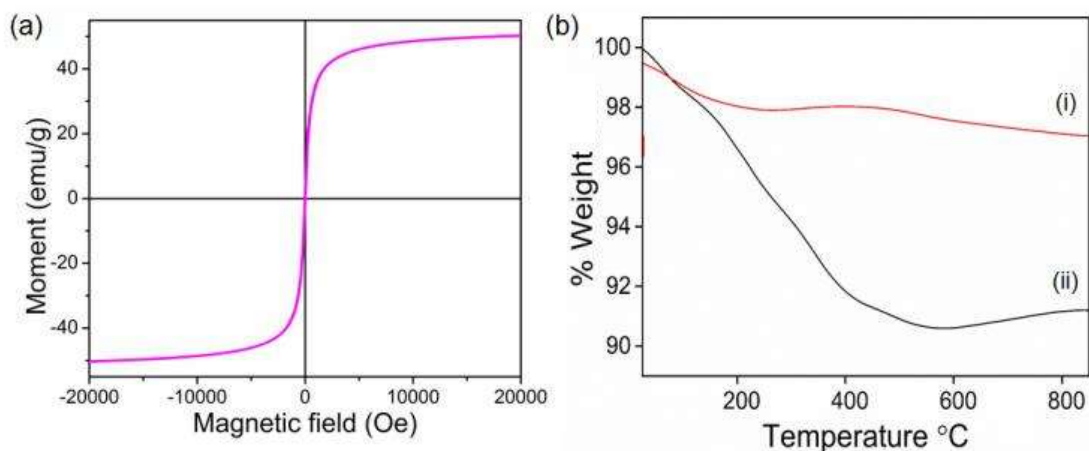
Figure 3.7 (a) Room temperature magnetization curves of Fe_3O_4-DOPA-Cu (b) TGA of (i) Fe_3O_4 (ii) Fe_3O_4-DOPA-CuNPs

Another important parameter for the practical applications of nanoparticles is revealed from the VSM curve shown in **Figure 3.7 (a)**. The hysteresis loops of powdered material showed almost negligible magnetic hysteresis, with both the magnetization and demagnetization curves passing through the origin, which clearly indicates the supermagnetic nature of the materials. This also means that the magnetic material can only be aligned under an applied magnetic field, but it will not retain any residual magnetism upon removal of the field. Thus, Fe_3O_4-DOPA-Cu nanoparticles are sufficiently magnetic so that it can be easily separated from the reaction mixture by using an external magnet. The thermal stability of the synthesized nanocatalyst was also investigated by performing thermogravimetric analysis. The major weight loss was observed after 350 ℃ due to the decomposition of chemisorbed material i.e. L-DOPA. This confirms that thermal stability of the synthesized catalyst maintained at higher temperature.

3.2.2 Catalytic activity

3.2.2.1 Catalytic studies for the synthesis of dihydropyrimidinone (4a-e)

After characterization and demonstration of the structure and morphology of nanocatalyst, we examined its efficiency in the synthesis of 3,4-DHP derivatives under microwave irradiation. The effect of solvent on reaction was examined along with catalyst amounts. Based on the results as shown in **Figure 3.9**, 25 mg of Fe3O4-DOPA-Cu was considered as the optimum amount of catalyst and EtOH/H_2O as best suitable solvent. After the optimization of solvent and catalyst amount, we further examined the effects of the microwave power and temperature on the yield of the reaction. From obtained results depicted in **Figure 3.8**, optimized power of microwave oven was 100 W at 80 °C. When the reaction has been carried out without using any catalyst it showed less yields in optimum time and after increasing time it gives quantitative yield. A comparative study with other synthetic method like conventional and ultrasonication has also been carried out, resulting best yield obtained by microwave irradiation in least reaction time (**Figure 3.10**). Regarding to the obtained desired reaction conditions, we developed the present method for the reaction between benzaldehyde derivatives, ethyl acetoacetate and urea in the presence of optimum amount of catalyst. As shown in **Table 3.1**, products have high to excellent yields both in case of aldehydes bearing electron donating and electron withdrawing groups obtained in shorter reaction time. Products were characterized using physical and spectroscopic methods such as melting point, ^{1}HNMR technique. A proposed mechanism for the formation of

dihydropyrimidines has been given in **Scheme 3.2** based on the mechanism suggested by Kappe **[49]**. Initially the catalyst activated the carbonyl group of aldehyde followed by condensation by urea forming the intermediate A. The role of nanocatalyst is to increase the electrophilicity of carbonyl carbons of both aldehyde and ethylacetoacetate. The formation of enol structure favoured by catalyst can be explained via HSAB theory. Here Cu^{+2} in the nanocatalyst act as harder acid due to the high charge density that is 6.2×10^2 nm^{-3} and the presence of low energy d-orbitals that can be used to hold the free electrons of the oxygen atom of ethylacetoacetate which can act as a base or nucleophile for chemical reactions. After that B intermediate was formed by nucleophilic addition of enol form of β-dicarbonyl to the intermediate A. Finally cyclization to the C intermediate subsequently proceeds by elimination of water to afford final product **[50].**
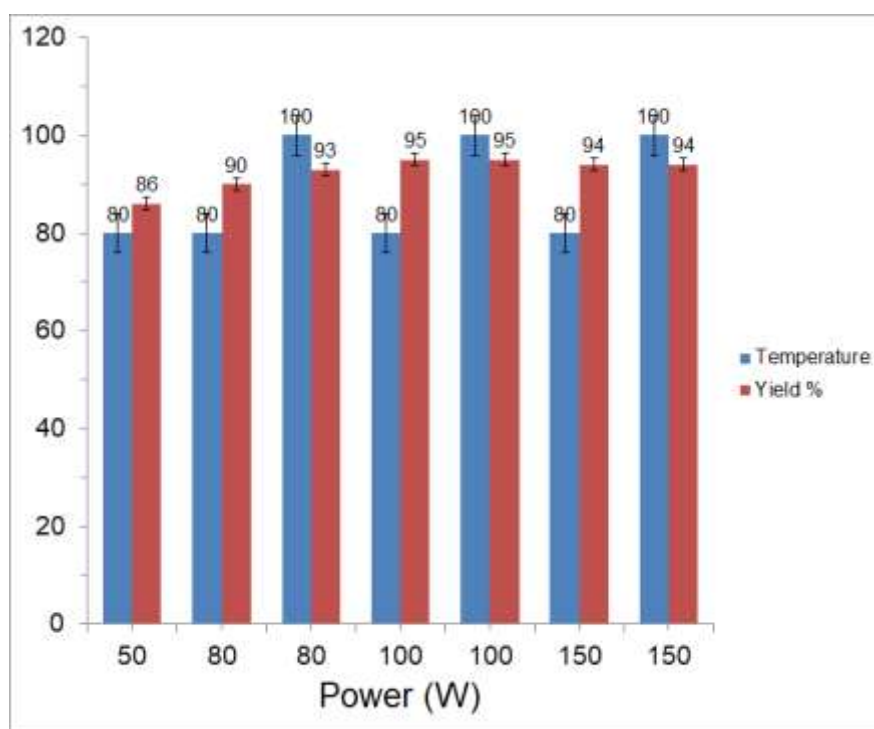
Figure 3.8 Optimization of microwave power and temperature (reaction conditions: benzaldehyde (1mmol), ethyl acetoacetate (1mmol), urea (1.2 mmol) in the presence of 25 mg of Fe_3O_4-DOPA-CuNPs in 5 ml EtOH/H_2O)
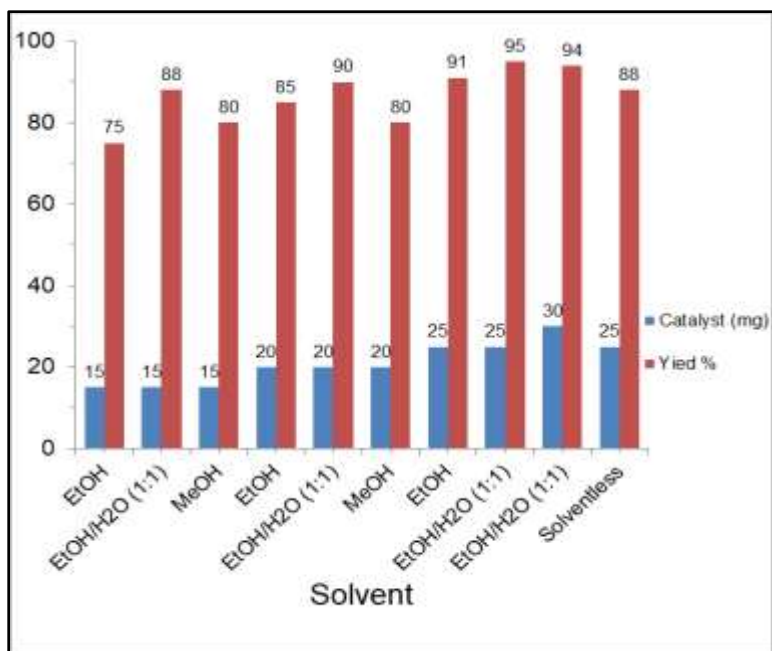
Figure 3.9 Optimization of solvent and catalyst loading (reaction conditions: benzaldehyde (1mmol), ethyl acetoacetate (1mmol), urea (1.2 mmol) at 100 W and 80 °C *in* 5 ml EtOH/H$_2$O)
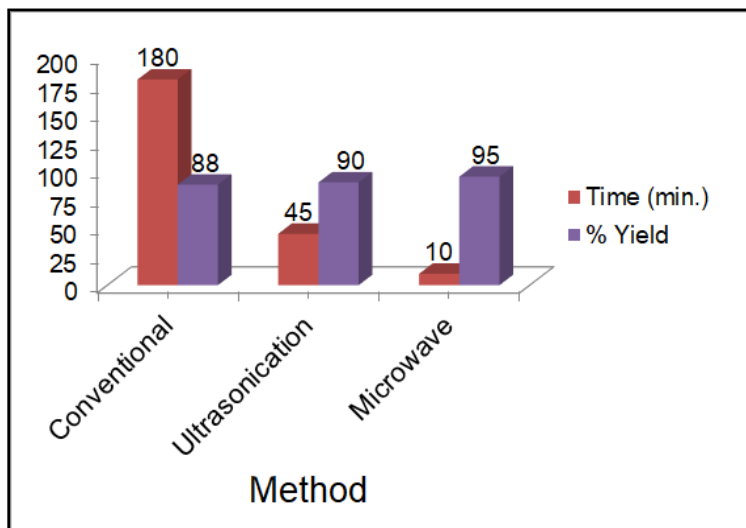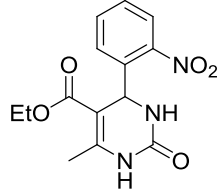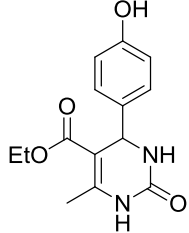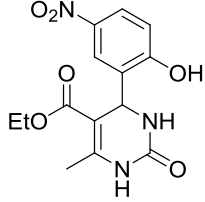
Figure 3.10 Optimization of various methods (reaction conditions: benzaldehyde (1mmol), ethyl acetoacetate (1mmol), urea (1.2 mmol) in the presence of 25 mg of Fe$_3$O$_4$-DOPA-CuNPs in 5 ml EtOH/H$_2$O and 80 °C)
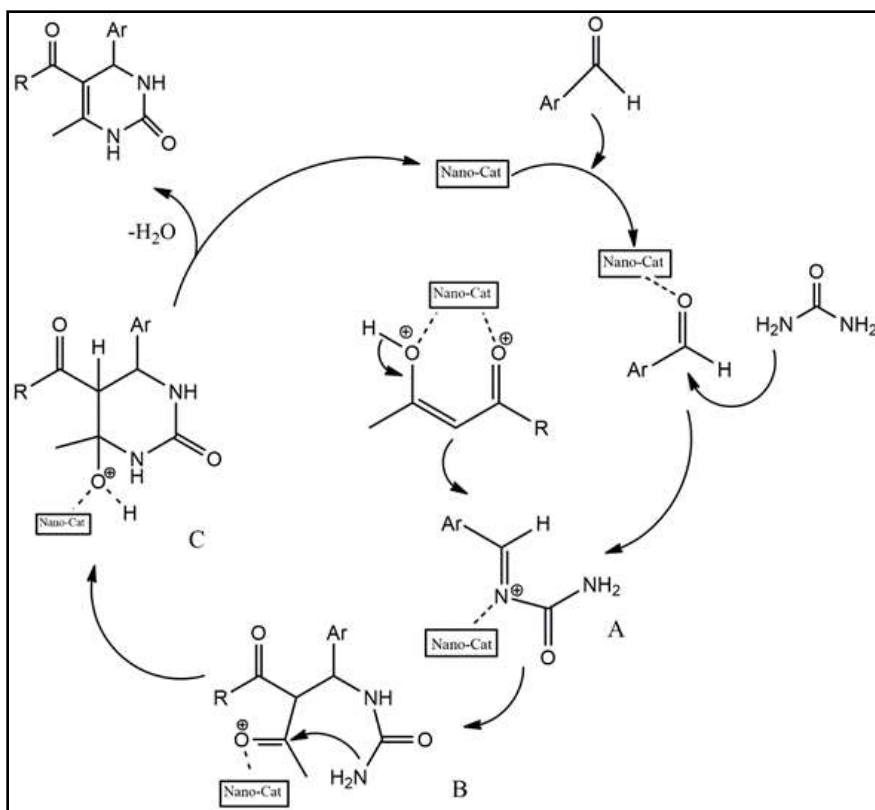
Scheme 3.2 Proposed mechanism for the synthesis of dihydropyrimidines by Fe_3O_4-DOPA-Cu nanocatalyst

Table 3.1 Fe_3O_4-DOPA-Cu catalyzed synthesis of 3,4 dihydropyrimidinones by Biginelli reaction[a]

Entry	Product	Time (min)	[b]Yield %
4a		10	95

4b		12	93
4c		05	96
4d		15	92
4e		12	90

[a]Reaction conditions: benzaldehyde (1 mmol), ethyl acetoacetate (1mmol), urea (1.2 mmol) in the presence of 25 mg of Fe_3O_4-DOPA-CuNPs in 5 ml EtOH/H_2O, 100 W and 80 °C) [b]Isolated yield

3.2.2.2 Catalytic studies for the synthesis of 2,4,5 trisubstituted imidazoles (8a-e)

To optimize the reaction conditions for the synthesis of 2,4,5 trisubstituted imidazoles, the reaction of benzaldehyde (1 mmol), benzil (1 mmol) and ammonium acetate (4 mmol) was used as a model reaction. Reactions were performed by varying microwave power and temperature, and the best optimum conditions obtained were 80 °C, 100 W. Further solvent optimization also carried out and the best suitable solvent observed was ethanol (Figure 3.11 and 3.12). Optimization for catalyst loading has been also carried out revealed that the optimum amount of catalyst was 30 mg. The reaction showed less yields in optimum time when it has been carried out without using any catalyst and after increasing time it gives quantitative yield. A

comparative study has been carried out for various synthetic methods and microwave irradiation opted out as best method **(Figure 3.13)**. After optimizing the reaction conditions, in order to explore the scope and generality of this protocol, various aldehydes were used as substrate for the synthesis of 2,4,5- trisubstituted imidazoles. The results are shown in **Table 3.2** and indicated that the reactions are equally facile with both electron withdrawing and electron donating groups present on the aromatic aldehydes, resulting in high yields of the corresponding imidazoles. Products were characterized using physical and spectroscopic methods such as melting point, ^{1}HNMR technique. The plausible mechanism for the synthesis of 2,4,5-trisubstituted imidazoles with the nanocatalyst shown in **Scheme 3.3.** Ammonium acetate is the source of ammonia molecule. At first the catalyst facilitates the formation of diamine intermediate (A) by increasing the electrophilicity of the carbonyl group of the aldehyde. Intermediate (A), undergo condensation with benzil to form intermediate (B) which further undergo condensation leading to intermediate (C) which rearranges via a [1,5]-sigmatropic shift to give the corresponding tri-substituted imidazole **[51].**
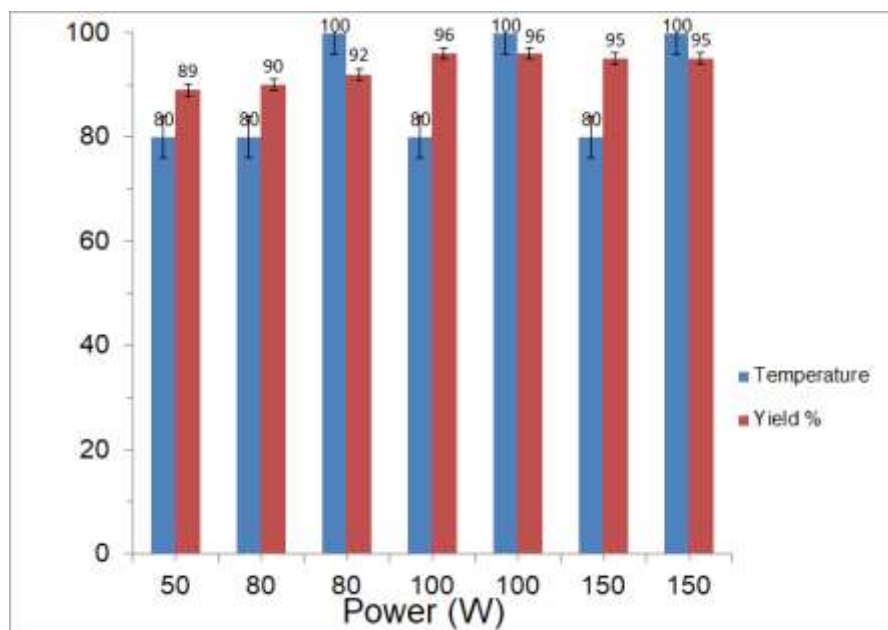
Figure 3.11 Optimization of microwave power and temperature (reaction conditions: benzaldehyde (1mmol), benzil (1mmol), ammonium acetate (4 mmol) in the presence of 30 mg of Fe_3O_4-DOPA-CuNPs in 5 ml EtOH)
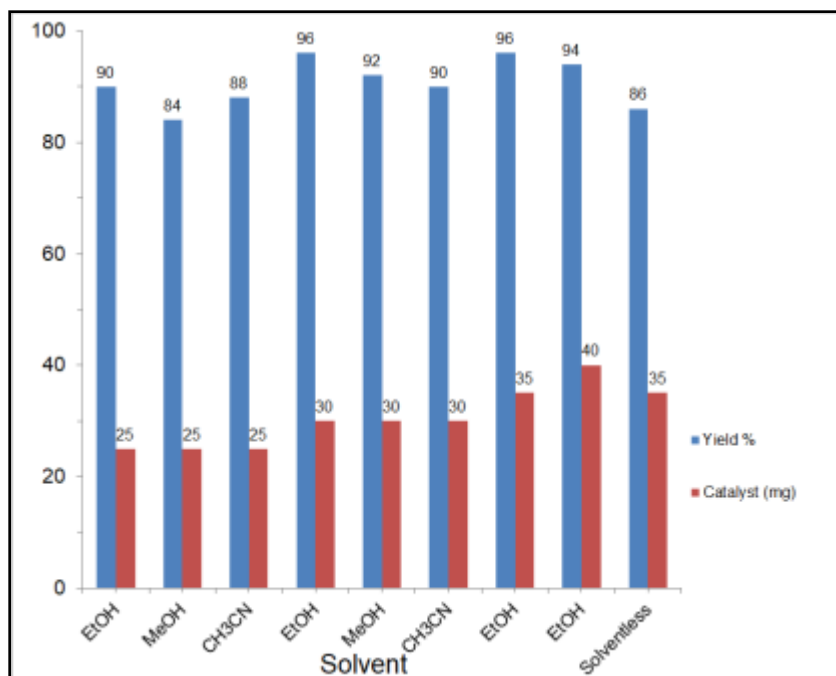
Figure 3.12 Optimization of solvent and catalyst loading (reaction conditions: benzaldehyde (1mmol), benzil (1mmol), ammonium acetate (4 mmol) at 100 W and 80 °C)
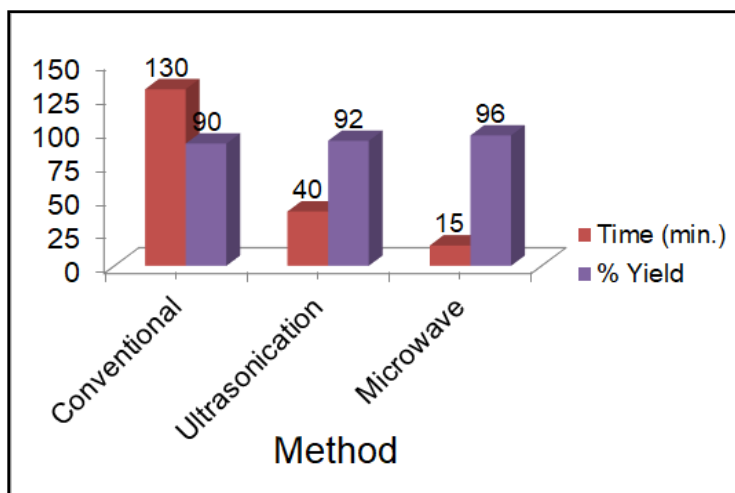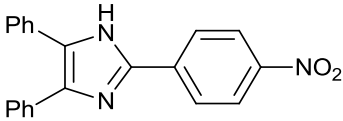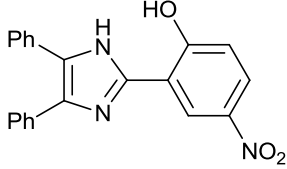
Figure 3.13 Optimization of various methods (reaction conditions: benzaldehyde (1mmol), benzil (1mmol), ammonium acetate (4 mmol) in the presence of 30 mg of Fe_3O_4-DOPA-CuNPs in 5 ml EtOH and 80 °C)
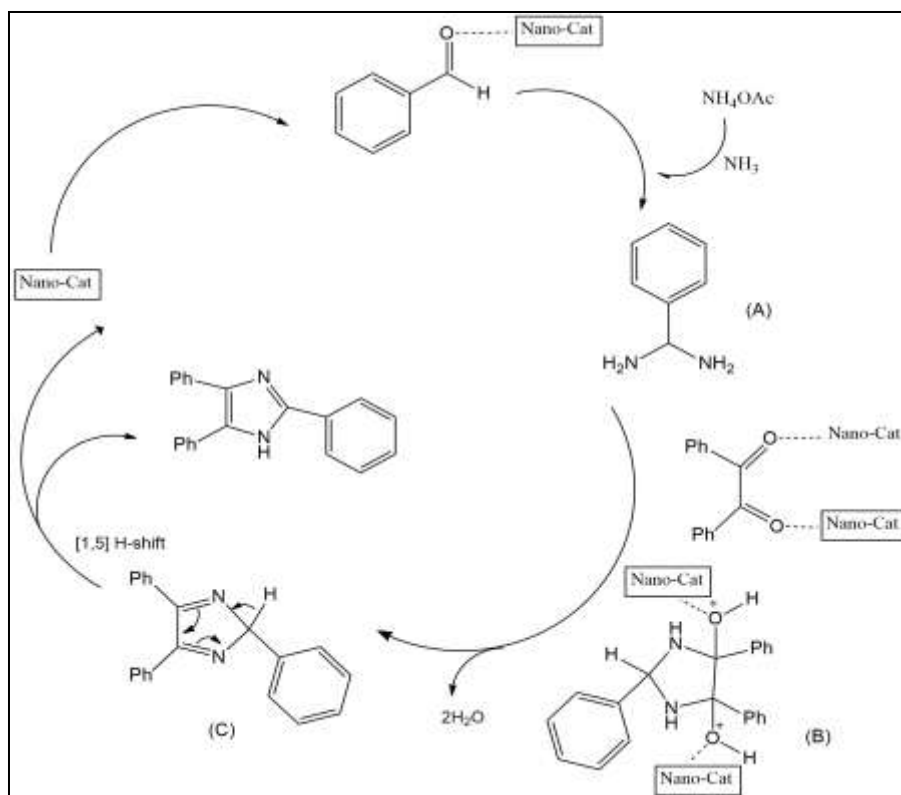
Scheme 3.3 Plausible mechanism for the synthesis of 2,4,5-trisubstituted imidazoles by Fe_3O_4-DOPA-Cu nanocatalyst

Table 3.2 Fe_3O_4-DOPA-Cu catalyzed synthesis of 2,4,5-trisubstituted imidazole[a]

Entry	Product	Time (min)	Yield %
8a		15	95
8b		18	92
8c		16	90

78

8d	Ph–C(=)–N(H)–...–NO_2 (4,5-diphenyl-2-(4-nitrophenyl)imidazole)	12	96
8e	Ph–C(=)–N(H)–...–OH, NO_2 (4,5-diphenyl-2-(2-hydroxy-5-nitrophenyl)imidazole)	15	96

[a]Reaction conditions **:** benzaldehyde (1 mmol), benzil (1 mmol), ammonium acetate (4 mmol) in the presence of 30 mg of Fe_3O_4-DOPA-CuNPs in 5 ml EtOH at 100 W and 80 °C) [b]Isolated yield

3.2.2.3 Catalytic studies for synthesis of 2-amino-4H- chromenes (12a-e)

Now to optimize the reaction conditions for the synthesis of 2-amino-4*H*-chromene, the reaction of benzaldehyde (1 mmol), malononitrile (1 mmol) and resorcinol (1mmol) was used as a model reaction. Reactions were performed at different microwave power, temperatures, solvents, and catalyst loading resulting that the best condition were 60 °C, 100 W, 45 mg of the catalyst and ethanol as a solvent (**Figure 3.14, 3.15**). The reaction has been carried out without using any catalyst also and it gives quantitative yield after increasing time but showed less yields in optimum time. For this reaction also a comparative study has been carried out for various synthetic methods and microwave irradiation opted out as best method (**Figure 3.16**). After optimizing the reaction conditions, various aldehydes were used as substrate for the synthesis of 2-amino-4*H*-chromene. As shown in **Table 3.3** aldehydes bearing either electron-withdrawing or electron donating groups showed equally well in the reaction and all 2-amino-4*H*-chromenes were prepared in high yields. Products were characterized using physical and spectroscopic methods such as melting point, ^{1}H NMR technique. The plausible reaction mechanism for the synthesis of 2-amino 4*H*-chromene derivatives in the presence of nanocatalyst is shown in **Scheme 3.4**. Firstly, catalyst binds with the oxygen of the carbonyl group makes the alpha hydrogen very acidic, thereby involving the Knoevenagel condensation reaction between aromatic aldehyde and malononitrile. In the second step, Knoevenagel product was reacted in a Michael addition with resorcinol to produce desired product after rearomatization and intramolecular cyclization with the help of nanocatalyst **[52]**.

79
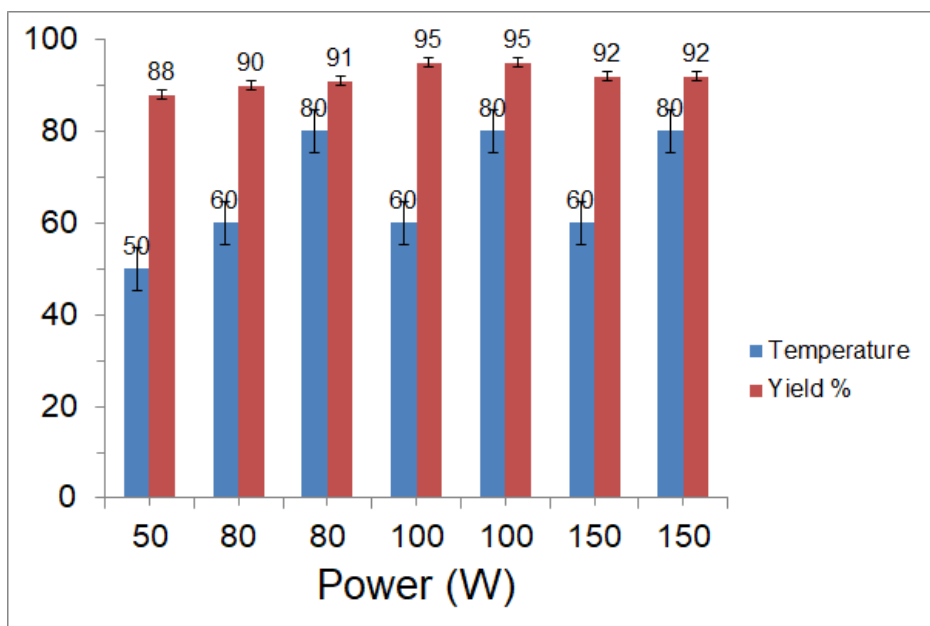
Figure 3.14 Optimization of microwave power and temperature (reaction conditions: benzaldehyde (1mmol), malononitrile (1mmol), resorcinol (1 mmol) in the presence of 45 mg of Fe_3O_4-DOPA-CuNPs in 5 ml EtOH)
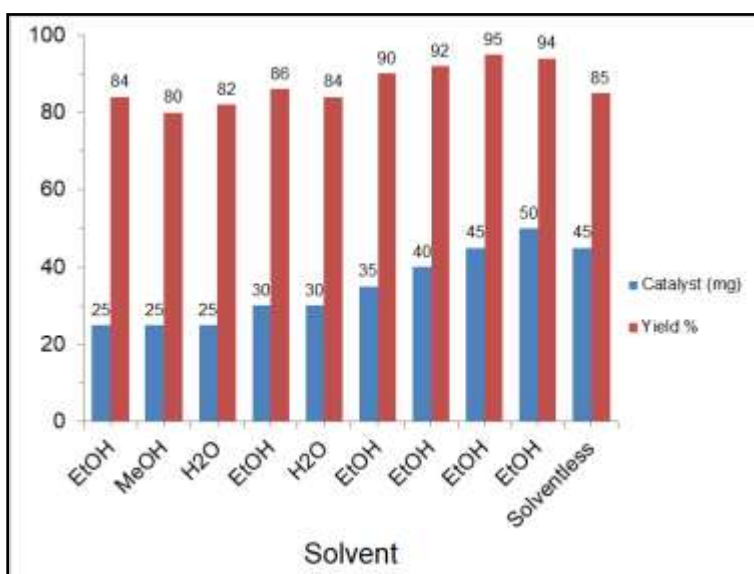
Figure 3.15 Optimization of solvent and catalyst loading (reaction conditions: benzaldehyde (1mmol), malononitrile (1mmol), resorcinol (1 mmol) at 100 W and 60 °C)
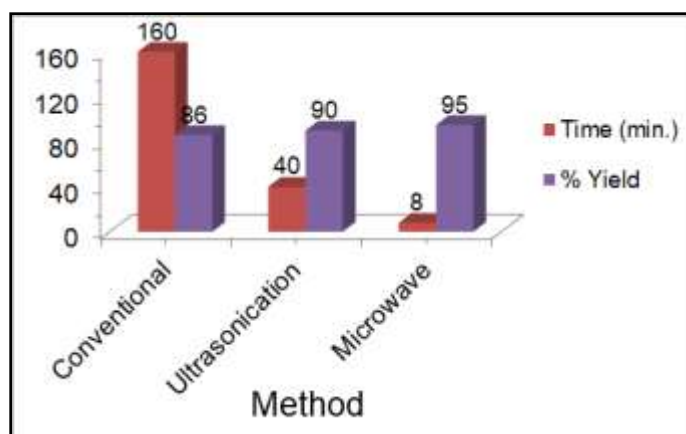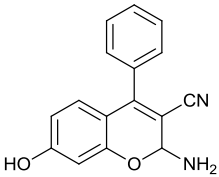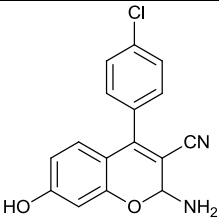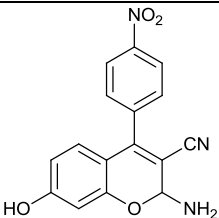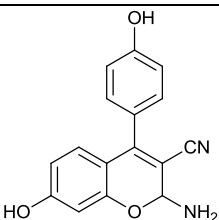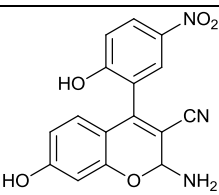
Figure 3.16 Optimization of various methods (reaction conditions: benzaldehyde (1mmol), malononitrile (1mmol), resorcinol (1 mmol) in 5 ml EtOH at 60 ℃)
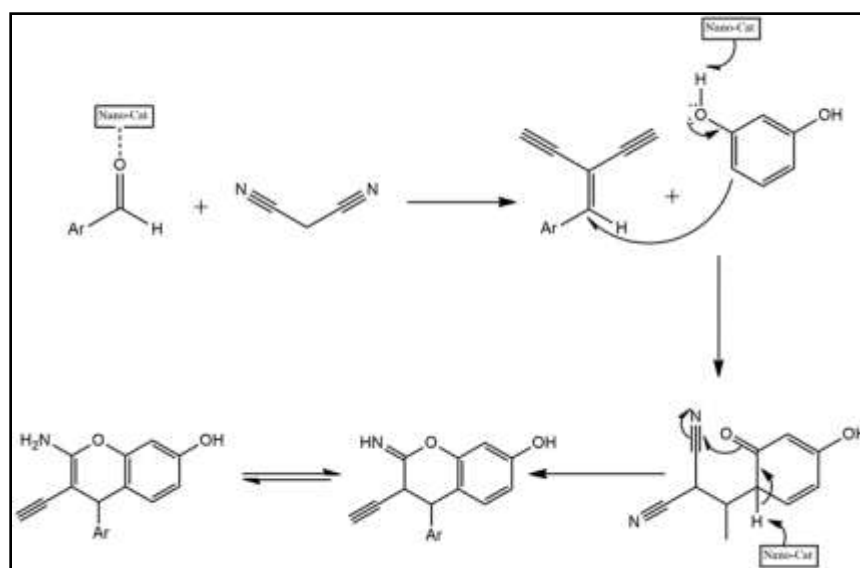
Scheme 3.4 Plausible mechanism for the synthesis of 2-amino-4*H*- chromene by Fe_3O_4-DOPA-Cu nanocatalyst

Table 3.3 Fe$_3$O$_4$-DOPA-Cu catalyzed synthesis of 2-amino-4H-chromenes[a]

Entry	Product	Time (min)	[b]Yield %
12a		08	95
12b		10	94
12c		05	98
12d		08	92
12e		10	92

[a]Reaction conditions : benzaldehyde (1mmol), malononitrile (1mmol), resorcinol (1 mmol) in the presence of 45 mg of Fe$_3$O$_4$-DOPA-CuNPs in 5 ml EtOH at 100 W and 60 °C) [b]Isolated yield

3.2.2.4 Catalytic studies for synthesis of 1,4-disubstituted 1,2,3-triazole (12a-d)

After preparing the catalyst, we examined its ability to promote the formation of the organic azide *in situ*, and subsequent 1,3-dipolar cycloaddition with the alkyne. We defined various parameters of analysis in order to optimize the reaction conditions. As can be seen from the **Figure 3.17** and **3.18** the influence of temperature, microwave power, solvent and catalyst loading were analysed. For the initial studies, we selected the reaction of benzyl bromide (1.2 mmol), sodium azide (1.5 mmol) and phenyl acetylene (1 mmol) as a model reaction to yield the 1,2,3-triazole. It was observed that the optimum condition for the synthesis of triazole achieved were 100 W, 120°C, 100 mg of the nanocatalyst and water as a solvent. In case of triazole synthesis, when the reaction was carried out without catalyst 1:1 of 1,4 and 1,5 cyclic adducts were obtained. The cycloaddition of alkyne and azide become region-selective and a very selective formation of 1,4 adduct in quantitative yield was observed with the help of Fe_3O_4–DOPA–Cu nanocatalyst. After independent optimization of the reaction conditions the same model reaction has been carried out under different synthetic methods like conventional heating, ultrasonication and microwave irradiation and results revealed that the best yield was obtained by microwave irradiation in less reaction time **(Figure 3.19)**. Further we extended these optimized conditions for different benzyl halides and terminal alkynes to check the versatility of the protocols and results obtained were mentioned in **Table 3.4.** Products were characterized using physical and spectroscopic methods such as melting point, ^{1}H NMR technique. Mechanism of copper catalyzed synthesis of 1,2,3-triazoles has been recently been reviewed by Fokin who proposed a revisited mechanism whereby a σ-bound Cu(I)-acetylide bearing a π complexed copper atom reacts with an organoazide forming a bridging dicopper μ-acetylide intermediate **[53-57]**. Based upon their studies we proposed following mechanism for the formation of 1,2,3-triazoles **(Scheme 3.5)**.
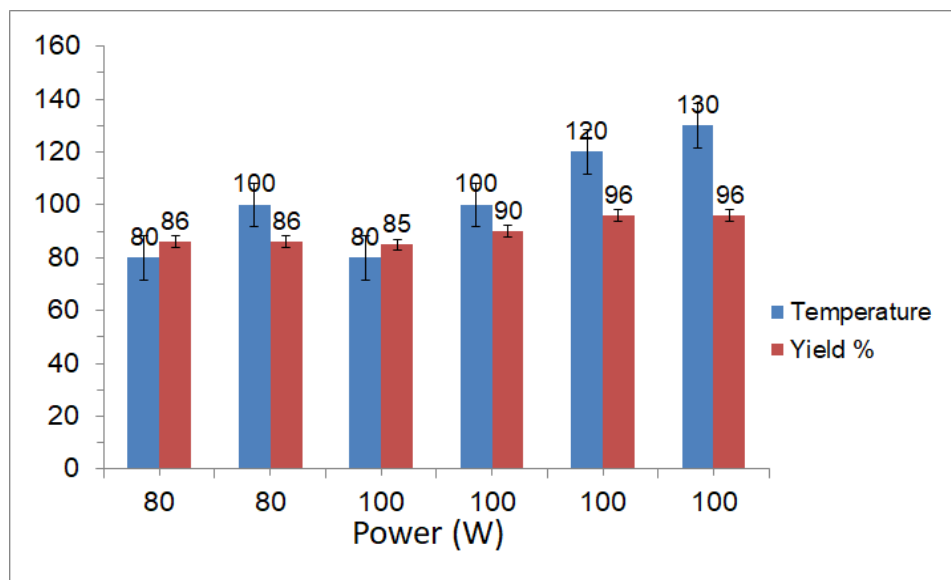
Figure 3.17 Optimization of microwave power and temperature (reaction conditions: benzyl bromide (1.2 mmol), sodium azide (1.5 mmol), phenyl acetylene (1 mmol) in the presence of 100 mg of Fe_3O_4-DOPA-CuNPs in 5 ml H_2O)
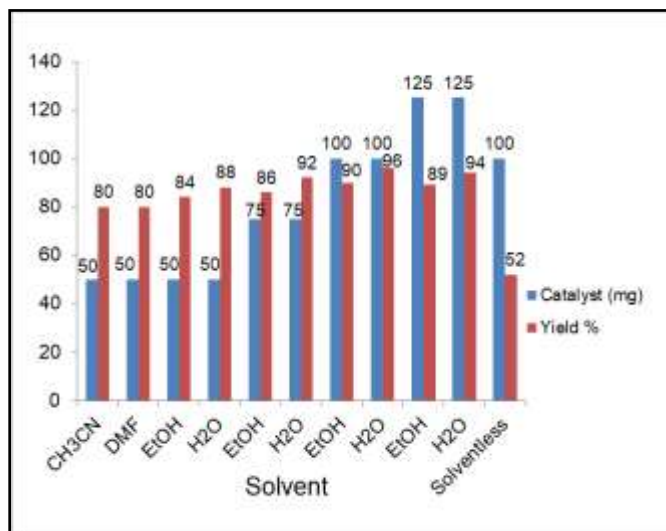
Figure 3.18 Optimization of solvent and catalyst loading (reaction conditions: benzyl bromide (1.2 mmol), sodium azide (1.5 mmol), phenyl acetylene (1 mmol) at 120 °C)

84
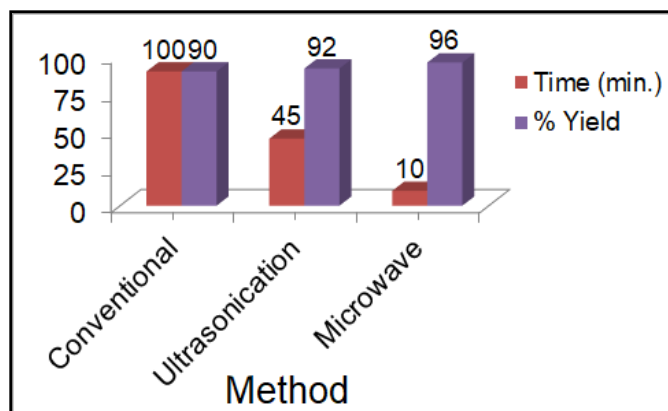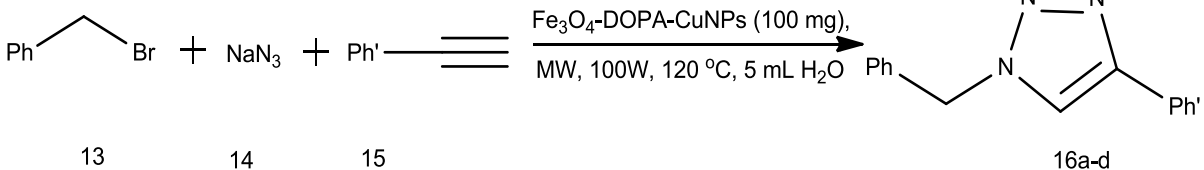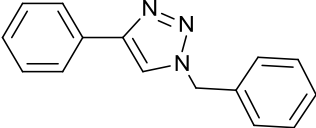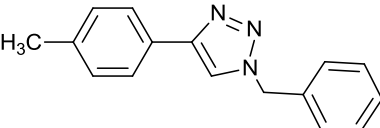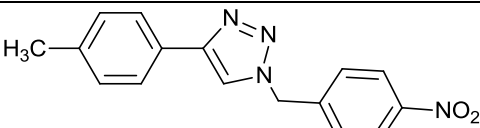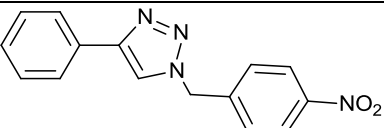
Figure 3.19 Optimization of various methods (reaction conditions: benzyl bromide (1.2 mmol), sodium azide (1.5 mmol), phenyl acetylene (1 mmol) in presence of 100 mg of Fe_3O_4-DOPA-CuNPs in 5 ml H_2O at 120 ℃)
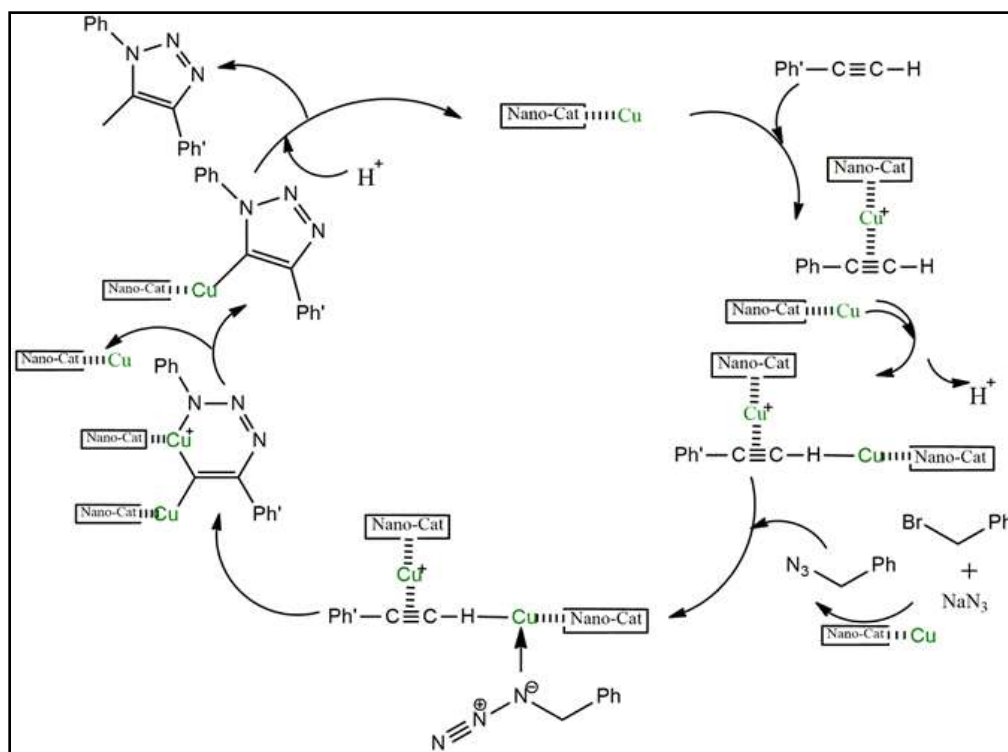
Scheme 3.5 Plausible mechanism for the synthesis of 1,2,3 triazole by Fe_3O_4-DOPA-Cu nanocatalyst

Table 3.4 Fe_3O_4-DOPA-Cu catalyzed synthesis of 1,2,3- triazoles by Click reaction[a]

$$Ph\text{-}Br \ + \ NaN_3 \ + \ Ph'\text{---}\equiv\text{---} \xrightarrow[\text{MW, 100W, 120 °C, 5 mL } H_2O]{Fe_3O_4\text{-DOPA-CuNPs (100 mg),}} Ph\text{-}N\text{-triazole-}Ph'$$
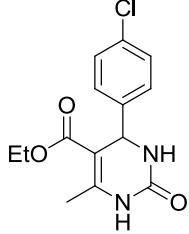
13　　　　14　　　15　　　　　　　　　　　　　　　　　　16a-d

Entry	Product	Time (min)	[b]Yield %
16a	4-phenyl-1-benzyl-1,2,3-triazole	10	96
16b	4-(4-methylphenyl)-1-benzyl-1,2,3-triazole	12	98
16c	4-(4-methylphenyl)-1-(4-nitrobenzyl)-1,2,3-triazole	10	94
16d	4-phenyl-1-(4-nitrobenzyl)-1,2,3-triazole	12	95

[a]Reaction conditions : benzyl bromide (1.2 mmol), sodium azide (1.5 mmol), phenyl acetylene (1 mmol) in presence of 100 mg of Fe_3O_4-DOPA-CuNPs in 5 ml H_2O at 120 °C) [b]Isolated yield

3.2.3 Recyclability and leaching aspect of the Fe_3O_4-DOPA-Cu nanocatalyst

The reusability of the nanocatalyst was also examined and it is an important advantage of magnetic nanocatalyst that being magnetically separable from the reaction mixture, easily recovered by using an external magnet and can be reused for subsequent cycles. After every reaction they were washed with hot ethanol, air-dried and used directly for next round of reactions. The nanocatalyst was found to exhibit good catalytic activity for upto five reaction cycles for Biginelli reaction and triazole synthesis and upto six runs for imidazole and chromene synthesis **(Figure 3.20)**.
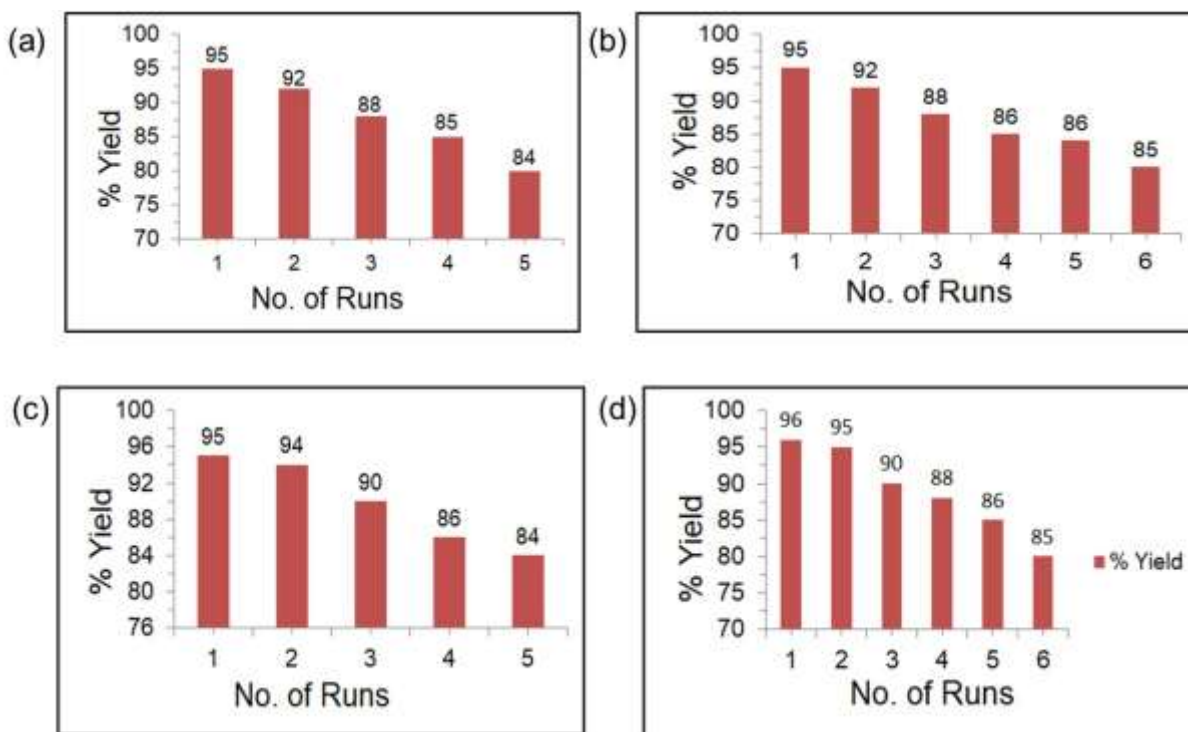
Figure 3.20 Recyclability of the Fe$_3$O$_4$-DOPA-Cu nanocatalyst in the respective model reaction for (a) biginelli reaction (b) imidazole (c) chromene (d) triazole synthesis

The leaching aspect of any copper after recycling was examined by determining the metal content of reaction solution using AAS (atomic absorption spectroscopy) and sample digestions were carried out in a microwave oven at 500 W for 10 min with 5 mL aqua regia. It was found that the concentration of copper in the reused catalyst was reduced to 1.34 wt% for Biginelli reaction and 1.89 wt% for triazole synthesis after 5th run, 2.65 wt% for imidazole synthesis and 2.39 wt% for chromene synthesis after 6th run. The small amount of copper leaching might be due to some changes that occurred on the surface of the magnetic catalyst. Major weight loss of catalyst at high temperature and a small amount of leaching also proves that the catalyst is highly stable at high temperature also.

3.3 Experimental

3.3.1 Materials and Characterizations

All chemicals and solvents purchased are of analytical grade and used without further purification. Infrared spectrum were collected on a Bruker Fourier transform infrared spectrophotometer (FTIR) (Alpha) with pressed KBr pellets and were recorded in the range of 4000-400 wave number (cm^{-1}). The visualization of surface morphology of MNPs was done by

using a field- emission scanning electron microscope (FESEM; NOVA nano SEM) operated at a voltage 10 kV. Samples were prepared by putting a little amount of fine powdered nanoparticles on black carbon tape. Their TEM images were recorded with a Technai G^2 20 (FEI) S-Twin high-resolution transmission electron microscope (HRTEM) operating at 200 kV. Samples were prepared by drying the droplet of dispersed solution of MNPs on a 400 mesh carbon coated copper grid under 100 W table lamp. Powder X-ray diffraction (XRD) pattern of the sample was obtained with X-ray Diffractometer (Panalytical X Pert Pro) using Cu Kα radiation. X-ray photoelectron spectroscopy (XPS) measurements recorded in ESCA[+] omicron nanotechnology oxford instrument. Thermo gravimetric analysis (TGA) and differential thermal analysis (DTA) was performed on a Mettler thermal analyzer in an inert atmosphere at a heating rate of 10 ℃/min. Melting points were determined in open glass capillaries using Gallenkamp melting point apparatus and are reported uncorrected. ^{1}H NMR were recorded on a Jeol ECS 400 MHz spectrophotometer using DMSO d_6 as a solvent. TMS was taken as an internal standard and chemical shifts are reported in δ ppm. Resonance multiplicities are described as s (singlet), d (doublet), t (triplet), q (quartet) and m (multiplet). Ultrasonic bath; Elma S 70 H with 37 KHz with an output frequency was used to carry out the sonochemical synthesis of nanoparticles and to carry out multicomponent reactions. CEM Discover Microwave was used to carry out all the multicomponent reactions. The purity of all the compounds was checked by TLC using silica gel as adsorbent and solvents of increasing polarity as mobile phase.

3.3.2 Preparation of Fe_3O_4- DOPA-Cu nanocatalyst

The magnetite nanoparticles were synthesized by chemical co-precipitation method similar to previously reported method with slight modification [42]. In a 250 ml round bottom flask 16 mmol of $FeCl_3.6H_2O$ (4.32 g) and 8 mmol of $FeCl_2.4H_2O$ (1.59 g) were taken in 50 mL of deionised (DI) water and ultrasonicated for 15 min at room temperature (25 ℃). Then slowly the temperature was raised to 60 ℃ and maintained for further 30 min. After that 50 mL of 1M NaOH solution was added dropwise at the same temperature till the pH of the solution became 10-11. It was further sonicated for another 30 min. The resulting black dispersion was then allowed to remain undisturbed for one night and the desired nanoparticles were separated by using an external magnet then washed thoroughly with deionised water (5 x 100 mL) followed by acetone, (2 x 50 mL) and finally dried in a vacuum oven for 6 h at 60 ℃. In order to graft L-

DOPA over Fe_3O_4 nanoparticles, the mixture of Fe_3O_4 (0.2 g) and L-DOPA (0.1 g) was ultrasonicated in deionized water (10 mL) at 80 °C for 2 h. Black precipitate of Fe_3O_4-DOPA was separated magnetically, washed with deionized water (3×20 mL) and dried under vacuum. Finally, for immobilization of Cu nanoparticles onto Fe_3O_4-DOPA, the aqueous solution of $CuCl_2.2H_2O$ (0.01 g, 3 mL) was added into the dispersed solution of Fe_3O_4-DOPA (0.1 g) in MeOH/ H_2O (1:1, 10 mL), and the reaction mixture was ultrasonicated at room temperature for 0.5 h. Hydrazine hydrate was added till the pH of the solution became 9 followed by addition of $NaBH_4$ (0.01g) into the reaction mixture which was further sonicated for 2 h. Fe_3O_4-DOPA-CuNPs so prepared was separated magnetically and washed successively with ethanol (2 × 20 mL) and water (2 × 20 mL). Finally, it was dried under vacuum at room temperature to get Fe_3O_4-DOPA-Cu nanoparticles as dark black powder (**Scheme 3.1**).
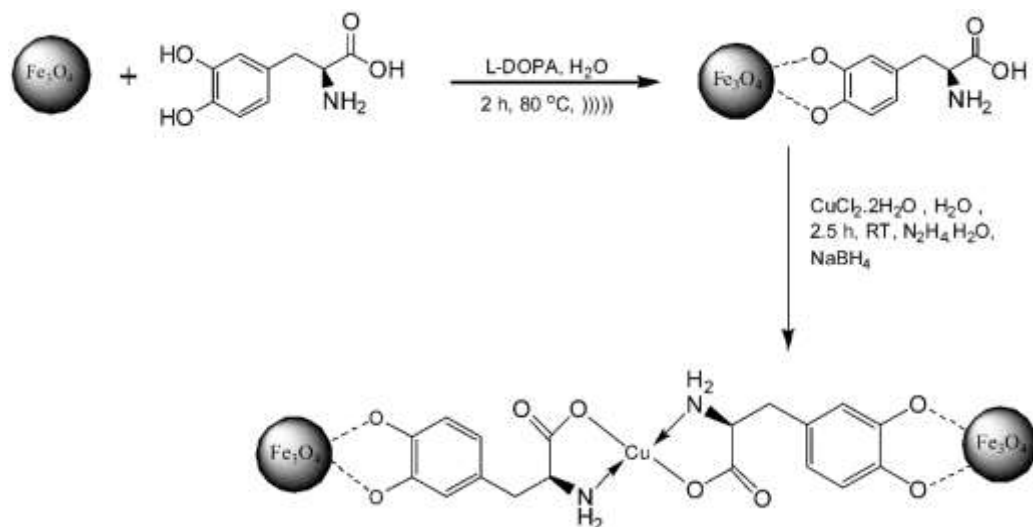
Scheme 3.1 Schematic representation of the synthesis of Fe_3O_4-DOPA-Cu nanocatalyst

3.3.3 General procedure for the synthesis of dihydropyrimidinones via Biginelli condensation under microwave irradiation by Fe_3O_4-DOPA-Cu nanocatalyst (4a-e)

25 mg of Fe_3O_4-DOPA-Cu nanocatalyst was added to a homogeneous mixture of aromatic aldehyde (1 mmol), ethylacetoacetate (1 mmol) urea (1.2 mmol) in a sealed pressure regulated 10 mL pressurized vial containing 5 ml of water/ethanol (1:1) with "snap-on" cap with a pressure sensor and a magnetic stirrer. The reaction tube was placed inside the cavity of a CEM Discover focused microwave synthesis system, operated at 80 °C, 100 Watts and 10-60 psi for 10-15 min.

The reaction progress was monitored by thin layer chromatography (TLC, eluent: petroleum ether : ethyl acetate : 8 : 2). After the completion of the reaction, the nano magnetite based catalyst was separated by using an external magnet and the reaction product was then poured into crushed ice. The obtained solid product was separated by simple filtration, washed with EtOH and dried and recrystallized from ethanol to afford pure product.

3.3.4 General procedure for the synthesis of 2,4,5-trisubstituted imidazoles under microwave irradiation by Fe_3O_4-DOPA-Cu nanocatalyst (8a-e)

Fe_3O_4-DOPA-Cu (30 mg) as an efficient magnetic nanocatalyst was added to a mixture of benzil (1 mmol), aromatic aldehyde (1 mmol), NH_4OAc (4 mmol) in a sealed pressure regulated 10 mL pressurized vial with a pressure sensor and a magnetic stirrer containing 5 mL of ethanol. The reaction tube was placed inside the cavity of a CEM Discover focused microwave synthesis system, operated at 80 °C, 100 Watts and 10-60 psi for 15-18 min. After the TLC (eluent: petroleum ether:ethyl acetate:7:3) indicates the disappearance of starting materials, the reaction was cooled to room temperature. The resultant solid was dissolved in acetone and the magnetic nanocatalyst was separated using an external magnet. The mixture was concentrated on a rotary evaporator under reduced pressure and the solid product obtained was washed with water and recrystallized from acetone-water 9:1 (v/v) to afford the pure 2,4,5-trisubstituted imidazole derivatives.

3.3.5 General procedure for the synthesis of 2-amino-3-cyano-4H-chromenes under microwave irradiation by Fe_3O_4-DOPA-Cu nanocatalyst

An equimolar mixture of resorcinol (1 mmol), malononitrile (1 mmol) and aromatic aldehyde (1 mmol) was placed in a sealed pressure regulated 10 mL pressurized vial containing ethanol (5 mL) and Fe_3O_4-PEG-Cu nanocatalyst (45 mg) with "snap-on" cap with a pressure sensor and a magnetic stirrer. The reaction tube was placed inside the cavity of a CEM Discover focused microwave synthesis system, operated at 60 °C, 100 Watts and 10-60 psi for 5-10 min. After completion of the reaction (TLC, eluent: petroleum ether:ethyl acetate:7:3), the mixture was poured into ice cold water. The resulting precipitate was filtered, dried and recrystallized from ethanol to afford pure 2-amino-4H-chromenes.

3.3.6 General procedure for synthesis of triazole via in situ generation of alkyl azide under microwave irradiation by Fe$_3$O$_4$-DOPA-Cu nanocatalyst

Alkyl halides (1.2 mmol), NaN$_3$ (1.5 mmol), alkyne (1.0 mmol) and Fe$_3$O$_4$-DOPA-Cu nanocatalyst (100 mg) in a sealed pressure regulation 10 mL pressurized vial containing 5 mL of water with "snap-on" cap with a pressure sensor and a magnetic stirrer. The reaction tube was placed inside the cavity of a CEM Discover focused microwave synthesis system, operated at 120 °C, 100 Watts and 10-60 psi for 10-12 min. After completion of the reaction, the catalyst was easily removed from reaction mixture using an external magnet. After separation of catalyst the solid product was filtered off or extracted with ethyl acetate and recrystallized or purified by column chromatography.

3.3.7 Analytical data of the synthesized compounds

Ethyl 6-methyl-2-oxo-4-phenyl-1,2,3,4-tetrahydropyrimidine-5-carboxylate (4a)
White solid; m.p 210-212 °C; ^{1}H NMR (400 MHz, DMSO-*d6*) δ_H (ppm): 1.07 (3H, t, OCH$_2$CH$_3$), 2.20 (3H, s, CH$_3$), 3.94 (2H, q, OCH$_2$CH3), 5.10 (1H, s, -CH), 7.10-7.32 (5H, m, Ar-H), 7.71 (1H, s, NH), 9.16 (1H, s, NH)); ^{13}C NMR (100 MHz, DMSO-*d6*) δ_H 14.48, 18.31, 54.34, 59.72, 99.81, 126.76, 127.80, 128.92, 145.31, 149.08, 152.95, 165.85

Ethyl 4-(4-chlorophenyl)-6-methyl-2-oxo-1,2,3,4-tetrahydropyrimidine-5-carboxylate (4b)
Off white solid; m.p 210-212 °C; ^{1}H NMR (400 MHz, DMSO-*d6*) δ_H (ppm): 1.07 (3H, t, OCH$_2$CH$_3$), 2.20 (3H, s, CH3), 3.93 (2H, q, OCH$_2$CH$_3$), 5.10 (1H, s, -CH), 7.10-7.32 (5H, m, Ar-H), 7.71 (1H, s, NH), 9.16 (1H, s, NH)); ^{13}C NMR (100 MHz, DMSO-*d6*) δ_H 14.51, 18.33, 54.09, 59.64, 99.50, 129.59, 131.63, 132.35, 144.65, 149.45, 152.65, 165.88

Ethyl 6-methyl-4-(2-nitrophenyl)-2-oxo-1,2,3,4-tetrahydropyrimidine-5-carboxylate (4c)
White solid; m.p 234-236 °C; 1H NMR (400 MHz, DMSO-*d6*) δ_H (ppm): 1.07 (3H, t, OCH$_2$CH$_3$), 2.23 (3H, s, CH3), 3.94 (2H, q, OCH$_2$CH$_3$), 5.65 (1H, s, -CH), 7.46-7.68 (4H, m, Ar-H), 7.80 (1H, s, NH), 9.32 (1H, s, NH)); ^{13}C NMR (100 MHz, DMSO-*d6*) δ_H 14.81, 18.68, 54.71, 59.94, 99.81, 124.70, 128.98, 133.44, 136.90, 139.67, 144.64, 146.81, 152.96, 165.90

Ethyl 4-(4-hydroxyphenyl)-6-methyl-2-oxo-1,2,3,4-tetrahydropyrimidine-5-carboxylate (4d)
White solid; m.p 230-232 °C; ^{1}H NMR (400 MHz, DMSO-*d6*) δ_H (ppm): 1.04 (3H, t, OCH$_2$CH$_3$), 2.18 (3H, s, CH3), 3.91 (2H, q, OCH$_2$CH$_3$), 4.98 (1H, s, -CH), 6.63-6.98 (4H, dd, Ar-H), 7.58 (1H, s, NH), 9.07 (1H, s, NH), 9.30 (1H, s, OH)); ^{13}C NMR (100 MHz, DMSO-*d6*) δ_H 14.49, 18.27, 54.32, 59.91, 100.21, 128.15, 129.52, 131.31, 144.93, 148.43, 152.95, 165.93

Ethyl 4-(2-hydroxy-5-nitrophenyl)-6-methyl-2-oxo-1,2,3,4-tetrahydropyrimidine-5-carboxylate (4e)
Yellow solid; m.p 126-128 °C; ^{1}H NMR (400 MHz, DMSO-*d6*) δ_H (ppm): 1.39 (3H, t, OCH$_2$CH$_3$), 2.25 (3H, s, CH3), 4.18 (2H, q, OCH$_2$CH$_3$), 4.80 (1H, s, -CH), 7.13 (d, 1H, ArH),

8.30 (d, 1H, ArH), 8.44 (s, 1H, ArH), 8.89 (s, 1H, NH), 10.26 (s, 1H, NH), 10.26 (s, 1H, NH), 12.56 (s, 1H, OH)); ^{13}C NMR (100 MHz, DMSO-$d6$) δ_H 14.51, 18.69, 54.77, 59.63, 99.08, 124.99, 126.72, 128.15, 131.27, 137.64, 140.09, 144.59, 148.06, 152.30, 166.59

2,4,5-triphenyl-1H-imidazole (8a)
White solid; m.p 270-272 ℃; ^{1}H NMR (400 MHz, DMSO-$d6$) δ_H (ppm): 7.57-8.06 (m, 15H, ArH), 10.01 (s, 1H, -NH)); ^{13}C NMR (100 MHz, DMSO-$d6$) δ_H 122.53, 127.82, 128.85, 129.56, 137.60

2-(4-chlorophenyl)-4,5-diphenyl-1H-imidazole (8b)
White solid; m.p 262-264 ℃; ^{1}H NMR (400 MHz, DMSO-$d6$) δ_H (ppm): 7.39-7.90 (m, 14H, ArH), 9.99 (s, 1H, -NH)); ^{13}C NMR (100 MHz, DMSO-$d6$) δ_H 122.56, 125.33, 126.42, 128.86, 130.28, 133.09, 144.20

4-(4,5-diphenyl-1H-imidazol-2-yl)phenol (8c)
Off white solid; m.p 198-201 ℃; ^{1}H NMR (400 MHz, DMSO-$d6$) δ_H (ppm): 6.82-7.90 (m, 14H, ArH), 9.68 (s, 1H, -NH), 12.38 (s, 1H, -OH)); ^{13}C NMR (100 MHz, DMSO-$d6$) δ_H 124.70, 127.83, 128.84, 129.89, 132.73, 146.66

2-(4-nitrophenyl)-4,5-diphenyl-1H-imidazole (8d)
Yellow solid; m.p 234-236 ℃; ^{1}H NMR (400 MHz, DMSO-$d6$) δ_H (ppm): 6.57-8.39 (m, 14H, ArH), 10.13 (s, 1H, -NH)); ^{13}C NMR (100 MHz, DMSO-$d6$) δ_H 118.42, 122.56, 124.30, 125.73, 126.05, 126.75, 127.85, 128.87, 129.56, 131.61, 132.73, 143.52, 148.81

2-(4,5-diphenyl-1H-imidazol-2-yl)-4-nitrophenol (8e)
Lemon yellow solid; m.p 240-242 ℃; ^{1}H NMR (400 MHz, DMSO-$d6$) δ_H (ppm): 7.56-7.90 (m, 14H, ArH), 8.25 (s, 1H, ArH), 10.18 (s, 1H, -NH), 12.19 (s, 1H, -OH)); ^{13}C NMR (100 MHz, DMSO-$d6$) δ_H 119.11, 124.29, 126.76, 127.47, 128.83, 129.58, 129.94, 130.92, 135.88, 145.65, 147.77

2-amino-7-hydroxy-4-phenyl-2H-chromene-3-carbonitrile (12a)
Pale yellow solid; m.p 232-233 ℃; ^{1}H NMR (400 MHz, DMSO-$d6$) δ_H (ppm): 4.61 (s, 1H, 4-H), 6.31 (s, 1H, 8-H), 6.44 (d, 1H, J=8.3 Hz, 6-H), 6.79 (d, 1H, J=8.3 Hz, 5-H), 6.89 (s, 2H, NH$_2$), 7.14-7.32 (m, 5H, ArH-aldehyde), 9.66 (s, 1H, OH); ^{13}C NMR (100 MHz, DMSO-$d6$) δ_H (ppm): 37.21, 55.05, 102.66, 112.40, 113.43, 112.56, 126.00, 127.82, 128.89, 129.54, 146.33, 148.38, 157.15, 159.28

2-amino-4-(4-chlorophenyl)-7-hydroxy-2H-chromene-3-carbonitrile (12b)
Off white solid; m.p 162-163 ℃; ^{1}H NMR (400 MHz, DMSO-$d6$) δ_H (ppm): 4.63 (s, 1H, 4-H), 6.42 (s, 1H, 8-H), 6.49 (d, 1H, J=8.4 Hz, 6-H), 6.80 (d, 1H, J=8.4 Hz, 5-H), 6.97 (s, 2H, NH$_2$), 7.18-7.49 (m, 4H, ArH-aldehyde), 9.73 (s, 1H, OH)); ^{13}C NMR (100 MHz, DMSO-$d6$) δ_H (ppm):37.26, 55.38, 102.63, 112.42, 114.83, 121.87, 126.05, 127.20, 128.87, 130.27, 146.33, 148.07, 158.96, 160.64

2-amino-7-hydroxy-4-(4-hydroxyphenyl)-2H-chromene-3-carbonitrile (12c)
Yellow solid; m.p 247-249 ℃; ^{1}H NMR (400 MHz, DMSO-$d6$) δ_H (ppm): 4.50 (s, 1H, 4-H), 6.23 (s, 1H, 8-H), 6.46 (d, 1H, J=8.2 Hz, 6-H), 6.73 (d, 1H, J=8.2 Hz, 5-H), 6.84 (s, 2H, NH$_2$), 6.97-7.30 (m, 4H, ArH-aldehyde), 9.12 (s, 1H, OH) ^{13}C NMR (100 MHz, DMSO-$d6$) δ_H 38.99, 55.78, 102.98, 112.10, 114.87, 121.52, 126.03, 127.87, 128.89, 129.91, 146.65, 148.40, 158.97, 161.72

2-amino-7-hydroxy-4-(4-nitrophenyl)-2H-chromene-3-carbonitrile (12d)
Dark yellowish red solid; m.p 172-174 ℃; ^{1}H NMR (400 MHz, DMSO-$d6$) δ_H (ppm): 4.49 (s, 1H, 4-H), 6.27 (s, 1H, 8-H), 6.42 (d, 1H, J=8.3 Hz, 6-H), 6.71 (d, 1H, J=8.3 Hz, 5-H), 6.90 (s, 2H, NH$_2$), 7.17-7.28 (m, 4H, ArH-aldehyde), 9.13 (s, 1H, OH); ^{13}C NMR (100 MHz, DMSO-$d6$) δ_H 38.62, 56.07, 102.97, 112.10, 114.84, 121.87, 126.02, 127.84, 128.82, 129.90, 146.35,

148.08, 158.96, 161.04

2-amino-7-hydroxy-4-(2-hydroxy-5-nitrophenyl)-2H-chromene-3-carbonitrile (12e)

Reddish brown solid; m.p 213-215 ℃; ^{1}H NMR (400 MHz, DMSO-*d6*) δ_H (ppm): 4.98 (s, 1H, 4-H), 6.13 (s, 1H, 8-H), 6.36 (d, 1H, J=8.2 Hz, 6-H), 6.42 (d, 1H, J=8.2 Hz, 5-H), 6.94 (s, 2H, NH$_2$), 7.32 (d, 1H, J=8.5 Hz), 7.47 (d, 1H, J=8.5 Hz), 7.57 (s, 1H), 9.15 (s, 1H, OH)); ^{13}C NMR (100 MHz, DMSO-*d6*) δ_H 38.60, 56.47, 103.65, 113.13, 114.52, 123.59, 125.73, 127.87, 129.89, 132.34, 134.46, 134.78, 147.08, 150.94, 159.28, 162.12

1-benzyl-4-phenyl-1H-1,2,3-triazole (16a)

White solid; m.p 125-127 ℃; ^{1}H NMR (400 MHz, DMSO-*d6*) δ_H (ppm): 5.61 (s, 2H), 7.32-7.82 (m, 10H, ArH), 8.61 (s, 1H)); ^{13}C NMR (100 MHz, DMSO-*d6*) δ_H 53.71, 122.11, 126.04, 127.41, 128.17, 128.42, 128.87, 128.59, 131.61, 136.89, 147.36

1-benzyl-4-(p-tolyl)-1H-1,2,3-triazole (16b)

Light brown solid; m.p 100-120 ℃ ^{1}H NMR (400 MHz, DMSO-*d6*) δ_H (ppm): 2.52 (s, 3H, CH$_3$) 5.59 (s, 2H), 7.26-7.74 (m, 9H, ArH), 8.56 (s, 1H)); ^{13}C NMR (100 MHz, DMSO-*d6*) δ_H 21.51, 54.74, 119.73, 125.66, 127.41, 128.17, 129.59, 129.88, 134.02, 138.67, 148.79

1-(4-nitrobenzyl)-4-phenyl-1H-1,2,3-triazole (16c)

Off white solid; m.p 140-142 ℃; ^{1}H NMR (400 MHz, DMSO-*d6*) δ_H (ppm): 5.81 (s, 2H), 7.31-7.84 (m, 10H, ArH), 8.69 (s, 1H)); ^{13}C NMR (100 MHz, DMSO-*d6*) δ_H 54.33, 119.14, 125.66, 128.17, 128.42, 129.59, 129.88, 133.79, 134.71, 138.67, 148.40

1-(4-nitrobenzyl)-4-(p-tolyl)-1H-1,2,3-triazole (16d)

Almond brown solid; m.p 128-130 ℃; ^{1}H NMR (400 MHz, DMSO-*d6*) δ_H (ppm): 2.58 (s, 3H, CH$_3$) 5.80 (s, 2H), 7.20-7.73 (m, 8H, ArH), 8.62 (s, 1H)); ^{13}C NMR (100 MHz, DMSO-*d6*) δ_H 21.83, 54.74, 119.41, 125.66, 128.17, 128,87, 129.21, 129.88, 133.40, 134.43, 138.33, 139.02, 148.40
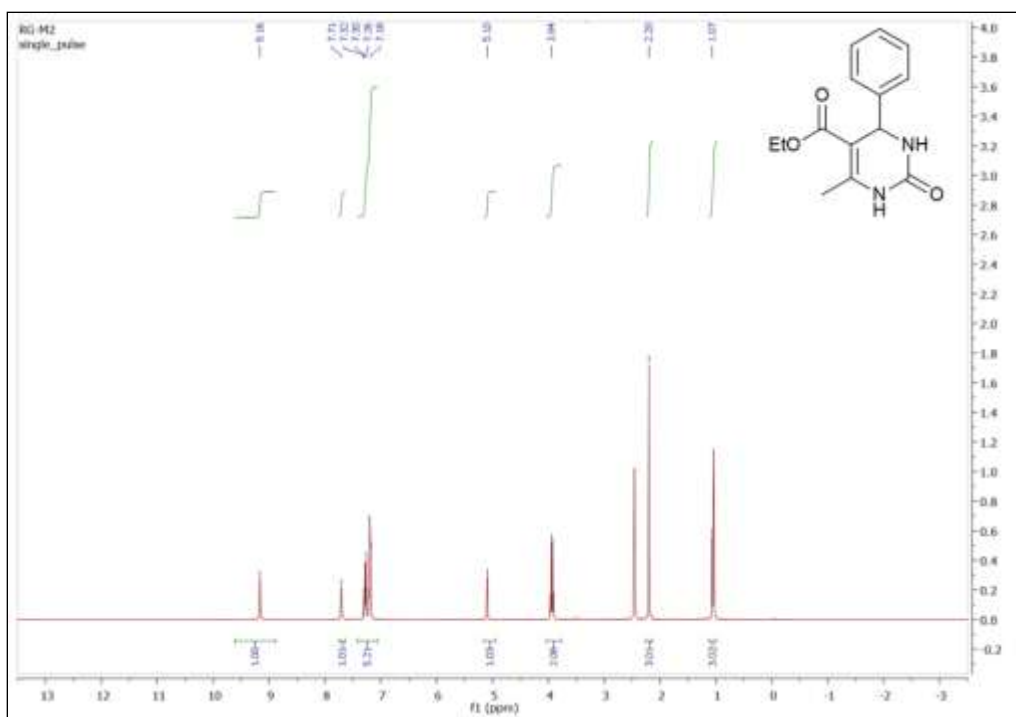
Figure 3.21 ^{1}H NMR spectrum of ethyl 6-methyl-2-oxo-4-phenyl-1,2,3,4-tetrahydropyrimidine-5-carboxylate **(4a)**
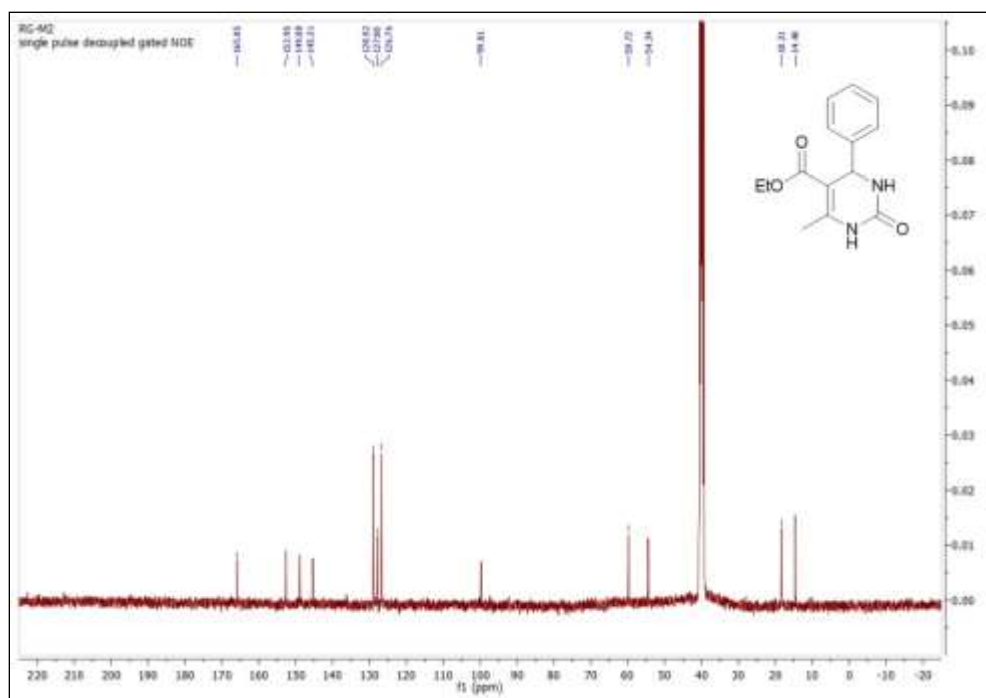
Figure 3.22 ^{13}C NMR spectrum of ethyl 6-methyl-2-oxo-4-phenyl-1,2,3,4-tetrahydropyrimidine-5-carboxylate **(4a)**
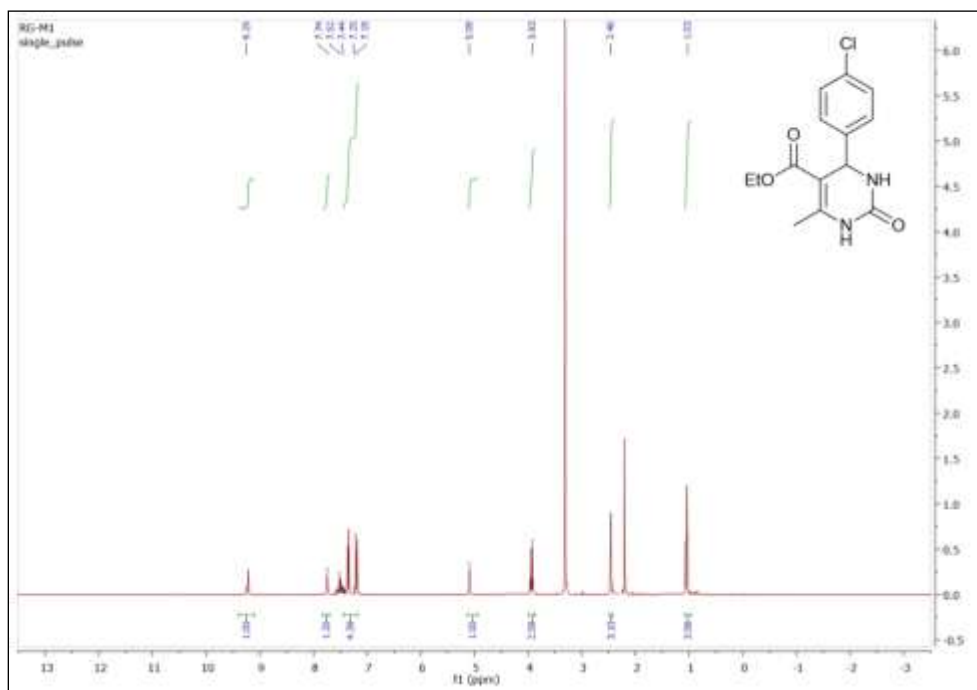
Figure 3.23 ^{1}H NMR spectrum of ethyl 4-(4-chlorophenyl)-6-methyl-2-oxo-1,2,3,4-tetrahydropyrimidine-5-carboxylate **(4b)**
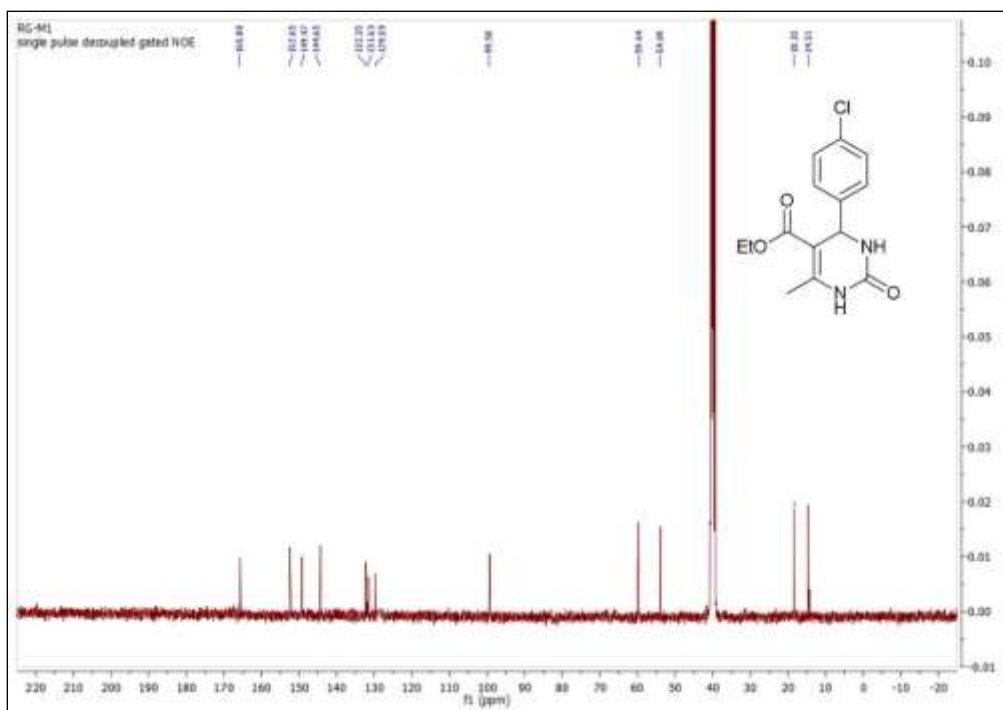
Figure 3.24 ^{13}C NMR spectrum of ethyl 4-(4-chlorophenyl)-6-methyl-2-oxo-1,2,3,4-tetrahydropyrimidine-5-carboxylate **(4b)**
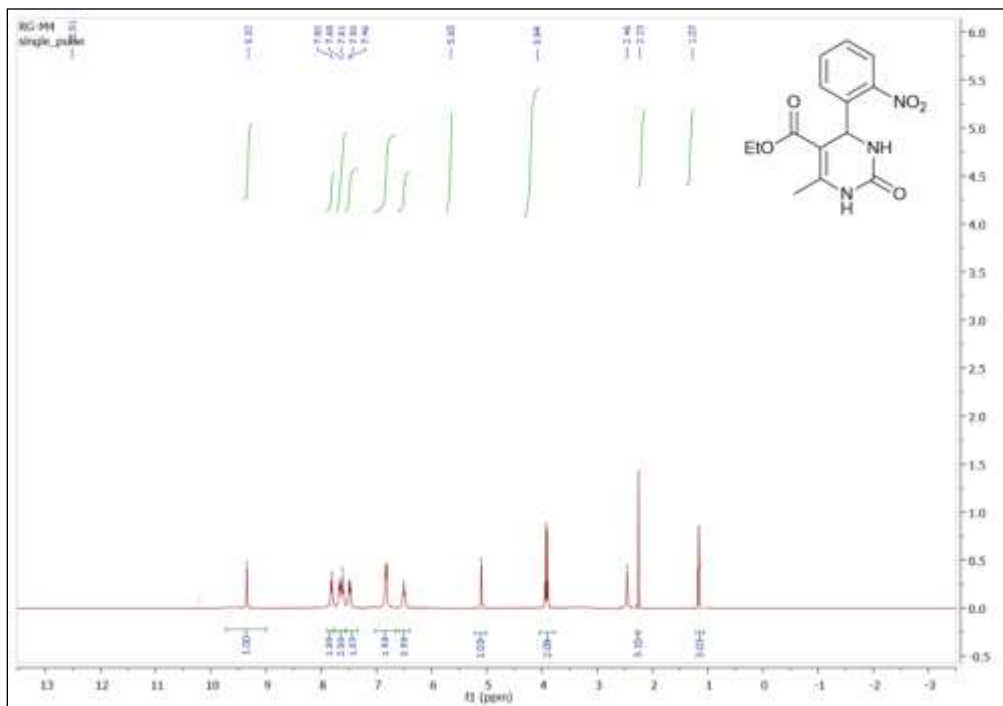
Figure 3.25 ^{1}H NMR spectrum of ethyl 6-methyl-4-(2-nitrophenyl)-2-oxo-1,2,3,4-tetrahydropyrimidine-5-carboxylate **(4c)**
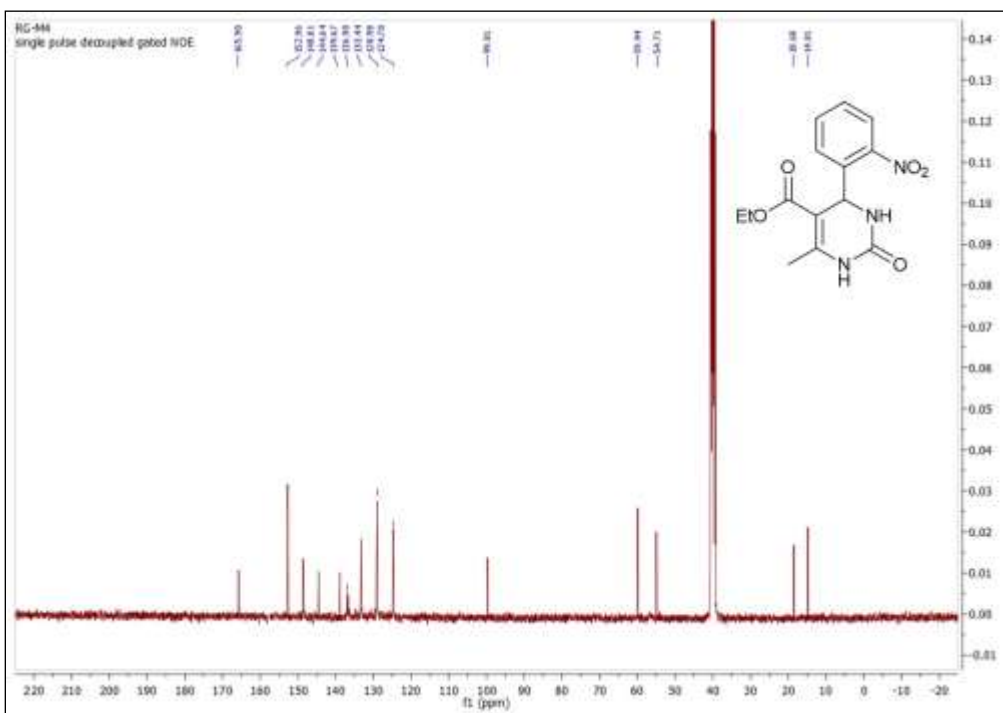
Figure 3.26 ^{13}C NMR spectrum of ethyl 6-methyl-4-(2-nitrophenyl)-2-oxo-1,2,3,4-tetrahydropyrimidine-5-carboxylate **(4c)**
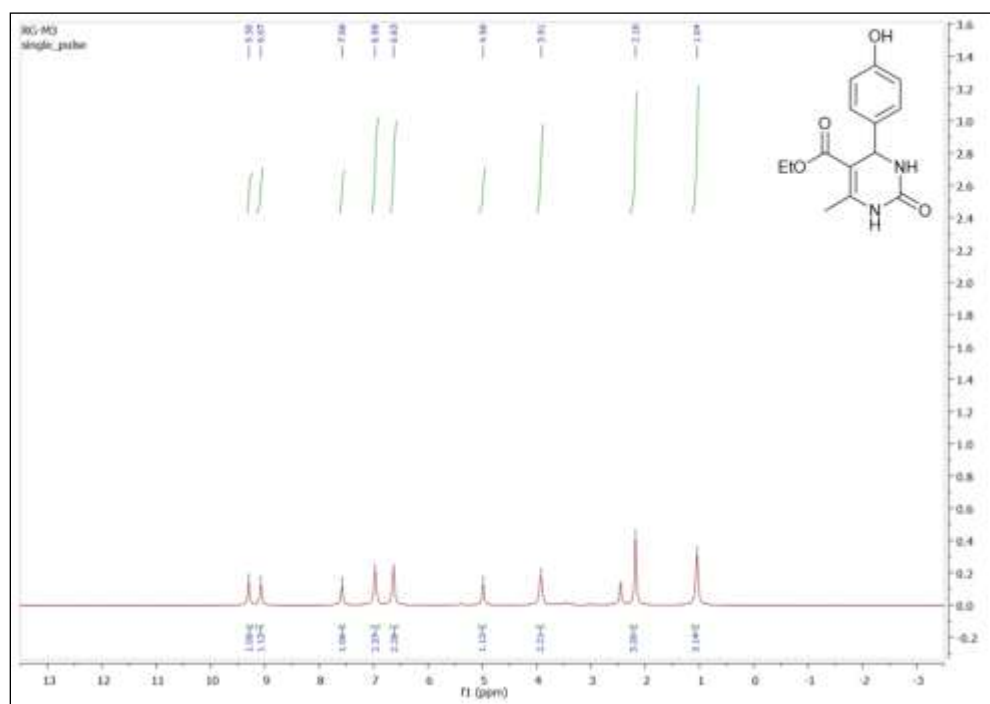
Figure 3.27 ^{1}H NMR spectrum of ethyl 4-(4-hydroxyphenyl)-6-methyl-2-oxo-1,2,3,4-tetrahydropyrimidine-5-carboxylate **(4d)**
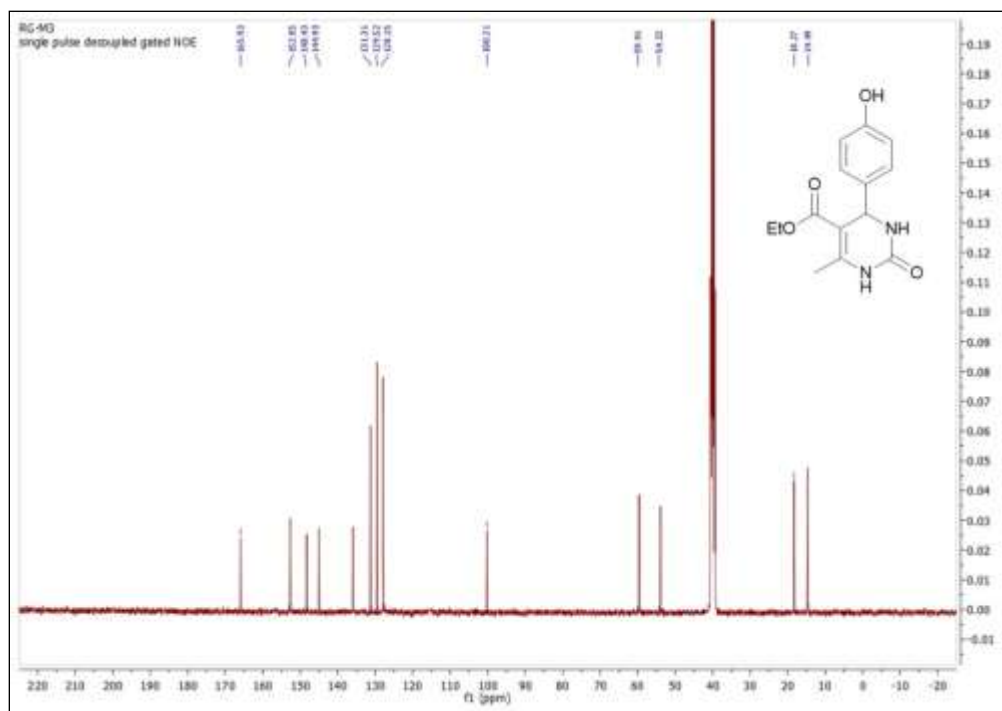
Figure 3.28 ^{13}C NMR spectrum of ethyl 4-(4-hydroxyphenyl)-6-methyl-2-oxo-1,2,3,4-tetrahydropyrimidine-5-carboxylate **(4d)**
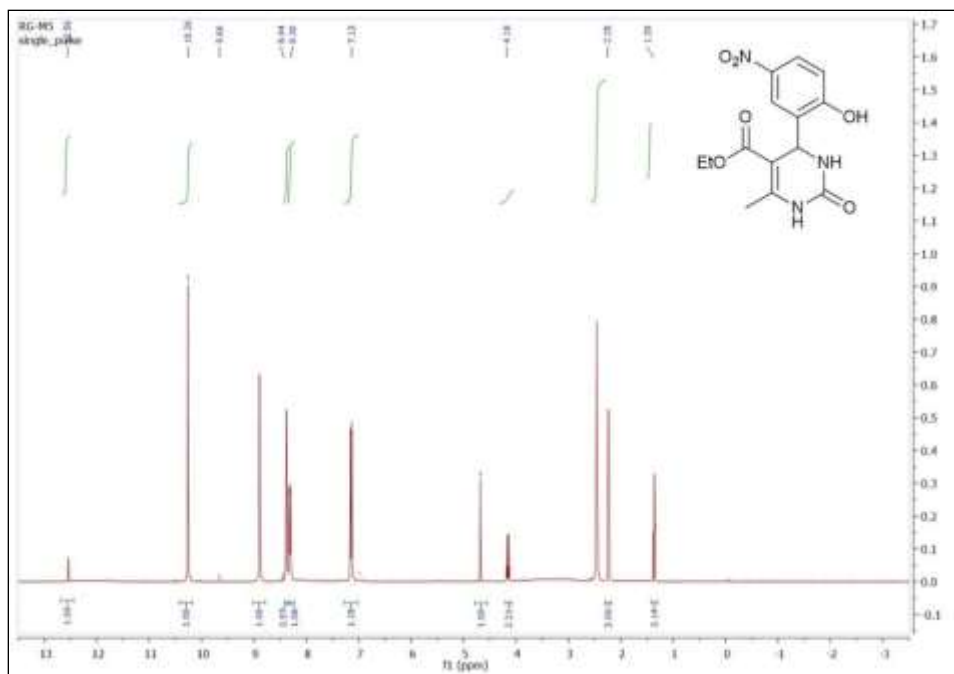
Figure 3.29 ^{1}H NMR spectrum of ethyl 4-(2-hydroxy-5-nitrophenyl)-6-methyl-2-oxo-1,2,3,4-tetrahydropyrimidine-5-carboxylate **(4e)**
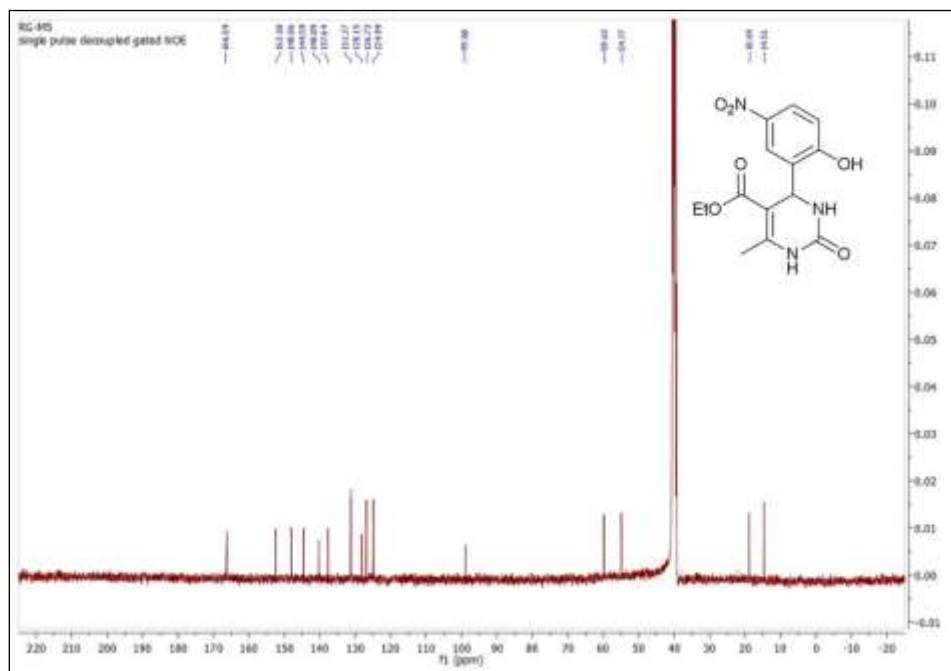
Figure 3.30 ^{13}C NMR spectrum of ethyl 4-(2-hydroxy-5-nitrophenyl)-6-methyl-2-oxo-1,2,3,4-tetrahydropyrimidine-5-carboxylate **(4e)**
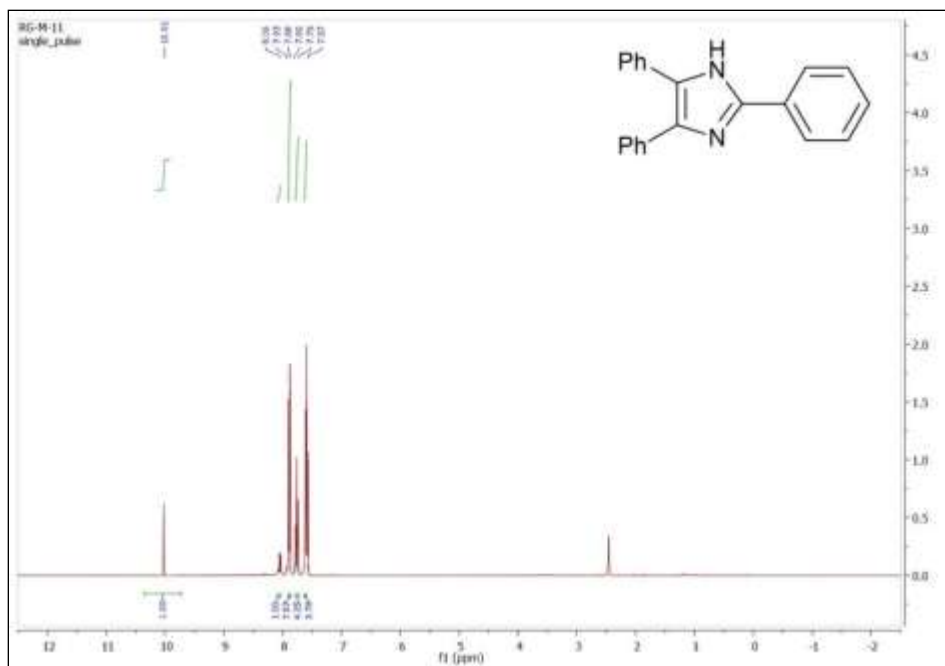
Figure 3.31 ^{1}H NMR spectrum of 2,4,5-triphenyl-1H-imidazole **(8a)**
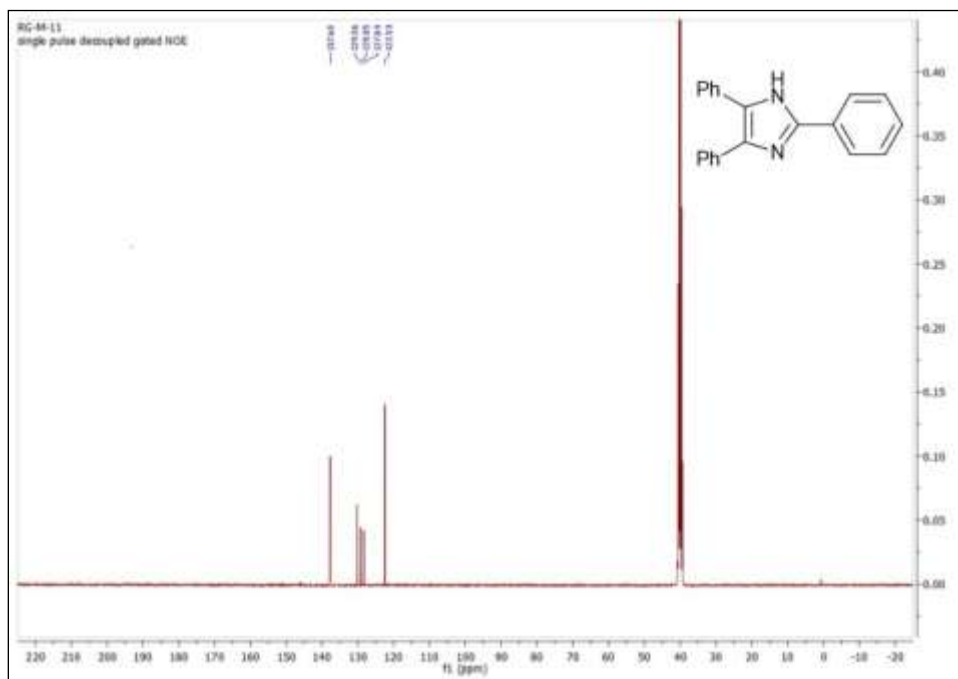
Figure 3.32 ^{13}C NMR spectrum of 2,4,5-triphenyl-1H-imidazole **(8a)**
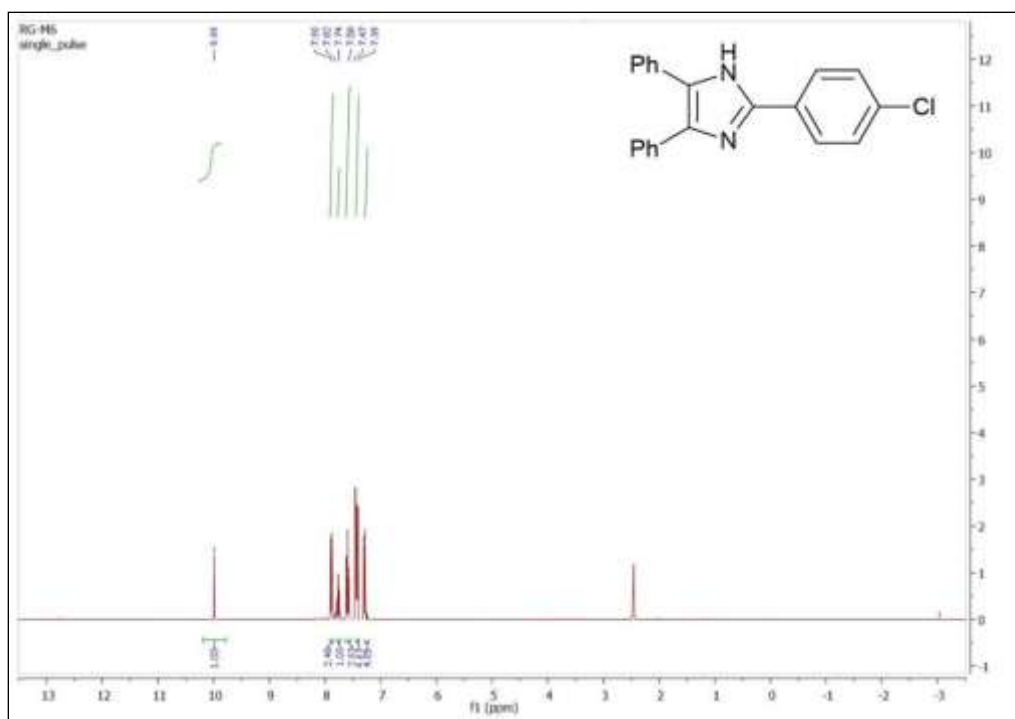
Figure 3.33 ^{1}H NMR spectrum of 2-(4-chlorophenyl)-4,5-diphenyl-1H-imidazole **(8b)**
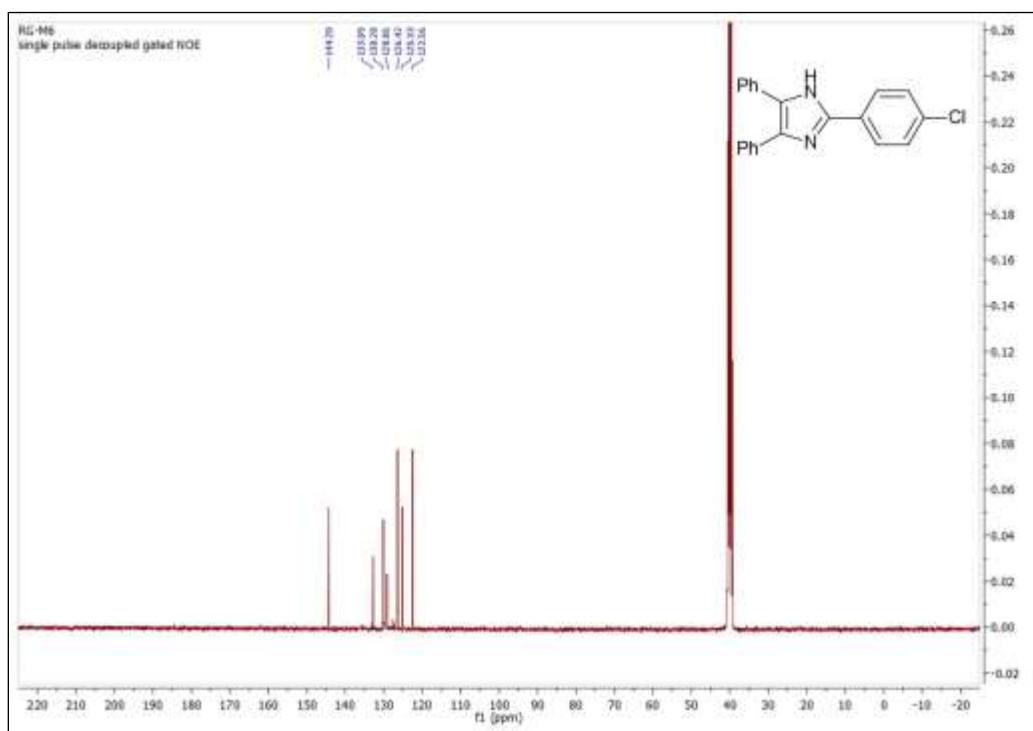
Figure 3.34 ^{13}C NMR spectrum of 2-(4-chlorophenyl)-4,5-diphenyl-1H-imidazole **(8b)**
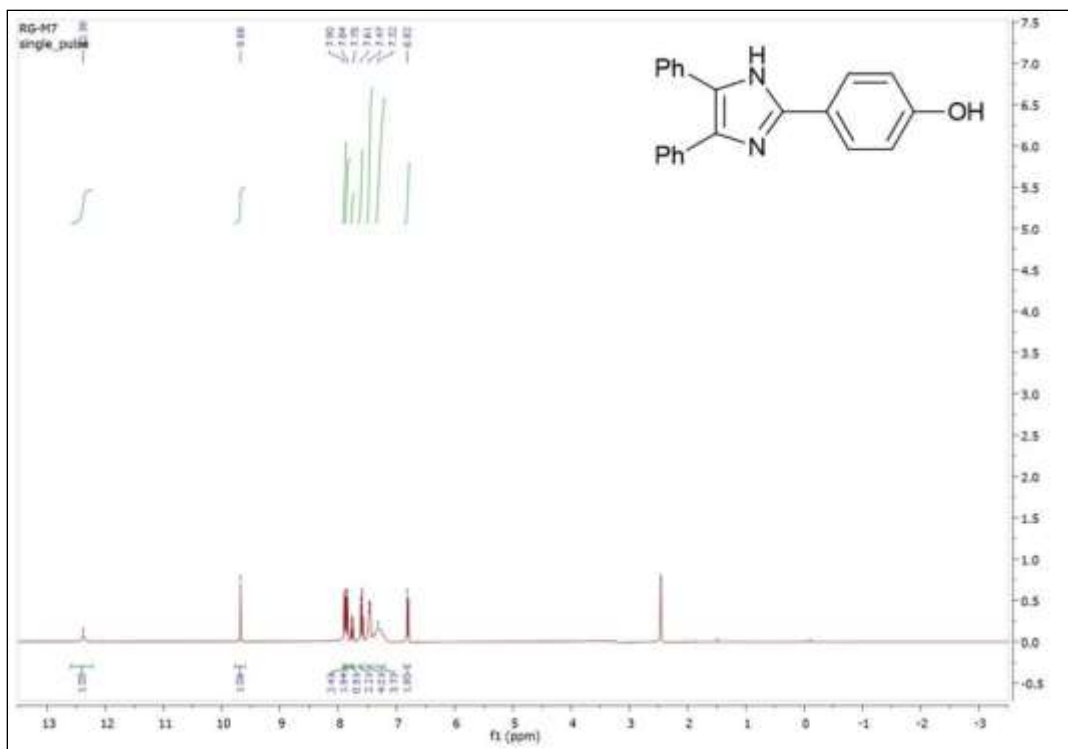
Figure 3.35 ^{1}H NMR spectrum of 4-(4,5-diphenyl-1H-imidazol-2-yl)phenol **(8c)**
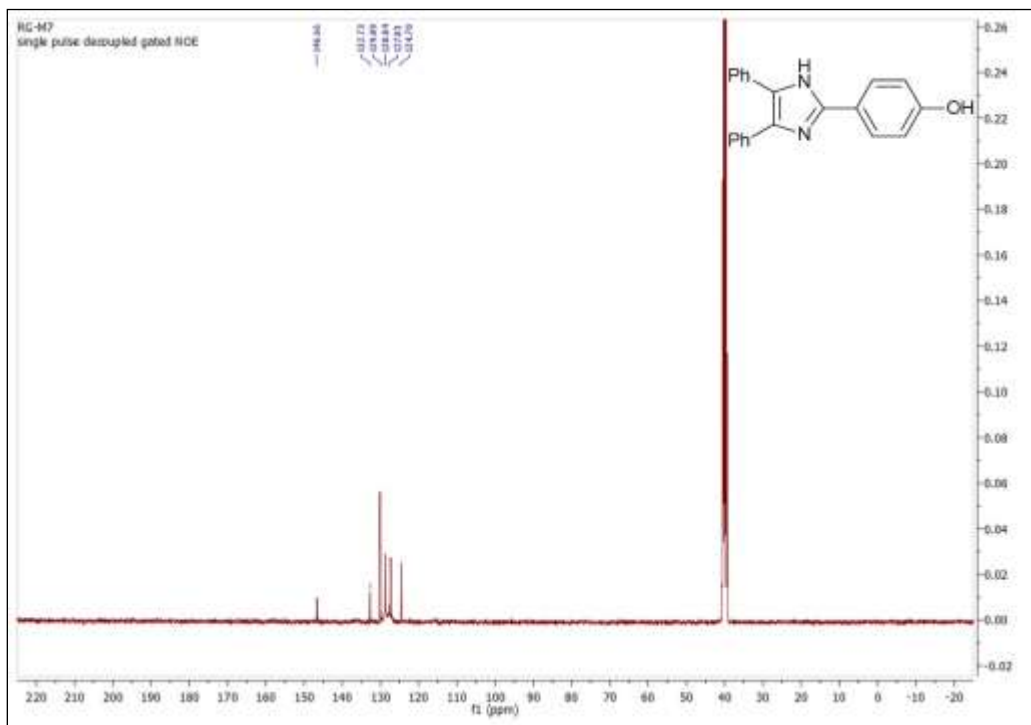
Figure 3.36 ^{13}C NMR spectrum of 4-(4,5-diphenyl-1H-imidazol-2-yl)phenol **(8c)**
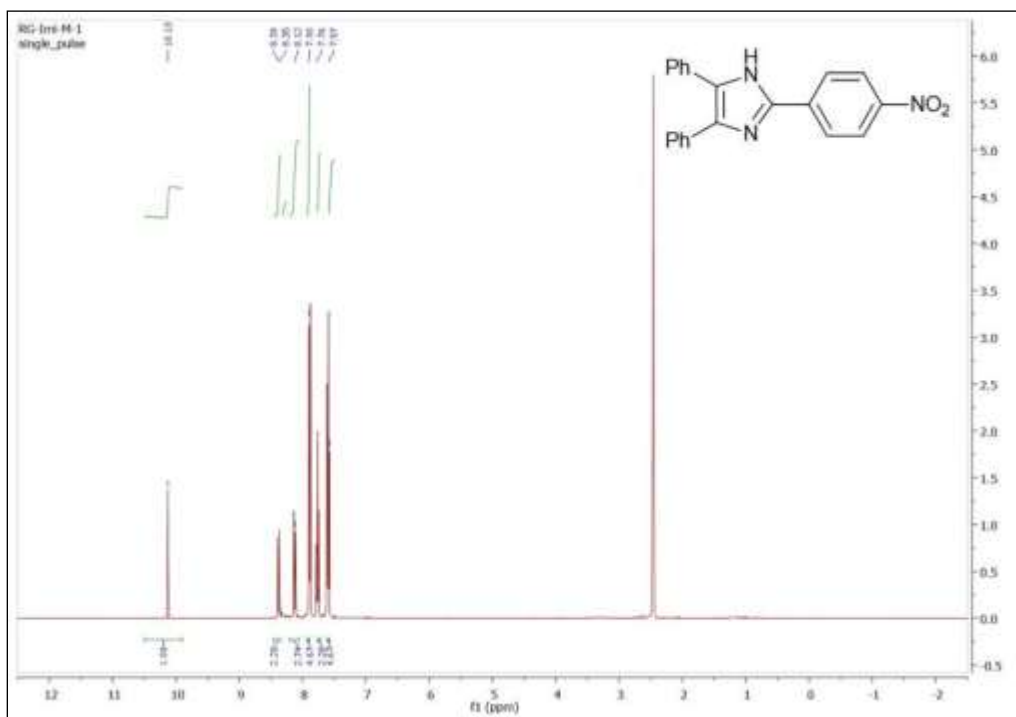
Figure 3.37 ^{1}H NMR spectrum of 2-(4-nitrophenyl)-4,5-diphenyl-1H-imidazole **(8d)**
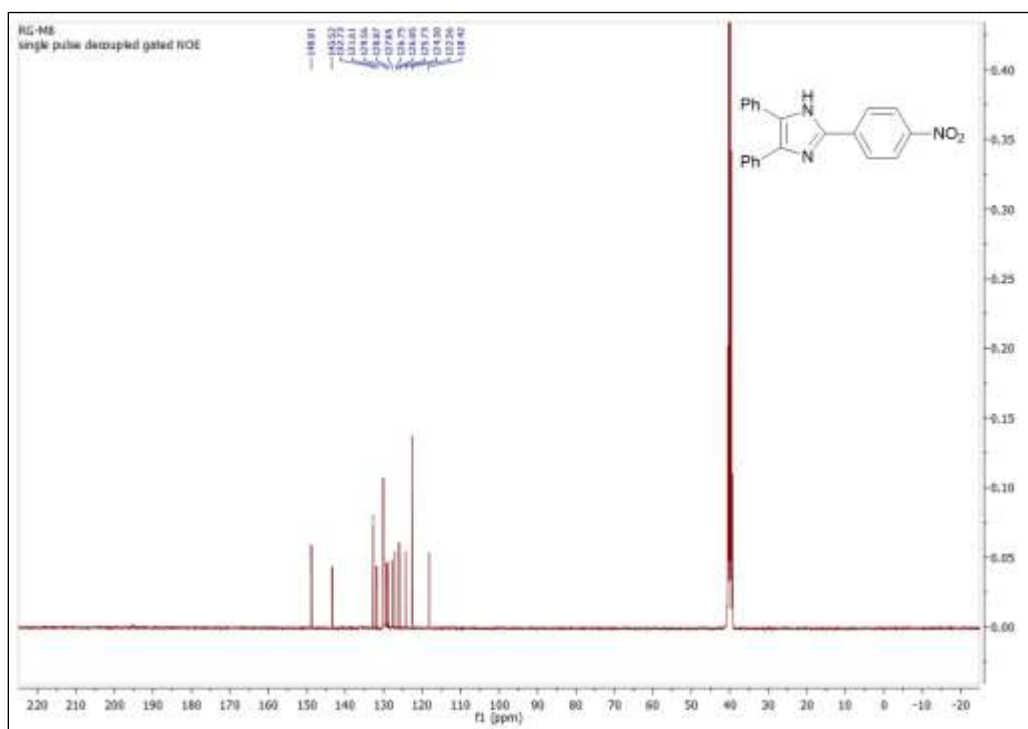
Figure 3.38 ^{13}C NMR spectrum of 2-(4-nitrophenyl)-4,5-diphenyl-1H-imidazole **(8d)**
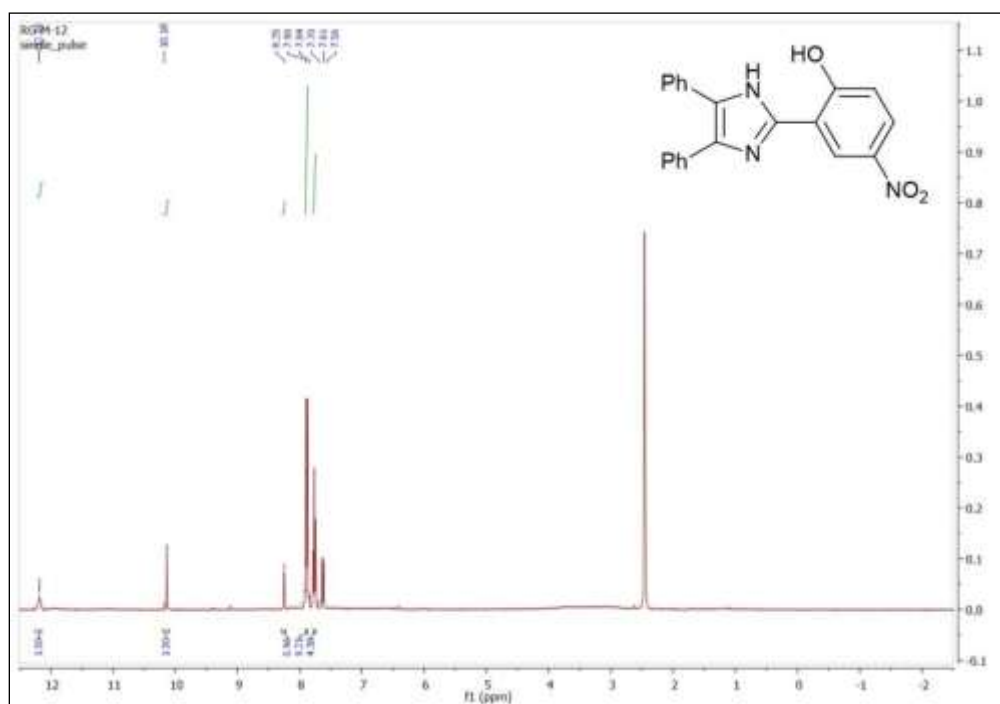
Figure 3.39 ¹H NMR spectrum of 2-(4,5-diphenyl-1H-imidazol-2-yl)-4-nitrophenol **(8e)**
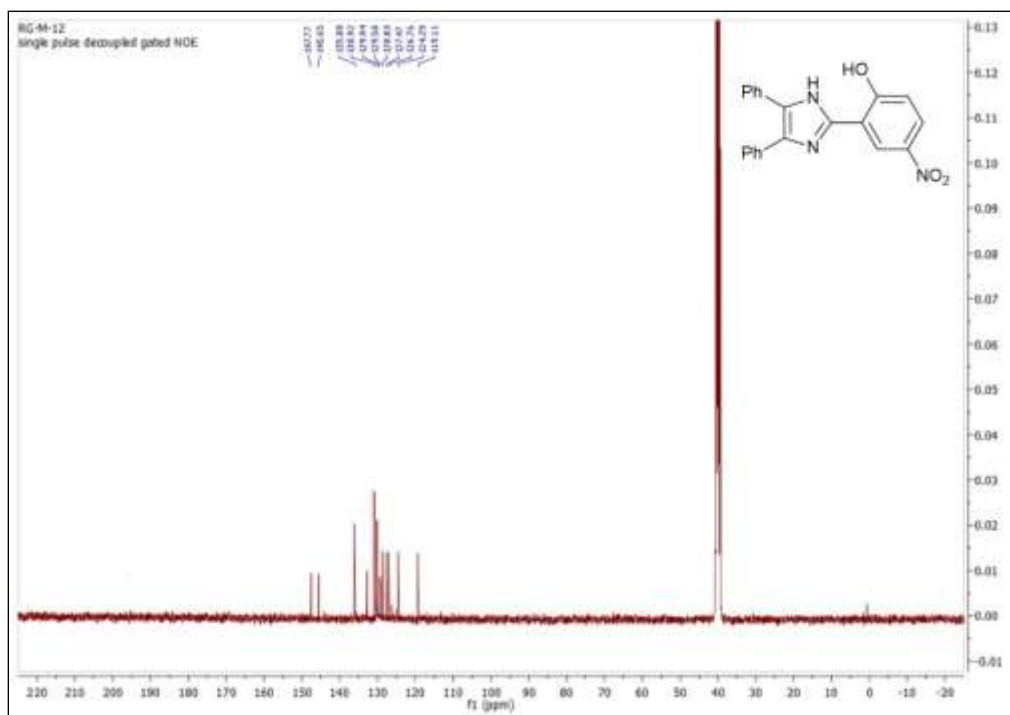
Figure 3.40 ¹³C NMR spectrum of 2-(4,5-diphenyl-1H-imidazol-2-yl)-4-nitrophenol **(8e)**
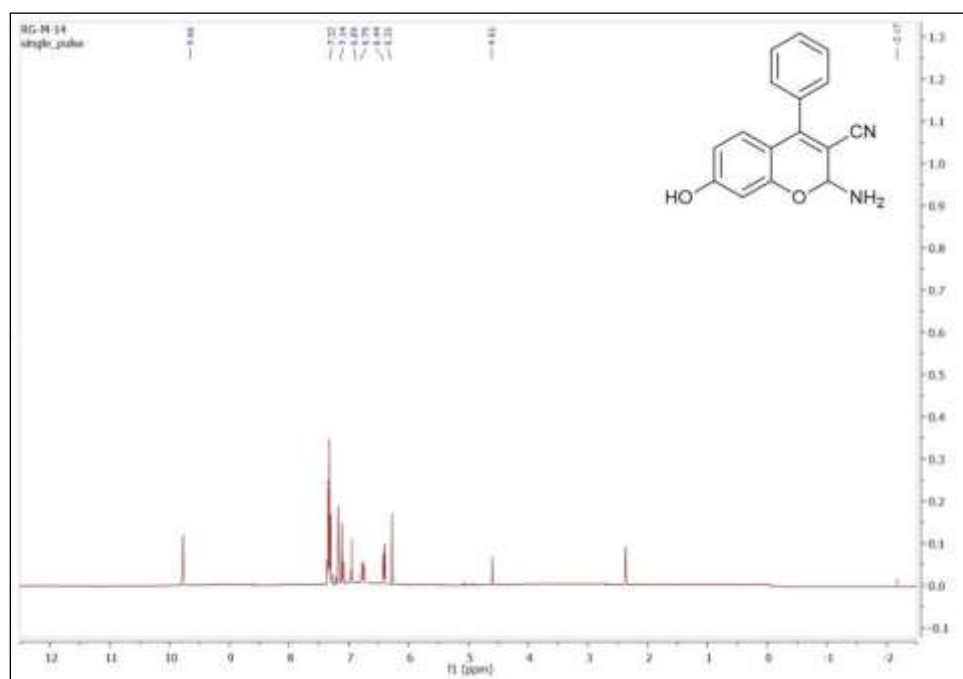
Figure 3.41 ^{1}H NMR spectrum of 2-amino-7-hydroxy-4-phenyl-2H-chromene-3-carbonitrile **(12a)**
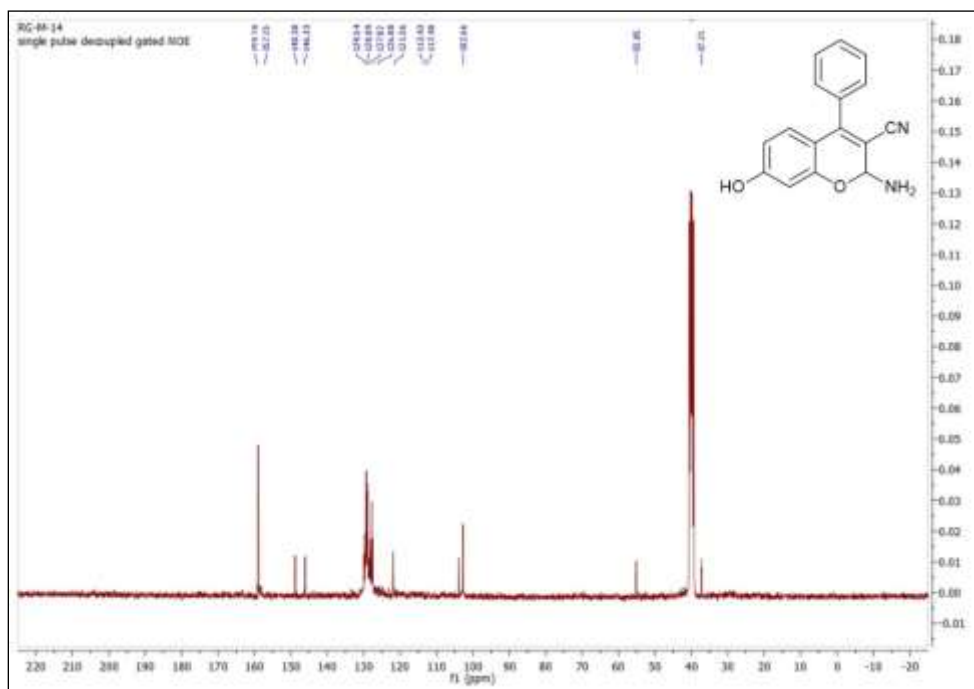
Figure 3.42 ^{13}C NMR spectrum of 2-amino-7-hydroxy-4-phenyl-2H-chromene-3-carbonitrile **(12a)**
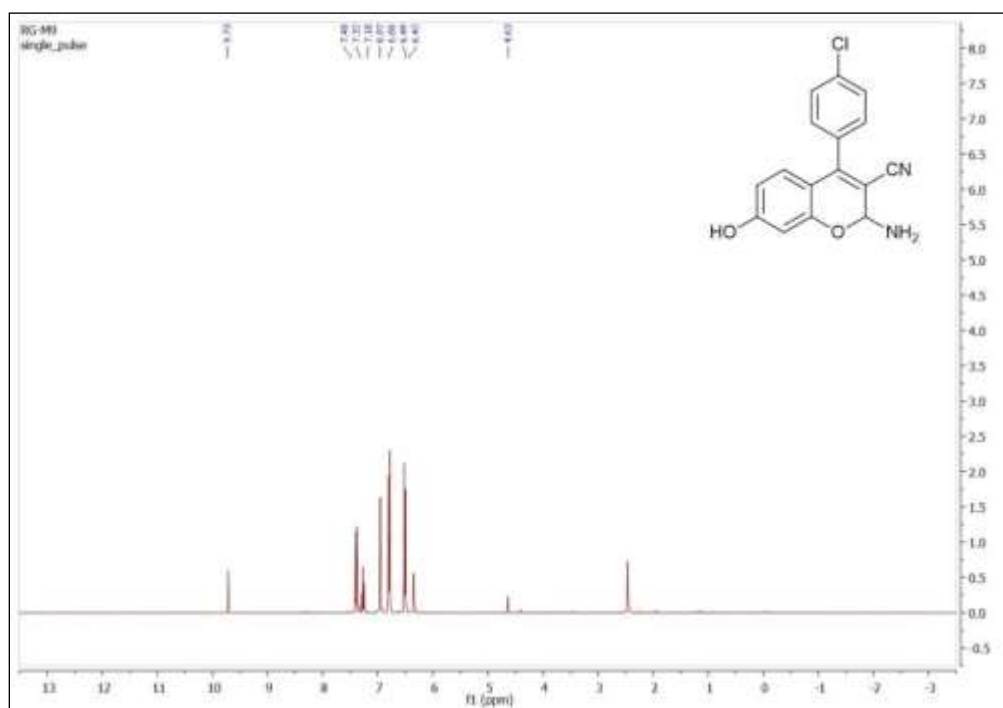
Figure 3.43 ¹H NMR spectrum of 2-amino-4-(4-chlorophenyl)-7-hydroxy-2H-chromene-3-carbonitrile (**12b**)
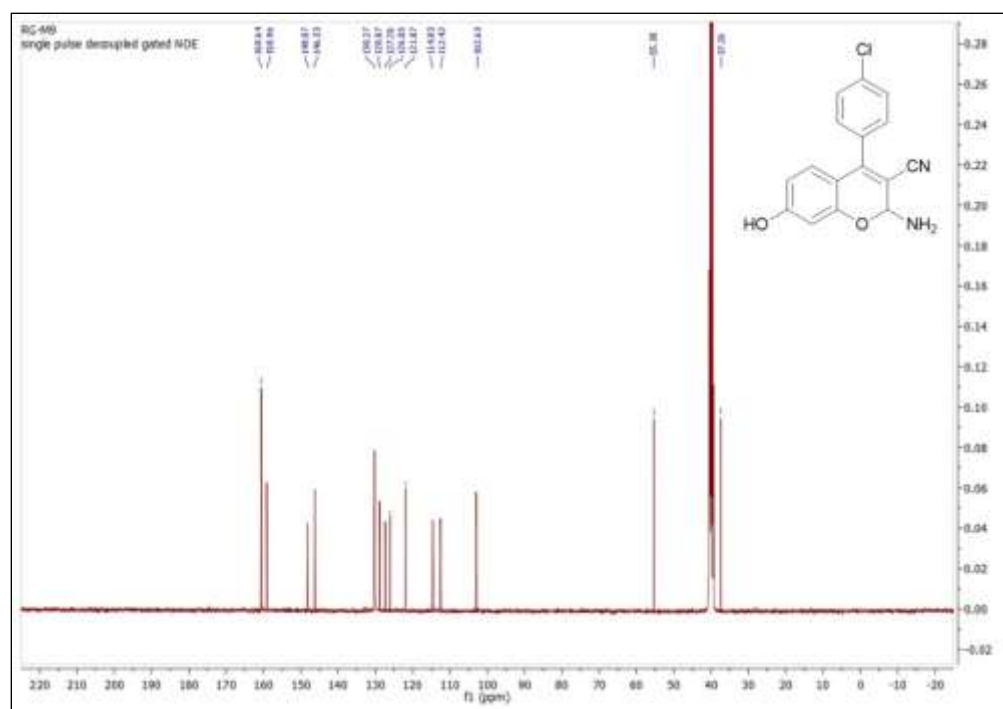
Figure 3.44 ¹³C NMR spectrum of 2-amino-4-(4-chlorophenyl)-7-hydroxy-2H-chromene-3-carbonitrile (**12b**)
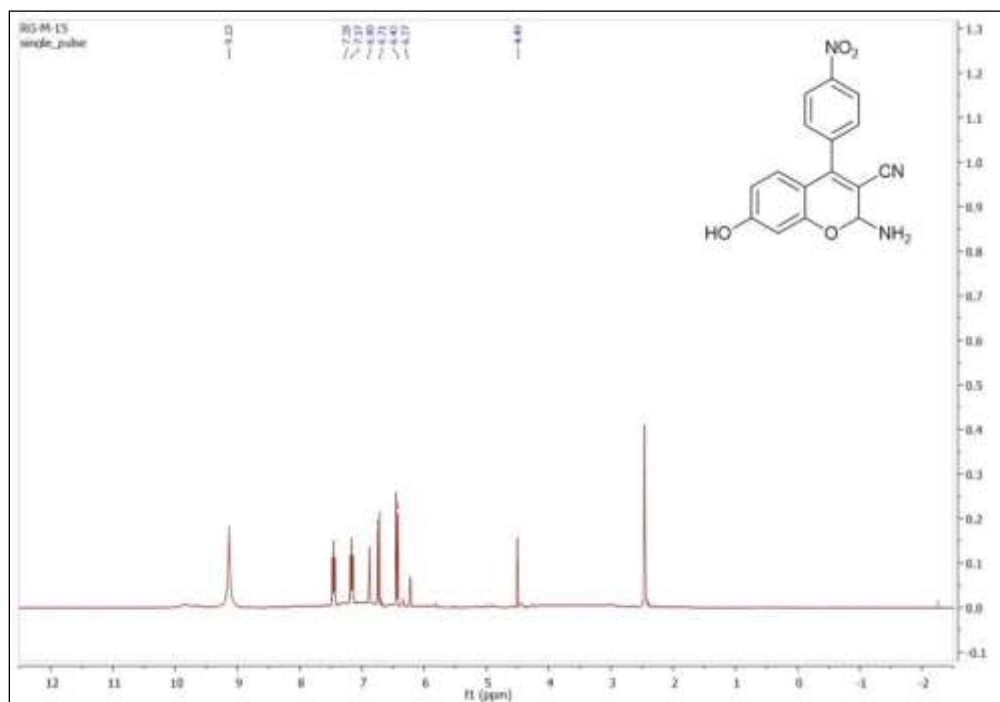
Figure 3.45 ^{1}H NMR spectrum of 2-amino-7-hydroxy-4-(4-hydroxyphenyl)-2H-chromene-3-carbonitrile (**12c**)
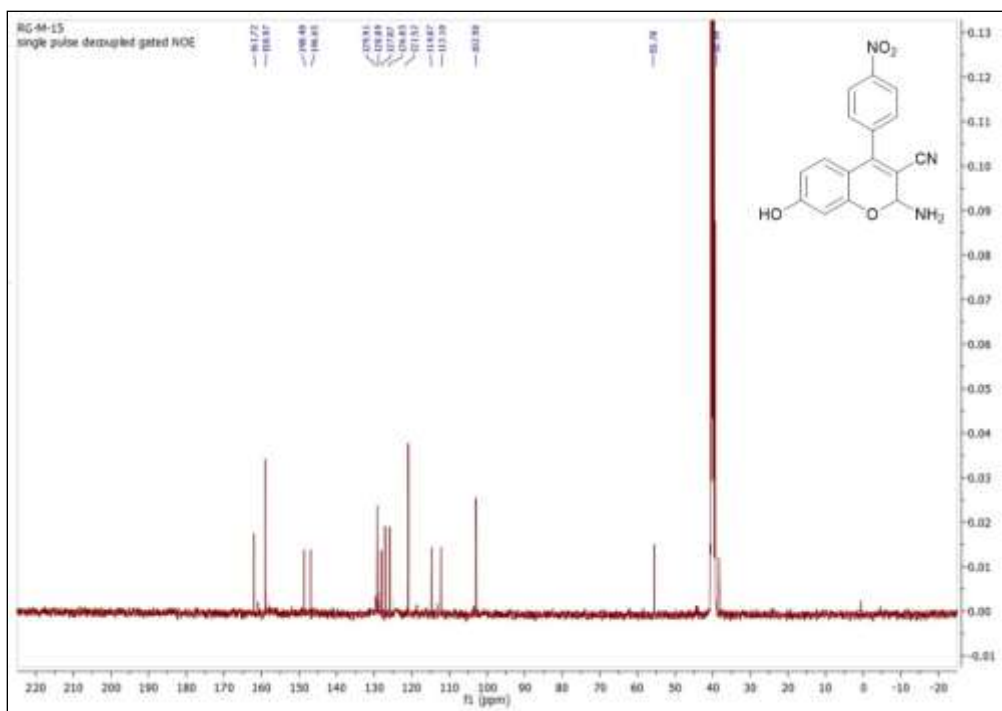
Figure 3.46 ^{13}C NMR spectrum of 2-amino-7-hydroxy-4-(4-hydroxyphenyl)-2H-chromene-3-carbonitrile (**12c**)
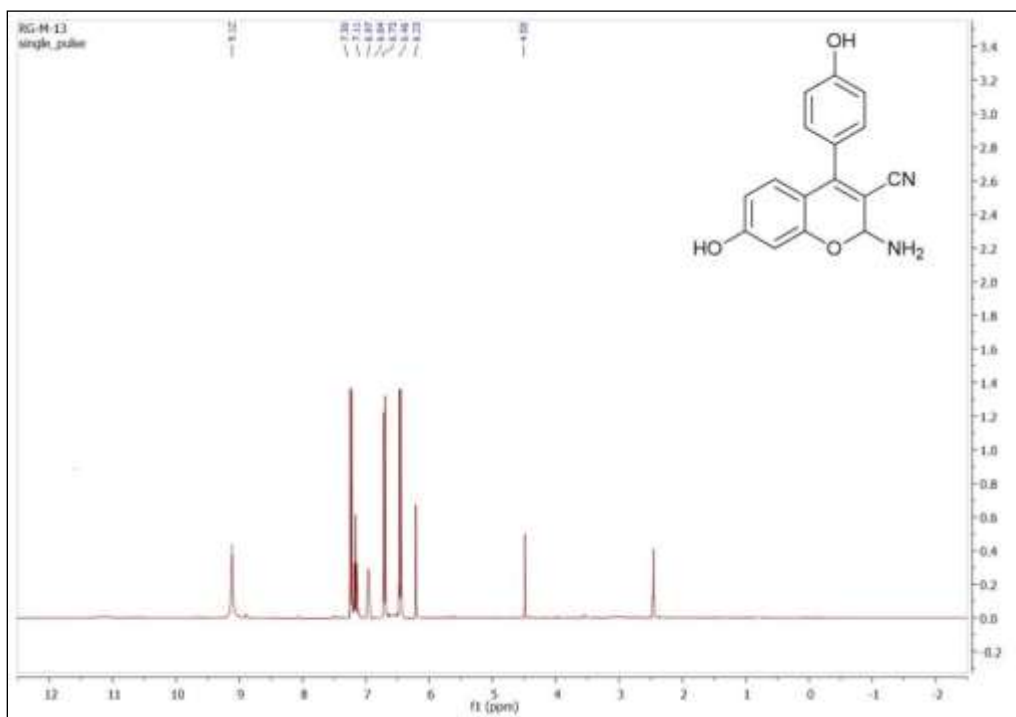
Figure 3.47 ^{1}H NMR spectrum of 2-amino-7-hydroxy-4-(4-nitrophenyl)-2H-chromene-3-carbonitrile **(12d)**
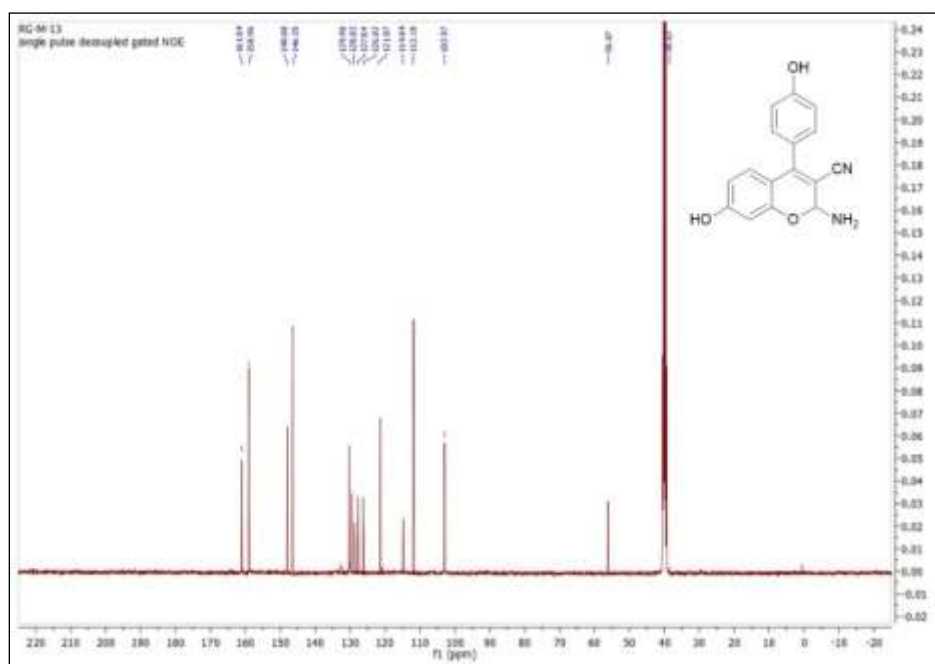
Figure 3.48 ^{13}C NMR spectrum of 2-amino-7-hydroxy-4-(4-nitrophenyl)-2H-chromene-3-carbonitrile **(12d)**

107
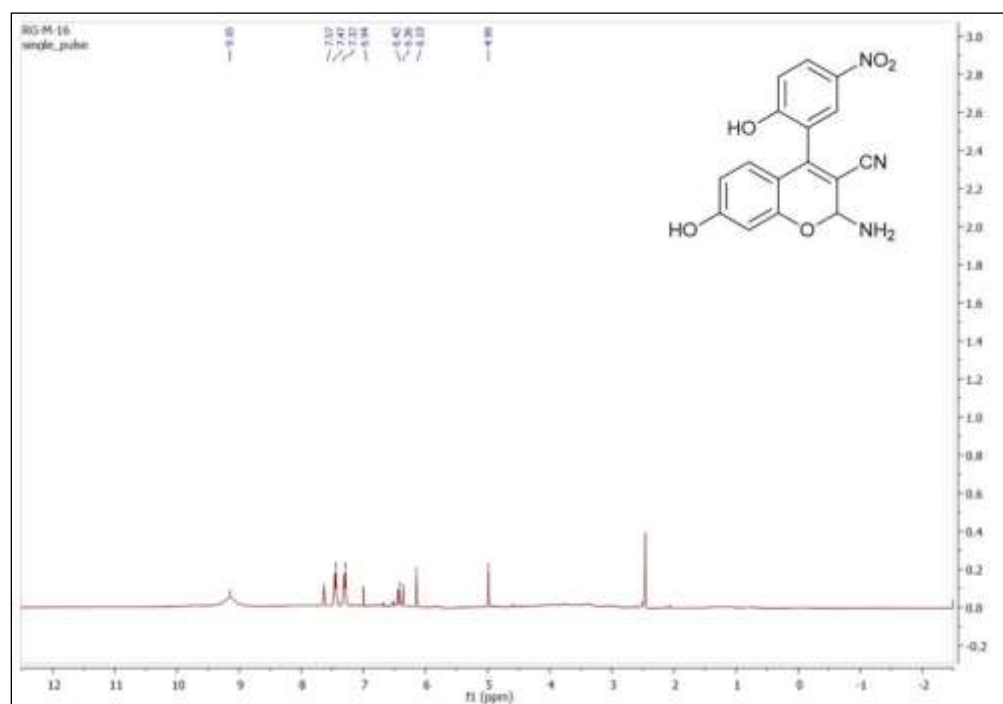
Figure 3.49 ¹H NMR spectrum of 2-amino-7-hydroxy-4-(2-hydroxy-5-nitrophenyl)-2H-chromene-3-carbonitrile **(12e)**
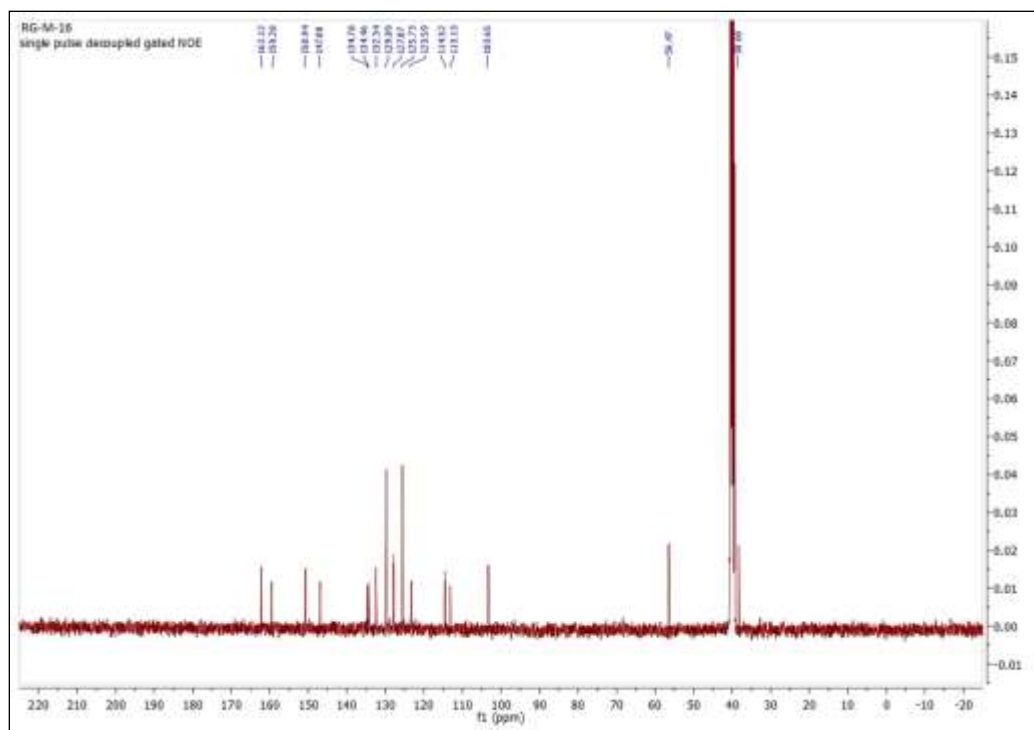
Figure 3.50 ¹³C NMR spectrum of 2-amino-7-hydroxy-4-(2-hydroxy-5-nitrophenyl)-2H-chromene-3-carbonitrile **(12e)**

108
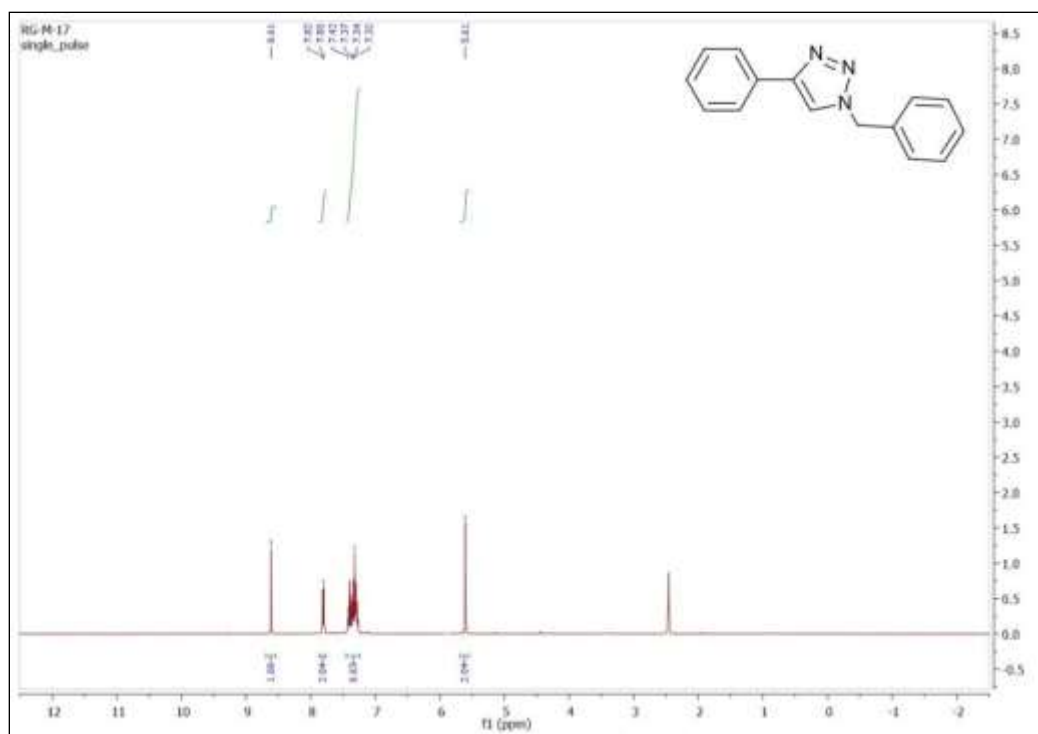
Figure 3.51 ¹H NMR spectrum of 1-benzyl-4-phenyl-1H-1,2,3-triazole **(16a)**
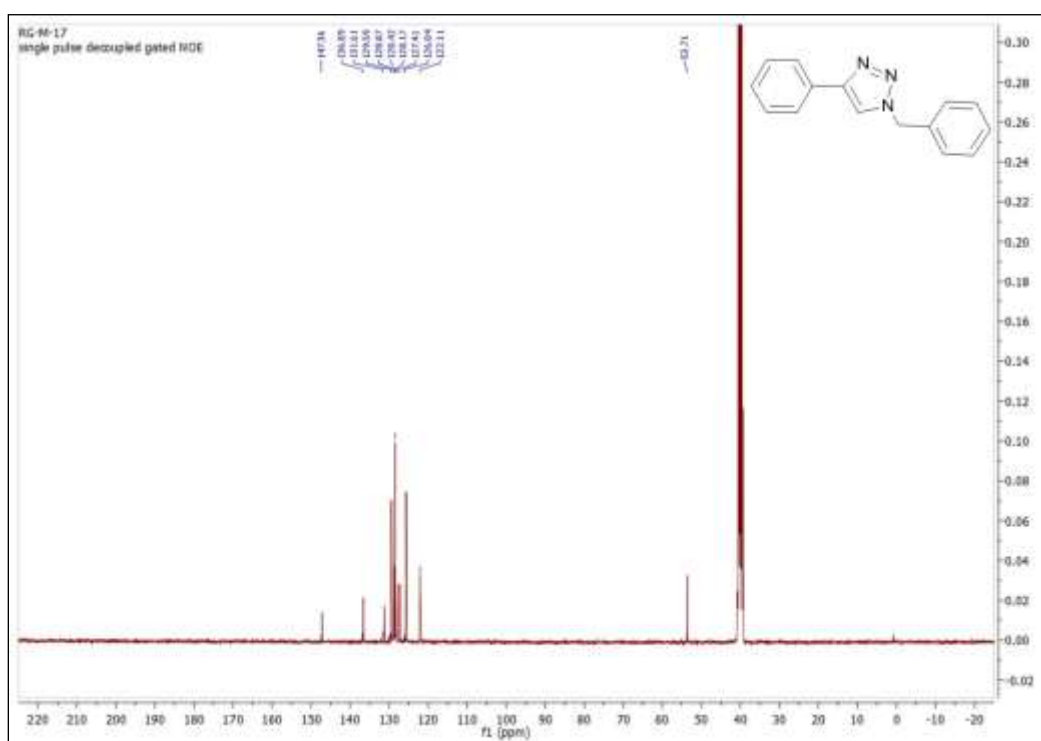
Figure 3.52 ¹³C NMR spectrum of 1-benzyl-4-phenyl-1H-1,2,3-triazole **(16a)**
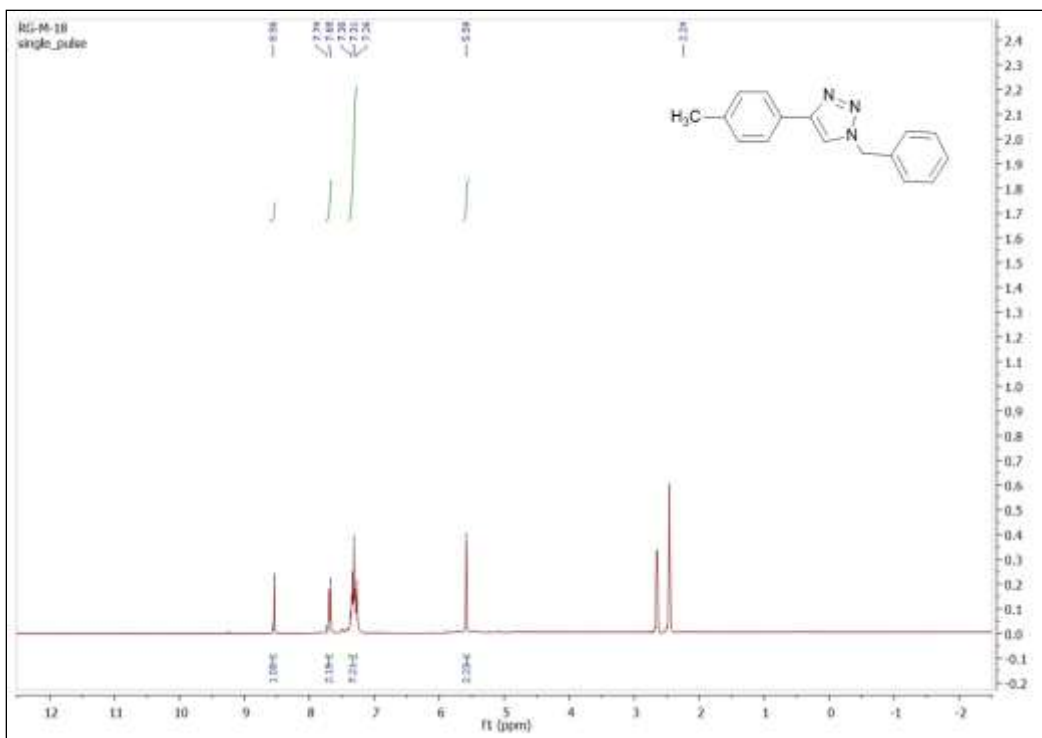
Figure 3.53 ^{1}H NMR spectrum of 1-benzyl-4-(p-tolyl)-1H-1,2,3-triazole **(16b)**
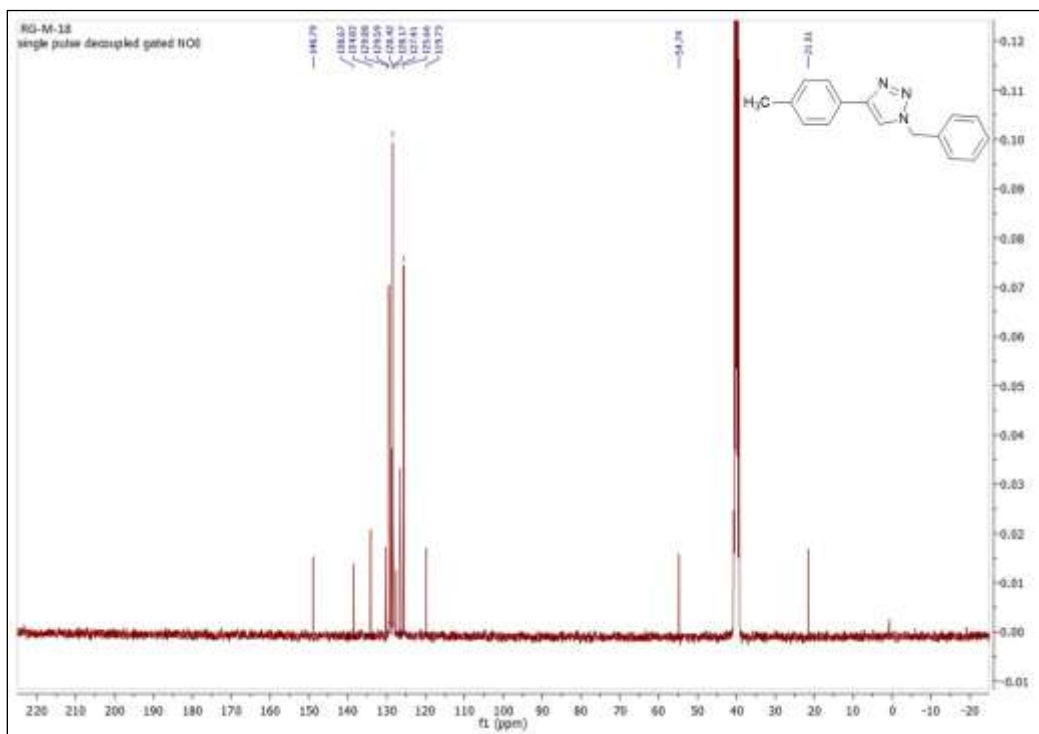
Figure 3.54 ^{13}C NMR spectrum of 1-benzyl-4-(p-tolyl)-1H-1,2,3-triazole **(16b)**
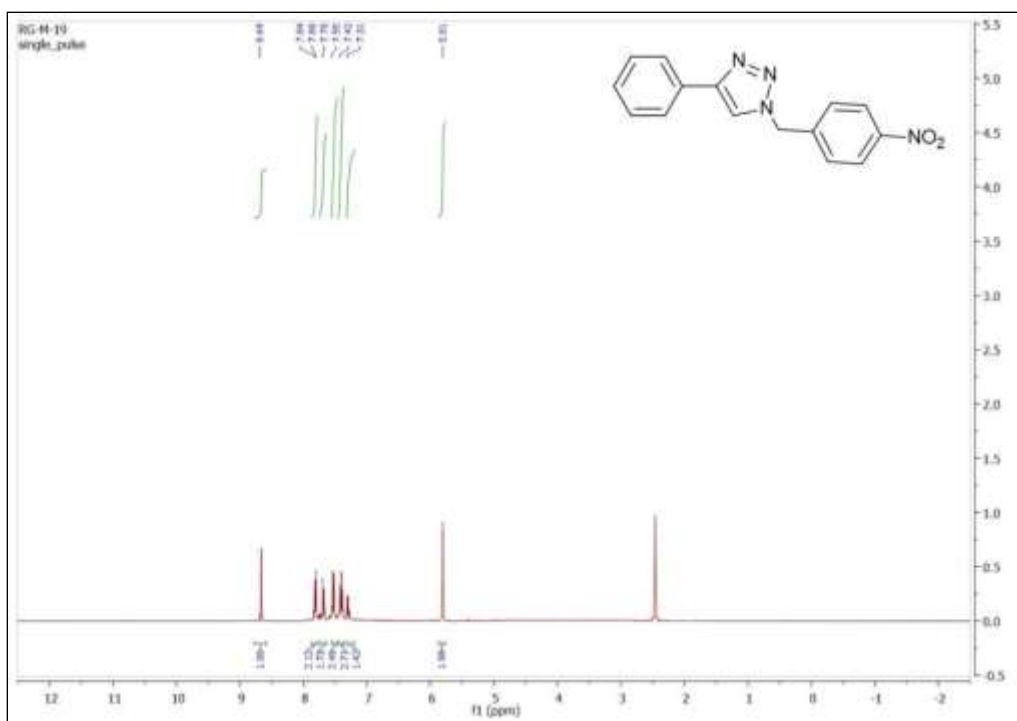
Figure 3.55 ^{1}H NMR spectrum of 1-(4-nitrobenzyl)-4-phenyl-1H-1,2,3-triazole (**16c**)
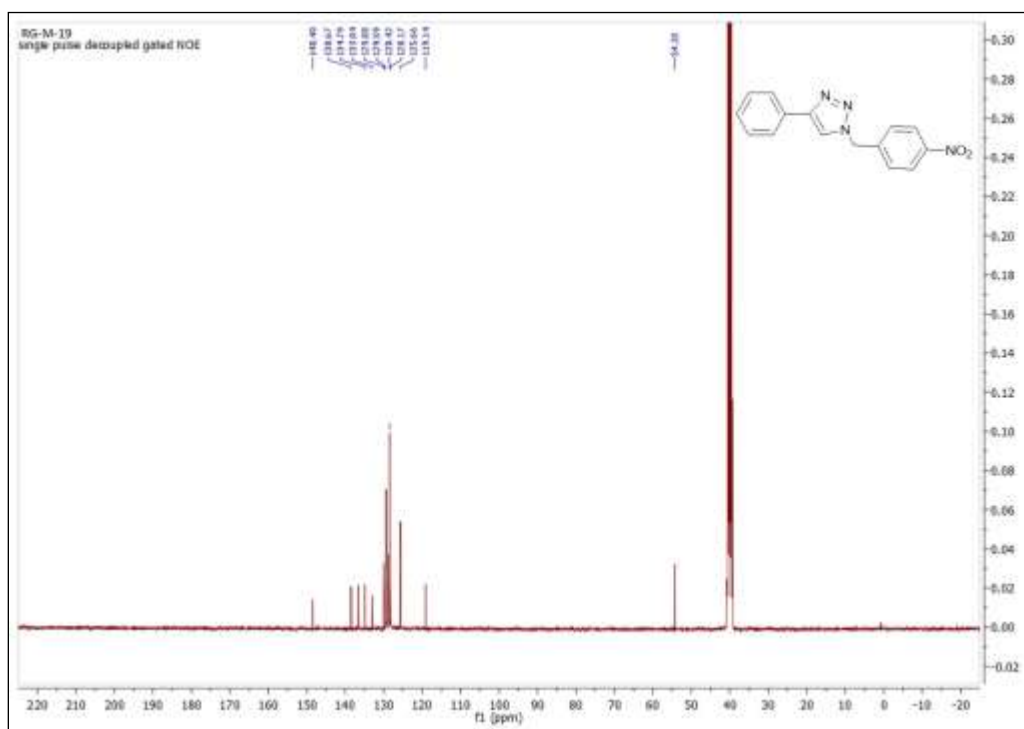
Figure 3.56 ^{13}C NMR spectrum of 1-(4-nitrobenzyl)-4-phenyl-1H-1,2,3-triazole (**16c**)
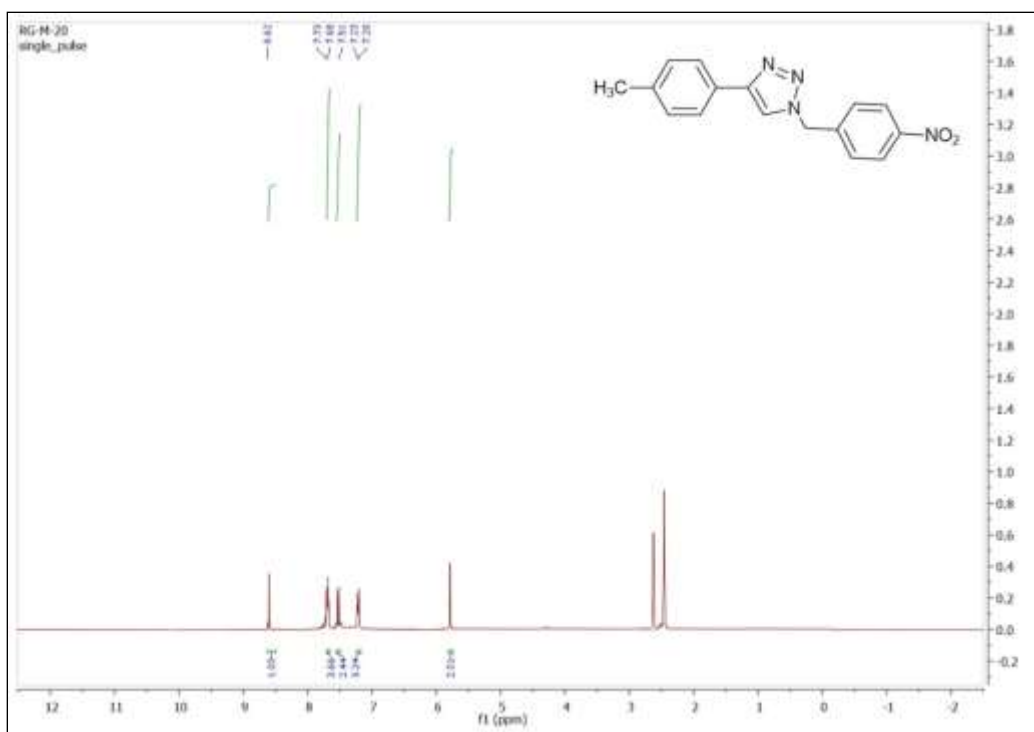
Figure 3.57 ¹H NMR spectrum of 1-(4-nitrobenzyl)-4-(p-tolyl)-1H-1,2,3-triazole **(16d)**
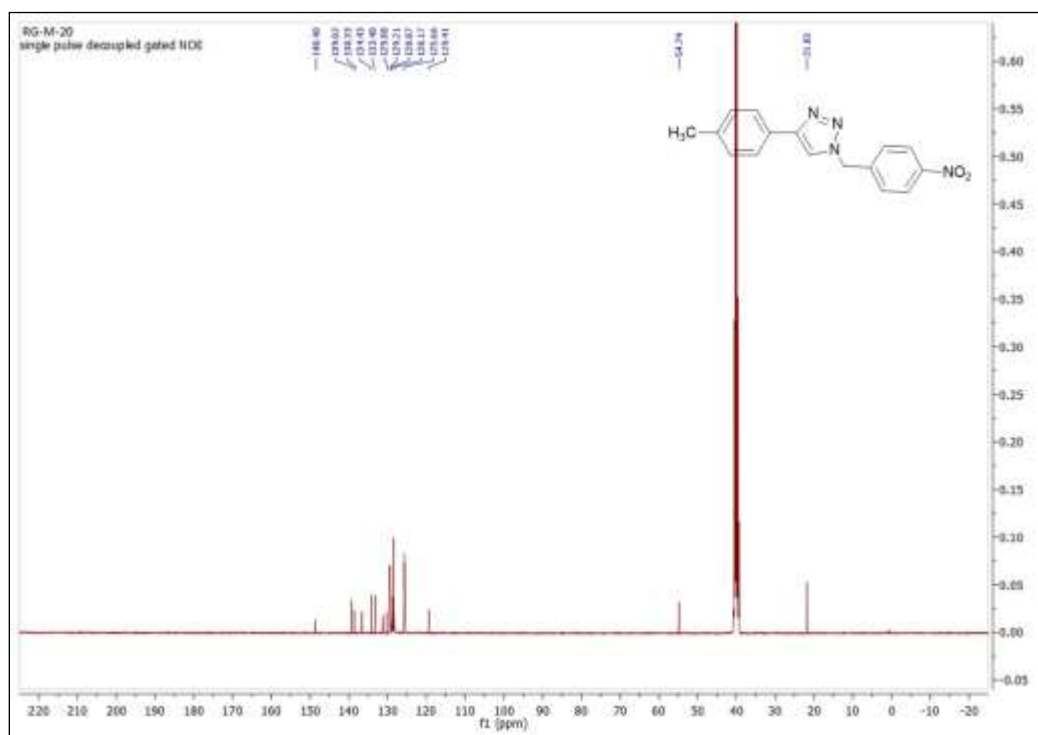
Figure 3.58 ¹³C NMR spectrum of 1-(4-nitrobenzyl)-4-(p-tolyl)-1H-1,2,3-triazole **(16d**

3.4 Conclusion

The synthesized catalyst (Fe_3O_4-DOPA-Cu) exhibits high catalytic activity towards (i) synthesis of DHPMs *via* Biginelli reaction (ii) synthesis of imidazoles (iii) synthesis of 2-amino-4H-chromenes (iv) 1,2,3-triazole derivatives by 'Click reaction' under microwave irradiation (MWI). The advantage of this catalyst are easy to prepare, inexpensive, and offers easy magnetic separation and reusability. Moreover the mild reaction conditions, operational simplicity, giving the desired product in high yields, easy work-up are the key advantages of this protocol. To the best of our knowledge, this is the first time one single catalyst is reported which shows its high activity for these four important multicomponent reactions and this fact makes it attractive.

3.5 References

[1] Nasir Baig, R. B.; Varma, R. S.; *Chem. Commun.* **2012**, *48*, 2582.

[2] Wang, D.; Astruc, D. *Chem. Rev.* **2014**, *114*, 6949.

[3] Gawande, M. B.; Monga, Y.; Zboril, R.; Sharma, R. K. *Coordination Chemistry Reviews* **2015**, *288*, 118.

[4] Shokouhimehr, M.; Hong, K.; Lee, T. H.; Moon, C. W.; Hong, S. P.; Zhang, K.; Suh, J. M.; Choi, K. S.; Varma, R. S.; Jang, H. W. *Green Chemistry* **2016**, *18*, 3184.

[5] Gawande, M. B.; Goswami, A.; Felpin, F. X.; Asefa, T.; Huang, X.; Silva, R.; Zou, X.; Radek, Varma, R. S. *Chem. Rev.* **2016**, *116*, 3722

[6] Nasr-Esfahani, M.; Rafiee, Z.; Montazerozohori, M.; Kashi, H. *RSC Adv*. **2016**, 6, 47298.

[7] Gawande, M. B.; Branco, P. S.; Varma, R. S. *Chem. Soc. Rev*. **2013**, *42*, 3371.

[8] Shelke, S. N.; Bankar, S. R.; Mhaske, G. R.; Kadam, S. S.; Murade, D. K.; Bhorkade, S. B.; Rathi, A. K.; Bundaleski, N.; Orlando, M. N. D.; Zboril, T. R.; Varma, R. S.; Gawande, M. B. *ACS Sustainable Chem. and Eng.* **2014**, *2*, 1699.

[9] Abu-Dief, A. M.; Fatah Abdel, S. M. J. *Basic Appl. Sci.* **2018**, *7*, 55–67

[10] (a) Li, B.; Gao, L.; Bian, F.; Yu, W. *Tetrahedron Lett.* 2013, 54, 1063 (b) Jin, X. K.; Sun, J.; Wang, J.; Dong, Z.; Li, R. *Catal. Commun.* **2012**, *26*, 199 (c) Esmaeilpour, M.; Sardarian, A. R.; Javidi, J. *Appl. Catal. A* **2012**, *445*, 359 (d) Ucoski, G. M.; Nunes, F. S.;

DeFreitas-Silva, G.; Idemori, Y. M.; Nakagaki, S. *Appl. Catal. A* **2013**, *459*, 121 (e) Sharma, R. K.; Monga, Y.; Puri, A.; Gaba, G. *Green Chem.* **2013**, *15*, 2800.

[11]   Yahyazadeh, A.; Gilandeh, E. A.; Hashjin, M. A. *Catal. Lett.* **2018**, *148*, 1254.

[12]   Allen, S. E.; Walvoord, R. R.; Salinas, R. P.; Kozlowski, M. C. *Chem. Rev.* **2013**, *113*, 6234.

[13]   Gawande, M. B.; Goswami, A.; Felpin F. X.; Asefa, T.; Huang, X.; Silva, R.; Zou, X.; Radek, Varma, R. S. *Chem. Rev.* **2016**, *116*, 3722.

[14]   Cioc, R. C.; Ruijter, E.; Orru, R. V. A. *Green Chem.* **2014,** *16*, 2958.

[15]   Chen, M. N.; Mo, L. P.; Cui, Z. S.; Zhang, Z. H. **2019**, *15*, 27.

[16]   Javidi, J.; Esmaeilpour, M.; Dodeji, F. N. *RSC Adv.* **2015**, 5, 308.

[17]   Khosropour, A. R.; Baltork, I. M.; Ghorbankhani, H. *Catal. Commun.* **2006**, *7*, 713.

[18]   Alvim, H. G. O.; Lima, T. B.; De-Oliveira, A. L.; De-Oliveira, H. C. B.; Silva, F. M.; Gozzo, F. C.; Souza, R. Y.; Da Silva, W. A.; Neto, B. A. D. *J. Org. Chem.* **2014**, *79*, 3383.

[19]   Ghosh, B. K.; Moitra, D.; Chandel, M.; Patra, M. K.; Vadera, S. R.; Ghosh, N. N. *Catal. Lett.* **2017**, *147*, 1061.

[20]   Prakash, G. K. S.; Lau, H.; Panja, C.; Bychinskaya, I.; Ganesh, S. K.; Zaro, B.; Mathew, T.; Olah, G. A. *Catal. Lett.* **2014**, *144*, 2012.

[21]   Zheng, H.; Shi, Q. Y.; Du, K.; Mei, Y. J.; Zhang, P. F. *Catal. Lett*. **2013**, *143*, 118.

[22]   (a) Ma Gee, D. I.; Bahramnejad, M.; Dabiri, M. *Tetrahedron Lett.* **2013**, *54*, 2591 (b) Keivanloo, A.; Bakherad, M.; Imanifar, E.; Mirzaee, M. *Appl. Catal. A* **2013**, *467*, 291

[23]   Gadekar, L. S.; Mane, S. R.; Katkar, S. S.; Arbad, B. R.; Lande, M. K. *Cent. Eur. J. Chem.* **2009**, *75*, 50.

[24]   (a) Koike, H.; Konse, T.; Sada, T.; Ikeda, T.; Hyogo, A.; Hinman, D.; Saito, H.; Yanagisawa, H. *Annu. Rep. Sankyo Res. Lab.* **2003**, *55*, 1 (b) Abrahams, S. L. R.; Hazen, J.; Batson, A. G.; Phillips, A. P. *J. Pharmacol Exp. Ther.* **1989**, *249*, 359 (c) Leister, C.; Wang, Y.; Zhao, Z.; Lindsley, C. W. *Org. Lett.* **2004**, *6*, 1453.

[25]   Ji, S. J.; Jiang, Z. Q.; Lu, J.; Loh, T. P. *Syn. lett.* **2004**, *5*, 0831.

[26]   Zhang, X. Y.; Li, Y. Z.; Fan, X. S.; Qu, G. R.; Hu, X. Y.; Wang, J. J. *Chin. Chem. Lett.* **2006**, *17*, 150.

[27]   Ivanciuc, O.; Ivanciuc, T.; Balaban, A. T. *Tetrahedron* **1998**, *54*, 9129.

[28]   Huynh, T. H.; Abrahamsen, B.; Madsen, K. K.; Gonzalez-Franquesa, A.; Jensen, A. A.; Bunch, L. *Bioorgan. Med. Chem.* **2012**, *20*, 6831.

[29]   Wang, J. L.; Liu. D.; Zhang, Z. J.; Shan, S.; Han, X.; Srinivasula, S. M.; Croce, C. M.; Alnemri, E. S.; Huang, Z. *Proc. Nat. Acad. Sci.* **2000**, *97*, 7124.

[30]   Manion, M. K.; Hockenbery, D. **2003**, *2*, 104.

[31]   Raj, T.; Bhatia, R. K.; Sharma, R. K.; Gupta, V.; Sharma, D.; Ishar, M. P. S. *Eur. J. Med. Chem.* **2009**, *44*, 3209.

[32]   Sabry, N. M.; Mohamed, H. M.; Khattab, E. S. A.; Motlaq, S. S.; ElAgrody, A. M. *Eur. J. Med. Chem.* **2011**, *46*, 765.

[33]   Vats, P.; Hadjimitova, V.; Yoncheva, K.; Kathuria, A.; Sharma, A.; Chand, K.; Duraisamy, A. J.; Sharma, A. K. *Med. Chem. Res.* **2014**, *23*, 4907.

[34]   Hajiashrai, T.; Karimi, M.; Heydari, A.; Tehrani, A. A. *Catal. Lett.* **2017**, *147*, 453.

[35]   Sharghi, H.; Ebrahimpourmoghaddam, S.; Doroodmand, M. M.; Purkhosrow, A. *Asian J. Org. Chem.* **2012**, *1*, 377.

[36]   Naeimi, H.; Nejadshafiee, V. *New J. Chem.* **2014**, *38*, 5429.

[37]   Bhardwaj, M.; Jamwal, B.; Paul, S. Catal. Lett. **2016**, *146*, 629.

[38]   Gawande, M. B.; Luque, R.; Zboril, R. T. *Chem Cat Chem*. **2014**, *6*, 3312.

[39]   Gawande, M. B.; Bonifaˊcio, V. D. B.; Luque, R.; Branco, P. S.; Varma, R. S. *Chem. Soc. Rev.* **2013**, *42*, 3371.

[40]   Kumari, M.; Gupta, R.; Jain, Y. *Synth. Commun.* **2019**, *49*, 529.

[41]   Jain, Y.; Gupta, R.; Yadav, P.; Kumari, M. *ACS Omega* **2019**, *4*, 3582.

[42]   Saha, S.; Pal, A.; Kundu, S.; Basu, S.; Pal, T. *Langmuir* **2010**, *26*, 2885.

[43]   Niu, J.; Wang, F.; Zhu, X.; Zhao, J.; Ma, J. *RSC Adv.* **2014**, *4*, 37761.

[44]   Sharma, H.; Bhardwaj, M.; Kour, M.; Paul, S. *Mol. Catal.* **2017**, *435*, 8.

[45]   Sharma, H.; Mahajan, H.; Jamwal, B.; Paul, S. *Catal. Comm.* **2018**, *107*, 68.

[46]   Rathore, P. S.; Patidar, R.; Thakore, S. *RSC Adv.* **2014**, *4*, 41111.

[47]   Hussain, N.; Gogoi, P.; Azhaganand, V. K.; Shelke, M. V.; Das, M. R. *Catal. Sci. Technol*. **2015**, *5*, 1251.

[48]   Mondal, P.; Sinha, A.; Salam, N.; Roy, A. S.; Jana, N. R.; Islam, S. M. *RSC Adv.* **2013**, *3*, 5615.

[49]   Kappe, C. O. *Acc. Chem. Res.* **2000**, *33*, 879.

[50]   Diarjani, E. S.; Rajabi, F.; Yahyazadeh, A.; Santiago, A. R. P.; Luque, R. *Materials* **2018**, *11*, 2458.

[51]   Zarnegar, Z.; Safari, J. *New J. Chem.* **2014**, *38*, 4555

[52]   Akocak, S.; Şen, B.; Lolak, N.; Şavk, A.; Koca, M.; Kuzu, S.; Şen, F. *Nano-Structures & Nano-Objects* **2017**, *11*, 25.

[53]   Ayouchia, H. B. E.; Bahsis, L.; Anane, H.; Domingo, L. R.; Stiriba, S. E. *RSC Adv.* **2018**, *8*, 7670.

[54]   Rostovtsev, V. V.; Green, L. G.; Fokin, V. V.; Sharpless, K. B. *Angew Chem. Int. Ed.* **2002**, *41*, 2596.

[55]   Worrell, B.; Malik, J. A.; Fokin, V. V. *Science* **2013**, *340*, 457.

[56]   Liang, L.; Astruc, D. *Coord. Chem. Rev.* **2011**, *255*, 2933.

[57]   Iacobucci, C.; Reale, S.; Gal, J. F.; Angelis, F. D. *Angew Chem. Int. Ed.* **2015**, *54*, 3065.

Chapter - 4

Fe₃O₄ – Glutathione stabilized Ag nanoparticles: A new magnetically separable robust and facile catalyst for aqueous phase reduction of nitroarenes
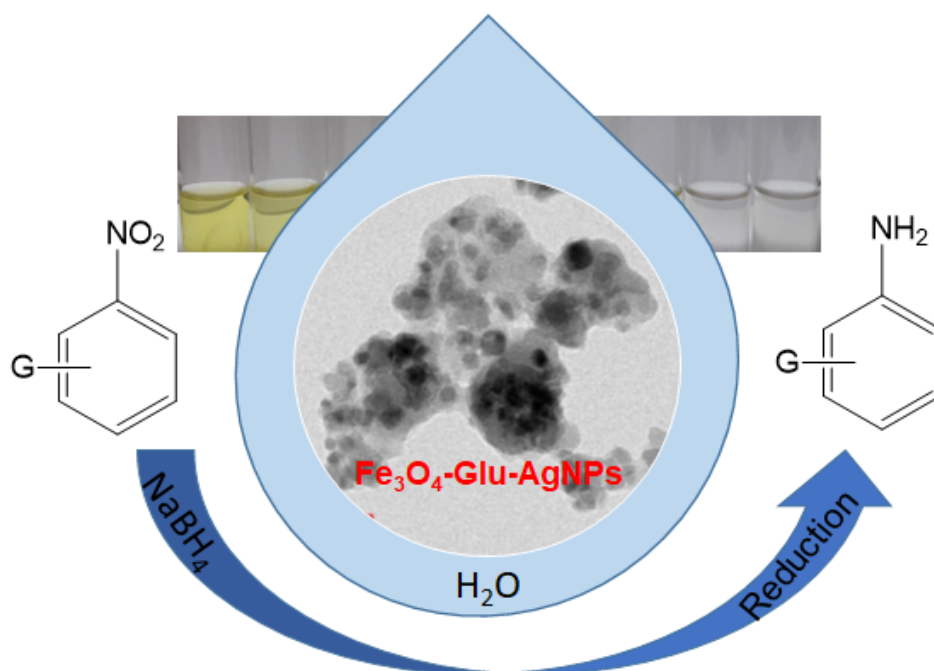
4.1 Introduction

The reduction of nitroarenes has attracted a great deal of attention as the resulting anilines are important intermediates for the manufacture of pharmaceuticals, dyes, polymers, and fine chemicals [1]. 4-nitrophenol being one of the toxic pollutant as the United States Environmental Agency has listed 4-nitrophenol as 'priority pollutant' because it can be hardly removed through natural degradation as a refractory pollutant and will cause serious risk to both animal and human [2]. Generally, the synthesis of anilines entails catalytic [3-5] and non-catalytic methods employing different reducing agents [6-8]. The non-catalytic processes uses either Bechamp or sulfide reduction technology which generates large amounts of undesirable waste that is detrimental to the environment [9]. On the other hand, catalysts used for the catalytic reduction of nitro compounds give priority to the precious metals, such as Pd and Pt, which are expensive and usually sensitive to both air and moisture [10-13]. Another type of catalyst was the iron-based compounds, including $FeCl_3$, iron oxides and FeOOH, which were mainly explored for the reduction of nitroarenes [14]. The preparation and use of magnetic nanoparticles (MNPs) offers advantages in clean and sustainable chemistry as they are non-toxic, readily accessible, and retrievable [15]. However, Fe_3O_4 nanoparticles as supports are vulnerable to the air [16]. Thus, it was needed to functionalized it with organic and inorganic supports [17]. Additionally, the activity and selectivity of magnetic nanocatalysts could be manipulated by their surface modification [18-19].

The first stride in the development of this concept was the selection of amino acids for the functionalization of magnetic nanoparticles. We decided to explore highly benign tripeptide Glutathione, an essential component of plants and human cell systems, as an organocatalyst. An additional benefit of using Glutathione is the presence of the highly reactive thiol group, which could be used for anchoring to the nano ferrite surfaces [20], keeping active sites free for catalysis. The support needed to be chemically stable, convenient for the immobilization of Ag NPs as powdered Ag NPs were not suitable for large scale applications in heterogeneous catalysis because they tend to aggregated owing to their high surface energy, thus resulting in a rapid reduction of their catalytic activity [21]. Ag NPs furthermore difficult to be separated and recycled from the reaction solution because of their ultrafine size. To overcome the above problems, immobilization of Ag NPs on the surface of suitable supporting substances such as metal oxides, polymers, carbon materials becomes efficient and the most adopted approach [22-

27].

In our study, silver nanoparticles were immobilized on magnetite functionalized glutathione which was used as catalyst for the preparation of aromatic amines by the reduction of nitroarenes. The reaction was carried out with sodium borohydride ($NaBH_4$) in water. From earlier reports it can be seen that quite a few noble metal catalysts based on Pt, Pd, Ru, Au, Ag etc. have been designed for this transformation (Xie et al. 2013; Shil et al. 2012; Kim et al. 2012; Liu et al. 2013; Nemanashi et al. 2013). Except Ag, all noble metals are very expensive. Thus, Ag-based recyclable catalysts reduce the cost of the reaction **[28]**. Additionally, the catalytic reduction of nitroarene compounds in sustainable method with green solvent like water which has been one of the most important method for decontamination of nitroarene compounds **[29-44]**. Sodium borohydride ($NaBH_4$) was a common reductant for hydrogenation. When it was used for reduction reactions with the help of transition metal catalysts, although normal pressure and room temperature was available, substantial molar excess of $NaBH_4$ relative to the substrates, usually exceeding 100-fold excess, was needed **[45-46]**. It is important to search suitable catalyst which could increase the catalytic efficiency and decrease the amount of $NaBH_4$ **[47]**. By considering all the above mentioned points and in the course of our investigations into the development of novel inorganic-organic hybrid heterogeneous nanocatalysts in organic transformation, the aim of this presented work is to highlight the synergistic effects of the combined properties of magnetically stabilized Glutathione, in the trapping and stabilizing of the Ag nanoparticles in order to synthesize high efficient and a reusable nanocatalyst for reduction of nitroarenes and heteronitroarenes to the corresponding aromatic amines by using $NaBH_4$ as reducing agent in aqueous medium. Consequently, the optimized conditions were used for the synthesis of various aromatic amines.

4.2 Results and Discussions

4.2.1 Characterization of Fe₃O₄-Glu-Ag nanocatalyst

The synthetic route for the preparation of Ag incorporated glutathione conjugated magnetic nanoparticle, as prepared with a multistep process has been outlined in **Scheme 4.1**. Firstly Fe_3O_4 nanoparticles was prepared by co-precipitation of ferrous and ferric ions in basic aqueous solution followed by thermal treatment. Because of the sensitivity of the Fe_3O_4 nanoparticles its surface was coated with glutathione. Finally, embedding of the silver nanoparticles into the

nanocomposite magnetite-glutathione has been carried out by chemical reduction $AgNO_3$ by hydrazine hydrate and sodium borohydride.
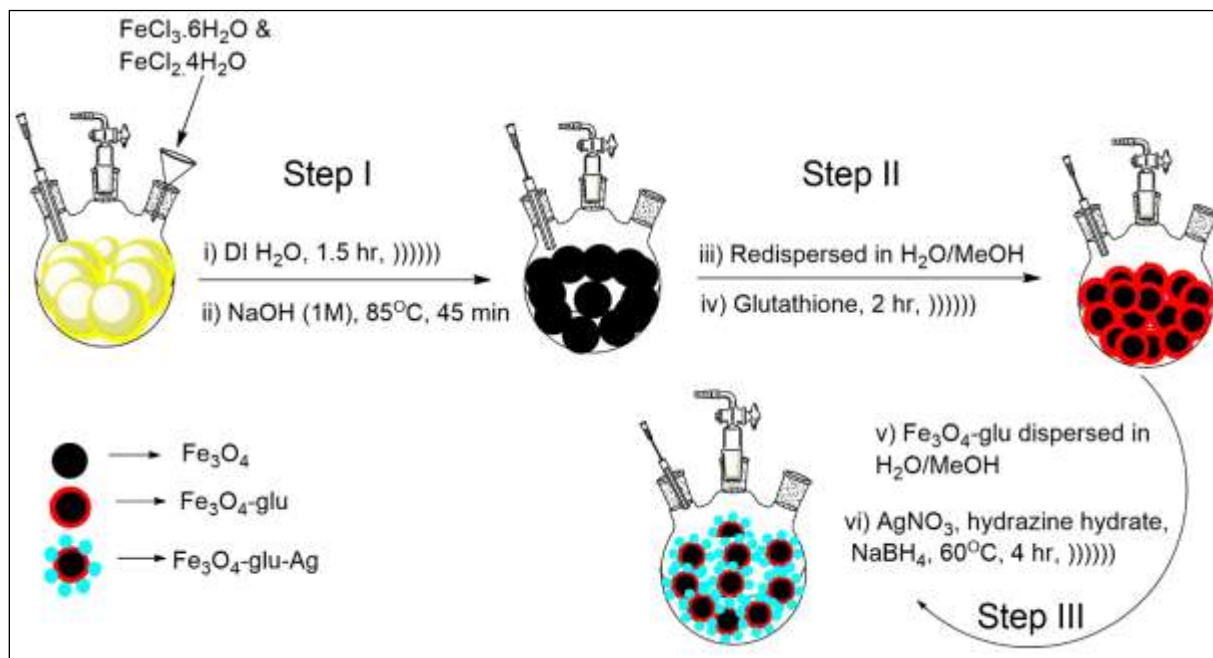
Scheme 4.1 Pictorial depiction for the preparation of Fe_3O_4-Glu-AgNps

The chemical structure of Fe_3O_4-Glu-AgNPs was analysed by using various microscopic and spectroscopic techniques such as FTIR, FESEM, EDS mapping, XRD, HRTEM and TGA. To confirm the immobilization of the active components, FTIR spectroscopy was initially utilized. A strong band at 583 cm^{-1} in **Figure 4.1(b)** was due to the vibration of the Fe–O of ferrite. Three characteristic bands 2947 cm^{-1} (C-H stretching), 1648 cm^{-1} (cysteine carbonyl), and 1629 cm^{-1} (glutamic acid-carbonyl) evidently confirmed the attachment of glutathione on nano ferrite surfaces. The molecule was firmly anchored via the thiol group, as the IR band at 2558 cm^{-1} for S–H stretching was diminished after anchoring. In the IR spectrum of magnetite the characteristic Fe–O stretching peak initially comes at 583 cm^{-1} shifted to 596 cm^{-1} in Fe_3O_4-Glu-AgNPs. **Figure 4.2** shows the X-ray diffraction patterns of the Fe_3O_4, glutathione and Fe_3O_4-Glu-AgNPs. According to JCPDS card no. 19-0629, six diffraction peaks appearing in **Figure 4.2** located at 30.4°, 35.5°, 43.3°, 53.4°, 57.2° and 62.8° can be assigned to diffraction of Fe_3O_4 crystal with an inverse spinel structure from the (220), (311), (400), (422), (511), and (440).

XRD pattern of Fe_3O_4-Glu-AgNPs shows same diffraction peaks as of magnetite. In addition, obvious diffraction peaks at 2θ values of 38.2°, 64.3° and 77.3° has been also observed which were corresponding to the (111), (220), and (311) planes of silver, respectively.
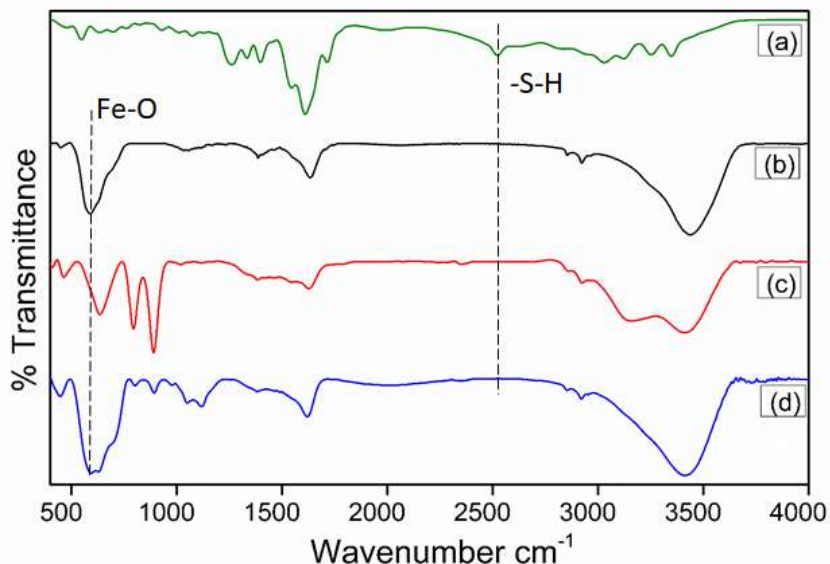
Figure 4.1 FTIR spectrum of (a) glutathione (b) Fe_3O_4 (c) Fe_3O_4-Glu (c) Fe_3O_4-Glu-Ag

Figure 4.2 shows the X-ray diffraction patterns of the Fe_3O_4, glutathione and Fe_3O_4-Glu-AgNPs. According to JCPDS card no. 19-0629, six diffraction peaks appearing in **Figure 4.2** located at 30.4°, 35.5°, 43.3°, 53.4°, 57.2° and 62.8° can be assigned to diffraction of Fe_3O_4 crystal with an inverse spinal structure from the (220), (311), (400), (422), (511), and (440). XRD pattern of Fe_3O_4-Glu-AgNPs shows same diffraction peaks as of magnetite. In addition, obvious diffraction peaks at 2θ values of 38.2°, 64.3° and 77.3° has been also observed which were corresponding to the (111), (220), and (311) planes of silver, respectively. Thermal gravimetric analysis (TGA) of bare magnetite Fe_3O_4-Glu-AgNPs was performed within the range of 25-900˚C under an inert atmosphere of nitrogen.
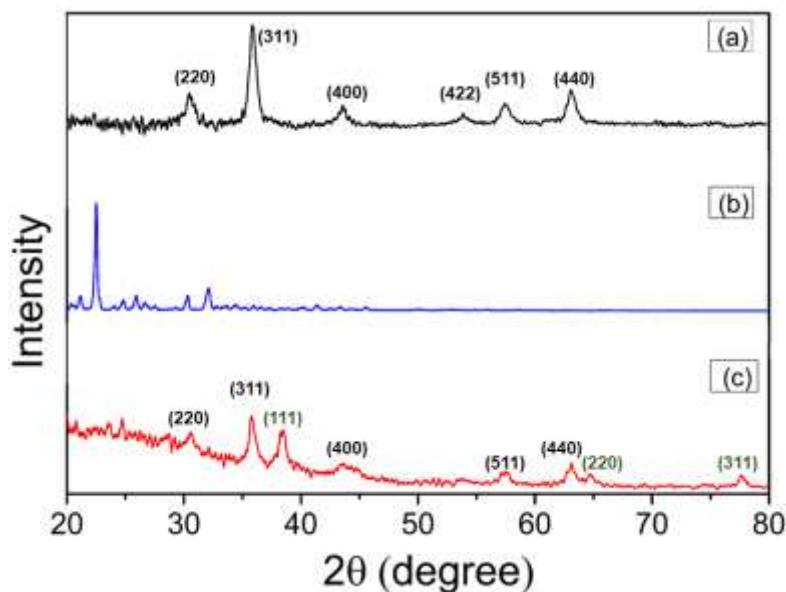
Figure 4.2 XRD of (a) Fe$_3$O$_4$ (b) glutathione (c) Fe$_3$O$_4$-Glu-AgNPs

As shown in **Figure 4.3 (a)** 3.5% weight loss was observed due to presence of water and OH group deterioration present on the surface of magnetite. **In Figure 4. 3 (b)** major weight loss of 18 % at high temperature was observed which confirms that glutathione was chemically bounded to the magnetic nanoparticles. It implies that thermal stability of synthesised Fe$_3$O$_4$-Glu-AgNPs have been maintained at higher temperature.
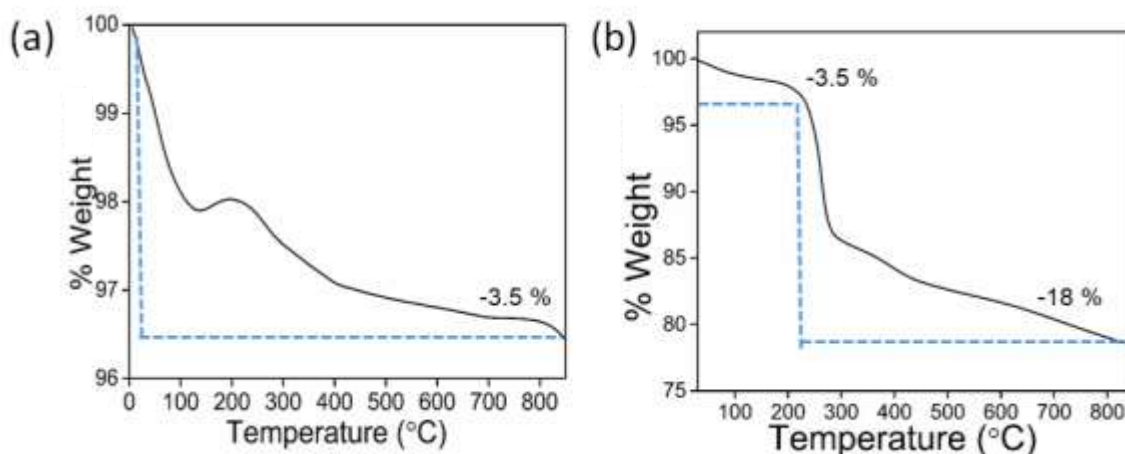
Figure 4.3 TGA curve of (a) Fe$_3$O$_4$ (b) Fe$_3$O$_4$-Glu-AgNPs

Furthermore, the chemical composition of the Fe_3O_4-Glu-Ag nanocomposite was determined by energy X-ray spectroscopy (EDS). It is found that the peaks of C, N, S, O, Fe and Ag were observed. The percentage of each element of nanocatalyst were obtained from energy dispersive X-ray spectrum **(Figure 4.5)**. The presence of silver centers in the nanocomposite support Fe_3O_4-Glu was confirmed by elemental mapping images **(Figure 4.4)**. The result showed uniform distribution of silver nanoparticles over the structure of the glutathione supported magnetite.
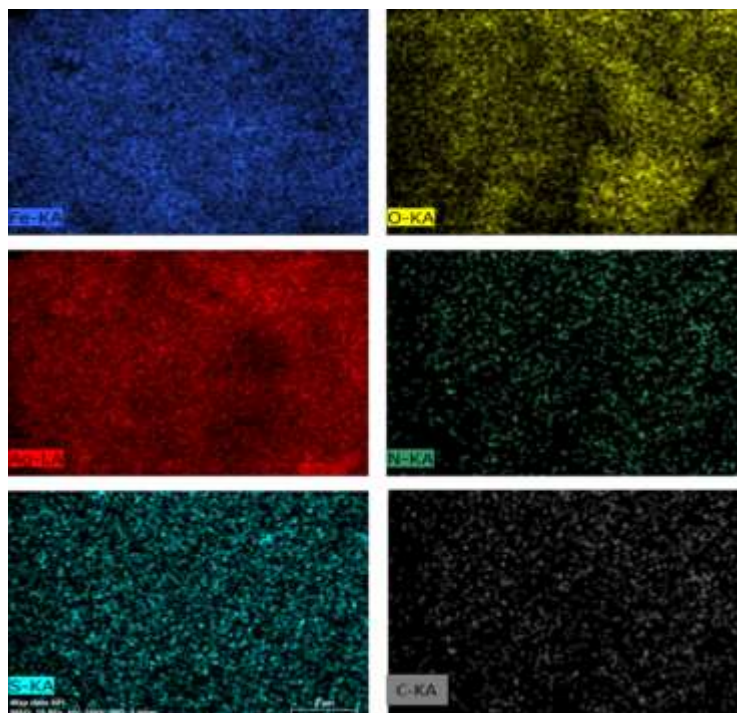
Figure 4.4 EDS elemental mapping of the Fe_3O_4-Glu-AgNPs

Transmission electron-microscopy studies as shown in **Figure 4.6 (a, b, c)** depicts the low magnification TEM image of the Fe_3O_4, Fe_3O_4-Glu and Fe_3O_4-Glu-Ag nanoparticles and revealed that the particles were almost spherical and multifaceted cuboid in shape while the histogram **Figure 4.6 (d)** showed that the size ranges from 1-25 nm with dominant particles in the range of size 11-15 nm. Some dark spots in the TEM image of Fe_3O_4-Glu-Ag **Figure 4.6 (e)** could be attributed to the presence of silver nanoparticles in catalyst and revealed that the Ag nanoparticles have been incorporated in the Fe_3O_4-Glu successfully. The selected area electron diffraction pattern as shown in **Figure 4.6 (f)** displayed that the particles were polycrystalline in nature.
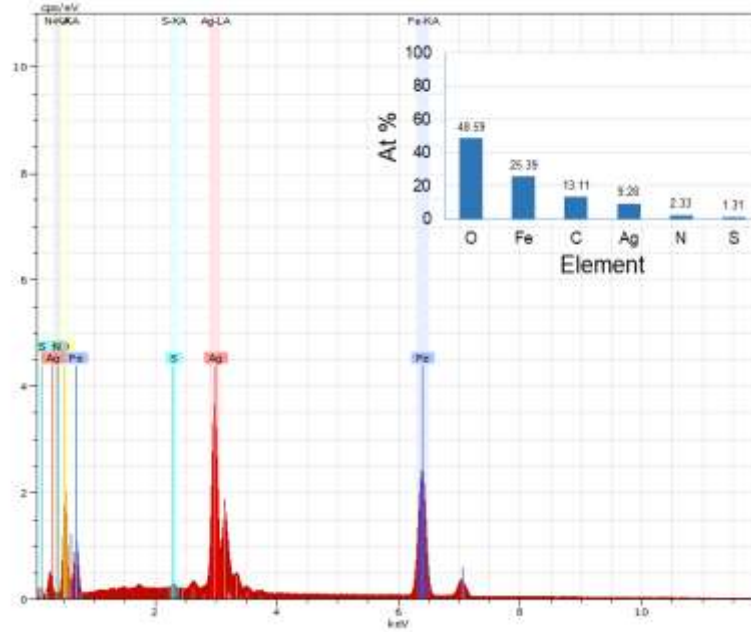
Figure 4.5 EDS spectrum of Fe_3O_4-Glu-AgNPs
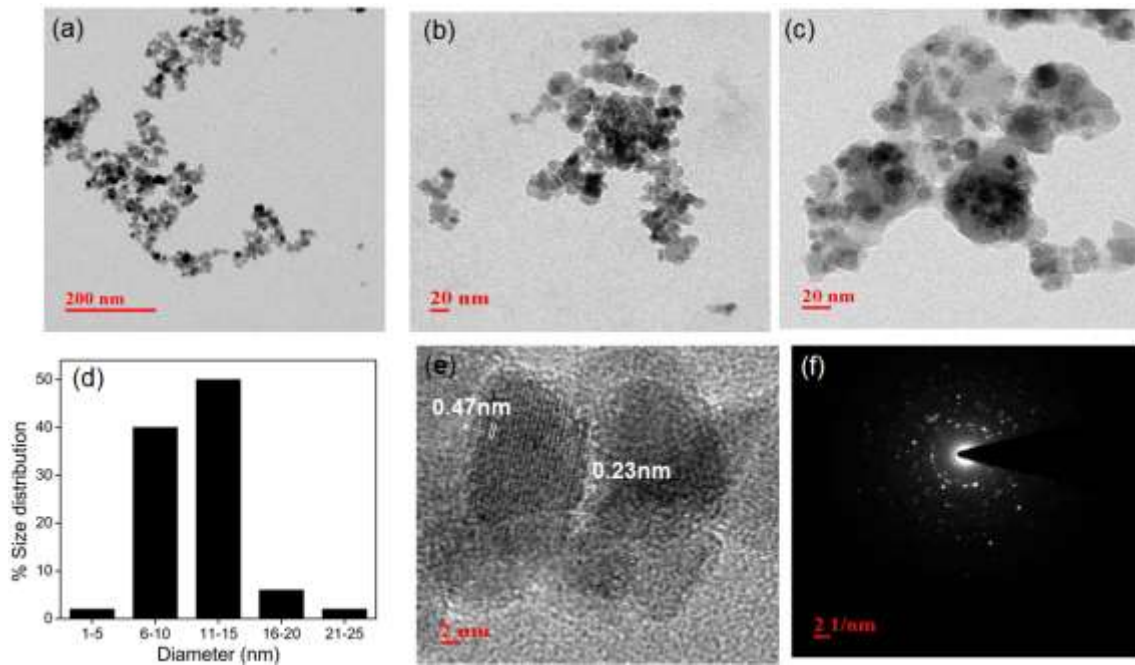
Figure 4.6 Low magnification TEM image of (a) Fe_3O_4 (b) Fe_3O_4-Glu (c) Fe_3O_4-Glu-Ag (d) Histogram showing size distribution of Fe_3O_4-Glu-AgNPs (e) HRTEM image showing the interlayer planes (f) SAED pattern of the corresponding low magnification TEM image of Fe_3O_4-Glu-AgNPs

4.2.2 Reduction of nitro compounds by Fe$_3$O$_4$-Glu-Ag nanocatalyst

After the successful preparation and characterization of the Fe$_3$O$_4$-Glu-AgNPs, catalytic performance of the nanocatalyst have been explored in the reduction of 4-nitrophenol (4-NP) as model reaction in the presence of NaBH$_4$ as a reductant. Three experiments were performed initially under ultrasonication (i) reduction in the absence of the catalyst Fe$_3$O$_4$-Glu-Ag, no product obtained; (ii) reduction was also performed in the presence of bare magnetite only, negligible conversion of reactant was observed; (iii) when reaction was performed in the presence of Fe$_3$O$_4$-Glu-Ag nanoparticles, products were obtained in good yield.
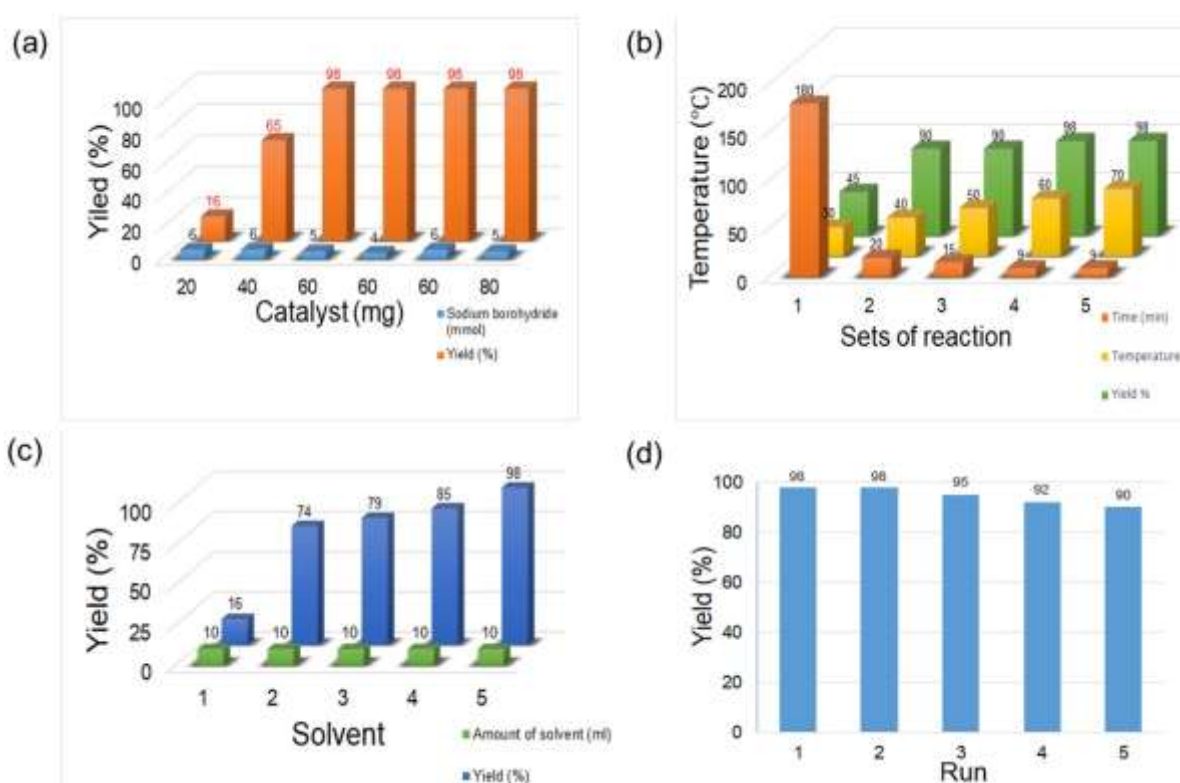
Figure 4.7 (a) Optimization of reductant amount and catalyst loading for reduction of 4-NP (b) Optimization of time and temperature for reduction of 4-NP (c) Standardization of various solvents (1. Toluene 2. MeOH 3. EtOH 4. MeOH/H$_2$O 5. H$_2$O) (d) Recyclability of Fe$_3$O$_4$-Glu-AgNPs in the reduction of 4-NP under optimized conditions.

To explore the optimum amount of needed catalyst and reductant, different catalyst loadings (20, 40, 60, 80) were investigated at different mmol (4, 5, 6) of reductant **(Figure 4.7 (a))** which revealed that 60 mg of the catalyst and 4 mmol of reductant were the optimum that afforded 98%

of aminophenol. Next, the reduction of nitrophenol was investigated varying temperature and time (**Figure 4.7 (b)**). A poor yield was obtained at 30 ℃ and at a time of 180 min. Then, the temperature and time for the reaction was changed to 40 ℃ and 20 min, respectively, giving 90% of yield of 4-aminophenol. The temperature when increased to 60 ℃ over a time period of 9 min, excellent yield was observed of 98%. No notable change in yield was observed at temperature greater than 60 ℃ and thus 60 ℃ and 9 min were chosen as the optimized reaction temperature and time respectively. As shown in **Figure 4.7 (c)** the effect of different solvents on the reduction of 4-nitrophenol was also investigated and it was discerned that the product yield was not satisfactory in toluene as the reducing agent was less soluble in it compared to other polar solvents. Ethanol and methanol afforded moderate yield and mixture of methanol and water showed good yield. The product yield improved with the polarity of solvents and the yield was highest in water as the solubility of $NaBH_4$ in water is high and thus water served as the best solvent. The kinetics of the catalytic reduction was also studied in a standard quartz cuvette with 1 cm path length and 4.5 ml volume. Then 3 ml of water was mixed with 20 µl (10^{-2} M) of 4-nitrophenol solution, finally 150 µl (10^{-1}M) was added. After mixing these solutions, 3 mg of Fe_3O_4-Glu-AgNPs were added in cuvette to study the reduction reaction. UV-visible spectrum were recorded at every 3 min interval in the range of 200-600 nm for 9 minutes. The rate constant was determined by measuring the change in absorbance (**Figure 4.8 (a)**) of a peak at 400 nm, the initially observed peak for the nitrophenolate ion, as a function of time. The peak shows a gradual decrease in intensity with time and a new peak appeared at 295 nm indicating the formation of 4-aminophenol. A linear correlation between ln (A_t/A_0) and reaction time, where A_t and A_0 represented the absorbance at the fixed intervals and the absorbance at the initial stage, respectively (**Figure 4.8 (b)**). This result confirmed that the reaction is a pseudo-first order and its rate constant (k) was calculated from the slope to be 0.510 min^{-1}.
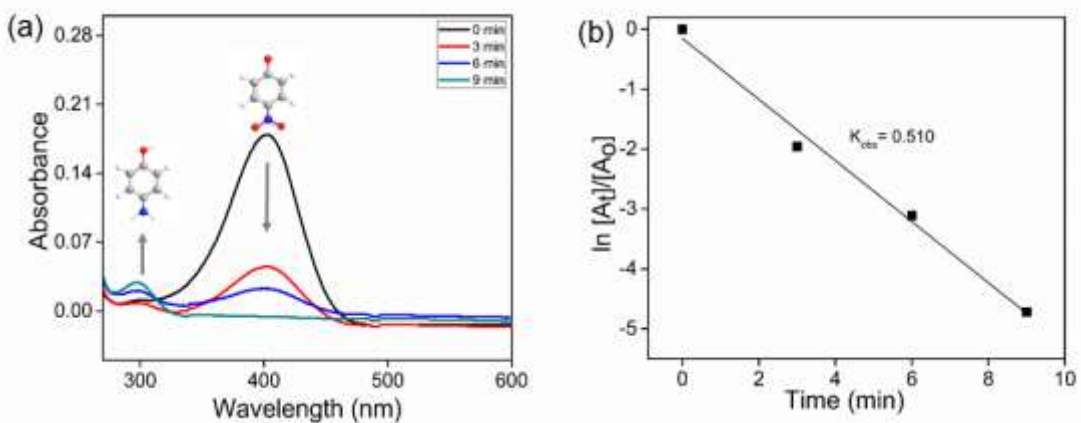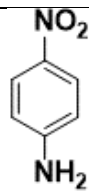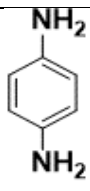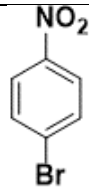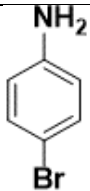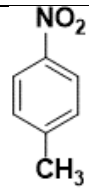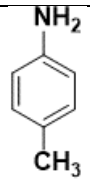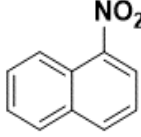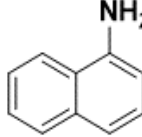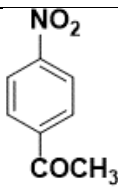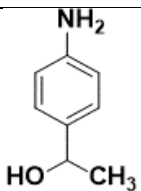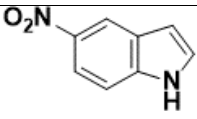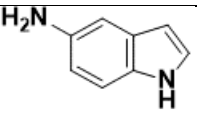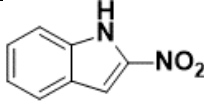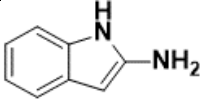
Figure 4.8 (a) Time-dependent UV-visible absorption spectrum for the reduction of 4-nitrophenol over Fe_3O_4-Glu-AgNPs in aqueous media at 60 °C, and **(b)** Plot of ln (A_t/A_0) versus time for reduction of 4-nitrophenol

Table 4.1 Catalytic reduction of nitroarenes over Fe_3O_4-Glu-Ag nanocatalyst

S. No	Nitro Compound	Product	Time (min)	Yield (%)
1			9	98
2			9	97
3			12	98

4	4-nitroaniline (NO₂ and NH₂ on benzene)	benzene-1,4-diamine (NH₂ and NH₂)	10	95
5	4-bromonitrobenzene (NO₂, Br)	4-bromoaniline (NH₂, Br)	15	92
6	4-nitrotoluene (NO₂, CH₃)	4-methylaniline (NH₂, CH₃)	15	90
7	1-nitronaphthalene (NO₂)	1-naphthylamine (NH₂)	10	95
8	4-nitroacetophenone (NO₂, COCH₃)	1-(4-aminophenyl)ethanol (NH₂, HO–CH–CH₃)	10	94
9	5-nitroindole (O₂N, indole NH)	5-aminoindole (H₂N, indole NH)	18	90
10	2-nitroindole (indole NH, NO₂)	2-aminoindole (indole NH, NH₂)	15	88

Reaction conditions: 4-nitrophenol (0.5 mmol), NaBH₄ (4 mmol), Fe₃O₄-Glu-Ag (60 mg), 10 mL of H₂O, 60 ℃, ultrasonicated in open air

128

Using the optimized reaction conditions, (0.5 mmol of 4-nitrophenol, 4 mmol of $NaBH_4$, 60 mg of the catalyst at 60 ℃ in aqueous solution) the activity and synthetic scope of the catalyst was demonstrated by reduction of a series of nitroarenes **(Table 4.1)**. As shown in **Table 4.1**, activated and deactivated groups have a very small authority on the reaction times and yields. In all cases, corresponding amines were found to be the exclusive product of the reactions according to TLC and the azo, hydrazo and azoxy groups as the usual side products in the reduction of nitroarenes were not detected. A plausible reaction mechanism for the reduction of aromatic nitro compounds to corresponding amine using Fe_3O_4-Glu-Ag catalyst with $NaBH_4$ as hydrogen source is shown in **Scheme 4.2**. The mechanism was proposed based on the reported literature **[28]**.The reaction pathway follow direct route where $[BH_4]^-$ ion and the substrate adsorption-desorption takes place at the silver nanoparticle surface. The aromatic nitro compound then get reduced to the corresponding nitroso compounds. Those were again converted to hydroxylamine and lastly after further reduction, desired substituted aromatic amines were obtained.
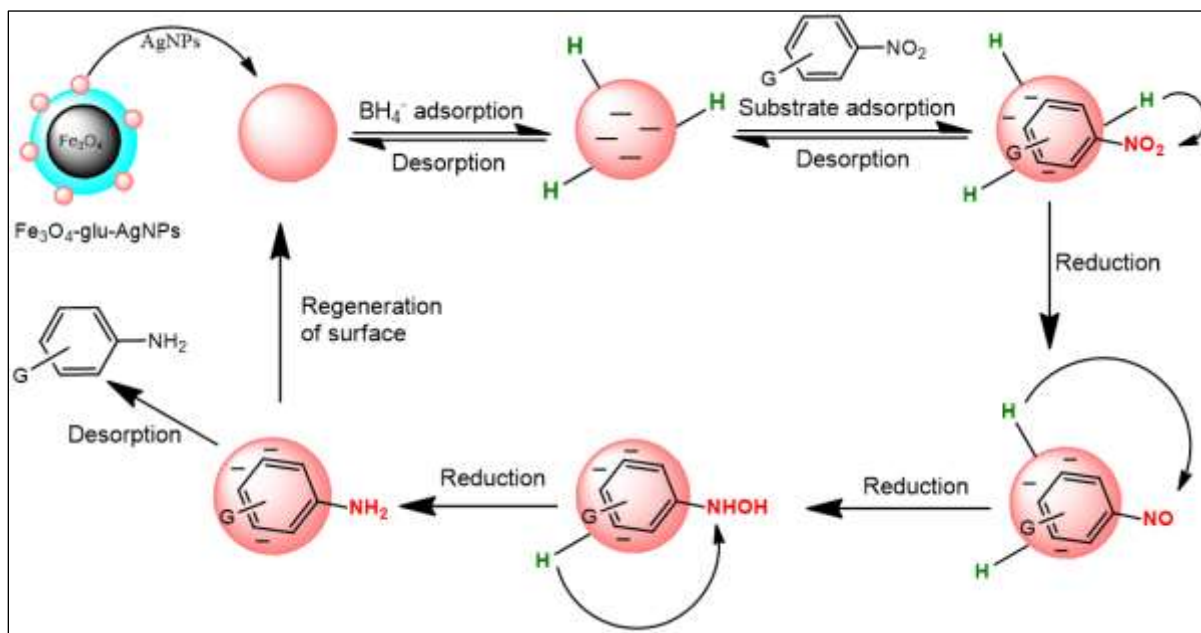
Scheme 4.2 Possible reaction pathway for the catalytic reduction of nitroarene

The recyclability of the catalyst is essential, therefore we examined the recyclability of our developed catalyst for the reduction of 4-NP as a model substrate under the optimized conditions. After completion of the reaction, the catalyst could be easily separated using an external magnet. The separated spent catalyst was then washed with ethanol and dried before

reuse. This process was repeated 5 times successfully without any noticeable decrease in catalytic activity **(Figure 4.7 (d)**. The leaching aspect of any silver after recycling was examined by determining the metal content of reaction solution using AAS (atomic absorption spectroscopy) after removing of the catalyst and founded that metal leaching was negligible. To demonstrate the superiority of Fe_3O_4-Glu-Ag over the reported catalysts, the reduction of 4-NP was considered as a representative example **(Table 4.2)**. The results clearly demonstrate that the nanocomposite is an equally or more efficient catalyst for this reaction. A gram scale reaction was also setup with a Fe_3O_4-Glu-Ag nanocatalyst to show industrial application. In our present study, 4-nitrophenol (10 mmol), $NaBH_4$ (80 mmol), were added in water (40 ml). Then add 1.2 gm of the catalyst to the reaction mixture and ultrasonicated at 60 ℃ for 10 min. After completion of the reaction as indicated by TLC (EtOAc/n-hexane as eluent: 2/8), the nanocatalyst was separated out using an external magnet and reaction mixture was extracted with ethyl acetate and concentrated in rota vapor to get the desired product. Further purification of the compounds were carried out by column chromatography.

Table 4.2 Comparative study of catalytic activity of Fe3O4-Glu-Ag for reduction of nitroarene with previously reported systems

Entry	Catalyst	Catalyst amount	Reaction Conditions	Rate constant k	Reference
1.	mPMF-Ag nanocatalyst	40 mg	H_2O, 60 °C	Not mentioned	28
2.	Ag-SiO$_2$NWs	2 mg mL^{-1}, 100 μL	H_2O, RT	2.535×10^{-3} s^{-1}	49
3.	Au@NiAg	0.06 mL, 0.250 mL	H_2O, RT	0.0266 s^{-1}	50
4.	Cu$_2$O-Ag NPs	1 mg	H_2O, RT	0.38 min^{-1} mg^{-1}	51
5.	PSMAA/Ag	2 mg	H_2O, RT	$3.19 \pm 0.22 \times 10^{-3}$ s^{-1}	52
6.	Fe$_3$O$_4$@P(MBAAm-co-MAA)@Ag	2 mg	H_2O, RT	1.5285 min^{-1}	53
7.	Ag-NP-SPBs	5.0×10^{-4} mol dm^3	H_2O, RT	0.1772 min^{-1}	54
8.	Ag@PS	1 mg	H_2O, RT	0.54 min^{-1}	55
9.	Ag@Gd-MOFs	1.0 mg	H_2O, RT	21.33×10^{-3} s^{-1}	56
10.	Fe$_3$O$_4$-Glu-AgNPs	60 mg	H_2O, 60 °C	0.510 min^{-1}	-

4.3 Experimental

4.3.1 Materials and instruments

All chemicals and solvents purchased are of analytical grade and used without further purification. Ferric chloride hexahydrate (FeCl$_3$.6H$_2$O, CDH), ferrous chloride tetrahydrate (FeCl$_2$.4H$_2$O, Sigma Aldrich), sodium hydroxide (NaOH, 98% Alfa Aesar), reduced glutathione powder (CDH), silver nitrate (Molychem). Infrared spectrum were collected on a Bruker Fourier transform infrared spectrophotometer (FTIR) (Alpha) with pressed KBr pellets and were recorded in the range of 4000-400 wavenumber (cm^{-1}). The visualization of surface morphology

of MNPs was done by using a field-emission scanning electron microscope (FESEM; NOVA nano SEM) operated at a voltage 10 kV. Samples were prepared by putting a little amount of fine powdered nanoparticles on black carbon tape. Their TEM images were recorded with a Tecnai G^2 20 (FEI) S-Twin high-resolution transmission electron microscope (HRTEM) operating at 200 kV. Samples were prepared by drying the droplet of dispersed solution of MNPs on a 400 mesh carbon coated copper grid under 100 W table lamp. Powder X-ray diffraction (XRD) pattern of the sample was obtained with X-ray Diffractometer (Panalytical X Pert Pro) using Cu Kα radiation. Thermogravimetric analysis (TGA) was performed on a Mettler thermal analyzer in an inert atmosphere at a heating rate of 10 ℃/min. Melting points were determined in open glass capillaries and are reported uncorrected. ^{1}H NMR were recorded on a Jeol ECS 400 MHz spectrophotometer using DMSO-d_6 as a solvent. TMS was taken as an internal standard and chemical shifts are reported in δ ppm. Resonance multiplicities are described as s (singlet), d (doublet), t (triplet), q (quartet) and m (multiplet). Ultrasonic bath; Elma S 70 H with 37 KHz with an output frequency was used to carry out the sonochemical reactions. UV-visible spectrum were recorded on a Shimadzu UV-1800 in standard 3.5 ml quartz cells with 10 mm path length. The purity of all the compounds was checked by TLC using silica gel as adsorbent and solvents of increasing polarity as mobile phase.

4.3.2 Synthesis of Ag decorated Fe$_3$O$_4$ -Glutathione nanoparticles

Step I: The magnetite nanoparticles were synthesized by chemical co-precipitation method similar to previously reported method with slight modification [**48**]. In a 250 ml round bottom flask 16 mmol of FeCl$_3$.6H$_2$O (4.32 g) and 8 mmol of FeCl$_2$.4H$_2$O (1.59 g) were taken in 50 ml of deionized (DI) water and ultrasonicated for 15 minutes at room temperature (25 ℃). Then slowly the temperature was raised to 60 ℃ and maintained for further 30 minutes. After that 50 ml of 1M NaOH solution was added dropwise at the same temperature till the pH of the solution became 10-11. It was further sonicated for another 30 minutes. The resulting black dispersion was then allowed to remain undisturbed for one night and the desired nanoparticles were separated by using an external magnet then washed thoroughly with deionised water (100 x 3 ml) followed by acetone, (2 x 50 ml) and finally dried in a vacuum oven for 6 h at 60 ℃.

Step II: Nano Fe_3O_4 (0.5 gm) was dispersed in deionised water (20 ml) and methanol (10 ml) and sonicated for 20 min. Reduced glutathione powder (0.2 gm) dissolved in deionized water (5 ml) was added to the above solution and again sonicated for another 2 h. The glutathione functionalized magnetic nanomaterial was then isolated by using an external magnet, washed with water (2 x 30 ml) and methanol (2 x 30 ml), and dried in an oven at 50-60 ℃ for 3 hr.

Step III: Glutathione functionalized nano Fe_3O_4 (1 gm) was dispersed in 20 ml of water-methanol mixture (1:1). Silver nitrate (100 mg) solution in water was added to the reaction mixture. Hydrazine monohydrate solution in water was added drop wise to bring the pH of the mixture to 9-10 followed by the addition of 0.1 gm of $NaBH_4$. The reaction mixture was then sonicated for 4 h after which it was cooled down to room temperature and the black precipitate of functionalised magnetic nanoparticles settled down under the influence of an external magnet. They were retrieved by magnetic decantation and washed with deionised water (20 ml x 5). Thereafter they were dried in vacuum oven for 2 h at 60 ℃.

4.3.3 General procedure for the reduction of nitro compounds, catalyzed by Fe_3O_4-Glu-AgNps

In this protocol of reduction, to the suspension of 4- nitro phenol (0.5 mmol) in water (10 ml), $NaBH_4$ (4 mmol) was added. Then add 60 mg of the catalyst to the reaction mixture and ultrasonicated at 60 ℃ for 9 min. After completion of the reaction as indicated by TLC (EtOAc/n-hexane as eluent: 2/8), the nanocatalyst was separated out using an external magnet and reaction mixture was extracted with ethyl acetate and concentrated in rota vapor to get the desired product. Further purification of the compounds were carried out by column chromatography. The products were confirmed by their melting points and ^{1}H NMR spectroscopy.

4.3.4 Analytical data of the synthesized compounds
4-Aminophenol (4a)
Light brown solid; Reported m.p. 185-189 ℃; Observed m.p. 186 ℃; ^{1}H NMR: (DMSO, 400 MHz) δ 6.40-6.42 (d, 2H), 6.48 – 6.82 (d, 2H), 8.44 (s, 1H), 8.22 (s, 2H)

Aniline (4b)

Colourless liquid; ^{1}H NMR: (DMSO, 400 MHz) δ 6.12 (s, 1H), 6.70-6.82 (d, 2H), 6.98 – 7.12 (d, 2H), 3.45 (s, 2H)

Benzene-1,2-diamine (4c)

Light Brown solid; Reported m.p. 256-258 ℃; Observed m.p. 256 ℃; ^{1}H NMR: (DMSO, 400 MHz) δ 6.48-6.50 (m, 2H), 6.35-6.38 (m, 2H), 4.40 (s, 4H)

Benzene-1,4-diamine (4d)

Off white solid; Reported m.p. 138-143 ℃; Observed m.p. 141 ℃; ^{1}H NMR: (CDCl$_3$, 400 MHz) δ 6.45 (s, 4H), 4.27 (s, 4H)

4-Bromoaniline (4e)

Off white solid; Reported m.p. 60-64 ℃; Observed m.p. 62 ℃; ^{1}H NMR: (DMSO, 400 MHz) δ 7.10-7.14 (d, 2H), 6.50-6.53 (d, 2H), 5.35 (s, 2H).

p-aminotoluene (4f)

Off white solid; Reported m.p. 44-46 ℃; Observed m.p. 43 ℃; ^{1}H NMR: (DMSO, 400 MHz) δ 7.21-7.24 (d, 2H), 4.99-6.50 (d, 2H), 5.29 (s, 2H), 3.25 (s,3H)

1-napthylamine (4g)

Dark brown solid; Reported m.p. 300-302 ℃; Observed m.p. 304 ℃ ; ^{1}H NMR: (DMSO, 400 MHz) δ 6.67-8.13 (m, 7H), 5.25 (s, 2H)

1-(4-aminophenyl)ethanol (4h)

Brown solid; ; Reported m.p. 70-74 ℃ ;Observed m.p. 74 ℃; ^{1}H NMR: (DMSO, 400 MHz) δ 8.15-8.17 (d, 2H),7.55-7.58 (d, 2H), 4.58 (s, 2H), 5.50 (s, 1H), 1.47 (s, 1H), 3.47 (s, 3H)

1H-indol-5-amine (4i)

Pinkish brown solid; Reported m.p. 131-133 ℃; Observed m.p. 130 ℃ ; ^{1}H NMR: (DMSO, 400 MHz) δ 6.47 (d, 1H), 6.55 (s, 1H), 7.24 (d, 1H), 7.25 (d, 1H), 6.21 (s, 1H), 10.15 (s, 1H)

2-aminobenzimidazole (4j)

Light orange brown solid; Reported m.p. 226-230 ℃;Observed m.p. 227 ℃ ; ^{1}H NMR: (DMSO, 400 MHz) δ 6.72 (d, 2H), 7.10 (d, 2H), 7.24 (d, 1H), 6.15 (s, 2H), 10.18 (s, 1H)
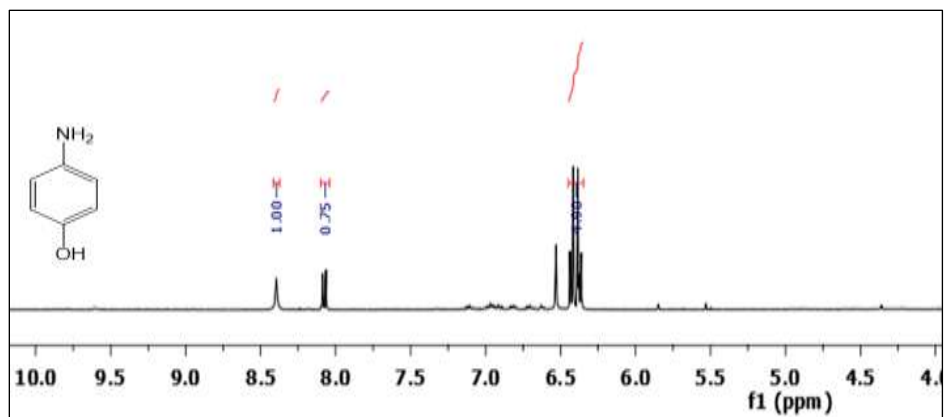
Figure 4.9 ^{1}HNMR of 4-aminophenol **(4a)**
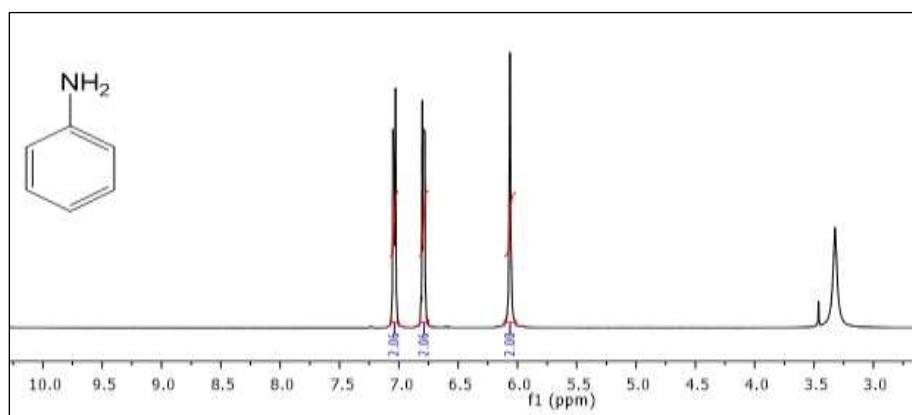
Figure 4.10 ^{1}HNMR of aniline **(4b)**
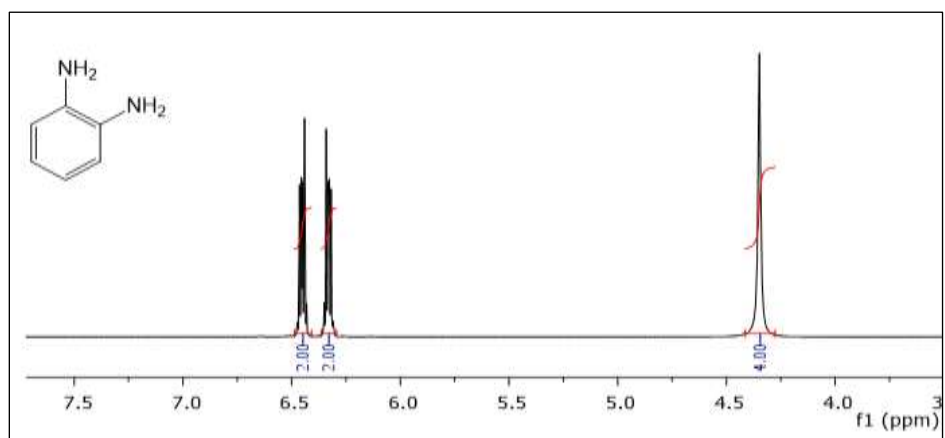
Figure 4.11 ^{1}HNMR of benzene-1,2-diamine **(4c)**

135
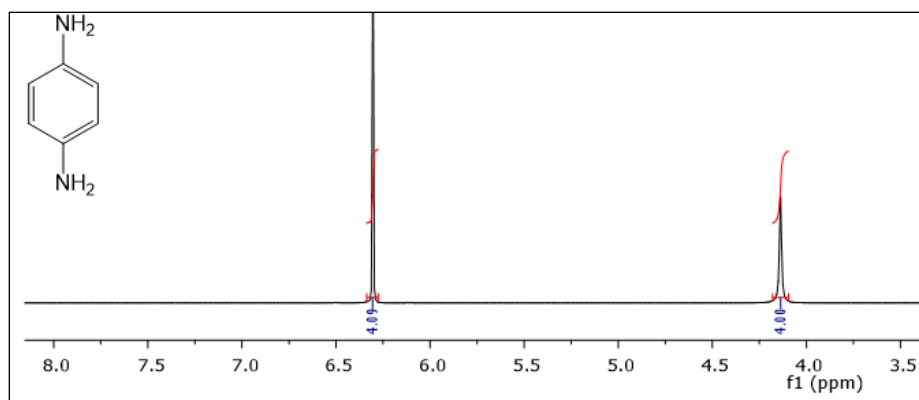
Figure 4.12 ^{1}HNMR of benzene-1,4-diamine (**4d**)
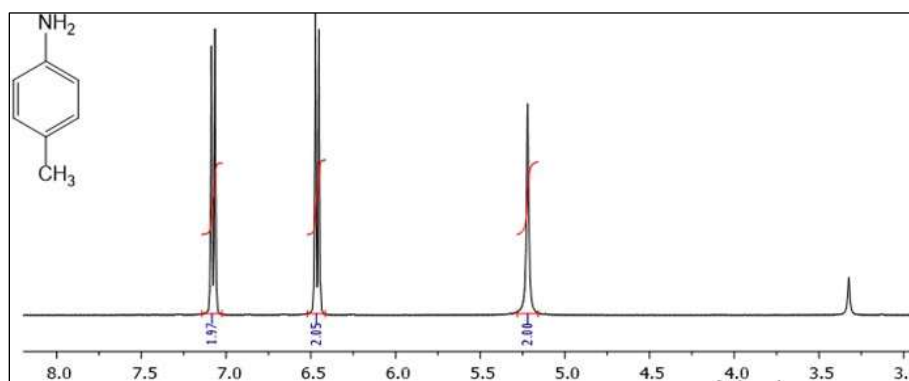
Figure 4.13 ^{1}HNMR of p-toluidine (**4f**)
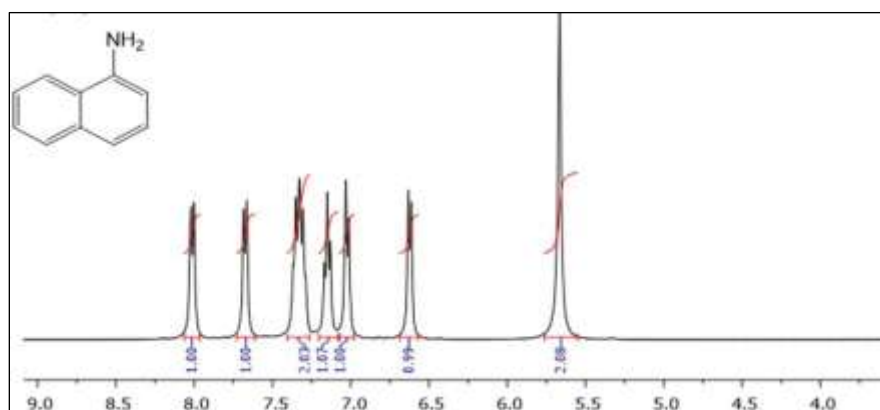
Figure 4.14 ^{1}HNMR of 1-napthylamine (**4g**)
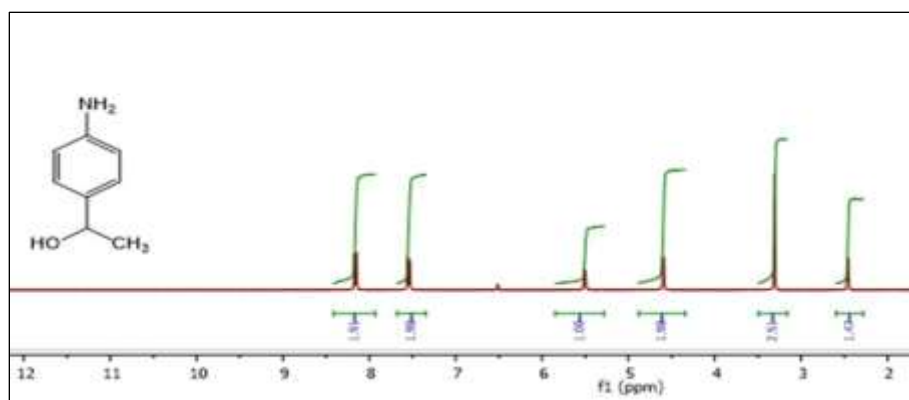
Figure 4.15 ^{1}HNMR of 1-(4-aminophenyl)ethanol **(4h)**
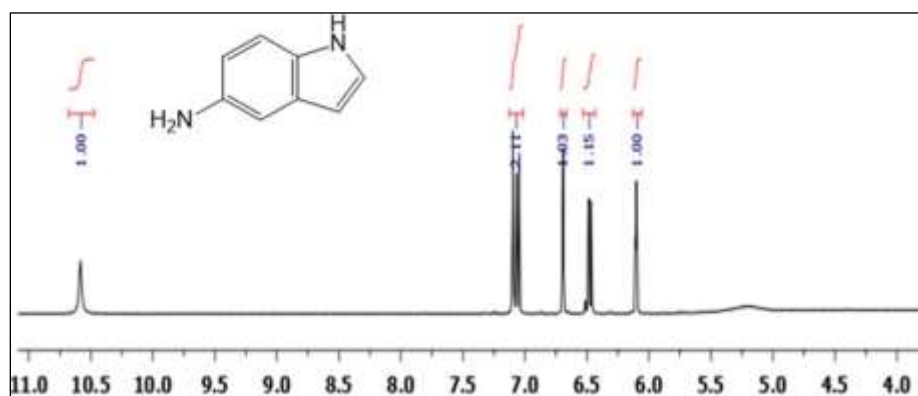
Figure 4.16 ^{1}HNMR of 1H-indol-5-amine **(4i)**
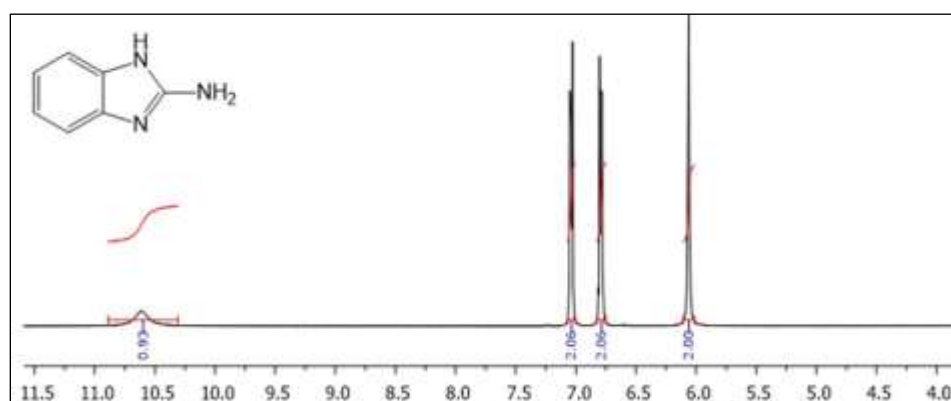
Figure 4.17 ^{1}HNMR of 1H-indol-2-amine **(4j)**

4.3 Conclusion

In conclusion, we have established a robust, chemoselective and magnetically recyclable catalyst for the reduction of industrially valuable nitroarenes substrates in the presence of other sensitive reducible functional groups. The catalyst could be recovered from the reaction mixture by using an external magnetic field and reused for five consecutive runs without any significant loss of yield. The simple work up, separation procedure, purity of product and using water as reaction media makes the whole process green and sustainable for environment.

4.5 References

[1] Doherty, S.; Knight, J. G.; Backhouse, T.; Bradford, A.; Saunders, Bourne, R. A.; Chamberlain, T. W.; Stones, R.; Clayton, A.; Lovelock, K. *Catal. Sci. Technol.* **2018**, *8*, 1454.

[2] Xiao, G.; Zhao, Y.; Li, L.; Pratt, J. O.; Su, H.; Tan, T. *Nanotechnology.* **2018**, *29*, 155601.

[3] Tafesh, A. M.; Weiguny, *J. Chem. Rev.* **1996**, *96*, 2035.

[4] Sorribes, I.; Wienhöfer, G.; Vicent, C.; Junge, K.; Llusar, R.; Beller, M. *Angew Chem Int.* 2012, *51*, 7794.

[5] Wienhöfer, G.; Sorribes, I.; Boddien, A.; Westerhaus, F.; Junge, K.; Junge, H.; Llusar, R.; Beller, M. *J Am Chem Soc*. 2011, *133*, 12875.

[6] Cantillo, D.; Baghbanzadeh, M.; Kappe, C. O. *Angew Chem Int*. **2012**, *51*, 10190.

[7] Corma, A.; Serna, P.; Garcia, H. *J. Am. Chem. Soc*. **2007**, *129*, 6358.

[8] Jagadeesh, R. V.; Wienhöfer, G.; Westerhaus, F. A.; Surkus, A. E.; Pohl, M. M.; Junge, H.; Junge, K.; Beller, M. *Chem. Commun*. **2011**, *47*, 10972.

[9] Yang, X. J.; Chen, B.; Zheng, L. Q.; Wu, L. Z.; Tung, C. H. *Green Chem*. **2014**, *16*, 1082.

[10] Li, M.; Hu, L.; Cao, X.; Hong, H.; Lu, J.; Gu, H. *Chem Eur. J.* **2011**, *17*, 2763.

[11] Gawande, M. B.; Luque, R.; Zboril, R. T. *Chem Cat Chem*. **2014**, *6*, 3312.

[12] Wu, H.; Zhuo, L. M.; He, Q.; Liao, X. P.; Shi, B. *Appl. Catal. A. Gen.* **2009**, *366*, 44.

[13] Amali, A. J.; Rana, R. K. *Green Chem*, **2009**, *11*, 1781.

[14] Rusevova, K.; Kopinke, F.-D.; Georgi, A. *J. Hazard. Mater.* **2012**, *433*, 242.

[15] (a) Baig, R. B. N.; Varma, R. S. *Chem Commun*, **2013**, *49*, 752; (b) Polshettiwar, V.; Varma, R. S. *Green Chem*. **2010**, *12*, 743.

[16] Yazdani, F.; Seddigh, M. *Materials Chemistry and Physics*. **2016**, *184*, 318.

[17] Azaroon, M.; Kiasat, A. R. *Catal. Lett*. **2017**, 148, 745.

[18] Lamei, K.; Eshghi, H.; Bakavoli, M.; Rostamnia, S. *Catal Lett*, **2016**, *312*, 215.

[19] Rathore, P. S.; Patidar, R.; Shripathi, T.; Thakore, S. *Catal. Sci. Technol*. **2014**, *55*, 2912.

[20] Polshettiwar, V.; Baruwati, B.; Varma, R. S. *Chem Commun*. **2009**, *0*, 1837.

[21] Woo, H.; Lee, K.; Park, S.; Park, K. H. *Molecules*. **2014**, *19*, 699.

[22] Shiraishi, Y.; Kanzaki, T.; Sawai, H.; Asano, H.; Du, Y.; Toshima, N. *Bull. Soc. Photogr. Imag. Japan*. **2017**, *27*, 13.

[23] Liang, Y.; Lin, C.; Guan, J.; Li, Y. *RSC Adv*. **2017**, *7*, 7460.

[24] Nasab, M. J.; Kiasat, A. R. *RSC Adv*. **2016**, *6*, 41871.

[25] Saravanan, R.; Gupta, V. K.; Mosquera, E.; Gracia, F.; Narayanan, V.; Stephen, A. *J Saudi Chem Soc*. **2015**, *19*, 521.

[26] Saravanan, R.; Khan, M. M.; Gupta, V. K.; Mosquera, E.; Gracia, F.; Narayanan, V.; Stephen, A. *RSC Adv*. **2015**, *5*, 34645.

[27] Saleh, T. A.; Gupta, V. K. *Environ. Sci. Pollut. Res*. **2012**, *19*, 1224.

[28] Islam, S. S.; Molla, R. A.; Ghosh, K.; Das, D.; Islam, S. M. *Natural resources & Engineering*. **2017**, *2*, 13.

[29] Li, P.; Li, S.; Wang, Y.; Zhang, Y.; Han, G. *Colloids & Surf A*. **2017**, *520*, 26.

[30] Luo, G.; Kang, L.; Zhu, M.; Dai, B. *Fuel Process Technol*. **2014**, *118*, 20.

[31] Lu, A. S.; Yu, J.; Cheng, Y.; Barras, A.; Xu, W.; Szunerits, S.; Cornu, D.; Boukherroub, R. *Appl. Surf. Sci*. **2017**, *411*, 163.

[32] Saravanan, R.; Gupta, V. K.; Mosquera, E.; Gracia, F. *J. Mol. Liq*. **2014**, *198*, 409.

[33] Saravanan, R.; Prakash, T.; Gupta, V. K.; Stephen, A. *J. Mol. Liq*. **2014**, *193*, 160.

[34] Saravanan, R.; Karthikeyan, N.; Gupta, V. K.; Thirumal, E.; Thangadurai, P.; Narayanan, V.; Stephen, A. *Mater Sci Eng* C. **2013**, *33*, 2235.

[35] Saravanan, R.; Gupta, V. K.; Narayanan, V.; Stephen, A. *J. Mol Liq*. **2013**, *181*, 133.

[36] Gupta, V. K.; Nayak, A. *Chem Eng J*. **2012,** *180*, 81.

[37] Saleh, T. A.; Gupta, V. K.; *J. Colloid Interface Sci*. **2012**, *371*, 101.

[38] Saravanan, R.; Sacari, E.; Gracia, F.; Khan, M. M.; Mosquera, E.; Gupta, V. K. *J Mol Liq*.

2016, *221*, 1029.

[39] Devaraj, M.; Saravanan, R.; Deivasigamani, R.; Gupta, V. K.; Gracia, F.; Jayadevan, S. *J Mol Liq*, **2016**, *221*, 930.

[40] Rajendran, S.; Khan, M. M.; Gracia, F.; Qin, J.; Gupta, V. K.; Arumainathan, S. *Sci Rep*. **2016,** *6*, 31641.

[41] Saleh, T. A.; Gupta, V. K. *J Colloid Interface Sci*. **2011**, *362*, 337.

[42] Ahmaruzzaman, M.; Gupta, V. K. *Ind. Eng. Chem. Res*. **2011**, *50*, 13589.

[43] Mohammadi, N.; Khani, H.; Gupta, V. K.; Amereh, E.; Agarwal, S. *J Colloid Interface Sci* , **2011**, *362*, 457.

[44] Saravanan, R.; Gracia, F.; Khan, M. M.; Poornima, V.; Gupta, V. K.; Narayanan, V.; Stephen, A. *J. Mol. Liq*. **2015**, *209*, 374.

[45] Wei, H.; Lu, Y. *Chem Asian J*. **2012,** 7, 680**.**

[46] Kurodaa, K.; Ishidaa, T.; Haruta, M. *J Mol Catal A-Chem.* **2009,** 298**,** 7**.**

[47] Layek, K.; Lakshmi-Kantam, M.; Shirai, M.; Nishio-Hamane, D.; Sasaki, T.; Maheswaran, M. *Green Chem.* **2012,** 14, 3164**.**

[48] Saha, S.; Pal, A.; Kundu, S.; Basu, S.; Pal, T. *Langmuir.* **2010,** 26, 2885**.**

[49] Zhang, H.; Duan, T.; Zhu W.; and Yao, W.-T. *J. Phys. Chem. C*. **2015**, *119*, 21465.

[50] Kulkarni, S.; Jadhav, M.; Raikar, P.; Raikar S.; Raikar, U. *Ind. Eng. Chem. Res.* **2019**, *58*, 3630.

[51] Sasmal, A. K. J.; Pal, Sahoo, R.; Kartikeya, P.; Dutta, S.; Pal, T. *J. Phys. Chem. C*, **2016**, *120*.

[52] Liao, G.; Chen, J.; Zeng, W.; Yu, C.; Yi, C.; Xu, Z. *J. Phys. Chem. C*. **2016**, *120*, 25935.

[53] Zhou, W.; Zhou, Y.; Liang, Y.; Feng, X.; Zhou, H. *RSC Advances*. **2015**, *5*, 50505.

[54] Liu, J.; Wang, J.; Zhu, Z.; Li, L.; Guo, X.; Lincoln, S. F.; Prud'homme, R. K. *AIChE Journal*. **2014**, *60*, 1977.

[55] Hu, X.; Zhang, Z.; Lu, Y.; Liu, R.; Sun, L.; Parkin, I. P.; Zhang, X. *Appl. Organomet. Chem.* **2019**, *33*, 4428.

[56] Wu, Y. P.; Xu, G. W.; Dong, W. W.; Zhao, J.; Li, D. S.; Zhang, J.; Bu, X. *Inorg Chem* **2017**, *56*, 1402.

Chapter - 5

Preparation of Fe$_3$O$_4$-Cys-Cu magnetic nanocatalyst for synthesis of C$_3$ symmetric tripodal receptors for naked eye selective fluoride ion recognition: A theoretical and experimental slant
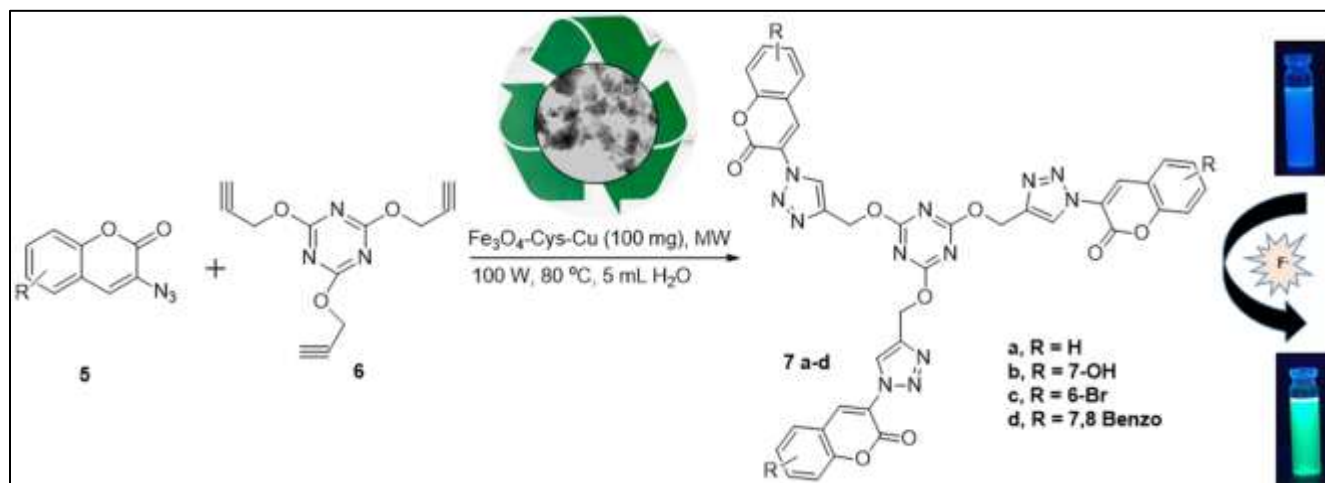
5.1 Introduction

Nanocatalysts have large surface-to-volume ratio, that is why they are attractive alternatives to conventional catalysts. Substantial enhancements in their catalytic activity, selectivity, and stability can be done by tailoring their size, shape, composition, and electronic structure. Nanocatalysts are isolated and recovered through filtration or centrifugation methods, whereas the inconvenience and inefficiency of these tedious methods caused by the nano size of the catalyst particles hamper the sustainability and economics of the nanocatalytic strategy **[1-11]**.

To overcome these issues, use of magnetic nanoparticles (MNPs) appears to be the most logical solution. Magnetic nanocatalysts are simply and efficiently removed from reaction mixtures with an external magnetic field, and MNPs have emerged as ideal catalysts or supports. This field has indeed been the subject of excellent reviews **[12-17]**. However ultrafine bare MNPs tend to undergo agglomeration due to their inherent instability and hydrophobic nature results in big clusters over time in the absence of any surface coating which reduces their surface energy. To address the issue of agglomeration of MNPs a passive coating of inert organic and organic materials such as carbons, silicon and polymers on the surfaces of MNPs could be feasible to prevent their aggregation and improve their stability **[18-21]**. L-cysteine a biocompatible, water soluble, sulphur containing amino acid with three functional groups (-SH, -NH$_2$, -COOH) has a strong metal chelating capability, which has been widely used for adsorption of transition metal ions **[22-28]**. The chemistry of copper is extremely rich because it can easily access Cu°, Cu^I, Cu^{II}, and Cu^{III} oxidation states allowing it to act through one electron or two electron process. This unique characteristic of Cu based nanocatalyst have made it suitable for many applications in nanotechnology, including catalytic organic transformations, electrocatalysis and photocatalysis. Because of the leaching effect and poor recyclability neat metal and oxide must be incorporated on some supports **[29-30]**. Therefore L-cysteine has been used as a solid support on which copper nanoparticles strongly bounded. The copper-catalysed cycloaddition reaction of terminal alkynes with organic azides (CuAAC) is one of the most attractive synthetic tools for formation of highly regioselective 1,4-disubstituted 1,2,3-triazole derivatives **[31]**. Nitrogen heterocyclic compounds obtained from the click reaction have different industrial applications for the preparation of dyes, drugs, corrosion inhibitors (of copper and copper alloys), photostabilizers, photographic materials, and agrochemicals **[32]**. In recent years, different heterogeneous and homogeneous copper catalysts have been applied for click reaction **[33-34]**.

142

However, to date few magnetic copper catalysts have been prepared and successfully applied for azide-alkyne cycloaddition reaction **[35]**. Fluoride ion is one of the essential micronutrient of body useful in dental care and osteoporosis but its excessive use is toxic to biological tissues and causes abdominal pain, nausea, dental or skeleton fluorosis, gastric disorder and nephrotoxic changes. Therefore, there is need to design and develop new binding motifs which can mimic the efficiency of anion binding based biological processes and are capable of recognizing fluoride ion selectively by the employment of non-covalent interactions. The creation of an artificial receptor which is preferentially selective towards fluoride ion requires the presence of multiple interactions between anion and receptor in a complimentary **[36-48]**. Topology of receptor must be organized to complement the size and shape of the anion to gain selectivity. Among the various approaches, the C_3 symmetric tripodal anion receptors are of special interest due to their rational control of binding properties like high sensitivity, selectivity, stability, simplicity in detecting low concentration of anions **[49]**. Due to these advantages, design of artificial tripodal receptor is an active thrust area amongst researchers. A considerable number of receptors for fluoride ion detection based on coumarin scaffold have been reported, however, tripodal receptors based on coumarin moiety are very few or not has been reported so far **[50-51]**. Inspired by the above facts and due to continuation of our research interest in the development of sustainable protocols **[52-54]** and application of nanocatalyst, a copper (II) immobilized on Fe_3O_4–Cys MNPs was prepared and its catalytic activity was also investigated in one-pot synthesis of 1,2,3-triazoles by reaction of terminal alkynes and azides under microwave irradiation in aqueous media. Further some new tripodal triazoles were also synthesized by taking cyanuric alkyne and coumarin azide as precursors, and among them, only **7b** acted as a receptor and found capable of exhibiting spectruml change selectively in presence of fluoride ion and therefore its fluoride binding property was examined further.

5.2 Results and Discussion

5.2.1 Characterization of the Fe_3O_4-Cys-Cu nanocatalyst

Based on our preliminary work on the synthesis of transition metal-based nanocatalyst, the synthetic route for the preparation of Fe_3O_4-Cys-Cu magnetic nanoparticles is outlined in **Scheme 5.1**. The magnetite nanoparticle was initially synthesized by co-precipitation method **[55]**.
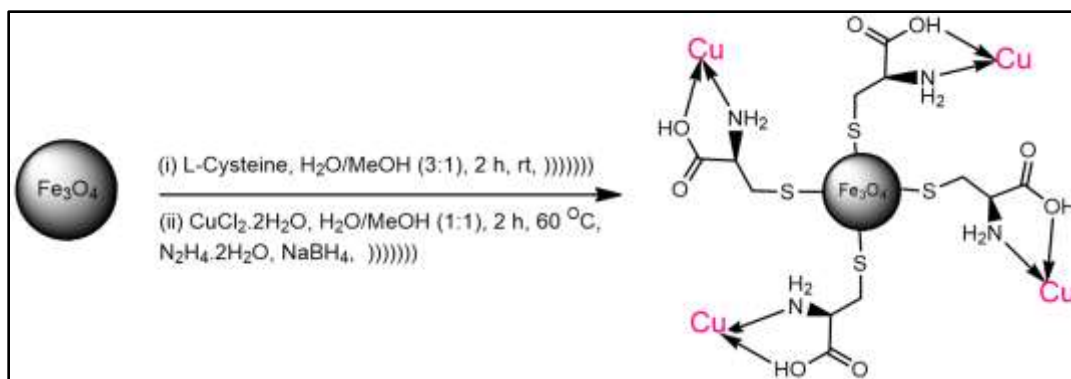
Scheme 5.1 Pictorial representation of the preparation of Fe$_3$O$_4$-Cys-Cu nanocatalyst

After that coating of a layer of carbonaceous material L-cysteine (Cys) on the surface of magnetite has been carried out and the loaded with copper nanoparticles **(Scheme 5.1)**. The prepared nanocatalyst was analyzed by using FTIR, XRD, FE-SEM, EDS mapping, XPS, and TGA analysis. Initially FTIR spectroscopy was utilized to confirm the chemical structure of the nanocatalyst as shown in **Figure 5.1**.
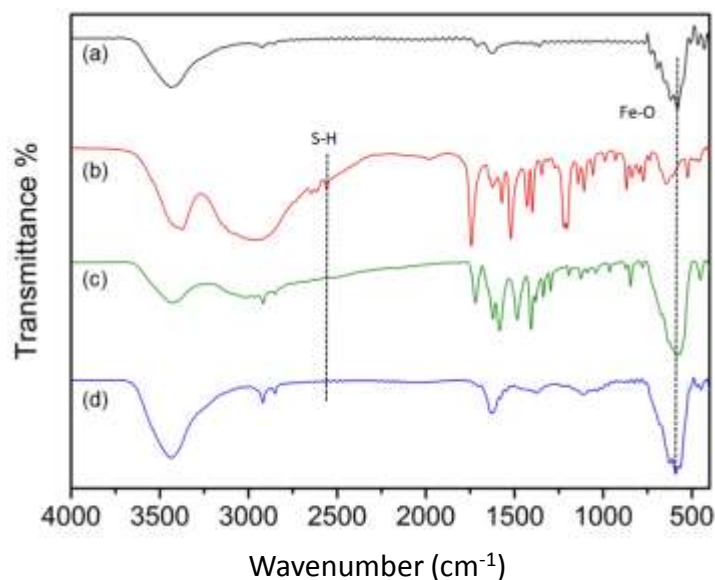
Figure 5.1 FTIR spectrum of (a) Fe$_3$O$_4$ (b) Cysteine pure (c) Fe$_3$O$_4$-Cys (d) Fe$_3$O$_4$-Cys-Cu

For pure Fe$_3$O$_4$ nanoparticles, the band at 573 cm^{-1} corresponds to the stretching vibration of the Fe–O bond. Additional, the peaks at 1628 and 3425 cm^{-1} could be attributed to the stretching vibration of the hydroxyl (–OH) groups on the surface of Fe$_3$O$_4$ nanoparticles. For the FTIR spectrum of L-cysteine **(Figure 5.1 (b))**, the characteristic absorption bands appeared at 3463

cm^{-1} was assigned to N–H stretching mode of amino group. The bands in the range of 2750-3200 cm^{-1} could be assigned to the asymmetric and symmetric –CH stretching vibration of the CH$_2$ group. A weak peak at 2548 cm^{-1} confirmed the presence of S–H group and an intense band at 1743 cm^{-1} indicated the presence of stretching vibration of C=O group of carboxylic acid of cysteine. After coating of cysteine on magnetite surface, Fe–O stretching vibrational peak shifted to 582 cm^{-1} and intensity of all the peaks decreased to some extent also **(Figure 5.1 (c))**. In the FTIR spectrum of Fe$_3$O$_4$-Cys-Cu as shown in **Figure 5.1 (d)**, the strong band at 3438 cm^{-1} was attributed to the –OH and –NH stretching and the broad band at 1635 cm^{-1} was due to C=O stretching and at 1340 cm^{-1} was due to N–H bending vibrational mode. A very weak peak at 1195 cm^{-1} was ascribed to C–N stretching. In addition, the peak at 2548 cm^{-1} disappeared, implying that the cysteine molecule was bound onto the surface of Fe$_3$O$_4$ MNPs via the formation of the covalent bond Fe–S [56].
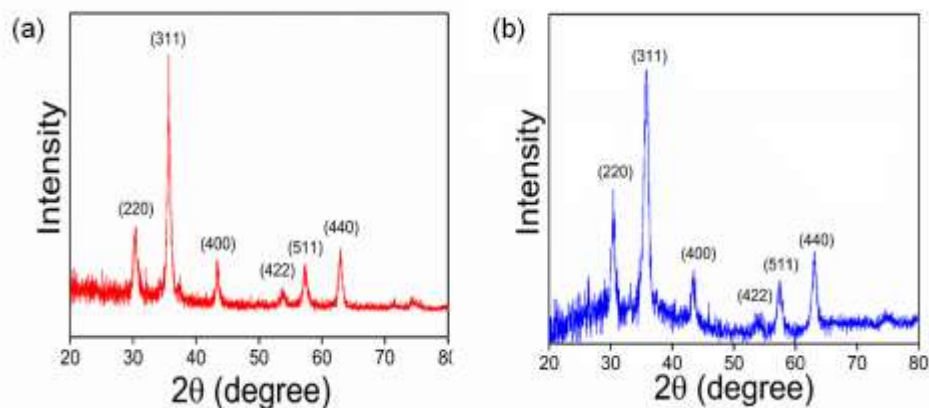
Figure 5.2 XRD of (a) Fe$_3$O$_4$ (b) Fe$_3$O$_4$-Cys-Cu

The XRD pattern of the Fe$_3$O$_4$ and Fe$_3$O$_4$-Cys-Cu shown in **Figure 5.2**. The diffraction peaks appeared at 30.4°, 35.5°, 43.3°, 53.4°, 57.2°, and 62.8° were correspond to the crystal planes of (220), (311), (400), (422), (511), and (440) of the magnetite (JCPDS -19-0629) respectively. The same diffraction peaks were observed for the Fe$_3$O$_4$-Cys-Cu nanoparticles with a slight broadening of the peaks, indicated that surface coating of the magnetite did not change its phase composition. As shown in **Figure 5.3 (a)** TGA curve of Fe$_3$O$_4$-Cys-Cu showed weight loss in two stage. The first stage weight loss occurred below 200 ℃ was about 3.1 %, due to the evaporation of residual water and second major weight loss was observed in the range of 200-450 ℃, which resulted from the decomposition of the L-cysteine. It implies that the loading of

cysteine in the optimal catalyst was about 16 %. DTA curve of the catalyst as shown in **Figure 5.3 (b)** revealed only one endothermic peak at 260 ℃ which assigned to the melting point of L-cysteine.
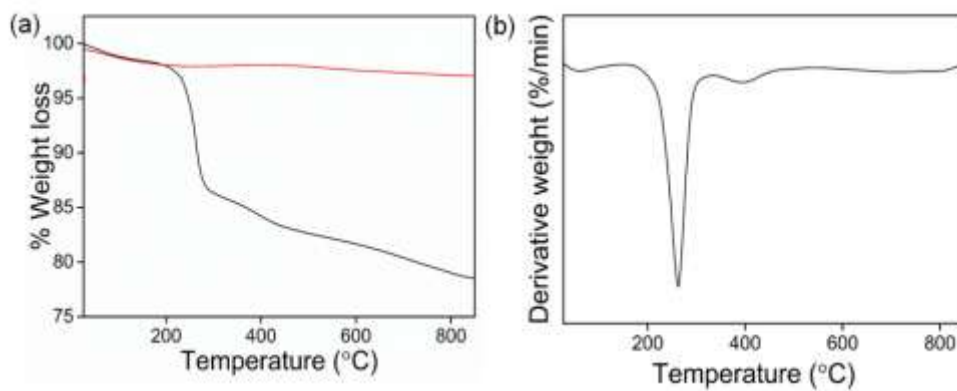
Figure 5.3 TG-DTA analysis of Fe_3O_4-Cys-Cu nanocatalyst
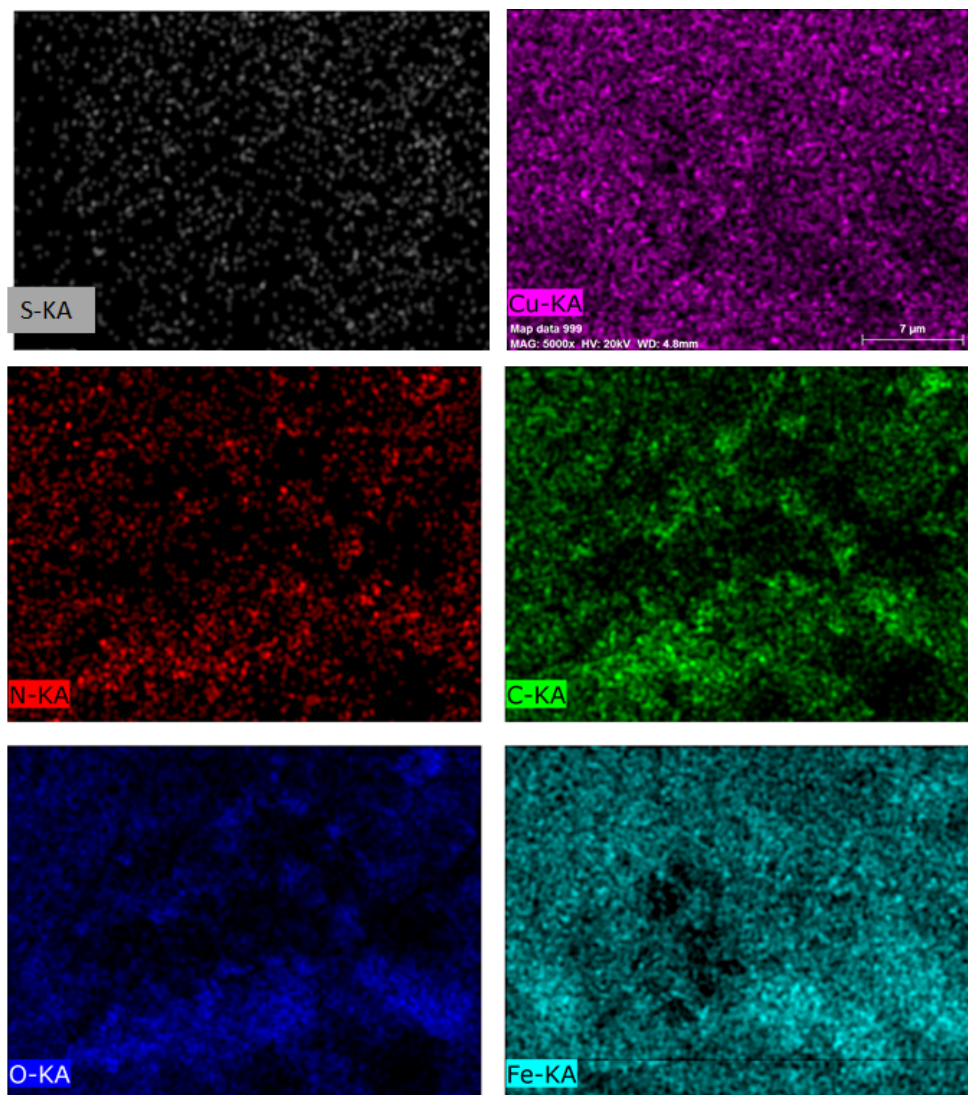
Figure 5.4 Elemental mapping of the Fe_3O_4-Cys-Cu
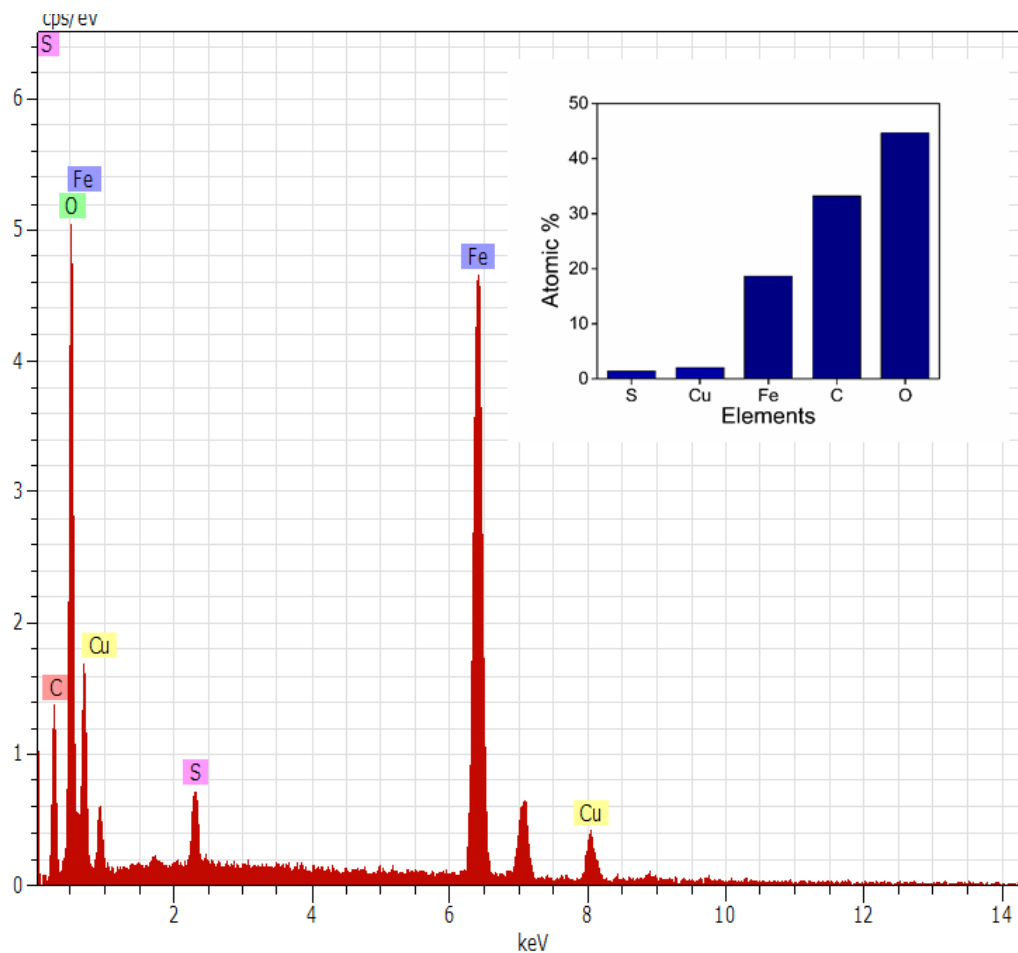
Figure 5.5 EDS spectrum of the Fe$_3$O$_4$-Cys-Cu

The chemical composition of the Fe$_3$O$_4$-Cys-Cu nanocatalyst was further determined by energy dispersive X-ray spectroscopy (EDS). The peaks of C, N, O, Fe, S, and Cu were observed. (**Figure 5.5**. The images shown in **Figure 5.4** revealed well distribution of copper over the structure of the cysteine support.
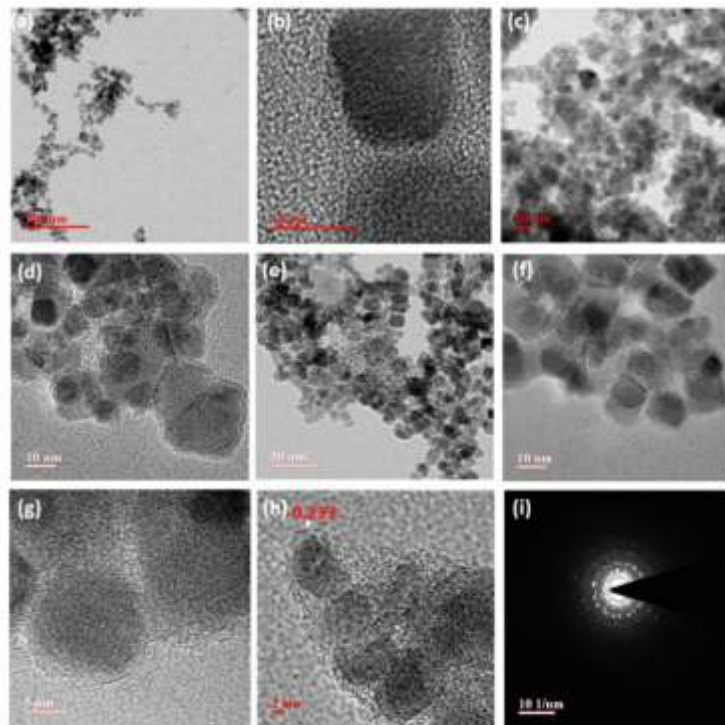
Figure 5.6 (a) TEM image of Fe_3O_4 (b) HRTEM image of Fe_3O_4 (c) TEM image of Fe_3O_4 –Cys (d) HRTEM image of Fe_3O_4 –Cys (e) TEM image of Fe_3O_4- Cys-CuNPs (f) and (g) (h) HRTEM image of Fe_3O_4- Cys-CuNPs (i) SAED pattern of the of Fe_3O_4-Cys-CuNPs

TEM images of the nanocatalyst show a quasi-spherical morphology with an average particle size of 9-20 nm. The HRTEM image in **Figure 5.6 (h)** revealed clearly a coating of cysteine over magnetite with an average diameter of 1 nm. Also the characteristic lattice fringes with d-spacing 0.233 corresponds to the [311] plane of Fe_3O_4 [**58**].
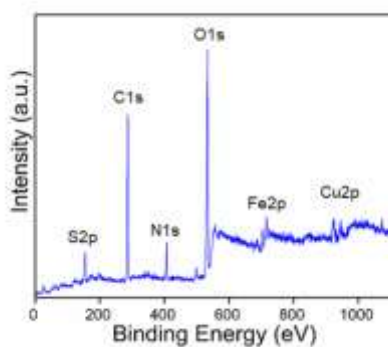
Figure 5.7 XPS spectrum of Fe_3O_4- Cys-CuNPs
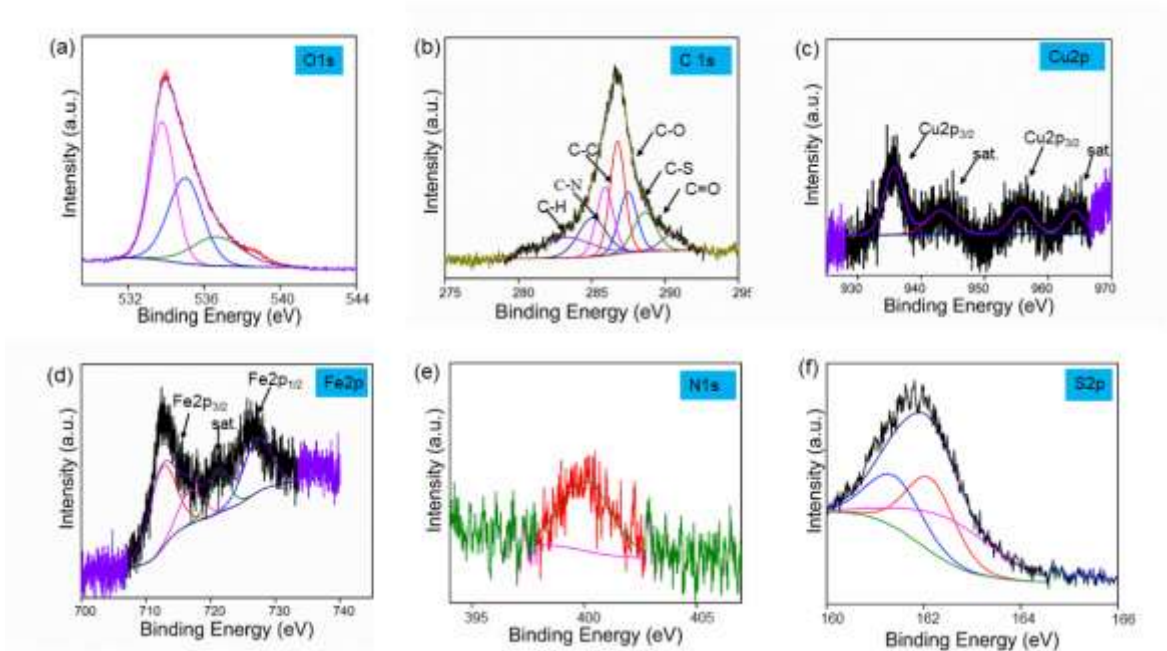
Figure 5.8 High resolution XPS spectrum of (a) O1s (b) C1s (c) Cu2p (d) Fe2p (e) N1s (f) S2p

XPS spectrum of the catalyst for Fe2p, N1s, O1s, C1s, S2p and Cu2p were recorded (**Figure 5.7**). The C1s binding energy for the carbon in the COOH group was observed at 288 eV which assigned to the unperturbed carboxylic group according to the literature. The same phenomena were observed for the N1s binding energy in the NH$_2$ group (400eV) and for O1s binding energy (BE) 533 eV. These results suggest that there is no chemical bonding for the Fe atom to the O atom in COOH group, or for the Fe atom to the amino group [**59**].

The peak due to S–H group usually appears at 162.0 eV. In the XPS spectrum of catalyst additionally a new peak at BE of 161 eV was developed [**60**]. The peak at 161 eV matches well with the early data of the sulphur in FeS, revealed a peak at 161.04 eV (**Figure 5.8 (f)**). Hence it is clear that the cysteine molecules bind directly to the Fe$_3$O$_4$ via Fe–S bonds. This result also excludes the possibility of forming a Fe–O–S bond. Indeed, the Fe–S bonding by 9 Kcal/mol (77 Kcal/mol vs. 68 Kcal/mol) [**61**].

XPS spectrum of Fe2p revealed two peaks at 711 eV and 728 eV due to Fe2p$_{3/2}$ and Fe2p$_{1/2}$ and one satellite peak at 720 eV. In order to provide evidence of the formation of Cu^{2+} cysteine complex over magnetite [**62-63**], XPS has been demonstrated. XPS spectrum of Cu2p shows main peak at binding energy of about 936.5 eV and 956.5 eV that assigned to the Cu2p$_{3/2}$ and Cu2p$_{1/2}$ respectively. Two other peaks were also obtained at 944.5 eV and 963.8 eV that

attributed to the $Cu2p_{3/2}$ and $Cu2p_{1/2}$ satellite peaks. So it can be concluded that the oxidation state of copper in the nanocatalyst is +2 [**64**].

5.2.2 Catalytic activity of the nanocatalyst for the synthesis of 1,4 disubstituted 1,2,3-triazole

Substitution of traditional heating (oil bath, sand bath, heating jacket, water bath or hot air) by microwave irradiation is a convenient method to accelerate organic reactions and thus reduce their reaction times. The use of microwave irradiation has been applied successfully in organic synthesis and, in particular, in the synthesis of heterocyclic compounds, among others. In order to develop an efficient protocol for this multicomponent reaction under microwave irradiation, a mixture of benzyl bromide, NaN_3, phenyl acetylene in H_2O (5 mL) were irradiated with different catalyst loading, powers, temperatures and times (**Table 5.1**) and taken as a model reaction. When reaction performed at 70 ℃ for 10 min at 50 W of power with 50 mg of the catalyst, the reaction led to the formation of product in 73 % yield (**Table 5.1, entry 1**). Raising the amount of catalyst did not lead to any appreciable increment in the yield (**Entry 2-4**). Raising the power and temperature along increased amount of catalyst, product obtained with yield 88-80 % (**Entries 5-9**). When power raised to 100 W and carried out at 80 ℃ with 100 mg of the catalyst for 10 min, an excellent yield 98 % of product was obtained (**Entry 10**). Further in the same reaction conditions by increasing the reaction time to 15 min, yield was decreased (**Entry 11**). The use of high power (**150 W**) did not lead to improvement in the yield (**Entry 12**). Also raising the temperature to 100 ℃ did not lead to increased yield (**Entry 13**). Decrease in the product yield were observed in reactions performed for reduced reaction times (**Entries 14-15**). To our satisfaction, by reducing (**Entry 16**) and increasing (**Entries 17-18**) the amount of catalyst, caused a dramatic decrease in the product yield. After optimizing all the reaction parameters it has been concluded that the best suitable condition for maximum product yield of 98 % were 100 W, 80 ℃, 100 mg of the catalyst and 10 min of time. After optimization of the reaction conditions, we extended these conditions for a series of different simple triazole (**4a-d**) and also four new tripodal triazoles (**7a-d**) were also synthesized using the same optimized reaction conditions as shown in **Table 5.2**. All the reactions proceeded smoothly generating the products with excellent yields. All new products were characterized using spectroscopic methods such as ^{1}H NMR and ^{13}C NMR, high resolution mass spectrometry technique**.** Mechanism of

copper catalysed synthesis of 1,2,3-triazoles has been recently been reviewed by Fokin who proposed a revisited mechanism whereby a σ-bound Cu(I)-acetylide bearing a π complexed copper atom reacts with an organoazide forming a bridging dicopper μ-acetylide intermediate **[65]**. The reusability of the nanocatalyst was also examined **(Figure 5.19)** and it is an important advantage of magnetic nanocatalyst that being magnetically separable from the reaction mixture, easily recovered by using an external magnet and can be reused for subsequent cycles. After every reaction they were washed with hot ethanol, air-dried and used directly for next round of reactions. The nanocatalyst was found to exhibit good catalytic activity for up to six reaction cycles for triazole synthesis.

The leaching aspect of any copper after recycling was examined by determining the metal content of reaction solution using AAS (atomic absorption spectroscopy) and sample digestions were carried out in a microwave oven at 500 W for 10 min with 5 mL aqua-regia. It was found that the concentration of copper in the reused catalyst was reduced to 1.89 wt% for triazole synthesis. The small amount of copper leaching might be due to some changes that occurred on the surface of the magnetic catalyst. Major weight loss of catalyst at high temperature and a small aunt of leaching also proves that the catalyst is highly stable at high temperature also.
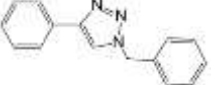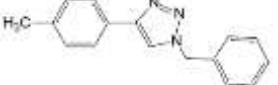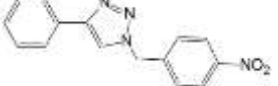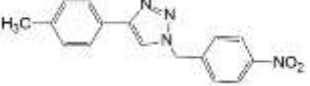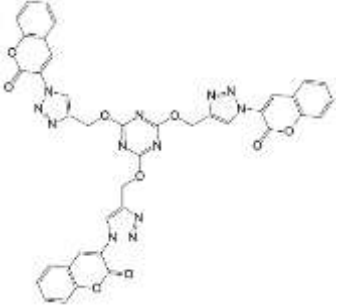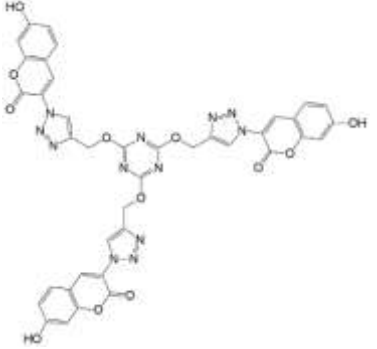
Table 5.1 Optimization of the reaction conditions for the synthesis of 1,4-disubstituted 1,2,3-triazole under microwave irradiation using Fe_3O_4-Cys-Cu nanocatalyst[a]
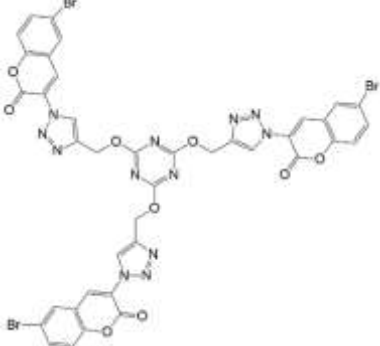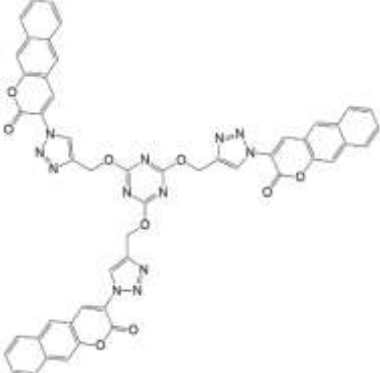
Reactions were performed using benzyl bromide (1.2 mmol), sodium azide (1.5 mmol), phenyl acetylene (1 mmol), Fe_3O_4-Cys-Cu in water (5 mL)

[b]Isolated yield

Entry	Power (W)	Temp (°C)	Catalyst (mg)	Time (min)	Yield (%)[b]
1	50	70	50	10	73
2	50	70	60	10	75
3	50	70	75	10	77
4	50	70	100	10	82
5	70	80	100	10	85
6	70	100	100	10	84
7	70	100	125	10	80
8	80	80	100	10	88
9	80	100	100	10	94
10	100	80	100	10	98
11	100	80	100	15	89
12	150	80	100	10	87
13	100	100	100	10	95
14	100	80	100	08	91
15	100	80	100	05	88
16	100	80	80	10	92
17	100	80	120	10	89
18	100	80	130	10	84

Table 5.2 Scope of the 1,3 dipolar cycloaddition reaction for the synthesis of 1,4 disubstituted 1,2,3-triazole under microwave irradiation using Fe_3O_4-Cys-Cu nanocatalyst [a]

Entry	Product	Time (min)	Yield (%)[b]	Product code
1		10	98	**4a**
2		12	98	**4b**
3		08	96	**4c**
4		12	95	**4d**
5		10	94	**7a**
6		15	92	**7b**

154

7			12	96	**7c**
8			15	94	**7d**

[a]Reactions were performed using benzyl bromide (1.2 mmol), sodium azide (1.5 mmol), phenyl acetylene (1 mmol) for 4 a-d and cyanuric alkyne (0.2 mmol) with coumarin azide (0.66 mmol) for 7 a-d at 100 W, 80 °C, Fe_3O_4-Cys-Cu (100 mg) in water (5 mL).
[b]Isolated yield

5.2.3 Anion binding studies

5.2.3.1 UV-vis titration experiment

For anion binding studies UV-visible spectrum of all the tripodal triazoles **7a-d** (1×10^{-5} M in DMSO) were recorded upon addition of different anions viz.; fluoride, chloride, bromide, iodide, acetate, nitrate and dihydrogen phosphate as tetrabutylammonium salts (TBA). Triazoles **7a, 7c** and **7d** failed to exhibit any spectruml change even at high concentration (10^{-3} M). Only **7b** acted as a receptor and found capable of exhibiting spectruml change in presence of fluoride ion and therefore its fluoride binding property was examined further.
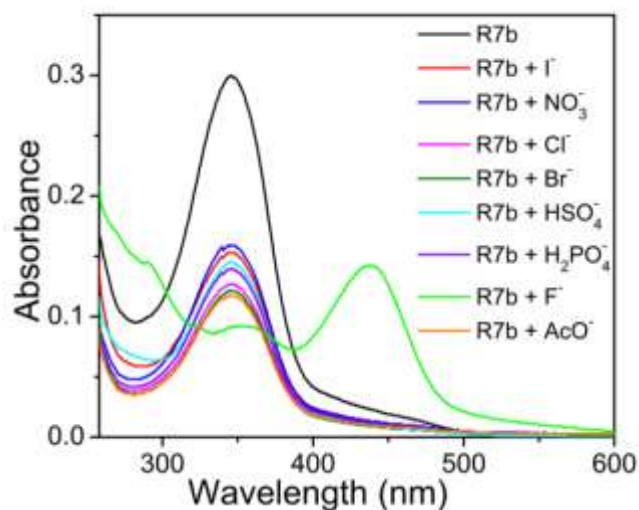
Figure 5.9 UV-vis spectrum of receptor **R7b** (1×10^{-5} M in DMSO) on titration with different ion (TBA salt, 1×10^{-4} M in DMSO)

UV-visible spectrum of receptor **7b** (1×10^{-5} M) exhibited absorption band centered at 346 nm. Interestingly, upon addition of fluoride ion (1×10^{-4} M), band at 346 nm disappeared completely and a new band formed at 437 nm, which indicated association between receptor **7b (R7b)** and fluoride ion. The receptor **7b (R7b)** proves selectivity for fluoride ion because with other anions no obvious spectruml changes were observed **(Figure 5.9)**. This reveals that –OH group of **R7b** showed binding affinity with fluoride ion. The effect of concentration of fluoride ion on UV-vis spectrum was evaluated by UV-vis titration which has been carried out with increasing fluoride ion concentration from 1×10^{-6} M to 1×10^{-4} M in DMSO **(Figure 5.10)**. Intensity of new band at 437 nm increases with increasing concentration of fluoride ion. Formation of stable complex between receptor and fluoride ion was confirmed by distinct isosbestic points which were observed at 303 nm and 382 nm. These spectruml changes could be rationalized on the basis of interactions between fluoride ion and receptor.
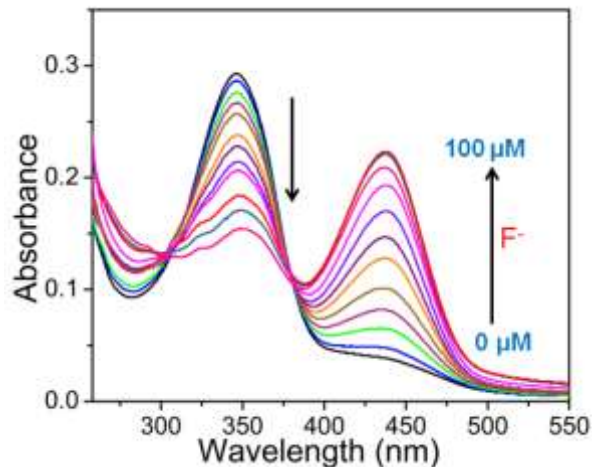
Figure 5.10 UV-vis spectrum of receptor **R7b** (1×10^{-5} M in DMSO) on titration with fluoride ion (TBA salt) from 1×10^{-6} M to 1×10^{-4} M in DMSO

Using continuous variation method, stoichiometric ratio of the complex formed between receptor and fluoride ion was determined by keeping the same concentration of both receptor and fluoride ion (1×10^{-4} M in DMSO). The molar fraction of fluoride/(receptor + fluoride) was continuously varied. In the UV-vis spectrum the absorbance reached its maxima at the molar concentration of 0.75 indicating that receptor forms 1:3 complex with fluoride ion **(Figure 5.11 (a))**. By mass spectrum of **R7b** with fluoride ion (TBA salt), which exhibited a peak at 860.1506 [calcd for **R7b** + 3F$^-$ + H$^+$: 860.1505], it was also proved that receptor bind with three fluoride ion respectively **(Figure 5.32)**. The receptor associates with F$^-$ in a 1:3 stoichiometry is also confirmed by the Benesi-Hildebrand analysis. When assuming a 1:3 association between 1 and F$^-$, the Benesi-Hildebrand equation is given as follows:

$$1/A\text{-}A_o = (a/b\text{-}a) \ (1/K[F^-]^3+1)$$

K is the binding constant (M^{-3}), and [F$^-$] is the concentration of F$^-$ added (M). As shown in **Figure 5.11 (b)**, plot of $1/(A\text{-}A_O)$ against $1/[F^-]^3$ shows a linear relationship, indicating that **R7b** actually associates with F$^-$ in a 1:3 stoichiometry. Binding constant K, calculated from the ratio of intercept/slope was found to be 3.11×10^{15} M^{-3}.
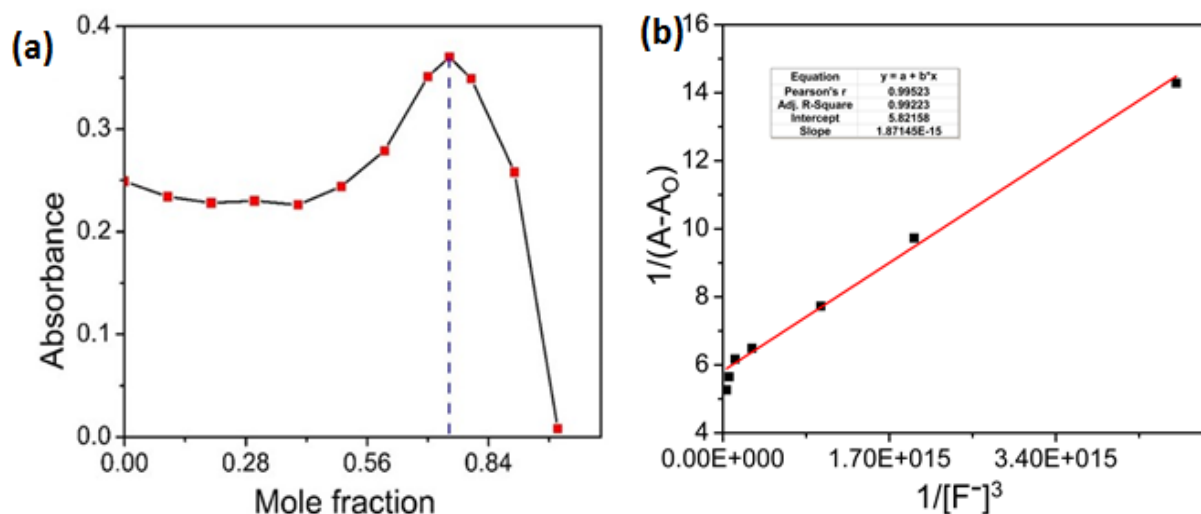
Figure 5.11 (a) Job's Plot with receptor **R7b** and TBA salt in 1×10^{-4} M in DMSO (b) Fitting curve of Benesi Hildebrand equation

5.2.3.2 Fluorescence titration experiment

The fluorescence response of **R7b** was carried out with various anions as their TBA salts. Receptor alone displayed weak fluorescence emission at 400 nm, when excited at 355 nm. Upon addition of various anions, no significant changes were observed. But on addition of fluoride ion, fluorescence enhancement was observed along with the appearance of a new emission peak at 456 nm (**Figure 5.12**). Using a UV lamp, the receptor in the presence of fluoride ion showed fluorescent intense green color which was initially blue fluorescent itself while at the same time with other ions addition no change was observed (**Figure 5.13 (a)**) and without UV lamp i.e. under naked eye, the receptor shows pale yellow color which turns to green color on addition of fluoride ion and no change with addition of other anions (**Figure 5.13 (b)**).
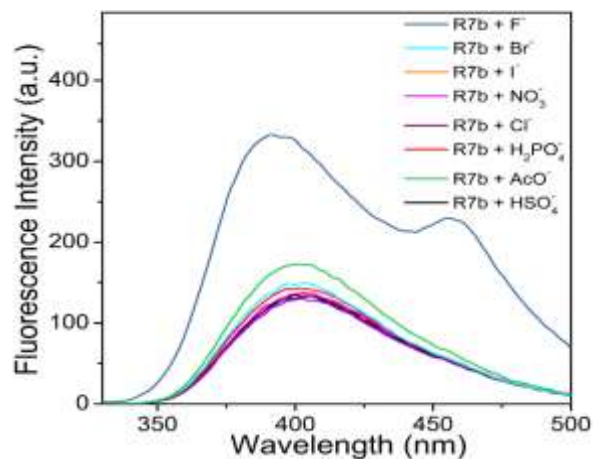
Figure 5.12 Fluorescence spectrum of receptor **R7b** (1×10^{-5} M in DMSO) with different anions (TBA salt, 1×10^{-4} M in DMSO)
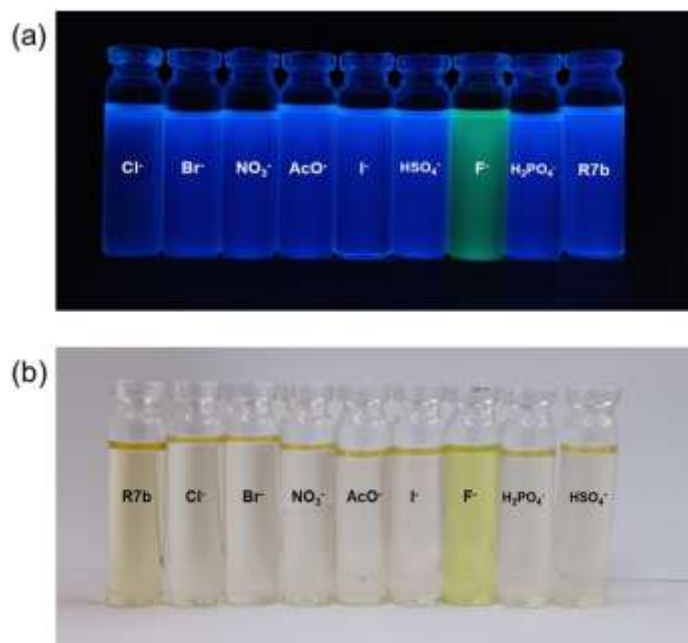
Figure 5.13 (a) Change in color of receptor **R7b** (1×10^{-5} M in DMSO) in the presence of various ions (TBA salt, 1×10^{-4} M in DMSO) under UV-lamp (b) under naked eye or normal day light

Comprehensive fluoride ion binding study was performed by preparing different solutions of varying concentration of fluoride anion salt from 1×10^{-4} M **(Figure 5.14)**. On increasing the equivalent of fluoride ion, intensity of receptor peak as well as new peak increases which might be due to the increase in rigidity of receptor's structure upon fluoride complexation.
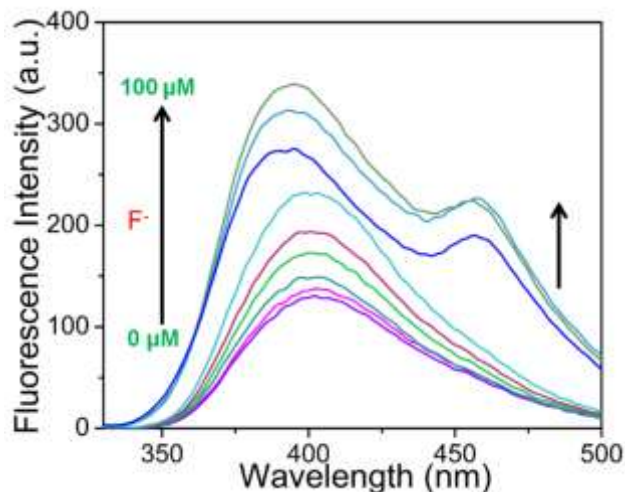
Figure 5.14 Fluorescence spectrum of receptor **R7b** (1×10^{-5} M in DMSO) with fluoride ion (TBA salt, 1×10^{-6} M to 1×10^{-4} M in DMSO)

Further to investigate the anti-interference study of receptor **R7b**, competition experiments in presence of various anions such as I⁻, NO₃⁻, Cl⁻, Br⁻, HSO₄⁻, H₂PO₄⁻, F⁻, OAc⁻ were carried out **(Figure 5.15)**. The orange bars represent the absorption intensities of receptor **R7b** in the presence of various metal ions. The blue bars represent the change in absorption intensity that occurred upon addition subsequent addition of fluoride ion to the above mentioned solution. Addition of other ions did not show any significant change in intensity, which indicated that the presence of other anions does not interfere with the fluorescence enhancement of receptor.
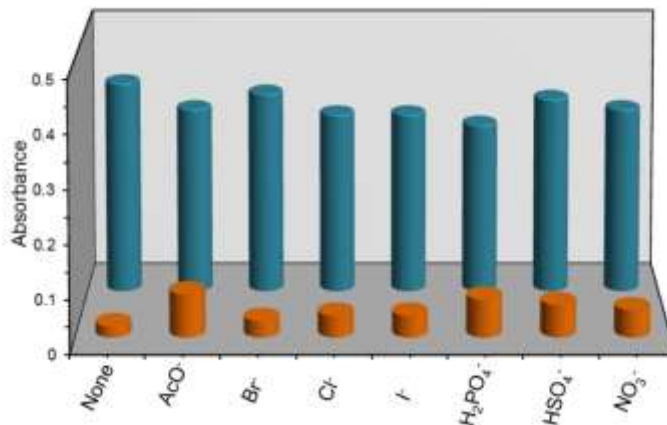
Figure 5.15 Variation of absorption intensity of receptor **R7b** (1×10^{-5} M in DMSO) in the presence of fluoride ion with co-existing competitive anions (1×10^{-4} M in DMSO)

5.2.3.3 Calculation of detection limit

The calibration curve of receptor **R7b** was plotted between absorbance and fluoride ion concentration (1×10^{-6} M to 1×10^{-4} M in DMSO), which showed a linear dependence of absorption intensity with fluoride ion concentration ($R^2 = 0.99$). The detection limit (DL) of receptor **R7b** for fluoride ion was determined from the following equation [66]: DL $= 3 \times$ Sbl/S, Where Sbl is the standard deviation of y-axis; S = slope of the calibration curve. The detection limit calculated was 2.4×10^{-6} M, which proves the sensitivity of receptor towards fluoride ion (**Figure 5.16**).
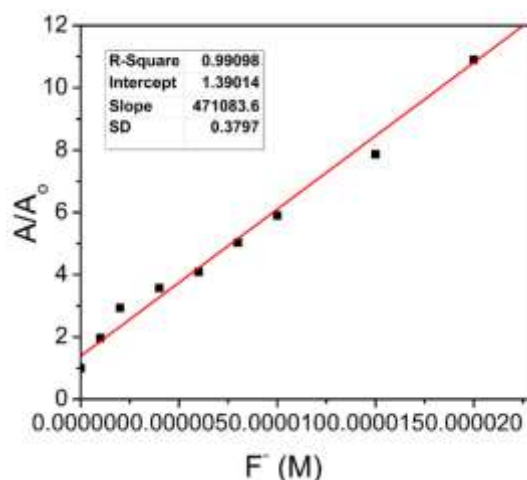
Figure 5.16 Calibration curve of receptor **R7b** (1×10^{-4} M in DMSO) against increasing concentration of fluoride ion (1×10^{-6} M to 1×10^{-4} M in DMSO)

5.2.3.4 ^{1}H NMR and ^{19}F NMR studies

In order to obtain an insight into fluoride binding event, the interaction of receptor **R7b** with fluoride was explored with ^{1}H NMR titration, performed using DMSO-d_6 solvent. In the ^{1}HNMR spectrum, the –OH signal which appears at 11.14 ppm disappears immediately upon addition of TBAF suggesting the binding occurs almost instantly when it comes in contact with the anion [67]. On addition of high equivalent of fluoride (TBAF), the appearance of a triplet at around 16 ppm observed due to the formation of HF_2^- [68]. In the excess of TBAF a marked variation of triazole C-H peak observed. The triazole proton (8.53 ppm) moves downfield by 1 ppm as the fluoride concentration increases from 0 to 8 eq. Perusal of literature revealed that triazole C-H is acidic in nature and also participate in H-bonding [69-72]. Desheilding effect in the triazole C-H

161

protons has been observed suggesting the polarizing, hydrogen-bonding like interaction with the fluoride anion. The proton ortho to the –OH group also moves upfield 8.36 to 8.31 ppm which advocates the increased electron density with a through-bond propagation [73]. Interestingly, the signal of the HF_2^- shifts downfield and increases in intensity during the titration, suggesting that the free HF_2^- is in fast exchange on the chemical shift time scale with the complexed HF_2^- [74]. ^{19}F-NMR titration of receptor **R7b** with TBAF has also been performed. Spectrum of TBAF in DMSO-d_6 revealed a singlet at δ -102 ppm due to F^- ion and a weak doublet at δ -142 ppm due to HF_2^-. The plot of titration shows that the signal of HF_2^- appears at around -152 ppm and shows an upshift to -142 ppm up to 3 eq. of F^- added; when an excess of TBAF is present in solution the signal of F^- appears at around -102 ppm. This supports the hypothesis of the initial deprotonation of the hydroxyl of receptor **R7b** with the subsequent formation of HF_2^- [74]. Further, the upshift of the signal of the HF_2^- species confirms that the deprotonated receptor initially interacts with the HF_2^- species, being the shift due to fast exchange on the chemical shift time scale between a free and a complexed HF_2^-. At around 7.5 eq. the resonance of HF_2^- is stable at approximately -142 ppm and the peak of F^- present in solution shifted upfield up to -103 ppm. **(Figure 5.17 and 5.18).**
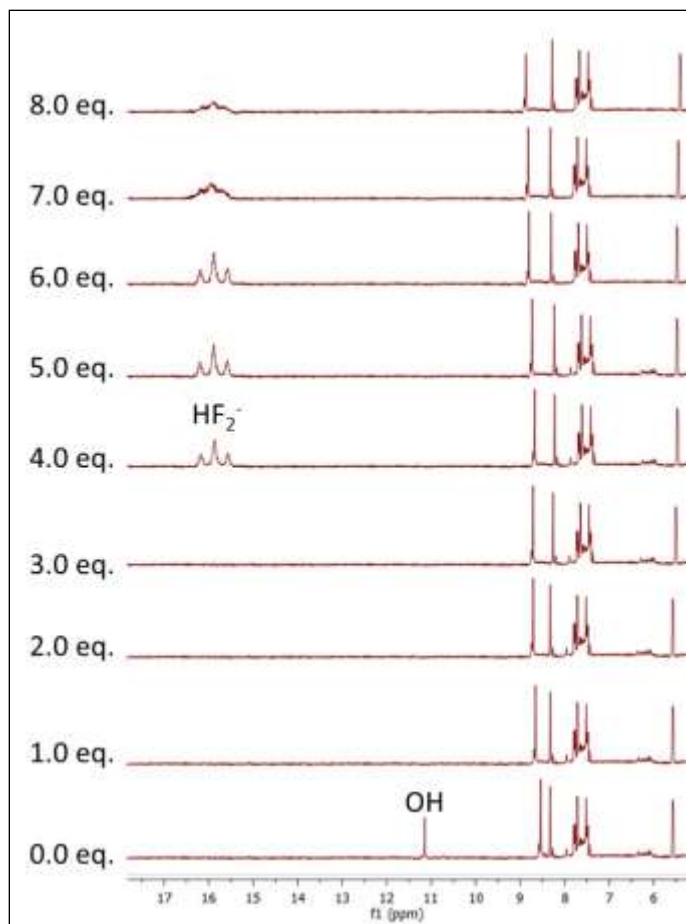
Figure 5.17 Changes in ^{1}H NMR spectrum of receptor **R7b** in DMSO-d_6 upon increasing equivalents of TBAF (0 to 8 equivalent)
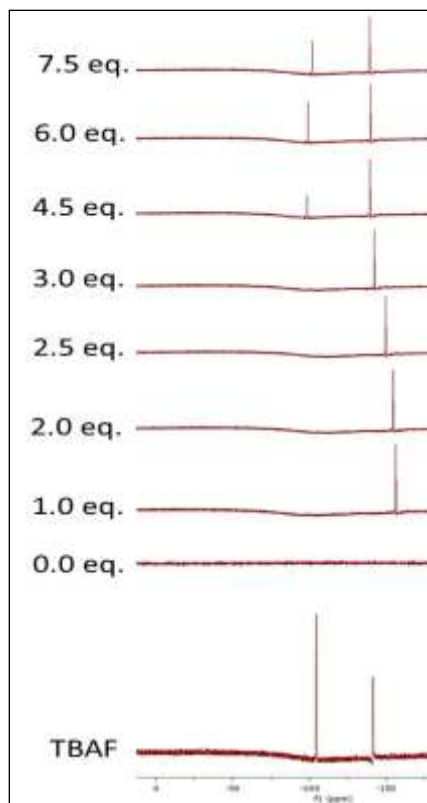
Figure 5.18 Changes in ^{19}F NMR spectrum of receptor **R7b** in DMSO-d_6 upon increasing equivalents of TBAF (0 to 8 equivalent)

5.2.4 Computational study

The foregoing results indicated that binding mechanism involved hydrogen bonding interaction between three hydroxyl group proton of tripodal receptor and fluoride ion. Computational calculation under density functional theory was carried out using Materials Studio (version 8.0) program suite to gain a clearer insight into the binding nature of fluoride ion. The geometry optimization has been performed without constraints using DMoL[3] module, PWC (Perdew Wang Correlations) local DFT functional and DND (4.4) basis set in DMSO as solvent. Graphics were obtained using Materials Studio visualizer [**75-76**]. Investigation of the highest occupied molecular orbital (HOMO) and lowest unoccupied molecular orbital (LUMO) have also been carried out at the same level of theory.
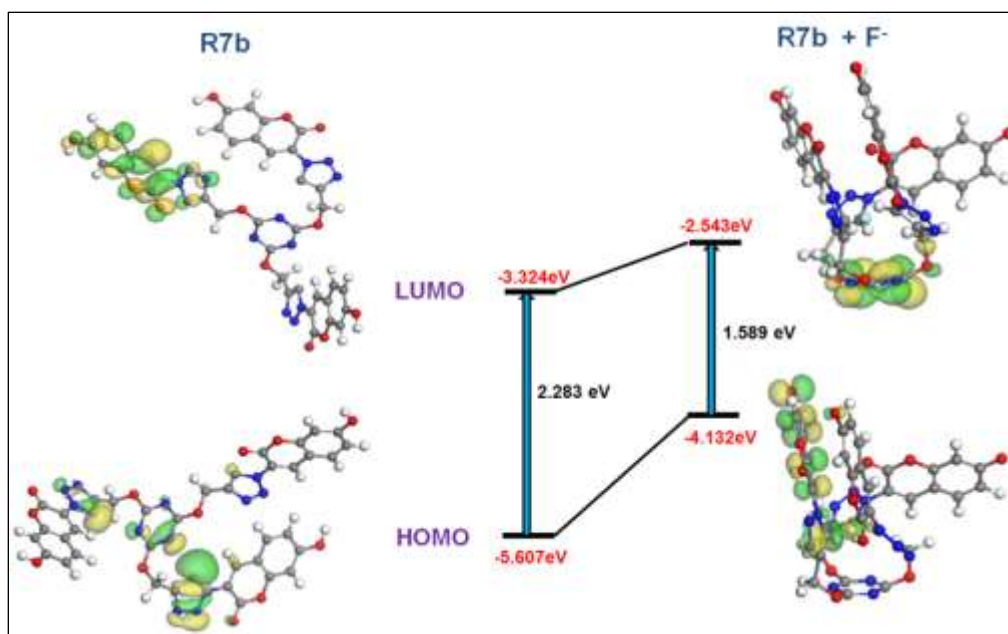
Figure 5.19 HOMO and LUMO energy levels and the interfacial plots of the orbitals for free receptor (**R7b**) and receptor + fluoride complex (**R7b** + 3F⁻)

The total energy of receptor-fluoride complex (-85272.3521 eV) is lower than the total energy of receptor (-82566.5033 eV) alone in solvent DMSO, which reveals formation of stable complex between receptor and fluoride ion. The optimized structure of free receptor and receptor + F⁻ complex with the distribution of their HOMO and LUMO levels were represented in **Figure 5.19**. The energy difference between HOMO and for receptor and receptor + F⁻ complex were 2.283 eV and 1.589 eV respectively. A significant decrease in band gap by 0.694 eV confirms the presence of deprotonation of the hydroxyl group along with hydrogen bonding with the triazole C-H during fluoride ion binding process [**77**]. Obtained results by computational study were found in good agreement of the experimental results.

5.3 Experimental

5.3.1 Materials and Characterization

All chemicals and solvents purchased are of analytical grade and used without further purification. Infrared spectrum were collected on a Bruker Fourier transform infrared spectrophotometer (FTIR) (Alpha) with pressed KBr pellets and were recorded in the range of 4000-400 wave number (cm⁻¹). The visualization of surface morphology of MNPs was done by

using a field- emission scanning electron microscope (FESEM; NOVA nano SEM) operated at a voltage 10 kV. Samples were prepared by putting a little amount of fine powdered nanoparticles on black carbon tape. Their TEM images were recorded with a Tecnai G^2 20 (FEI) S-Twin high-resolution transmission electron microscope (HRTEM) operating at 200 kV. Samples were prepared by drying the droplet of dispersed solution of MNPs on a 400 mesh carbon coated copper grid under 100 W table lamp. Powder X-ray diffraction (XRD) pattern of the sample was obtained with X-ray Diffractometer (Panalytical X Pert Pro) using Cu Kα radiation. X-ray photoelectron spectroscopy (XPS) measurements recorded in ESCA$^+$ omicron nanotechnology oxford instrument. Thermo gravimetric analysis (TGA) and differential thermal analysis (DTA) was performed on a Mettler thermal analyzer in an inert atmosphere at a heating rate of 10 ℃/min. Melting points were determined in open glass capillaries using Gallenkamp melting point apparatus and are reported uncorrected. ^{1}H NMR and ^{13}C NMR were recorded on a Jeol ECS 400 MHz spectrophotometer using DMSO d_6 as a solvent. TMS was taken as an internal standard and chemical shifts are reported in δ ppm. Resonance multiplicities are described as s (singlet), d (doublet), t (triplet), q (quartet) and m (multiplet). Mass spectrum were recorded on a Xevo G2-S Q-Tof (Waters, USA), capable of recording high resolution mass spectrum (HRMS) in the ESI (Electrospray Ionization) mode. Electronic spectruml studies were performed on a Shimadzu UV-L800 Spectrophotometer. The emission data were collected on a Perkin Elmer LS 55 Fluorescence Spectrophotometer at room temperature (298 K). Ultrasonic bath; Elma S 70 H with 37 KHz with an output frequency was used to carry out the sonochemical synthesis of nanocatalyst. CEM Discover Microwave was used to carry out the reactions. The purity of all the compounds was checked by TLC using silica gel as adsorbent and solvents of increasing polarity as mobile phase.

5.3.2 Synthesis of Fe$_3$O$_4$-Cys-Cu nanocatalyst

The magnetic nanoparticles were synthesized by chemical co-precipitation method as reported earlier [55]. For surface modification of cysteine over magnetite, initially 0.5 g of Fe$_3$O$_4$ was dispersed in H$_2$O/MeOH (3:1) and ultrasonicated for 10 min. Then L-cysteine 0.15 g added to the above solution and further sonicated for another 2 h at room temperature. The resulting nanomaterial allowed to remain undisturbed and were separated by using an external magnet and thoroughly washed with deionized water (2 x 50 mL) and methanol (2 x 50 mL) to remove any

unbounded L-cysteine. Finally functionalized nanoparticles were dried in an oven for 5 h at 60 °C. Cysteine functionalized nano Fe_3O_4 (1 g) was dispersed in $H_2O/MeOH$ (1:1) mixture. After that solution of $CuCl_2.H_2O$ (80 mg) in 2 mL of water was added to the above solution and sonicated for 5 min. Then hydrazine hydrate was added to it till the pH of the solution becomes 9-10 followed by addition of $NaBH_4$ (0.1 g) and sonication carried out for another 2 h at 60 °C. Fe_3O_4-Cys-Cu nanoparticles so prepared were separated by an external magnet and washed with water (2 x 50 mL) followed by methanol (2 x 50 mL). Finally the nanocatalyst was dried in an oven at 60 °C for 6-8 h.

5.3.3 General procedure for the synthesis of 1,4 disubstituted 1,2,3-triazole under microwave irradiation

In a crimp sealed thick walled glass tube equipped with a pressure sensor and a magnetic stirrer, benzyl bromide (1.2 mmol), sodium azide (1.5 mmol), phenyl acetylene (1.0 mmol) and for tripodal reaction as shown in Scheme 1 coumarin azide (0.66 mmol) and cyanuric alkyne (0.2 mmol) were taken with Fe_3O_4-Cys-Cu nanocatalyst (100 mg) and 5 mL of water. The reaction tube was placed inside the cavity of CEM discover focused microwave system. The reaction was carried out at 80 °C and 100 W under 10-60 psi for 08-15 min. After completion of the reaction, catalyst was separated from the reaction mixture by using an external magnet. The product was extracted from water with ethyl acetate (3 x 10 mL), the organic layers were combined, dried over Na_2SO_4 and the solvent removed under rota vapor. A crude solid product was obtained which was later purified by column chromatography. The catalyst was recycled up to six runs without any significant loss of yield (**Figure 5.19**).
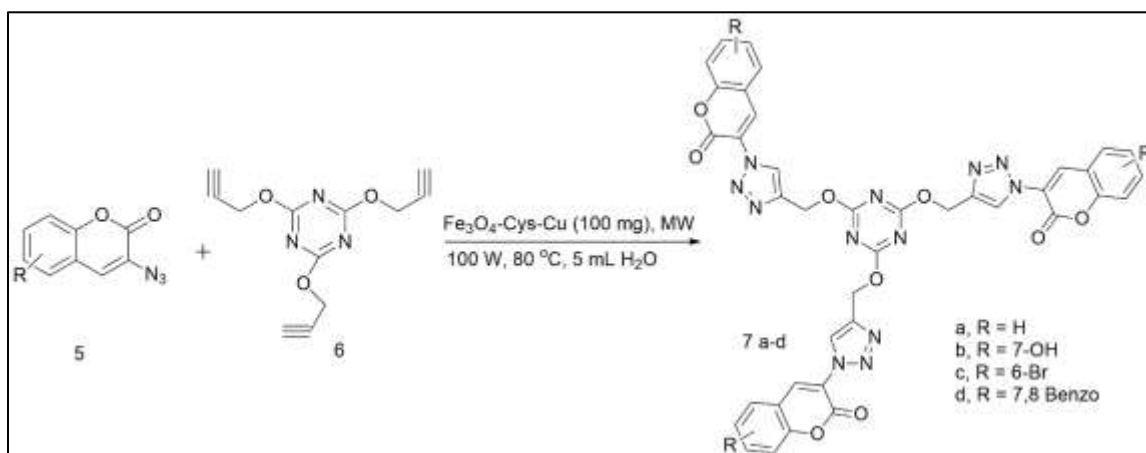
Scheme 5.2 Synthesis of tripodal triazole by using Fe_3O_4-Cys-Cu nanocatalyst (**7a-d**)
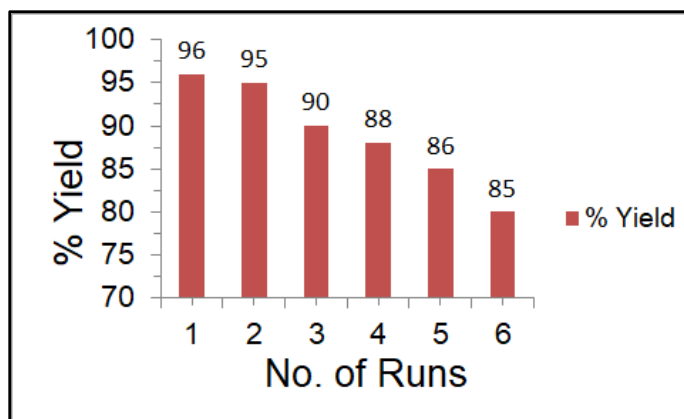
Figure 5.20 Recyclability of the nanocatalyst (reaction conditions**:** benzyl bromide (1.2 mmol), sodium azide (1.5 mmol), phenyl acetylene (1 mmol) in presence of 100 mg of Fe_3O_4-Cys-CuNPs in 5 ml H_2O at 100 W and 80 $^{\circ}$C

5.3.4 Analytical data

3,3',3''-(4,4',4''-(((1,3,5-triazine-2,4,6-triyl)tris(oxy))tris(methylene))tris(1H-1,2,3-triazole-4,1-diyl))tris(2H-chromen-2-one) (7a)

Yield: 94 %; m.p.: 155 ℃; ^{1}H NMR (400 MHz, DMSO-d_6, ppm) δ 5.34 (s, 6H, OCH$_2$), 7.41-7.89 (m, 12H, ArH), 8.39 (s, 3H, ArH), 8.45 (s, 3H, 3×CH); ^{13}C NMR (100 MHz, DMSO-d_6, ppm) δ 71.83, 116.59, 122.56, 123.98, 124.69, 125.72, 126.74, 130.60, 132.73, 149.11, 157.15, 164.17, 172.19; MS (ESI) m/z = 805.1861 [M+H]+ Calculated for $C_{39}H_{24}N_{12}O_9$: 804.1789.

3,3',3''-(4,4',4''-(((1,3,5-triazine-2,4,6-triyl)tris(oxy))tris(methylene))tris(1H-1,2,3-triazole-4,1-diyl))tris(7-hydroxy-2H-chromen-2-one) (7b)

Yield: 92 %; m.p.: 162 ℃; ^{1}H NMR (400 MHz, DMSO-d_6, ppm) δ 5.53 (s, 6H, OCH$_2$), 7.49-7.83 (m, 9H, ArH), 8.36 (s, 3H, ArH), 8.53 (s, 3H, 3×CH), 11.14 (s, 1H, OH); ^{13}C NMR (100 MHz, DMSO-d_6, ppm) δ 69.71, 115.95, 121.86, 123.29, 124.28, 125.33, 125.73, 131.30, 133.07, 150.51, 157.51, 164.87, 173.28; MS (ESI) m/z = 853.1712 [M+H]+ Calculated for $C_{39}H_{24}N_{12}O_{12}$: 852.1637.

3,3',3''-(4,4',4''-(((1,3,5-triazine-2,4,6-triyl)tris(oxy))tris(methylene))tris(1H-1,2,3-triazole-4,1-diyl))tris(7-bromo-2H-chromen-2-one) (7c)

Yield: 96 %; m.p.: 220 ℃; ^{1}H NMR (400 MHz, DMSO-d_6, ppm) δ 5.60 (s, 6H, OCH$_2$), 7.28-7.59 (m, 9H, ArH), 7.97 (s, 3H, ArH), 8.54 (s, 3H, 3×CH); ^{13}C NMR (100 MHz, DMSO-d_6, ppm) δ 70.83, 117.32, 122.13, 123.58, 124.67, 125.30, 126.73, 130.30, 132.71, 149.11, 157.85, 164.55,

171.16; MS (ESI) m/z = 1038.9176 [M+H]+ Calculated for $C_{39}H_{21}Br_3N_{12}O_9$: 1037.9105.

3,3',3''-(4,4',4''-(((1,3,5-triazine-2,4,6-triyl)tris(oxy))tris(methylene))tris(1H-1,2,3-triazole-4,1-diyl))tris(2H-benzo[g]chromen-2-one) (7d)

Yield: 94 %; m.p.: 159 °C; ^{1}H NMR (400 MHz, DMSO-d_6, ppm) δ 5.49 (s, 6H, OCH$_2$), 7.20-8.22 (m, 18H, ArH), 9.09 (s, 3H, ArH), 9.27 (s, 3H, 3×CH); ^{13}C NMR (100 MHz, DMSO-d_6, ppm) δ 72.54, 113.10, 121.55, 122.69, 123.30, 124.0, 126.0, 126.6, 127.12, 128.89, 129.59, 130.57, 131.67, 138.93, 150.91, 164.87, 173.96; MS (ESI) m/z = 955.2334 [M+H]+ Calculated for $C_{51}H_{30}N_{12}O_9$: 954.2259.
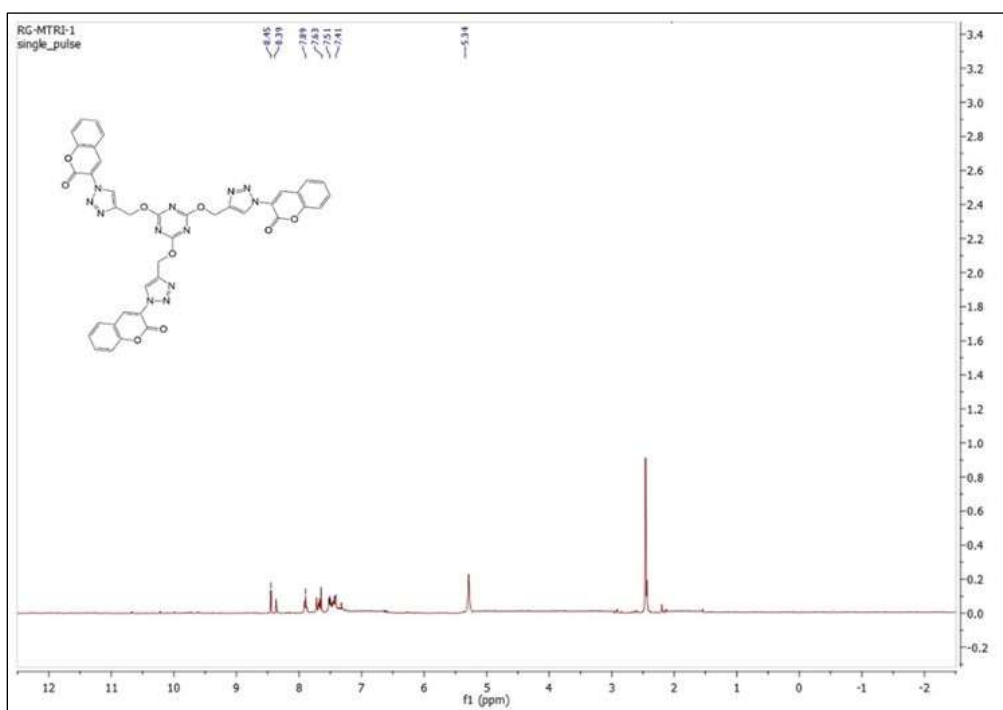
Figure 5.21 ^{1}HNMR of 3,3',3''-(4,4',4''-(((1,3,5-triazine-2,4,6-triyl)tris(oxy))tris(methylene))tris(1H-1,2,3-triazole-4,1-diyl))tris(2H-chromen-2-one) **(7a)**
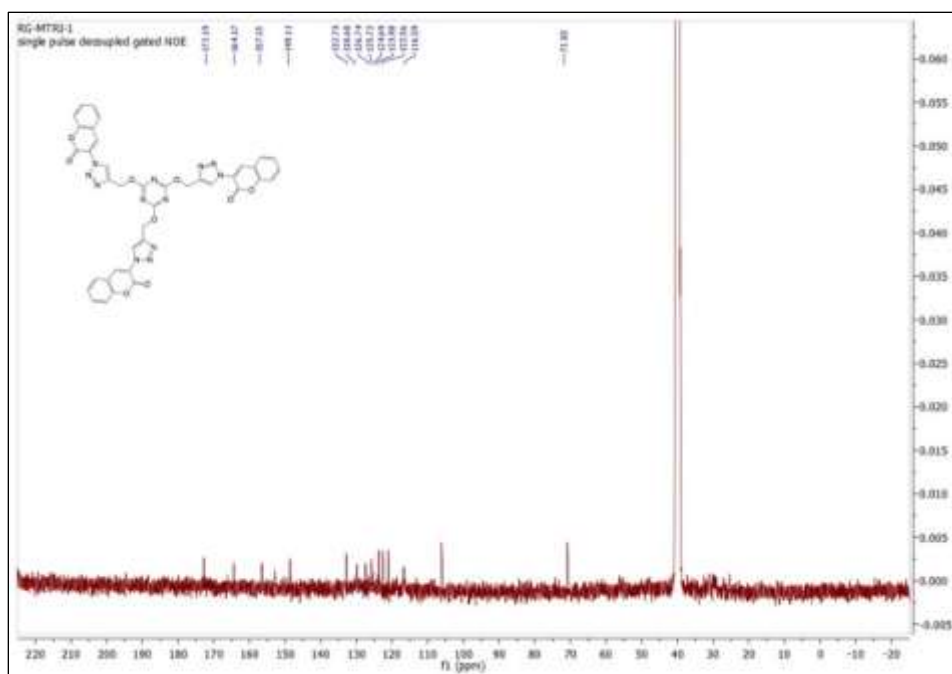
Figure 5.22 ^{13}C NMR of 3,3',3''-(4,4',4''-(((1,3,5-triazine-2,4,6-triyl)tris(oxy))tris(methylene))tris(1H-1,2,3-triazole-4,1-diyl))tris(2H-chromen-2-one) **(7a)**
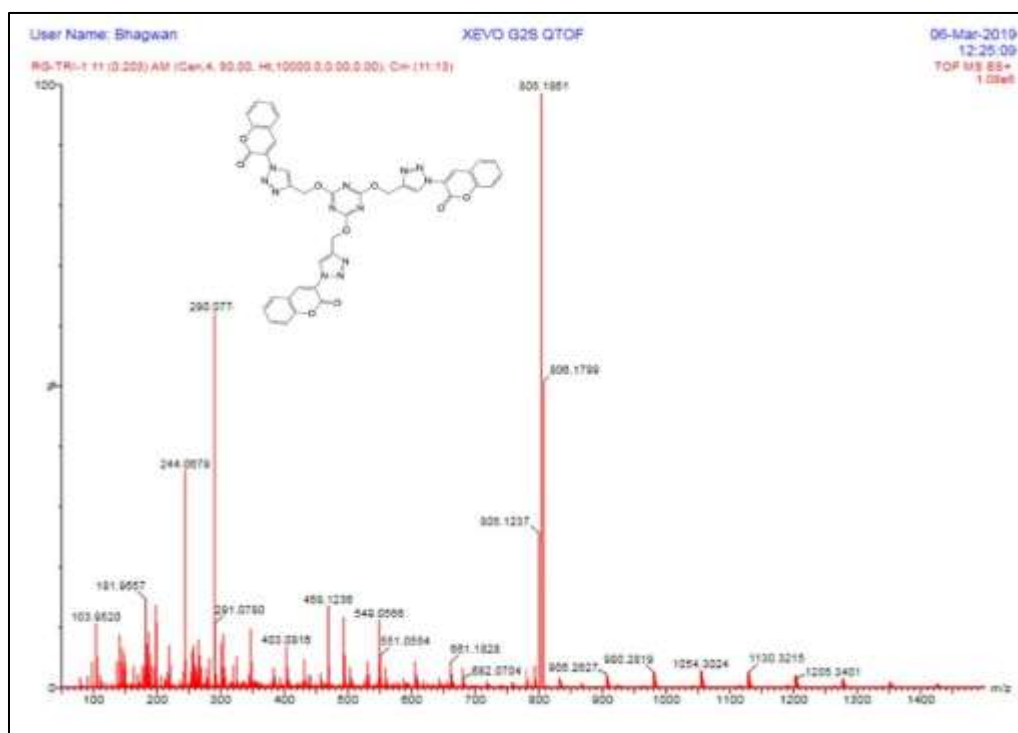
Figure 5.23 Mass spectrum of 3,3',3''-(4,4',4''-(((1,3,5-triazine-2,4,6-triyl)tris(oxy))tris(methylene))tris(1H-1,2,3-triazole-4,1-diyl))tris(2H-chromen-2-one) **(7a)**
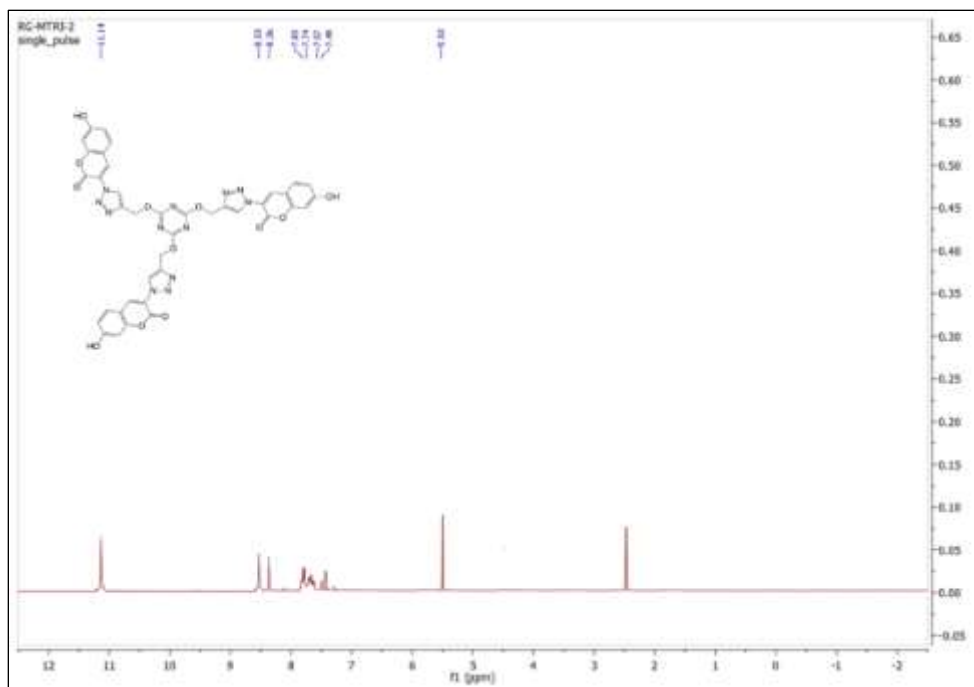
Figure 5.24 ¹H NMR of 3,3',3''-(4,4',4''-(((1,3,5-triazine-2,4,6-

triyl)tris(oxy))tris(methylene))tris(1H-1,2,3-triazole-4,1-diyl))tris(7-hydroxy-2H-chromen-2-one)

(7b)
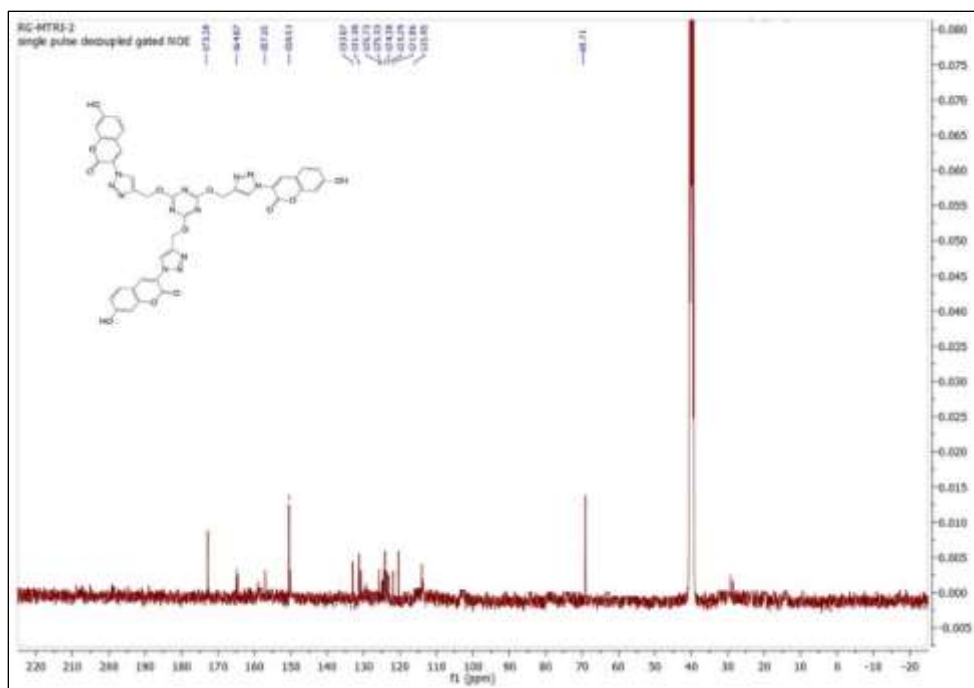
Figure 5.25 ¹³C NMR of 3,3',3''-(4,4',4''-(((1,3,5-triazine-2,4,6-
triyl)tris(oxy))tris(methylene))tris(1H-1,2,3-triazole-4,1-diyl))tris(7-hydroxy-2H-chromen-2-one)
(7b)
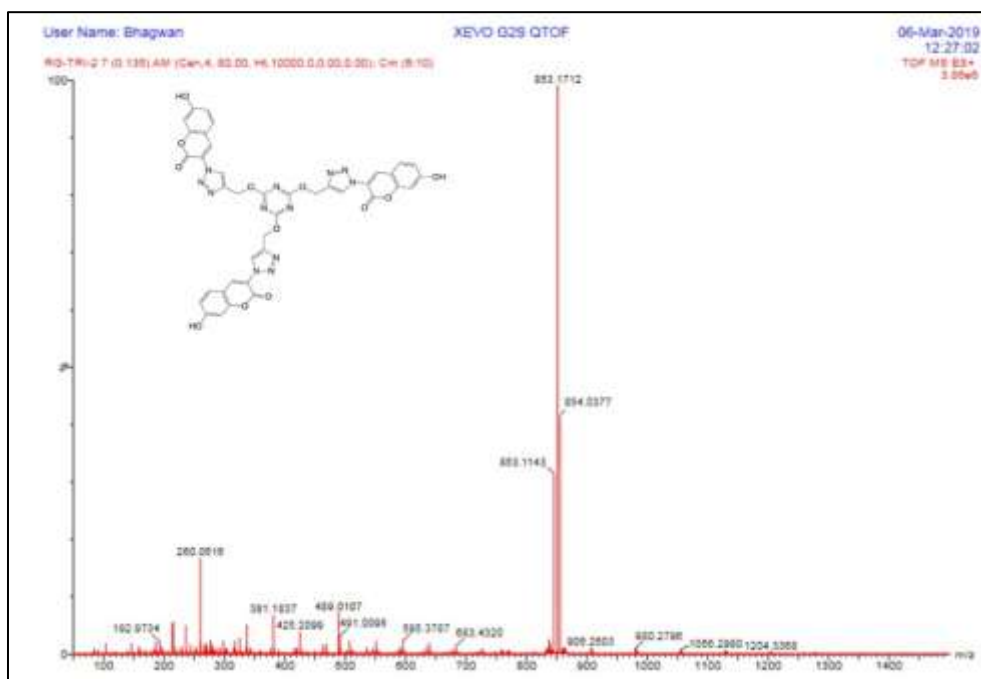
Figure 5.26 Mass spectrum of 3,3',3''-(4,4',4''-(((1,3,5-triazine-2,4,6-triyl)tris(oxy))tris(methylene))tris(1H-1,2,3-triazole-4,1-diyl))tris(7-hydroxy-2H-chromen-2-one) **(7b)**
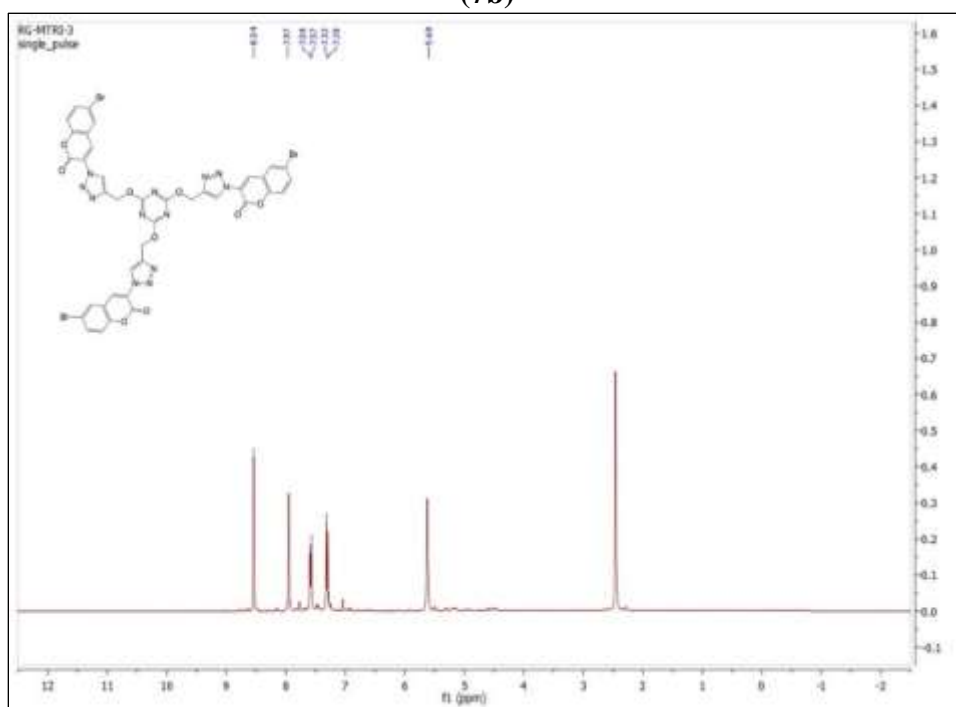
Figure 5.27 1 ^{1}HNMR of 3,3',3''-(4,4',4''-(((1,3,5-triazine-2,4,6-triyl)tris(oxy))tris(methylene))tris(1H-1,2,3-triazole-4,1-diyl))tris(7-bromo-2H-chromen-2-one) **(7c)**
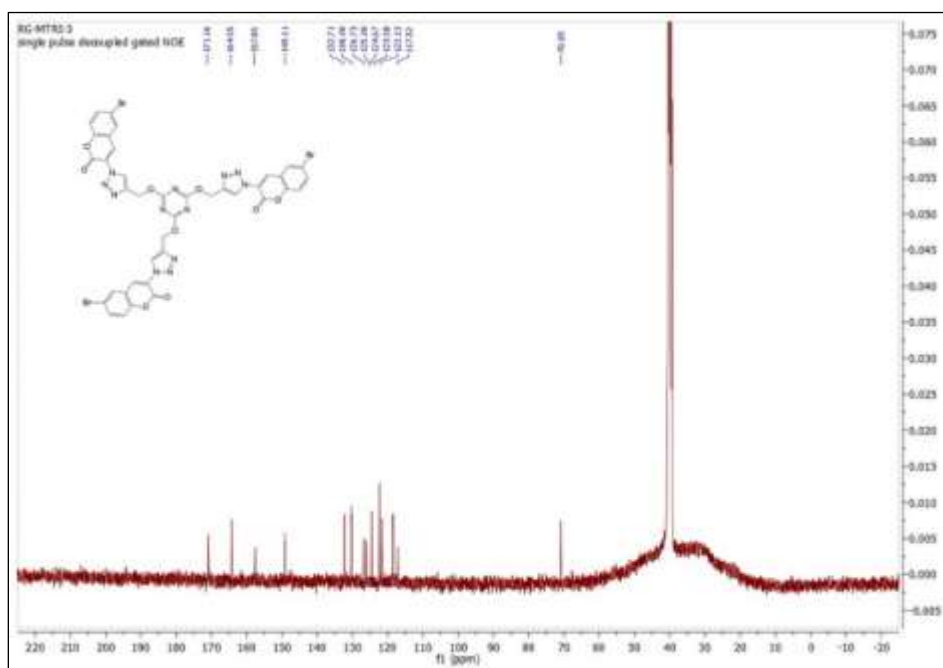
Figure 5.28 ^{13}C NMR of 3,3',3''-(4,4',4''-(((1,3,5-triazine-2,4,6-triyl)tris(oxy))tris(methylene))tris(1H-1,2,3-triazole-4,1-diyl))tris(7-bromo-2H-chromen-2-one) **(7c)**
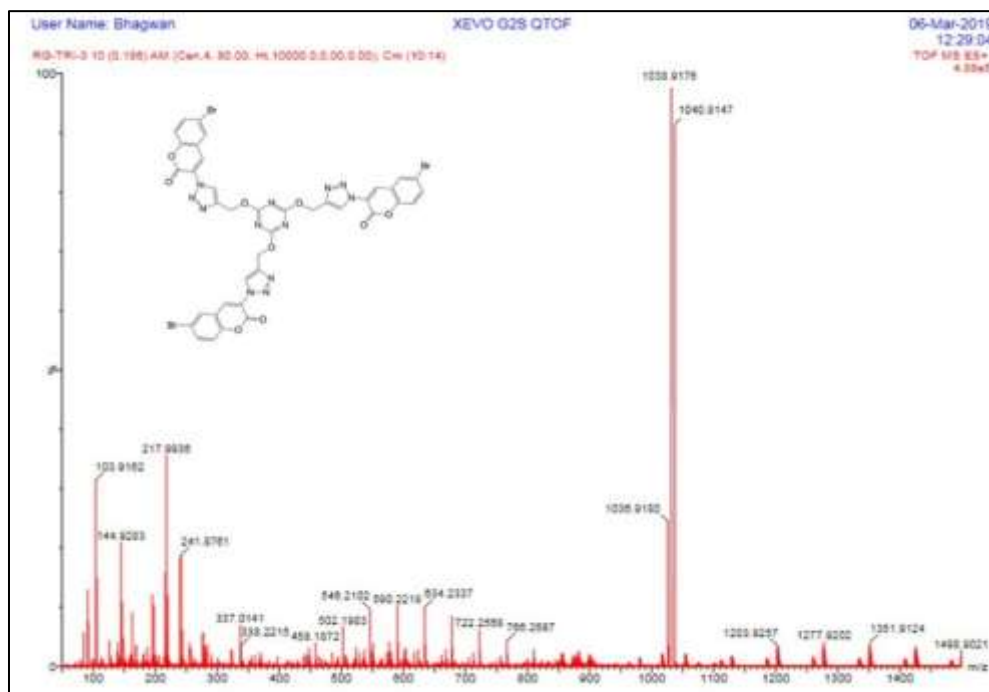
Figure 5.29 Mass spectrum of 3,3',3''-(4,4',4''-(((1,3,5-triazine-2,4,6-triyl)tris(oxy))tris(methylene))tris(1H-1,2,3-triazole-4,1-diyl))tris(7-bromo-2H-chromen-2-one) **(7c)**

Figure 5.30 ^{1}HNMR of 3,3',3"-(4,4',4"-(((1,3,5-triazine-2,4,6-triyl)tris(oxy))tris(methylene))tris(1H-1,2,3-triazole-4,1-diyl))tris(2H-benzo[g]chromen-2-one)
(7d)

Figure 5.31 ^{13}C NMR of 3,3',3"-(4,4',4"-(((1,3,5-triazine-2,4,6-triyl)tris(oxy))tris(methylene))tris(1H-1,2,3-triazole-4,1-diyl))tris(2H-benzo[g]chromen-2-one)
(7d)
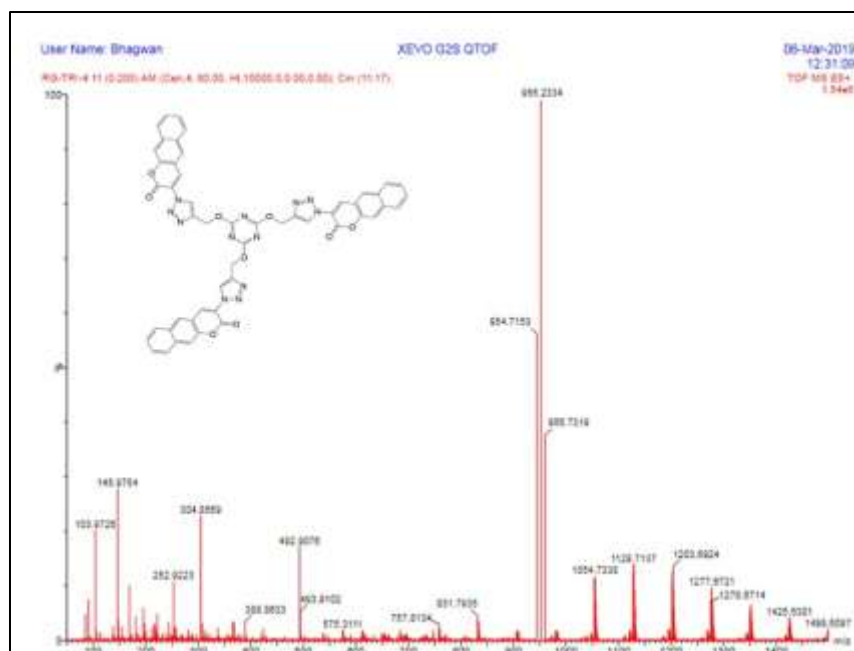
Figure 5.32 Mass spectrum of 3,3',3''-(4,4',4''-(((1,3,5-triazine-2,4,6-triyl)tris(oxy))tris(methylene))tris(1H-1,2,3-triazole-4,1-diyl))tris(2H-benzo[g]chromen-2-one) **(7d)**
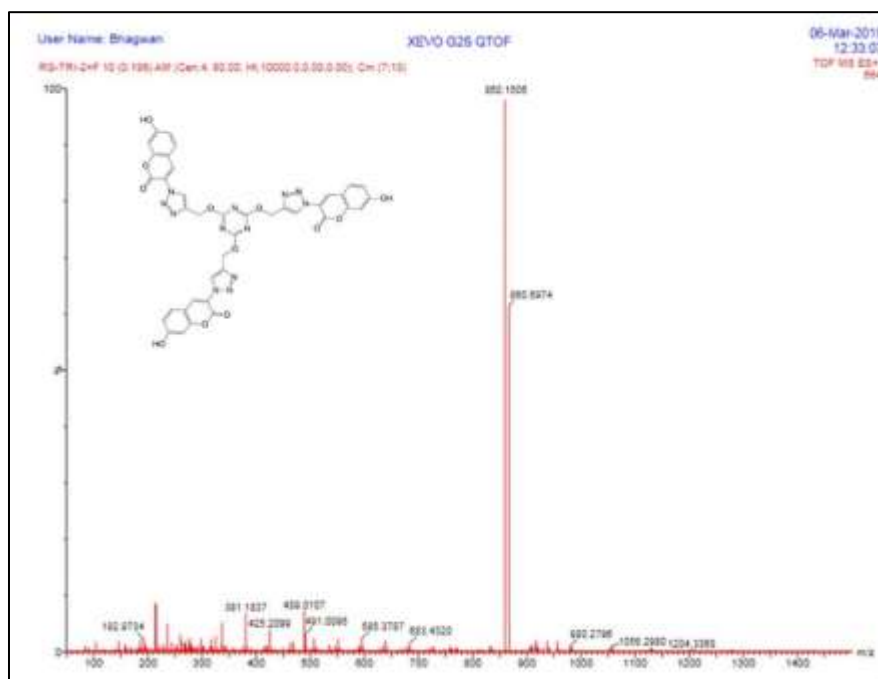
Figure 5.33 Mass spectrum of 3,3',3''-(4,4',4''-(((1,3,5-triazine-2,4,6-triyl)tris(oxy))tris(methylene))tris(1H-1,2,3-triazole-4,1-diyl))tris(2-oxo-2H-chromene-7,3-diyl) trihypofluorite (**7b**+3F⁻)

175

5.4 Conclusion

We have successfully developed a clean, inexpensive and high yield synthesis of 1,2,3-triazoles by using a highly water dispersible, efficient and magnetically separable Fe_3O_4-Cys-Cu nanocatalyst in an aqueous medium. Using this catalyst, some new tripodal triazoles were also successfully synthesized and explored for their anion binding affinity. Triazole 7b exhibit good sensitivity and selectively binds with fluoride ion in 1:3 stoichiometry which further theoretically proved by DFT studies suggesting lowering of the $\Delta E_{\text{HOMO-LUMO}}$ energy gap due to the deprotonation.

5.5 References

[1] Roduner, E. *Chem. Soc. Rev.* **2006**, *35*, 583.

[2] Astruc, D.; Lu, F.; Ruiz, *J. Angew. Chem.*, *Int. Ed.* **2005**, *44*, 7852.

[3] Astruc, D., *Ed.; Wiley-VCH Verlag GmbH & Co. KGaA: Weinheim*, **2008**, *47*, 5504.

[4] Somorjai, G. A.; Frei, H.; Park, J. Y. *J. Am. Chem. Soc.* **2009**, *131*, 16589.

[5] Schatz, A.; Reiser, O.; Stark, W. *J. Chem. Eur. J.* **2010**, *16*, 8950.

[6] Goesmann, H.; Feldmann, C. *Angew. Chem., Int. Ed.* **2010**, *49*, 1362.

[7] Arpad, M. *Chem. Rev.* **2011**, *111*, 2251.

[8] Mondloch, J. E.; Bayram, E.; Finke, R. G. *J. Mol. Catal. A: Chem.* **2012**, *355*, 1.

[9] Bai, C.; Liu, M. *Nano Today* **2012**, *7*, 258.

[10] Chng, L. L.; Erathodiyil, N.; Ying, J. Y. *Acc. Chem. Res.* **2013**, *46*, 1825.

[11] Mitsudome, T.; Kaneda, K. *ChemCatChem.* **2013**, *5*, 1681.

[12] Lu, A. H.; Salabas, E. L.; Schüth, F. *Angew. Chem., Int. Ed.* **2007**, *46*, 1222.

[13] Shylesh, S.; Schünemann, V.; Thiel, W. R. *Angew. Chem., Int. Ed.* **2010**, *49*, 3428.

[14] Zhu, Y.; Stubbs, L. P.; Ho, F.; Liu, R.; Ship, C. P.; Maguire, J. A.; Hosmane, N. S. *ChemCatChem.* **2010**, *2*, 365.

[15] Polshettiwar, V.; Luque, R.; Fihri, A.; Zhu, H.; Bouhrara, M.; Basset, J.-M. *Chem. Rev.* **2011**, *111*, 3036.

[16]   Rossi, L. M.; Garcia, M. A. S.; Vono, L. L. R. J. Braz. *Chem. Soc*. **2012**, *23*, 1959.

[17]   Baig, R. B. N.; Varma, R. S. *Chem. Commun*. **2013**, *49*, 752.

[18]   Nasr-Esfahani, M.; Rafiee, Z.; Montazerozohori, M.; Kashi, H. *RSC Adv*. **2016**, *6*, 47298.

[19]   Gawande, M. B.; Branco, P. S.; Varma, R. S. *Chem. Soc. Rev.* **2013**, *42*, 3371.

[20]   Shelke, S. N.; Bankar, S. R.; Mhaske, G. R.; Kadam, S. S.; Murade, D. K.; Bhorkade, S. B.; Rathi, A. K.; Bundaleski, N.; Orlando, M. N. D.; Zboril, T. R.; Varma, R. S.; Gawande, M. B. *ACS Sustainable Chem. and Eng*. **2014**, *2*, 1699.

[21]   Abu-Dief, A. M.; Fatah Abdel S. M. J. *Basic Appl. Sci.* **2018**, *7*, 55.

[22]   Seenivasan, R.; Chang, W. J.; Gunasekaran, S. *ACS Appl. Mater. Interfaces* **2015**, *7,* 15935.

[23]   Li, Q.; Wang, Z.; Fang, D. M.; Qu, H. Y.; Zhu, Y.; Zou, H. J.; Chen, Y. R.; Du, Y. P.; Hu, H. L. *New. J. Chem.* **2014**, *38*, 248.

[24]   Liu, Y.; Li, Y.; Yan, X. P. *Adv. Funct. Mater*. **2008**, *18,* 1536.

[25]   White, B. R.; Stackhouse, B. T.; Holcombe, J. A. *J. Hazard. Mater*. **2009**, *161,* 848.

[26]   Zhou, L. M.; Wang, Y. P.; Liu, Z. R.; Huang, Q. W. *J. Hazard. Mater*. **2009**, *161,* 995.

[27]   Uzun, L.; Türkmen, D.; Yılmaz, E.; Bektas, S.; Denizli, A. *Colloid Surf. A Physicochem. Eng. Asp.* **2008**, *330,* 161.

[28]   Wildgoose, G. G.; Leventis, H. C.; Simm, A. O.; Jones, J. H.; Compton, R.G. *Chem. Commun*. **2005**, *41,* 3694.

[29]   Allen, S. E.; Walvoord, R. R.; Salinas, R. P.; Kozlowski, M. C. *Chem. Rev.* **2013**, *113*, 6234.

[30]   Gawande, M. B.; Goswami, A.; Felpin, F. X.; Asefa, T.; Huang, X.; Silva, R.; Zou, X.; Radek, Varma, R. S. *Chem. Rev.* **2016**, *116*, 3722.

[31]   (a) Huisgen, R.; *Pure Appl. Chem.* **1989**, *61*, 613-628; (b) Tornøe, C. W.; Christensen, C.; Meldal, M. *J. Org. Chem.* **2002**, *67*, 3057.

[32]   (a) Pérez, J. M.; Crosbie, P.; Lal, S.; Díez-González, S. *ChemCatChem*. **2016**, *8*, 2222-2226; (b) Liu, X.; Novoa, N.; Manzur, C.; Carrillo, D.; Hamon, J. *New J. Chem.* **2016**, *40*, 3308.

[33]   (a) Jang, S.; Sa, Y. J.; Joo, S. H.; Park, K. H. *Catal. Commun.* 2016, **81**, 24-28; (b) Holub, J. M.; Kirshenbaum, K. *Chem. Soc. Rev.* **2010**, *39*, 1325.

[34]   (a) Tabacaru, A.; Furdui, B.; Ghinea, I. O.; Cârâc, G.; Dinica, R. M. *Inorg. Chim. Acta* **2017**, *455*, 329; (b) Nie, R.; Sang, R.; Ma, X.; Zheng, Y.; Cheng, X.; Li, W.; Guo, L.; Jin, H.; Wu, Y. *J. Catal*. **2016**, *344*, 286; (c) Shin, J.-A.; Oh, S.-J.; Lee, H.-Y.; Lim, Y.-G. *Catal. Sci. Technol*. **2017**, *7*, 2450.

[35]   Zohreh, N.; Hosseini, S. H.; Pourjavadi, A.; Bennett, C. *Appl. Organomet. Chem.* **2016**, *30*, 73.

[36]   Shiraishi, Y.; Nakamura, M.; Matsushita, N.; Hirai, T. *New J. Chem*. **2016**, *40*, 195.

[37]   Zhao, L.; Liu, G.; Zhang, B. J. *Spectrochim. Acta A.* **2016**, *169*, 45.

[38]   Biswas, S.; Gangopadhyay, M.; Barman, S.; Sarkar, J.; Singh, N. D. P. *Sens. Actuators B.* **2016**, *222*, 823.

[39]   Kim, W.; Sahoo, S. K.; Kim, G. D.; Choi, H. J. *Tetrahedron.* **2015**, *71*, 8111.

[40]   Li, W.; Sun, J.; Shi, J.; Hao, S.; Liu, Q.; Yu, G. *Supramol. Chem*. **2016**, *28*, 686.

[41]   Ravikumar, I.; Ghosh, P. *Chem. Commun.* **2010**, 1082.

[42]   Yeap, Y.; Hrishikesan, E.; Chan, Y. H.; Mahmood, W. A. K. *J. Fluoresc*. **2016**, *27*, 105.

[43]   Wu, J. –S.; Wang, F.; Liu, W. –M. *Sens. Actuators B* **2007**, *125*, 447.

[44]   Sain, D.; Kumari, C.; Kumar, A.; Dey, S. *Supramol. Chem.* **2016**, *28*, 239.

[45]   Lin, L. –R.; Fang, W.; Yu, Y. *Spectrochim. Acta A*. **2007**, *67*, 1403.

[46]   Amendola, V.; Fabbrizzi, L.; Mosca, L. *Chem. Soc. Rev.* **2010**, *39*, 3889.

[47]   Martínez-Máñez, R.; Sancenon, F. Coord. *Chem. Rev*. **2006**, *250*, 3081.

[48]   Fabbrizzi, I.; Poggi, A. *Chem. Soc. Rev*. **2013**, *42*, 1681.

[49]   Ghosh, K.; Kar, D.; Joardar, S.; Samadder, A.; Khuda-Bukhsh, A. R. *RSC Adv.* **2014**, 4, 11590.

[50]   Zhao, L.; Lio, G.; Zhang, B.; *Spectrochim. Acta A*. **2016**, 169, 45.

[51]   Shiraishi, Y.; Nakamura, M.; Matsashita, N.; Hiral, T. *New J. Chem*. **2016**, 40, 195.

[52]   Kumari, M.; Gupta, R.; Jain, Y. Synth. Commun. **2019**, 49, 529.

[53]   Jain, Y.; Gupta, R.; Yadav, P.; Kumari, M. *ACS Omega* **2019***, 4, 3582.

[54]   Jain, Y.; Kumari M.; Gupta R. *Tetrahedron Lett*. **2019**, 60, 1215.

[55]   Saha, S., Pal, A., Kundu, S.; Basu, S**.;** Pal, T. *Langmuir.* 2010*, 26***, 2885.**

[56]   Shen, X.; Wang, Q.; Chen, W. L.; Pang, Y. *Appl Surf Sci* 2014**, 317,** 1028**.**

[57]   Fan, Li H-L.; L.; Zhou, S-F.; Liu, Y-Z. *Ceram Int.* 2016**, 42,** 4228**.**

[58]   Rathore, P.S.; Patidar, R.; Thakore, S.; RSC Adv **2014**, 4, 1111.

[59]   Cohen, H.; Gedanken, A.; Zhong, Z**.** *J. Phys. Chem. C* **2008,** *112,* 15429.

[60]   Kataby, G., Prozorov, T.; Koltypin.Y.; Cohen. H.; Sukenik, C.N.; Ulman, A.; Gedanken, A.; *Langmuir* **1997**,   13, 6151.

[61]   Bain, C.D.; Troughten, E.B.; Tao, Y.T.; Evall, J.; Whitesides, G.M.; Nuzzo, R.G.; *J. Am. Chem. Soc.***1989**, 11, 321.

[62]   Cornell R. M.; Schwertmann, U. VCH: Weinheim, Germany, **1996**

[63]   Jung, C. W. *Magn. Reson. Imaging* **1995**, *13*, 675

[64]   Kumari, M.; Jain, Y.; Yadav, P.; Laddha, H.; Gupta, R.; Catalytic Lett. 2019

[65]   Mondal, P.; Sinha. A.; Salam. N.; Roy, A. S.; Jana, N. R.; Islam, S. M.; *RSC Adv* **2013,** 3, 5615

[66]   Ayouchia, H. B. E.; Bahsis, L.; Anane, H.; Domingo, L. R.; Stiriba, S. E. *RSC Adv.* **2018,** 8, 7670.

[67]   Khanmohammadi, H.; Rezaeian, K.; *RSC Adv* **2014**, 4, 1032

[68]   Ghosh, D,; Rhodes, S.; Hawkins, K.; Winder, D.; Atkinson, A.; Ming, W.; Padgett, C.; Orvis, J.; Aiken, K.; Landge, S. *New J. Chem.* **2015**, **39**, 295.

[69]   Tamgho, I. S.; Chaudhuri, S.; Verderame, Molly.; DiScenza, D. J.; Levine, M.; *RSC Adv* **2017**, 7, 28489

[70]   Sui, B.; Kim, B.; Zhang, Y.; Frazer, A.; Belfield, K. D. *Appl. Mater. Interfaces* **2013**, 5, 2920.

[71]   Kumar, M. S.; Ashok Kumar, S.L.; Sreekanth, A. *Materials Science and Engineering* C **2013**, 33, 3346.

[72]   Gale, P. A.; Howe, E. N.W.; Wu, X. *Chem 1*, **2016**, 351.

[73]   Peng, X.; Wu, Y.; Fan, J.; Tian, M.; Han, K.; J. Org. Chem. 2005, 70, 10524.

[74]   Juwarker, H.; Lenhardt, J. M.; Castillo, J. C.; Zhao, E.; Krishnamurthy, S.;
Jamiolkowski, R. M.; Kim K. H.; Craig, S. L. J. Org. Chem 2009, 74, 8924.

[75]   Shrivastava, A.; Gupta, V. B.; *Chron Young Sci*. **2011**, 2, 21.

[76]   Delly, B.; *J.Chem.Phys.* **1990**, 92, 508

[77]   Morakot, N.; Rakrai, W.; Keawwangchat, S.; Kaewtong, C.; Wamao, B.J.; *Mol.
Model* **2010**, 16, 129-136; (b) Amalraj, A.; Plus, A.J.; *Fluor. Chem.* **2015**, 178, 73.

CONCLUSIONS AND SCOPE OF THE FUTURE WORK

The present work describes a straight forward and more efficient methodology for efficient synthesis of the Schiff's bases, reduction of nitroarenes, an array of multicomponent reactions catalyzed by recyclable and reusable magnetic nanocatalyst under ultrasonication and microwave irradiation.

Citric acid immobilized magnetic nanoparticles (MNP@CA) have been synthesized and used for the preparation of bio-important antipyrine (1,5-dimethyl-2-phenyl-1,2-dihydro-3H-pyrazol-3-one) derived Schiff's bases in lesser reaction time with very high yield under ultrasonication. The functionalized nanoparticles were easily separated using an external magnet during work-up procedure and show excellent reusability up to 8 cycles without any significant loss in catalytic activity. All the synthesized compounds **(3a-k)** were screened by DPPH (2,2-diphenyl-1-picrylhydrazyl) method with respect to ascorbic acid for their antioxidant activity and some of them gave promising results.

A more facile route to synthesize magnetically separable copper loaded L-DOPA functionalized magnetite nanoparticles (Fe_3O_4-DOPA-CuNPs) has been presented. This single catalyst exhibits excellent catalytic activity towards (i) synthesis of DHPMs *via* Biginelli reaction (ii) synthesis of imidazoles (iii) synthesis of 2-amino-4H-chromenes (iv) 1,2,3-triazole derivatives by 'Click reaction' under microwave irradiation (MWI). Interestingly it could be easily recovered and reused for subsequent cycles for above mentioned four important multicomponent reactions without any significant decrease in its catalytic activity.

Heterostructured Ag nanoparticles decorated Fe_3O_4 Glutathione (Fe_3O_4-Glu-Ag) nanoparticles (NPs) were synthesized by sonicating glutathione (Glu) with magnetite and further surface immobilization of silver NPs on it. The prepared Fe_3O_4-Glu-Ag nanoparticles have proved to be an efficient and recyclable nanocatalyst with low catalyst loading for the reduction of nitroarenes and heteronitroarenes to respective amines in the presence of $NaBH_4$ using water as a green solvent which could be easily separated at the end of a reaction using an external magnet and can be recycled up to 5 runs without any significant loss in catalytic activity. Gram scale study for the reduction of 4-NP has also being carried out successfully and it has been observed that this method can serve as an efficient protocol for reduction of nitroarenes on industrial level.

A series of tripodal triazoles have been synthesized by recyclable and reusable Fe_3O_4-Cys-Cu magnetic nanocatalyst. One of the triazole was then evaluated as selective colorimetric and

fluorometric receptor for fluoride ion recognition. Colorimetric response upon addition of fluoride ion to receptor shows a color change from pale yellow to shiny green. Additionally, receptor showed the UV-vis red shift and fluorescent enhancement only in the presence of F^- ion. The 1:3 binding stoichiometry of receptor-fluoride ion was determined by Job's plot and further verified by ESI-HRMS data. ^{1}H NMR validate O-H$\cdots$F$^-$ hydrogen bonding interactions and also theoretical calculations using density functional theory confirms the deprotonation fluoride ion binding process.

Finding further applications of the magnetic nanocatalyst and search for cost-effective alternative developing reaction methodologies to work economically and with high efficiency will be the the critical goal of this research.

APPENDIX- I

LIST OF SYNTHESIZED COMPOUNDS

S. No.	Compd No.	Name of Synthesized Compounds
Chapter – 2		
1	**3a**	4-(benzylideneamino)-1,5-dimethyl-2-phenyl-1H-pyrazol-3(2H)-one
2	**3b**	4-((2-hydroxybenzylidene)amino)-1,5-dimethyl-2-phenyl-1H-pyrazol-3(2H)-one
3	**3c**	4-((4-hydroxybenzylidene)amino)-1,5-dimethyl-2-phenyl-1H-pyrazol-3(2H)-one
4	**3d**	4-((2,4-dihydroxybenzylidene)amino)-1,5-dimethyl-2-phenyl-1H-pyrazol-3(2H)-one
5	**3e**	4-((2-hydroxy-3-methoxybenzylidene)amino)-1,5-dimethyl-2-phenyl-1H-pyrazol-3(2H)-one
6	**3f**	4-((2-hydroxy-5-nitrobenzylidene)amino)-1,5-dimethyl-2-phenyl-1H-pyrazol-3(2H)-one
7	**3g**	1,5-dimethyl-4-((2-nitrobenzylidene)amino)-2-phenyl-1H-pyrazol-3(2H)-one
8	**3h**	4-(((1,5-dimethyl-3-oxo-2-phenyl-2,3-dihydro-1H-pyrazol-4-yl)imino)methyl)benzonitrile
9	**3i**	4-((4-chlorobenzylidene)amino)-1,5-dimethyl-2-phenyl-1H-pyrazol-3(2H)-one
10	**3j**	4-((4-(diethylamino)-2-hydroxybenzylidene)amino)-1,5-dimethyl-2-phenyl-1H-pyrazol-3(2H)-one
11	**3k**	4-(((2-hydroxynaphthalen-1-yl)methylene)amino)-1,5-dimethyl-2-phenyl-1H-pyrazol-3(2H)-one (3k)
Chapter – 3		
12	**4a**	Ethyl 6-methyl-2-oxo-4-phenyl-1,2,3,4-tetrahydropyrimidine-5-

		carboxylate
13	**4b**	Ethyl 4-(4-chlorophenyl)-6-methyl-2-oxo-1,2,3,4-tetrahydropyrimidine-5-carboxylate
14	**4c**	Ethyl 6-methyl-4-(2-nitrophenyl)-2-oxo-1,2,3,4-tetrahydropyrimidine-5-carboxylate
15	**4d**	Ethyl 4-(4-hydroxyphenyl)-6-methyl-2-oxo-1,2,3,4-tetrahydropyrimidine-5-carboxylate
16	**4e**	Ethyl 4-(2-hydroxy-5-nitrophenyl)-6-methyl-2-oxo-1,2,3,4-tetrahydropyrimidine-5-carboxylate
17	**8a**	2,4,5-triphenyl-1H-imidazole
18	**8b**	2-(4-chlorophenyl)-4,5-diphenyl-1H-imidazole
19	**8c**	4-(4,5-diphenyl-1H-imidazol-2-yl)phenol
20	**8d**	2-(4-nitrophenyl)-4,5-diphenyl-1H-imidazole
21	**8e**	2-(4,5-diphenyl-1H-imidazol-2-yl)-4-nitrophenol
22	**12a**	2-amino-7-hydroxy-4-phenyl-2H-chromene-3-carbonitrile
23	**12b**	2-amino-4-(4-chlorophenyl)-7-hydroxy-2H-chromene-3-carbonitrile
24	**12c**	2-amino-7-hydroxy-4-(4-hydroxyphenyl)-2H-chromene-3-carbonitrile
25	**12d**	2-amino-7-hydroxy-4-(4-nitrophenyl)-2H-chromene-3-carbonitrile
26	**12e**	2-amino-7-hydroxy-4-(2-hydroxy-5-nitrophenyl)-2H-chromene-3-carbonitrile
27	**16a**	1-benzyl-4-phenyl-1H-1,2,3-triazole
28	**16b**	1-(4-nitrobenzyl)-4-phenyl-1H-1,2,3-triazole
29	**16c**	1-benzyl-4-(p-tolyl)-1H-1,2,3-triazole
30	**16d**	1-(4-nitrobenzyl)-4-(p-tolyl)-1H-1,2,3-triazole
	Chapter-4	
31	**4a**	4-Aminophenol
32	**4b**	Aniline
33	**4c**	Benzene-1,2-diamine

34	**4d**	Benzene-1,4-diamine
35	**4e**	4-Bromoaniline
36	**4f**	p-amino toluene
37	**4g**	1-napthyl amine
38	**4h**	1-(4-aminophenyl)ethanol
39	**4i**	1H-indol-5-amine
40	**4j**	2-amino benzimidazole
		Chapter 5
41	**4a**	1-benzyl-4-phenyl-1H-1,2,3-triazole
42	**4b**	1-(4-nitrobenzyl)-4-phenyl-1H-1,2,3-triazole
43	**4c**	1-benzyl-4-(p-tolyl)-1H-1,2,3-triazole
44	**4d**	1-(4-nitrobenzyl)-4-(p-tolyl)-1H-1,2,3-triazole
45	**7a**	3,3',3''-(4,4',4''-(((1,3,5-triazine-2,4,6-triyl)tris(oxy))tris(methylene))tris(1H-1,2,3-triazole-4,1-diyl))tris(2H-chromen-2-one)
46	**7b**	3,3',3''-(4,4',4''-(((1,3,5-triazine-2,4,6-triyl)tris(oxy))tris(methylene))tris(1H-1,2,3-triazole-4,1-diyl))tris(7-hydroxy-2H-chromen-2-one)
47	**7c**	3,3',3''-(4,4',4''-(((1,3,5-triazine-2,4,6-triyl)tris(oxy))tris(methylene))tris(1H-1,2,3-triazole-4,1-diyl))tris(7-bromo-2H-chromen-2-one)
48	**7d**	3,3',3''-(4,4',4''-(((1,3,5-triazine-2,4,6-triyl)tris(oxy))tris(methylene))tris(1H-1,2,3-triazole-4,1-diyl))tris(2H-benzo[g]chromen-2-one)

APPENDIX-II

LIST OF PUBLICATIONS/ABSTRACT

Research Papers Published

1. **M Kumari**, R Gupta, Y Jain, *Synth. Commun.*, **2019**, 49, 529-538.

2. **M Kumari**, Y Jain, P Yadav, H Laddha, R. Gupta, *Catal. Lett.* **2019**, 8, 2180-2194.

3. Y Jain, R Gupta, P Yadav, **M Kumari**, *ACS Omega*, **2019**,4, 3582-3592.

4. Y Jain, **M Kumari**, H Laddha, R Gupta, *ChemistrySelect*, **2019**,4, 7015-7026.

5. Y Jain, **M Kumari**, R Gupta, *Tetrahedron Lett.*, **2019**, 60, 1215-1220.

6. N Sharma, V Sharma, Y Jain, **M Kumari**, R Gupta, S K Sharma, K Sachdev, *Macromolecular Symposia* **2017**, 376, 1700006.

7. A Jain, R Gupta, Y Jain, **M Kumari** and M Agrawal *Chemistry and biology interface*, **2017**,7, 2, 102-115.

8. Y Jain, **M Kumari**, M. Agarwal, R Gupta, Robust synthesis of sugar-coumarin based fluorescent 1, 4-disubstituted-1, 2, 3-triazoles using highly efficient recyclable citrate grafted β-cyclodextrin@ magnetite nano phase transfer catalyst in aqueous media, *Carbohydrate research,* **2019***,* 482, 107736.

9. **M Kumari**, R Gupta, Y Jain, Fe_3O_4 – Glutathione stabilized Ag nanoparticles: A new magnetically separable robust and facile catalyst for aqueous phase reduction of nitroarenes, *Appl Organometal Chem*. **2019**, *33*, 5223.

10. P Yadav, **M Kumari**, Y Jain, M Agarwal, R Gupta, Antipyrine based Schiff's base as a reversible fluorescence turn "off-on-off" chemosensor for sequential recognition of Al^{3+} and F^- ions: A theoretical and experimental perspective, *Spectrochimica Acta Part A: Molecular and Biomolecular Spectroscopy*, **2019**, 117596.

11. N Sharma, V Sharma, R Vyas, **M Kumari**, A Kaushal, R Gupta, SK Sharma, K Sachdev, A new sustainable green protocol for production of reduced graphene oxide and its gas sensing properties, *Journal of Science: Advanced Materials and Devices*, **2019**, 4(3), 473-482.

12. Y Jain, **M Kumari**, R. P. Singh, D Kumar, R Gupta, Sonochemical Decoration of Graphene Oxide with Magnetic Fe3O4@CuO Nanocomposite for Efficient Click Synthesis of Coumarin-Sugar Based Bioconjugates and Their Cytotoxic Activity. *Catal Lett* . **2019**. doi:10.1007/s10562-019-02982-6

1. **Publications in Conferences:**

Conferences, Seminar and Short-term course:

1. Attended 3 day National conference on "Recent advances in chemical sciences (RAICS 2015), 21-23 August, organized by Department of Chemistry, MNIT Jaipur.

2. Attended 2 day international conference on "Frontiers at the Chemistry-Allied Sciences Interface from 25th-26th April 2016 organized by center of advance science, Department of Chemistry, university of Rajasthan, Jaipur.

3. Attended 2 day International conference on Surface Engineering from December, 09 to 10, 2016 organised by Department of Metallurgical and Materials Engineering & Materials Research Centre.

4. Worked as co-ordinator and attend one day INDO-CANADIAN SYMPOSIUM ON "Materials, energy and Environment" on 31st December 2016 organised by Materials Research Centre.

5. Attended 2 day national conference on "Desalination and water purification for defence and civil applications" from 22-23rd organised by DRDO Jodhpur and Indian desalination association.

6. Attended five days intensive training programme on "Basics to Advanced NMR Theory & Practice" organized by Materials Research Center, Malaviya National Institute of Technology Jaipur from 3rd July-7^{th}July, 2017

7. Attended 3 day National conference recent advances in chemical sciences(RAICS 2015), 21-23 August, organized by Department of Chemistry, MNIT Jaipur

8. Attended 3 day International Conference on, "Frontiers at the Chemistry – Allied Sciences Interface, 25th- 26^{th}April, 2016, organized by Centre of Advanced Studies, Department of Chemistry, University of Rajasthan, Jaipur.

9. Attended 3 day International Conference on, "Frontiers at the Chemistry – Allied Sciences Interface, 25th- 26th April, 2016, organized by Centre of Advanced Studies, Department of Chemistry, University of Rajasthan, Jaipur.

10. Attended 3 day International Conference on, "Frontiers at the Chemistry – Allied Sciences Interface, 25th- 26th April, 2016, organized by Centre of Advanced Studies, Department of Chemistry, University of Rajasthan, Jaipur.

11. Attended 3 day international conference on "Frontiers Research in Chemistry and Biology Interface from 11th-13th Jan 2018 organized by Department of Chemistry, Manipal University of Rajasthan, Jaipur and Indian Society of Chemists & Biologists, Lucknow, India.

12. Attended five days short term course on "Electron Microscopy" organized by Department of Metallurgical & Materials Engineering and Materials Research Center, Malaviya National Institute of Technology Jaipur from 19th Feb-23rd Feb, 2018.

13. Attended one day National Seminar on "Recent Trends & Advances in Chemical Science and their Impact on Environment organized by Department of chemistry, Amity School of Applied Sciences, Amity University Rajasthan, Jaipur held on 13th, 2018.

14. Attended five days short term course on "Nano Forms of Carbon" organized by Materials Research Center, Malaviya National Institute of Technology Jaipur from 19th March-23rd March, 2018.

15. Attended five days short term course on "Properties of Nano Materials-why and How They Differ from their Bulk Counter-part" organized by Materials Research Center, Malaviya National Institute of Technology Jaipur from 13th -17th Nov, 2018.

16. Attended five days short term course on "Nanostructures-Nanoparticles & Thin Films : Synthesis and Characterization" organized by Materials Research Center, Malaviya National Institute of Technology Jaipur from 11th Feb-15th Feb, 2019

BRIEF BIODATA OF AUTHOR

Ms. Mitlesh Kumari was born in Alwar, Rajasthan in 1989. She has graduated in Science (Zoology, Botany and Chemistry) from St. Wilfred's PG College affiliated to Rajasthan University, Jaipur. She has pursued her Master's degree in Chemistry from Malaviya National Institute of Chemistry Jaipur, from 2011-2013 and awarded Gold Medal. She has cleared NET-JRF in 2015. She joined the research group of Dr. Ragini Gupta, Professor, Malaviya National Institute of Technology Jaipur, Jaipur in 2014 and being selected for INSPIRE Fellowship (IF140506). Her research work is on "Nanoparticles with magnetic core as a versatile catalyst for organic transformations."

She has presented her research work in various national and international conferences. She has good publications (research articles and review) in international journals in the area of Chemistry.

Check for updates

Preparation of a simple biocompatible magnetite@citric acid: An efficient reusable solid acid catalyst for the rapid synthesis of antipyrine Schiff's bases and study of their radical scavenging potential

Mitlesh Kumari[a], Ragini Gupta[a,b], and Yachana Jain[a]

[a]Department of Chemistry, Malaviya National Institute of Technology, Jaipur, India; [b]Materials Research Centre, Malaviya National Institute of Technology, Jaipur, India

ABSTRACT

Citric acid immobilized magnetic nanoparticles (MNPs@CA) have been synthesized and used for the preparation of bio-important anti-pyrine (1,5-dimethyl-2-phenyl-1,2-dihydro-3H-pyrazol-3-one) derived Schiff's bases (3a–k) in lesser reaction time with very high yield under ultrasonication. The catalyst was characterized by FT-IR, powder X-ray diffraction (XRD), field emission scanning electron microscopy (FESEM), high resolution transmission electron microscopy (HRTEM), and thermogravimetric analysis (TGA). The functional-ized nanoparticles were easily separated using an external magnet during work-up procedure and show excellent reusability upto 8 cycles without any significant loss in catalytic activity. All the synthe-sized compounds (3a–k) were screened by DPPH (2,2-diphenyl-1-pic-rylhydrazyl) method with respect to ascorbic acid for their antioxidant activity and some of them gave promising results.

GRAPHICAL ABSTRACT

EtOH, 50 °C, 15 min,)))),
85-96%

DPPH (red)
yellow

Synthesis of Fe₃O₄-DOPA-Cu Magnetically Separable Nanocatalyst: A Versatile and Robust Catalyst for an Array of Sustainable Multicomponent Reactions under Microwave Irradiation

Mitlesh Kumari[1] · Yachana Jain[1] · Priya Yadav[1] · Harshita Laddha[1] · Ragini Gupta[1,2]

Abstract

Herein, we are reporting a facile route to synthesize magnetically separable copper loaded L-DOPA functionalized magnetite nanoparticles (Fe₃O₄-DOPA-CuNPs), which are well characterized by FT-IR, PXRD, SEM, EDAX, HRTEM, XPS, TGA and VSM techniques. This single catalyst exhibits excellent catalytic activity towards (i) synthesis of DHPMs via Biginelli reaction (ii) synthesis of imidazoles (iii) synthesis of 2-amino-4H-chromenes (iv) 1,2,3-triazole derivatives by 'Click reaction' under microwave irradiation (MWI). Interestingly it can be easily recovered and reused for subsequent cycles for above mentioned four important multicomponent reactions without any significant decrease in its catalytic activity.

✉ Ragini Gupta
rgupta.chy@mnit.ac.in

[1] Department of Chemistry, Malaviya National Institute of Technology, Jaipur 302017, India

[2] Materials Research Centre, Malaviya National Institute of Technology, Jaipur 302017, India

🙋 Springer

FULL PAPER

WILEY Applied Organometallic Chemistry

Fe₃O₄ – Glutathione stabilized Ag nanoparticles: A new magnetically separable robust and facile catalyst for aqueous phase reduction of nitroarenes

Mitlesh Kumari[1] | Ragini Gupta[1,2] | Yachana Jain[1]

[1] Department of Chemistry, Malaviya National Institute of Technology, Jaipur 302017, India

[2] Materials Research Centre, Malaviya National Institute of Technology, Jaipur 302017, India

Correspondence
Ragini Gupta, Department of Chemistry, Malaviya National Institute of Technology Jaipur 302017, India.
Email:
Email: rgupta.chy@mnit.ac.in

The heterostructured Ag nanoparticles decorated Fe₃O₄ Glutathione (Fe₃O₄-Glu-Ag) nanoparticles (NPs) were synthesized by sonicating glutathione (Glu) with magnetite and further surface immobilization of silver NPs on it. The ensuing magnetic nano catalyst is well characterized by Fourier transform infrared spectroscopy (FTIR), scanning electron microscopy (SEM), high resolution transmission electron microscopy (HRTEM), powder X-ray diffraction (PXRD), thermogravimetric analysis (TGA). The prepared Fe₃O₄-Glu-Ag nanoparticles have proved to be an efficient and recyclable nanocatalyst with low catalyst loading for the reduction of nitroarenes and heteronitroarenes to respective amines in the presence of NaBH₄ using water as a green solvent which could be easily separated at the end of a reaction using an external magnet and can be recycled up to 5 runs without any significant loss in catalytic activity. Gram scale study for the reduction of 4-NP has also being carried out successfully and it has been observed that this method can serve as an efficient protocol for reduction of nitroarenes on industrial level.

KEYWORDS
Fe₃O₄-Glu-AgNPs, magnetically separable, reduction of nitroarenes, silver nanoparticles

1 | INTRODUCTION

The reduction of nitroarenes has attracted a great deal of attention as the resulting anilines are important intermediates for the manufacture of pharmaceuticals, dyes, polymers, and fine chemicals.[1] 4- nitrophenol being one of the toxic pollutant as the United States Environmental Agency has listed 4-nitrophenol as 'priority pollutant' because it can be hardly removed through natural degradation as a refractory pollutant and will cause serious risk to both animal and human.[2] Generally, the synthesis of anilines entails catalytic[3–5] and non-catalytic methods employing different reducing agents.[6–8] The non-catalytic processes uses either Bechamp or sulphide reduction technology which generates large amounts of undesirable waste that is detrimental to the environment.[9] On the other hand, catalysts used for the catalytic reduction of nitro compounds give priority to the precious metals, such as Pd and Pt, which are expensive and usually sensitive to both air and moisture.[10–13] Another type of catalyst was the iron-based compounds, including FeCl₃, iron oxides and FeOOH, which were mainly explored for the reduction of nitroarenes [14]. The preparation and use of magnetic nanoparticles (MNPs) offers advantages in clean and sustainable chemistry as they are non-toxic, readily accessible, and retrievable.[14,15] They have attracted more and more attention because of their unique properties, such as large surface area, multifunctionality, excellent loading capacity and great potential applications in catalysis, drug carriers

192